ON THE ANTARCTIC CONTRIBUTION TO HOLOCENE SEA-LEVEL

BY

IAN DAVID GOODWIN

B. SURV., M. APP. SC. (U.N.S.W.)

Submitted in fulfilment of the requirements
for the degree of Doctor of Philosophy

in the Institute of Antarctic and Southern Ocean Studies (IASOS)
University of Tasmania

June, 1995

STATEMENT

This thesis contains no material which has been accepted for the award of any other degree, diploma or higher degree in any tertiary institution, except by way of background information and duly acknowledged in the thesis, and to the best of my knowledge and belief, this thesis contains no material previously published or written by another person, except where due reference is made in the text of the thesis.

Ian David Goodwin
13 June, 1995

AUTHORITY OF ACCESS

This thesis may be made available for loan. Copying of any part of this thesis is prohibited for six months from the date this statement was signed; after that time limited copying is permitted in accordance with the *Copyright Act* 1968.

Ian David Goodwin
13 June, 1995

ACKNOWLEDGEMENTS

The research work which forms the core of this thesis was conducted whilst the author was employed as a Glaciologist with the Glaciology Section, Australian Antarctic Division from 1984 to 1990. Subsequently, the research work on the "Surface mass balance variability in Kemp Land, East Antarctica" was conducted whilst the author was employed as a Research Fellow in the School of Earth Sciences, University of Melbourne, and funded by an Antarctic Scientific Advisory Committee (ASAC) Grant to the author between 1991-1993. The later stages of thesis preparation were funded by an Antarctic CRC Scholarship between August, 1994 to April, 1995.

The thesis was supervised by Dr Ian Allison, Principal Research Scientist, Glaciology Program, Antarctic CRC and Australian Antarctic Division, and Professor Bill Budd, Antarctic CRC, University of Tasmania. Over a number of years many of the author's colleagues provided advice and actively participated in discussions and fieldwork relevant to the thesis. The glaciological research was principally supervised by Mr Neal Young, Dr Ian Allison and Mr Vin Morgan of the Glaciology Program. The author is grateful for the friendship, discussion and co-operation of his colleagues in the Glaciology Program over the last decade, especially Mr David Etheridge (CSIRO DAR), Mr Egon Wehrle, Mr Martin Higham, Mr Russell Brand, Mr Damien Jones and Mr Tim Medhurst. Mr Egon Wehrle developed specialised firn and ice coring drills for the fieldwork. Mr Martin Higham and Mr Gerry Love conducted the drilling program in Kemp Land in 1991/92 when the author was unable to participate. Professor Pat Quilty provided direction, assistance and useful discussions on Antarctic geoscience over the last decade, for which the author is grateful.

The extensive fieldwork which formed a major aspect of this research, involved dozens of people. Firstly, I wish to acknowledge the assistance and friendship of my fellow wintering ANARE expeditioners in 1985 at Casey Station, in particular, my companions on the eastern Wilkes Land Traverses, with whom I worked and lived continuously for fifteen months; Mr Ross Walsh, Mr Gerry Love, Mr Don Waugh, Mr Wayne Eastley, Mr Graeme Lawrence, and Mr Andy Crook.

I also wish to acknowledge the assistance of many of the ANARE expeditioners at Casey in 1985, 1986, 1987 and 1988 who accompanied the author on field trips along the coast of Law Dome and on the Windmill Islands, and aided in the glacial geological fieldwork, particularly Mr Ray Lindupp, Mr Russell Rachinger, Mr Blue

MacGibbon and Mr Simon Catley. I thank my ANARE colleagues at Mawson and at the Dovers field base in the Northern Prince Charles Mountains in 1988/89, particularly Dr Ian Allison, Mr Peter Mantell and Mr Rod Ledingham.

The author also thanks Dr Peter Barrett and Mr Alex Pyne, Antarctic Research Centre, Victoria University of Wellington, New Zealand for the invitation and assistance to participate in the 1989/90 NZARP summer program in glacial geological and sedimentological fieldwork at Granite Harbour and Mackay Glacier environs, McMurdo Sound, Victoria Land.

Many people assisted in the laboratory analysis of ice core samples and sediment samples. These include: the late Mr Ted Wishart and Mr Colin Wookey at Glaciology for some of the oxygen isotope analyses; Mr John Ivey and Ms. Diana Davies at AGAL, Kingston for the solute analyses; Mr John Head at the Australian National University Radiocarbon Laboratory for the ^{14}C dating, and Mr John Olley at CSIRO Division of Water Resources for the deuterium isotope measurements.

The author also wishes to acknowledge the generous assistance of people in the School of Earth Sciences, University of Melbourne, in particular Professor Ian Simmonds and Dr Bob Baird, who provided an office and access to facilities whilst this thesis was prepared.

Finally, I wish to thank my wife Deborah and children Angus and Erica for enduring my absence both in Antarctica and for long bouts 'in the office', and my father Keith, for encouragement. Last but not least, my thanks to Sir Edmund Hillary, who in 1968 inspired and encouraged me to seek adventure and science in the Antarctic.

ABSTRACT

Holocene glacial fluctuations of Antarctica are investigated using a combined glacial geological and glaciological approach. An understanding of the timing, forcing and sea-level contribution of these glacial fluctuations is crucial to the interpretation of global eustatic sea-level changes during the Holocene and the present. As a baseline for the Holocene studies, the recent surface mass balance rate distribution of Antarctica and its controlling factors are determined with respect to case studies in the Wilkes Land and the Lambert Glacier drainage basins. The variation in surface mass balance rates and mean annual oxygen isotope values over the last 50 years are interpreted from stratigraphic analyses of several shallow firn cores from these drainage basins. The surface mass balance rate is calculated to vary with surface air temperature by 20%/°C in the ice sheet interior, and by 25%/°C in the coastal margins. This variation is in response to changes in atmospheric circulation, surface air temperature and sea ice extent.

The Holocene climate pattern is analysed with respect to the oxygen isotope records from the deep ice cores and the oceanic sediment cores, and is defined into periods where temperature has deviated up to 1-2°C from the long-term Holocene mean. The corresponding terrestrial and marine glacial geological evidence for Holocene glacial fluctuations in the south-western Pacific Ocean, the Indian Ocean, and the Ross Sea sectors of East Antarctica is re-examined together with a case study of the Holocene glacial history of the Windmill Islands and the Law Dome ice sheet, in East Antarctica. An interpretation of the ice expansion during the Last Glacial Maximum and the subsequent melting history of the Law Dome ice sheet during the Early-Mid Holocene, is made from field observations of raised shorelines and the chronostratigraphy of lake sediments and abandoned Adélie penguin rookeries on the Windmill Islands. The Mid-Late Holocene evolution of the Law Dome ice sheet margin is determined from the stratigraphy, structure, morphology, isotopic, solute and sediment composition of basal ice exposures and the Løken Moraines. The results from the Law Dome case study support the view that contraction of the outlet glaciers was established before 8,000 years B.P. with the outer Windmill Islands, adjacent to the Vanderford Glacier, ice free at this time. Contraction of the grounded ice margins lagged the outlet glaciers with the inner Windmill Islands deglaciated by 5,500 years B.P.. Subsequently, the ice margin continued to retreat to a position further inland than the present until 4,500 years B.P.. During this period the East Antarctic outlet glaciers were at their maximum Holocene expansion. Between 4,000 to 1,000 years B.P. it is concluded that the Law Dome and the East Antarctic grounded ice margins expanded with a partial contraction between 500 years B.P. to the present.

Relative sea-level changes and variation in surface mass balance rates throughout the Holocene are tested by a sensitivity analysis of the Lambert Glacier/Amery Ice Shelf system, the Law Dome and Wilkes Land to determine the forcing mechanisms for the glacial fluctuations. The palaeo-surface mass balance rates are calculated for the Early Holocene Climatic Optimum, the Mid Holocene cool period, and the Late Holocene warm and cool phases, using the interpreted 20-25%/°C variation in surface mass balance with air temperature. The sensitivity analyses confirm that the size of Antarctica is controlled by its dual response to sea-level and climate changes, with expansion initiated by relative sea-level lowering and nourished by a positive surface mass balance. The relative sensitivities are characterised by the outlet glaciers leading the grounded ice sheet margins and the alpine glaciers, both in the Early Holocene contraction and in the Mid-Late Holocene expansion. It is hypothesised that variation in palaeo-surface mass balance rates during the Holocene has partially offset the sea-level rise contribution of the post-glacial contraction of Antarctica. An equivalent sea-level curve for Antarctica is constructed from the differential surface mass balance contributions and from the post-glacial melting history. The validity of the hypothesis is tested by comparing the derived sea-level curve to the relative sea-level records on mid-oceanic islands. The maximum contribution from Antarctica to post-glacial sea-levels occurred at 4,000 years B.P. when there was widespread retreat of the East Antarctic outlet glaciers, and the grounded ice sheet margins. This is synchronous with the geomorphological evidence for high sea-level stands on the mid-oceanic islands. Antarctica contributed a slight lowering to sea-level between 4,000 to 1,000 years B.P.. During this century the probable Antarctic sea-level contribution was calculated to have varied from a sea-level contribution of +0.25 mm a^{-1} prior to 1970 followed by a contribution of -0.15 mm a^{-1} since 1970. It is suggested that these contributions to Holocene sea-levels provide a better fit to the oceanic sea-level records than those produced by models based on the continuing exponential melting and retreat of the Antarctic Ice Sheet throughout the Holocene.

TABLE OF CONTENTS

LIST OF FIGURES

LIST OF TABLES

CHAPTER 1
INTRODUCTION

1.1 OVERVIEW

The majority of glacial geological and paleo-glaciological studies on Antarctica have focused on the extent of the ice sheet during the Late Pleistocene and the timing of the subsequent retreat of the expanded ice sheet during the Holocene. This has also been the case for Holocene sea-level studies which have been primarily oriented towards the melting contribution of Antarctica during the Early-Mid Holocene (Clark and Lingle, 1979, Peltier, 1988, Tushingham and Peltier, 1991). Little attention has been focused on the state of mass balance and the glacial fluctuations of the Antarctic Ice Sheet and glaciers during the Holocene. This has partly been due to the lack of terrestrial exposures in Antarctica where glacial fluctuations can be interpreted by glacial geological features. In addition the poor knowledge of the present mass balance of Antarctica and its temporal variation (Bentley and Giovinetto, 1990, Jacobs, 1992) have hindered investigations of Holocene glacial fluctuations. Nevertheless, glacial geologists throughout this century from Stillwell (1918) to Domack et al. (1991) and Baroni and Orombelli (1994) have observed features which indicate that regions of the Antarctic Ice Sheet have fluctuated in size during the Holocene. Such fluctuations, if they were regionally widespread have significant consequences for the interpretation of global sea-level changes during the Holocene and the patterns of hydro-isostasy and the emergence of mid-oceanic islands, in the Pacific, Indian and Atlantic Oceans.

Dual control of the volume and extent of the Antarctic Ice Sheet by precipitation and sea-level was first suggested by Denton et al. (1971). They concluded that 'sea-level controlled fluctuations along the periphery of the ice sheet, and that changes in accumulation rate controlled surface level oscillation in the interior of the Antarctic Ice Sheet'. This thesis investigates the hypothesis that the dual forcing of relative sea-level changes and fluctuations in the climate of Antarctica during the Holocene has resulted in variations in the size and extent of the ice sheet and the outlet glaciers which have contributed directly to global sea-level changes. To accomplish this study a multi-disciplinary approach has been taken with the intention of combining the glacial geological evidence on the ice sheet extent with the modern glaciological observations, measurements and theory. The majority of previous glacial geological and modern glaciological studies have not combined the results of each discipline to predict or reconstruct the palaeo-geography of the Antarctic Ice Sheet.

The early studies on the extent of the Late Pleistocene ice sheet have been based on the concept that the Antarctic ice sheet grows in response to global sea-level lowering and climate cooling (Hollin, 1962). Whilst the sea-level is the primary control on the growth of marine ice sheets, the concept of climate cooling controlling the establishment and growth of ice sheets had evolved from studies on the Late Pleistocene Northern Hemisphere ice sheets (Flint, 1955, Denton and Hughes, 1981). These ice sheets which include the present Greenland Ice Sheet experience significant summer melting and ablation which limits ice sheet growth (Paterson, 1981). In contrast, the Antarctic Ice Sheet experiences only minimal surface ablation and summer melting which is restricted to a narrow area around the margin (Robin, 1986). The growth of the Antarctic Ice Sheet is controlled instead, by climate warming in the absence of global sea-level lowering. Increased snow accumulation occurs over the ice sheet surface due to the increased moisture carrying capacity of the warmer air mass, increased ocean evaporation and a decrease in the extent and area of sea ice (Budd and Simmonds, 1991). The ice sheet thickens in response to the increased accumulation over short time scales before dynamical adjustments affect the ice sheet outflow (Whillans, 1978). Ice sheet growth will only occur if climate warming is less than 5°C above the present (Huybrechts and Oerlemans, 1990). If climate warming is greater than 5°C, it is estimated that surface ablation and runoff together with the basal melting of ice shelves would result in ice sheet decay. Studies such as Huybrechts and Oerlemans, (1990), Drewry (1990), Drewry and Morris (1991) and Budd and Simmonds (1991) have investigated the potential response of the Antarctic Ice Sheet to global warming and the resulting contribution to global sea-level. They have focused debate away from the cooler climate of the Late Pleistocene ice sheets and onto the future responses of the Antarctic Ice Sheet under a warmer climate.

Part of the research in this thesis aims to hindcast the changes in spatial ice sheet accumulation pattern in response to climate variations during the Holocene (which are outlined in section 1.2). The hindcasting is used to test the glacial geological evidence for fluctuations in ice sheet extent. A detailed study of the modern spatial and temporal accumulation patterns together with their controlling climatological and topographical factors was conducted to form a basis for the hindcasting of accumulation rates during the Holocene. This study is focused on Wilkes Land, Law Dome, Queen Mary Land, Mac.Robertson Land and Kemp Land (Figure 1.1). It involved the field survey of spatial accumulation rates and their relationship to topography and the surface katabatic windfield (Chapter 2), together with regional firn core stratigraphic analyses to determine the temporal variation in accumulation rates and oxygen isotope composition (Chapter 3). These field studies and laboratory

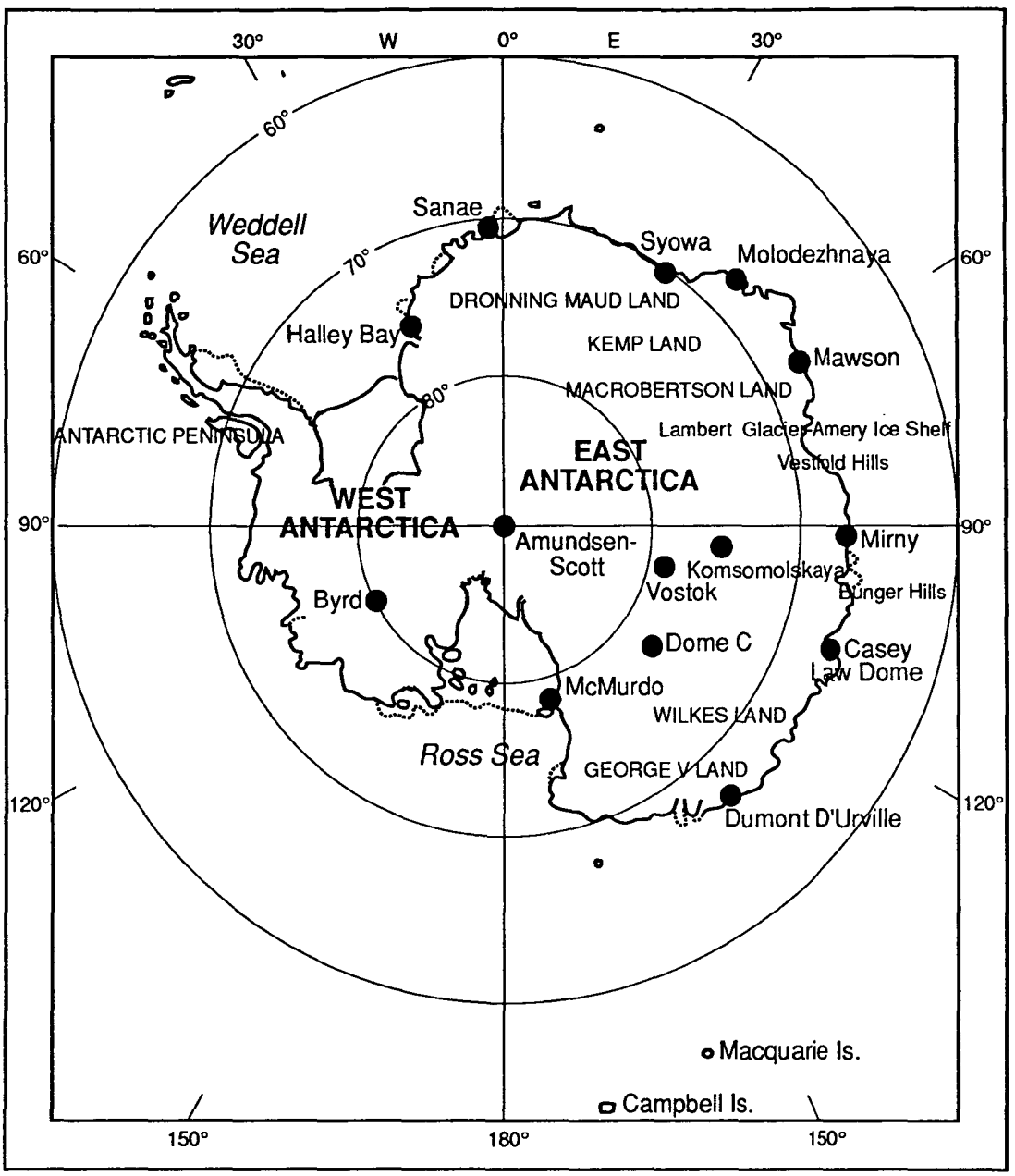

Figure 1.1 Antarctic locality map showing the major geographic regions of East and West Antarctica, together with the locations referred to in the study.

analyses enabled; the determination of relationships between accumulation rate and elevation; accumulation rate and coastal air temperature; and accumulation rate and sea ice extent. These relationships particularly between accumulation and air temperature were applied to the interpreted Holocene temperature variations, to determine an estimate of accumulation rates for these Holocene periods. A sensitivity analysis was applied to the Law Dome and Lambert Glacier Basin to determine the effect of climate forced variations in accumulation rate on ice sheet extent and mass balance (Chapter 7).

Relative sea-level changes at the margin alone can change the position of the margin without changes in the mass balance of the ice sheet interior (Hollin, 1962). A glacial geological study on the Early-Holocene retreat of the Late Pleistocene ice sheet and the glacio-isostasy at the East Antarctic ice margin was conducted to determine estimates of the relative sea-level changes during the Holocene (Chapter 4). The study also established the timing and extent of the retreat for use as a baseline to interpret subsequent glacial advances during the Mid-Late Holocene. This research involved a detailed case study of the Late Pleistocene-Mid Holocene glacial and glacio-isostatic history of the Law Dome ice margin together with a broad regional comparison along the East Antarctic ice margin. Similarly a case study of the Mid-Late Holocene glacial history of the Law Dome ice margin was investigated to determine the timing and extent of glacial fluctuations (Chapter 5). The glacial history was determined from a study of basal ice and sediments, proglacial sediments and the morphology of ice-cored terminal moraines. A regional comparison and analysis of evidence for Mid-Late Holocene glacial fluctuations was made along the East Antarctic ice margin (Chapter 6). A sensitivity analysis of the response of the Antarctic Ice Sheet to changes in relative sea-level around the margins was conducted to determine whether the interpreted variations in ice sheet extent from the glacial geological studies could be explained without changes in ice sheet mass balance (Chapter 7).

Global sea-level rose rapidly in the Late Pleistocene and Early Holocene as the Northern Hemisphere and Antarctic ice sheets melted and retreated. The melting of the Northern Hemisphere ice sheets was completed by 6,000 years B.P.. This has been determined by an enormous body of glacial geological research (Denton and Hughes, 1981). However, the Holocene high sea-level stands on oceanic islands are dated at between 4,000 to 2,000 years B.P. (Nakada and Lambeck, 1988,1989, Nunn, 1994). This indicates that water was being added to the world's oceans during this period. The most likely source of this water is from the continued melting of Antarctica (Nakada and Lambeck, 1988). However, most previous glacial geological studies have concluded that melting of the expanded Late Pleistocene Antarctic ice sheet was

completed by 6,000 years B.P.. The hypothesis tested in this thesis is that the variations in the extent and mass balance of Antarctica during the Holocene may have been responsible for the rise in sea-level to ~3,000 years B.P. and partially responsible for the subsequent slight lowering of sea-level. This has important consequences for the interpretation of both the hydro-isostatic response of the ocean basins to meltwater loading and of the present and future trends in sea-level. The hypothesis is based on the interpretation that ice sheet accumulation rates have oscillated in response to Holocene temperature fluctuations and have resulted in a temporal pattern of differential mass exchange between the ice sheet and the oceans. The differential mass exchange is estimated and an equivalent sea-level curve for Antarctica is calculated for the Holocene. The hypothesis is presented as an alternative to the hypothesis for the exponential melting of Antarctica throughout the Holocene presented by Nakada and Lambeck (1988). The validity of the hypothesis is tested by comparing the derived equivalent sea-level curve for Antarctica to the relative sea-level records on mid-oceanic islands. This thesis also examines the contribution of Antarctica to global sea-level during the Holocene and over the last 50 years (Chapter 8). The temporal accumulation patterns interpreted from the firn core stratigraphic studies are used to determine the recent contribution of surface mass balance to sea-level on the basis of direct mass transfer between ocean to ice sheet storage. The glacial geological evidence for glacial fluctuations in the Late Holocene is also used in the determination of the present mass balance state of Antarctica and its total contribution to global sea-level.

1.2 CHARACTERISTICS OF HOLOCENE CLIMATE IN ANTARCTICA

Data on the Holocene climate of Antarctica and the Southern Ocean region are rare in comparison with the voluminous data from the temperate and tropical regions (Goudie, 1983, Pielou, 1991). The primary sources of climate data have been derived from ice cores and marine sediment cores. The secondary sources of data have been derived from geomorphological, sedimentological and palynological studies which have produced indications of climate change. However, the profiles of the stable oxygen isotope ($\delta^{18}O$) and deuterium isotope (δD) ratios from ice cores and marine sediment cores present the most comprehensive proxy climate records because of the strong relationship between oxygen isotope and temperature. The marine sediment $\delta^{18}O$ records also represent changes in the $\delta^{18}O$ composition of the oceanic reservoir due to changes in ice volumes. The present knowledge of the Holocene climate pattern in Antarctica has been derived from the interpretation of both ice cores drilled in the East

Antarctic ice sheet and ocean sediment cores obtained from the circum-polar and sub-polar oceans.

Detailed proxy temperature records have been derived from oxygen and deuterium measurements on deep ice cores in the interior of East Antarctica (Figure 1.1) at:

- Dome C at 74° 30' S, 123° 10' E (Lorius et al., 1979),
- Vostok at 78° 28' S, 106° 48' E (Jouzel et al., 1987),
- Komsomolskaya at 74° 05' S, 97° 29'E (Ciais et al., 1992),

and from ocean sediment cores at :

- RC11-120 in the subantarctic Indian Ocean at 43° 31' S, 79° 52' E (Hays et al, 1976, Shackleton, 1978, Martinson et al., 1987),
- MD 73-025 and MD 84-527 in the subantarctic Indian Ocean at 43° 49' S, 51° 19' E (Labeyrie et al., 1987, Labracherie et al., 1989)

The oxygen isotope $\delta^{18}O$ composition of ice in Antarctic ice cores closely reflects the surface air temperature at the time water vapour condenses to form snow (Dansgaard, 1964) but is also primarily a function of the composition of the ocean reservoir, and the distance to the ocean source from which the water vapour was evaporated. It is also a function of the kinetic fractionation processes which occur during transportation and condensation, and the strength of the surface air temperature inversion above the ice sheet. There is also a strong linear relationship between the $\delta^{18}O$ water vapour composition and air elevation since temperature is linearly dependent upon elevation. Over much of the ice sheet the cloud height and the top of the surface air inversion follows the ice sheet surface closely and hence small changes in ice sheet elevation can cause proportional changes in the $\delta^{18}O$ composition of snow. Thus long-term $\delta^{18}O$ records determined from ice cores provide an accurate proxy record of temperature provided changes in the isotopic composition of the ocean water reservoir, the geographic source of the moisture, the elevation of the ice sheet and the strength of the inversion have not occurred during the period of the record, or can be estimated. If the temporal pattern in $\delta^{18}O$ is coincident between ice cores from sites separated by long distances then it is probable that significant relative changes in moisture source, ice sheet elevation and the inversion strength across the ice sheet have not occurred during the period represented by the ice core record. Hence the oscillations in the $\delta^{18}O$ records should primarily represent changes in temperature.

The deep ice core sites at Dome C, Vostok and Komsomolskaya are located on the East Antarctic plateau where neither significant ice flow conditions nor large changes (< 50-100 m) in ice sheet elevation or ice thickness are considered to have biased the climatic records during the Last Glacial Maximum to Holocene period (Ciais et al., 1992). Temperature series were derived by Ciais et al. (1992) following a detailed analysis of the δ value-temperature relationship and the isotopic temperature noise. The modern δ value-temperature relationship ($\delta = a\ T_s + b$) for this region of East Antarctica was first established by Lorius and Merlivat (1977) as $\delta^{18}O = 0.75‰$ per °C +10‰. However, because of past differences (glacial to interglacial) in the isotopic composition of the seawater reservoir from which the moisture is evaporated, and in ice sheet elevation, the intercept b value for the Holocene and the Glacial-Holocene Transition (15,000 to 11,000 yr B.P.) is subject to correction.

The choice of the appropriate correction values has important implications for the analysis of small temperature changes during the Holocene. The mean $\delta^{18}O$ isotopic value of oceanic waters was enriched by +1.1‰ during the Last Glacial Maximum (LGM) due to the storage of water (depleted in $\delta^{18}O$) in the global ice sheets (Chappell and Shackleton, 1986, Labeyrie et al., 1987). Therefore, the $\delta^{18}O$ isotopic value of the seawater reservoir and moisture source for ice sheet precipitation would have become more negative or depleted during the Glacial-Holocene Transition and the Early Holocene as the ice sheets (particularly in the Northern Hemisphere) melted. Similarly, a long-term latitudinal shift in the moisture source around Antarctica, due to the reduction in the sea ice extent and the expanded ice sheet margins may also have resulted in a more negative shift in the $\delta^{18}O$ value of ice sheet precipitation during the Glacial-Holocene Transition and the Early Holocene, according to the modern latitudinal gradient in $\delta^{18}O$ established by Bromwich and Weaver (1983). Thus the modern b intercept requires at least a correction for the seawater reservoir changes during the Glacial-Holocene Transition, and preferably for latitudinal shifts in the moisture source, before proxy temperature records can be determined. Ciais et al. (1992) approached this problem by correcting the b intercept according to the marine $\delta^{18}O$ time series calculated by Labeyrie et al. (1986) for the surface water isotopic changes in the southern Indian Ocean from benthic and planktonic foraminifera $\delta^{18}O_{PDB}$ measurements. They did not correct for shifts in the moisture source pattern, since this is unknown.

Elevation changes may also cause a shift in the value of the intercept b in the δ value-temperature relationship. Because the ice sheet responds very slowly (35,000 years) to changes in accumulation at Vostok and Dome C (Whillans, 1978) changes in the accumulation rate either raise or lower the surface elevation. Such changes affect the

isotope values because the surface inversion layer follows the ice sheet surface. At Vostok and Dome C the mean annual $\delta^{18}O$ value changes by 0.8‰ per 100 m change in elevation (Grootes and Stuiver, 1987), whilst at Law Dome near the coast, the mean annual $\delta^{18}O$ value changes by 0.55‰ per 100 m (Morgan and Budd, 1977). Since precipitation and accumulation rates are a function of temperature due to the saturation water vapour pressure, a change in temperature is usually associated with a change in ice sheet accumulation (Robin, 1977). Thus if the temperature and the accumulation rate at a site increased there would be two components of change in the mean annual $\delta^{18}O$ value. The temperature increase would result in an enrichment or more positive $\delta^{18}O$ value according to the relationship 0.74‰/°C for Dome C (Lorius et al., 1979). In contrast, the associated increase in the mean annual accumulation rate would cause a tendency towards an increase in elevation and progressively, a partial or total offset to the enrichment in $\delta^{18}O$ by causing a slight depletion or more negative $\delta^{18}O$ value. The elevation effect is more pronounced near the coast where accumulation rates are high compared to on the interior plateau.

There is considerable debate about the extent to which ice sheet elevations changed on the interior plateau between LGM to the Holocene. Jouzel et al (1989) calculated from ^{10}Be measurements that accumulation rates at Vostok were 50% lower during the LGM than the Holocene. This is equivalent to an ice sheet elevation increase of ~50 m over 5,000 years from the LGM to the Holocene. Alternatively, ice sheet elevation changes at Dome C and Vostok on the order of 100-150 m have been estimated from the total gas content in ice cores by Raynaud and Lebel (1979). More recently, Martinerie et al. (1994) have examined the processes which control the air content in ice cores and have concluded that ice sheet elevation changes were probably smaller than previously estimated. These are more in accord with those determined from the ^{10}Be measurements. An elevation increase of ~50 m during the glacial-interglacial transition would result in an equivalent depletion (more negative) in the mean $\delta^{18}O$ value. Thus a correction of ~+0.4‰ would be required in the b intercept to accommodate the elevation changes between LGM and the Holocene. Ciais et al. (1992) did not apply a correction for elevation changes between LGM and the Holocene, or during the Holocene.

The temporal noise in the isotope records also requires definition before estimates of significant fluctuations in temperature can be ascertained. The isotopic temperature noise is a function of the snow accumulation rate at the ice core site. At Dome C, Vostok and Komsomolskaya these accumulation rates are low at 34 kg m^{-2} a^{-1}, 23 kg m^{-2} a^{-1} and 50 kg m^{-2} a^{-1} respectively. Hence, the noise in the snow deposition and

subsequent redistribution by surface winds can result in relatively large interannual variability (discussed in detail in Chapter 3). Ciais et al. (1992) calculated from two adjacent cores at Vostok that the high frequency noise at Vostok accounted for ~20% of the signal and they concluded that for 50 year intervals derived temperature fluctuations above 0.32°C were statistically significant at one standard deviation At Dome C and Komsomolskaya this limit is likely to be reduced to ~0.2 to 0.25°C because of the relatively higher accumulation rates.

The resulting proxy temperature curve calculated by Ciais et al. (1992) for East Antarctica is shown in Figure 1.2 and was calculated as an average from the Vostok, Dome C and Komsomolskaya $\delta^{18}O$ and δD series. For comparison, the most detailed summer sea-surface temperature record (MD 84-527) from the Southern Ocean (Indian Ocean Sector) at 43° 49' S, 51° 19' E between Crozet and Heard Island, just north of the Antarctic Convergence (Polar Front), is shown in Figure 1.3 (after Labracherie et al., 1989). This record confirmed in greater detail the earlier summer sea-surface temperature record calculated from the nearby core MD 73026 which was reported by Labeyrie et al. (1986). The summer sea surface temperature record was calculated from the foraminiferal-based transfer function using multivariate statistical analysis of the distribution of the planktonic foraminifera species, *Neogloboquadrina pachyderma s.* and *Globigerina bulloides*, together with $\delta^{18}O_{PDB}$ series for these planktonic foraminifera species and the benthic formainifera, *Cibicides wuellerstorfi.* Both records show a strong correlation between the major fluctuations in temperature, although the sea-surface temperature fluctuations are generally greater in amplitude. For example during the Early Holocene Climatic Optimum between 11,000 to 9,000 yr B.P. the sea-surface temperatures were on average 1.5 °C warmer than at present (Labracherie et al, 1989), whilst the comparable ice sheet surface temperatures are estimated by Ciais et al. (1992) as ~0.7°C warmer than at present. This difference may be in part attributed to: the scaling of the modern b intercept for past changes in the isotopic composition of seawater by Ciais et al.(1992), using the marine $\delta^{18}O$ series for the polar front waters (Labeyrie et al., 1986), and; changes in atmospheric circulation patterns and the moisture sources of Antarctic precipitation, during deglaciation and the southward migration of the polar front.

However, the marine $\delta^{18}O$ series applied to the ice sheet $\delta^{18}O$ measurements was calculated by Labeyrie et al. (1986) from the benthic $\delta^{18}O_{PDB}$ series which included a +0.4‰ correction (relative to the glacial values) to the $\delta^{18}O$ of the benthic foraminifera aged between 0 to 9,000 yr B.P., to account for the 1.5°C increase in the Indian Ocean deep water which occurred at ~9,000 yr B.P.. This correction was applied to separate the isotopic changes due to reservoir composition (1.1‰) from those caused by deep

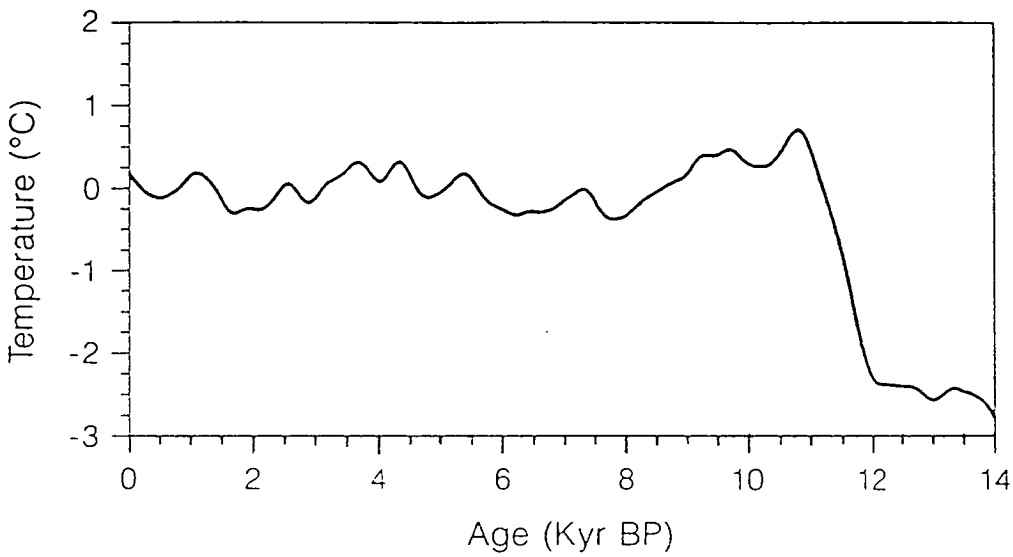

Figure 1.2 Holocene proxy temperature record for East Antarctica (after Ciais et al., 1992). The figure shows the average temperature curve obtained from $\delta^{18}O$ and δD measurements on the East Antarctic deep ice cores from Dome C, Vostok, Komsomolskaya. The temperature scales are relative to the mean of the last 5,000 years. Note that the temperatures during the Early Holocene (11,000 to 9,000 yr B.P.) may be underestimated by up to 0.5°C, since the marine $\delta^{18}O$ time series of Labeyrie et al. (1986) from the polar front location was applied to the ice core $\delta^{18}O$ records, to approximate the correction for changes in the seawater isotopic composition between the LGM and the Holocene. The $\delta^{18}O$ and δD measurements were also not corrected for probable ice sheet elevation increases in response to a 40% increase in accumulation rates during the Glacial-Holocene Transition (15,000 to 11,000 yr B.P.) (Jouzel et al., 1989).

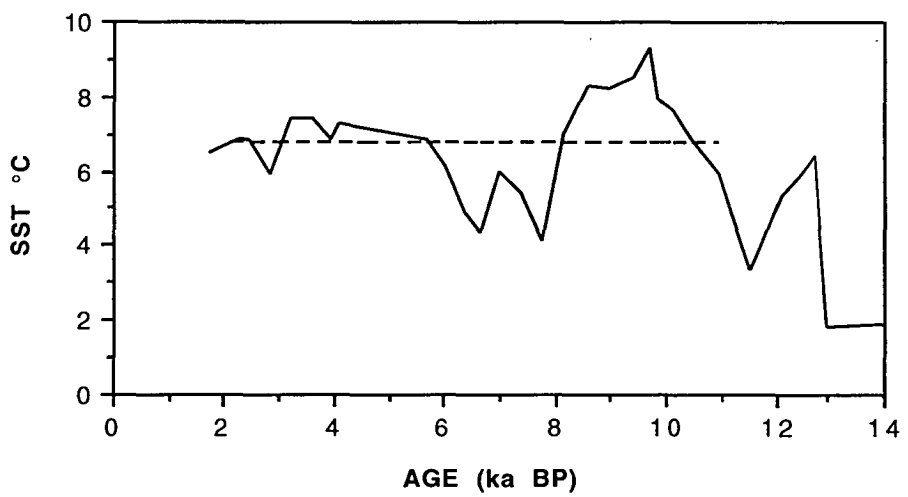

Figure 1.3 Holocene record of summer sea surface temperatures at MD 84-527, located at 44°S, 51°E in the Indian Ocean sector of the Southern Ocean, just north of the Antarctic Convergence, between Crozet and Heard Islands (after Labracherie et al., 1989). The sea surface temperature record was derived from the $\delta^{18}O$ measurements made on the planktonic foraminifera, *Globigerina bulloides* and *Neogloboquadrina pachyderma s.*, together with the multivariate statistical foraminifera temperature-transfer function. The dashed line represents the mean sea surface temperature between 2,000 to 11,000 yr B.P.

water temperature changes at the polar front (0.4‰). The increase in deep water temperature at the polar front was driven by the recommenced feeding of the North Atlantic Deep Water (NADW) into the Circumpolar Deep Water (CPDW) during the deglaciation of the northern hemisphere ice sheets (Duplessy et al., 1988). A more recent study by Charles and Fairbanks (1992) determined from a carbon isotope ($\delta^{13}C$) record in core RC11-83 (41°36' S, 9°48' E, in the South Atlantic Ocean sector of the Southern Ocean) that the NADW recommenced feeding into the Southern Ocean, earlier than 9,000 yr B.P.. The NADW is a major source of heat and salt in the CPDW which represents a mixture of NADW and recirculated deep water from the Indian and Pacific Oceans . The CPDW $\delta^{13}C$ values lie between those of the NADW (high $\delta^{13}C$ and low nutrients) and those of the Indo-Pacific Deep Water (low $\delta^{13}C$ and high nutrients) (Charles and Fairbanks, 1992). Charles and Fairbanks (1992) established the most detailed (to present) isotopic record of the deglacial period in the Southern Ocean. They determined a $\delta^{13}C_{PDB}$ record from the benthic foraminifera, *Cibicides wuellerstorfi*, together with AMS ^{14}C dates on the planktonic foraminifera *Globigerina bulloides*. The $\delta^{13}C_{PDB}$ record for core RC11-83 is shown in Figure 1.4, and shows an abrupt shift from low values characteristic of glacial conditions to high modern values at 12,600-12,200 yr B.P. (Charles and Fairbanks, 1992). Thus the +0.4‰ correction applied to the ice core $\delta^{18}O$ records since 9,000 yr B.P. should have been applied to the records since 12,000 yr B.P, to account for the increased temperature of the CPDW. Accordingly, the Holocene average ice sheet surface temperature record of Ciais et al. (1992) shown in Figure 1.2 was corrected for an increase in ocean temperature due to the earlier recommencement of NADW flux into the Southern Ocean by 12,000 yr B.P.. The revised Holocene proxy surface temperature record for East Antarctica is shown in Figure 1.5. This record is in close agreement with the sea surface temperature record of Labracherie et al. (1989) shown in Figure 1.3.

The upwelling of warmer CPDW during the Early Holocene, promoted warmer surface waters and the earlier retreat of sea ice in late winter and spring (Grobe and Mackensen, 1992). The reduced sea ice extent and concentration was probably a major influence on the circumpolar oceanic circulation, through the greater role of katabatic wind-driven currents and inshore polynya development (Grobe and Mackensen, 1992). Coupled with the reduction in the sea ice extent and concentration during the Early Holocene (Burckle and Cirilli, 1987), the geographic location of the moisture sources of the East Antarctic precipitation migrated southwards closer to the Antarctic continent. This is consistent with the annual cycle of sea ice growth and decay which parallels the migration of the primary moisture source region which is located in the vicinity of the 0 or 1°C sea surface isotherm (Bromwich and Weaver,

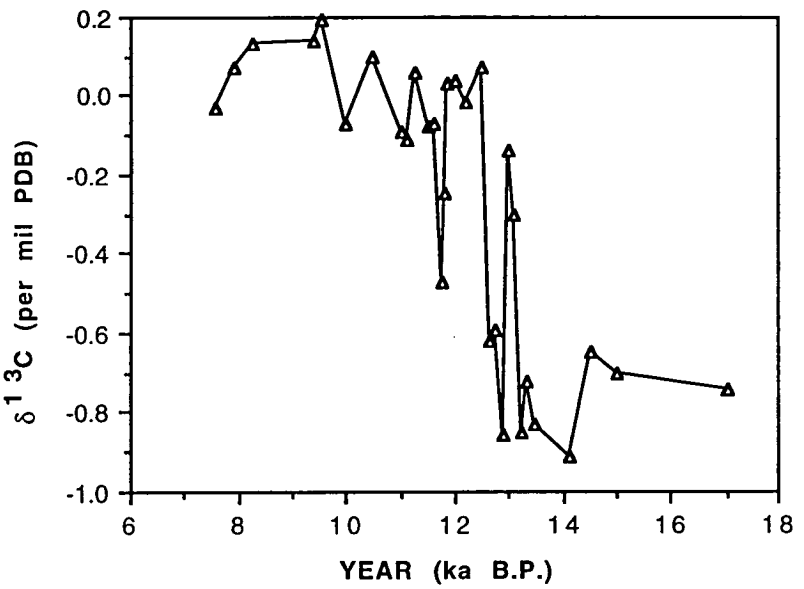

Figure 1.4 The $\delta^{13}C_{PDB}$ record for the deep sea core RC11-83 (41°36' S, 9°48' E, in the South Atlantic Ocean sector of the Southern Ocean) (after Charles and Fairbanks, 1992). The $\delta^{13}C_{PDB}$ record was determined from the benthic foraminifera, *Planulina wuellerstorfi*, together with AMS ^{14}C dates on the planktonic foraminifera *Globigerina bulloides*. A reservoir correction of 600 years was applied to the AMS ^{14}C dates by Charles and Fairbanks (1992). The $\delta^{13}C_{PDB}$ record shows an abrupt shift from low values characteristic of glacial conditions to high modern values at 12,600-12,200 yr B.P. (Charles and Fairbanks, 1992), which indicates that NADW recommenced flux into the CPDW at this time.

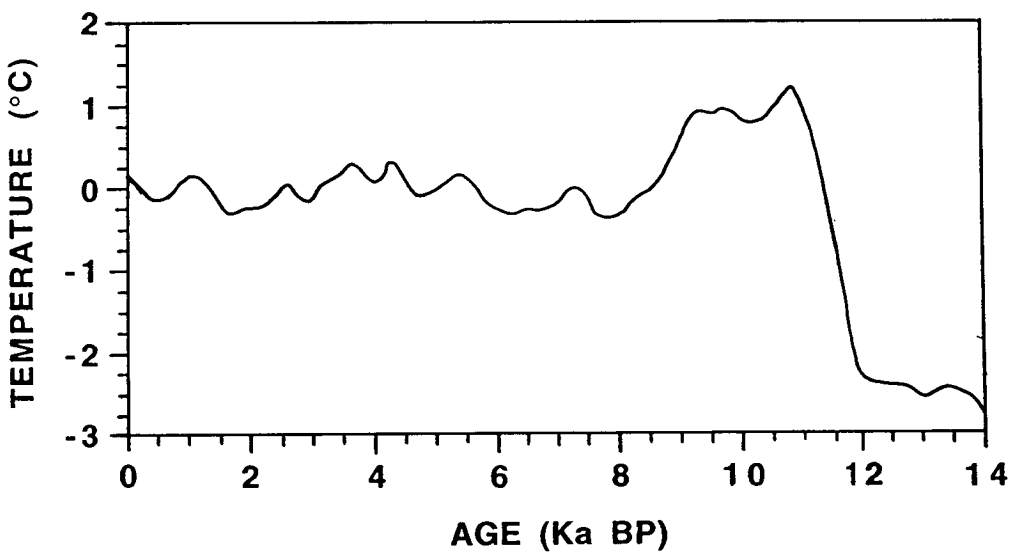

Figure 1.5 The revised Holocene proxy surface temperature record for East Antarctica (after Ciais et al., 1992). The temperature scales are relative to the mean of the last 5,000 years. The proxy temperatures between 0 to 9,000 yr B.P. (in Figure 1.2) have been corrected by -0.5 °C which is equivalent to -0.4‰ according to the modern isotope-temperature transfer function of 0.75‰ per °C (Lorius and Merlivat, 1977). This correction accounts for the earlier increase in CPDW temperature at 12,000 yr B.P., and its effect on the Holocene values in the marine $\delta^{18}O$ series of Labeyrie et al. (1986), used in the determination of the proxy temperature record for East Antarctica in Ciais et al. (1992).

1983). The post-glacial migration of the moisture source would have resulted in the average $\delta^{18}O$ of Antarctic precipitation becoming more negative compared to the average values during the Last Glacial Maximum, since the average $\delta^{18}O$ of sea surface waters becomes more negative towards Antarctica. It is likely that these changes in the average $\delta^{18}O$ of moisture source may have been at least the magnitude equivalent to offset the +0.4‰ correction applied to the marine series for the temperature increase in the deep waters, according to the present latitudinal gradient in average sea surface $\delta^{18}O$ of ~0.004‰/km (Chapter 3, this study). Therefore, the proxy temperatures for the ice sheet during the Holocene may be underestimated by ~0.4°C and be closer to the Holocene sea-surface temperature record.

A broad characterisation of the Early to Mid Holocene climate in Antarctica and the Southern Ocean can be made from these proxy temperature records. A rapid climate warming of about 8°C (Grootes and Stuiver, 1987) occurred at the end of the last glaciation. The temperature warmed by ~3°C between 12,500 to 11,000 years B.P. from the Younger Dryas cool interval to the beginning of the Holocene. The surface temperatures were 1°C above the present day values during the interval 11,000 to 9,000 years B.P. and represent the warmest temperatures during the Holocene (Ciais et al. 1992). Events on the order of centuries during this interval reached up to 1.5°C above the present values (after Lorius et al., 1979), and are not apparent in Figure 1.2 because of the coarse data smoothing. This interval is referred to in this study as the Early Holocene climatic optimum (EHCO) rather than the often used term, Hypsithermal. Between 8,000 and 6,000 years B.P. the temperature decreased to 0.4°C below present values and reached the minimum Holocene temperatures at 7,500 to 8,000 years B.P. (Ciais et al. 1992, Lorius et al., 1979). This period is referred to in this study as the Mid Holocene cool phase (MHCP). Since 5,500 years B.P. the climate is characterised by a series of warm spikes which last for ~1,000 years. These temperature characteristics are corroborated by the proxy summer sea-surface temperature record from the deep sea sediment cores MD84-527 shown in Figure 1.3, and RC11-120, located at 43° 31' S, 79° 52' E, in the Indian Ocean Sector of the Southern Ocean, to the east of Heard Island. This later record was derived from the determined percentages of the radiolarian *Cyladophora davisiana*, and the measured oxygen isotopic composition in the foraminifera *Globigerina bulloides* (Shackleton, 1978, Hays et al., 1976). Shackleton (1978) reported that the Holocene peak in summer sea surface temperatures occurred at 9,400 +/- 600 years B. P. and was 2°C warmer than the present (Martinson et al., 1987). The sea surface temperature records also show the MHCP and a subsequent second warm period centered at 3,500 yr B.P..

The smoothing filter used by Ciais et al. (1992) in the generation of the proxy ice surface temperature records was too coarse to enable a more detailed discussion of the temperature oscillations during the later half of the Holocene. Consequently, the detailed $\delta^{18}O$ record for Dome C and a preliminary record from the coastal site DSS at Law Dome summit (66° 46' S, 112° 59' E, 1,370 m) (after V. Morgan, Antarctic CRC, pers. comm., 1994) are shown in Figures 1.6 and 1.7. Before a discussion on climate oscillations during the later half of the Holocene it is important to distinguish if these smaller oscillations are affected by small ice sheet elevation changes. For example, the mean annual accumulation rate at Dome C is 0.037 m/a^{-1} (snow) and the mean annual accumulation rate at the Law Dome Summit (DSS) is 1.3 m/a^{-1} (ice). Hence a hypothetical 25% change in accumulation at each of these sites over a period of 500 years would change the elevation by ~4.6 m at Dome C and 160 m at DSS These elevation changes are comparable to changes in $\delta^{18}O$ of 0.004‰ and 0.9‰ respectively. Whilst the ice sheet would achieve such a change at Dome C, such a change would not occur at DSS because its response time before a new equilibrium between accumulation and ice flow is short at 330 years (after Whillans, 1978). Hence at DSS it is probable that an $\delta^{18}O$ oscillation representing a fluctuation in temperature should be smaller in amplitude than a similar change at a site such as Dome C where the elevation changes are significantly smaller. In addition at DSS the $\delta^{18}O$ signal should show a peak followed by a sharp decrease as the elevation increased.

The preliminary $\delta^{18}O$ record for DSS at Law Dome covers the last 4,000 years and has been smoothed using a 40 point filter equivalent to an 80 year interval. The Dome C record is composed of average measurements over 4 m sections of the ice core and each represent the mean value for 100 year intervals (Figure 1.6). Comparison of the major oscillations in these records over the 4,000 year period shows a remarkably similar pattern although the magnitude of the oscillations is generally less in the DSS record. Both records show a sharp increase in $\delta^{18}O$ at 1,000 years B.P., with two peaks in the signal between 1,000 to 1,400 years B.P. which represent a peak increase in temperature of 0.4°C above the present for the DSS and Dome C cores. The present mean temperature is defined in Figure 1.7 for DSS, as the mean for the last 200 years as determined by Morgan et al. (1991). The present mean temperature for the last 200 years at Dome C (Figure 1.6) is coincident with the mean for the Holocene (Lorius et al., 1979). The period 1,000 to 1,400 yr B.P. is referred to as the Little Climatic Optimum (LCO) and was previously reported for another core BHD on Law Dome (Morgan, 1985). Similarly a smaller peak occurs at 1,800 to 1,900 years B.P. in both cores although the DSS peak is of a smaller magnitude. The peak at 2,600 to 2,800 years B.P. also occurs in both records and the same pattern occurs between 3,500 to

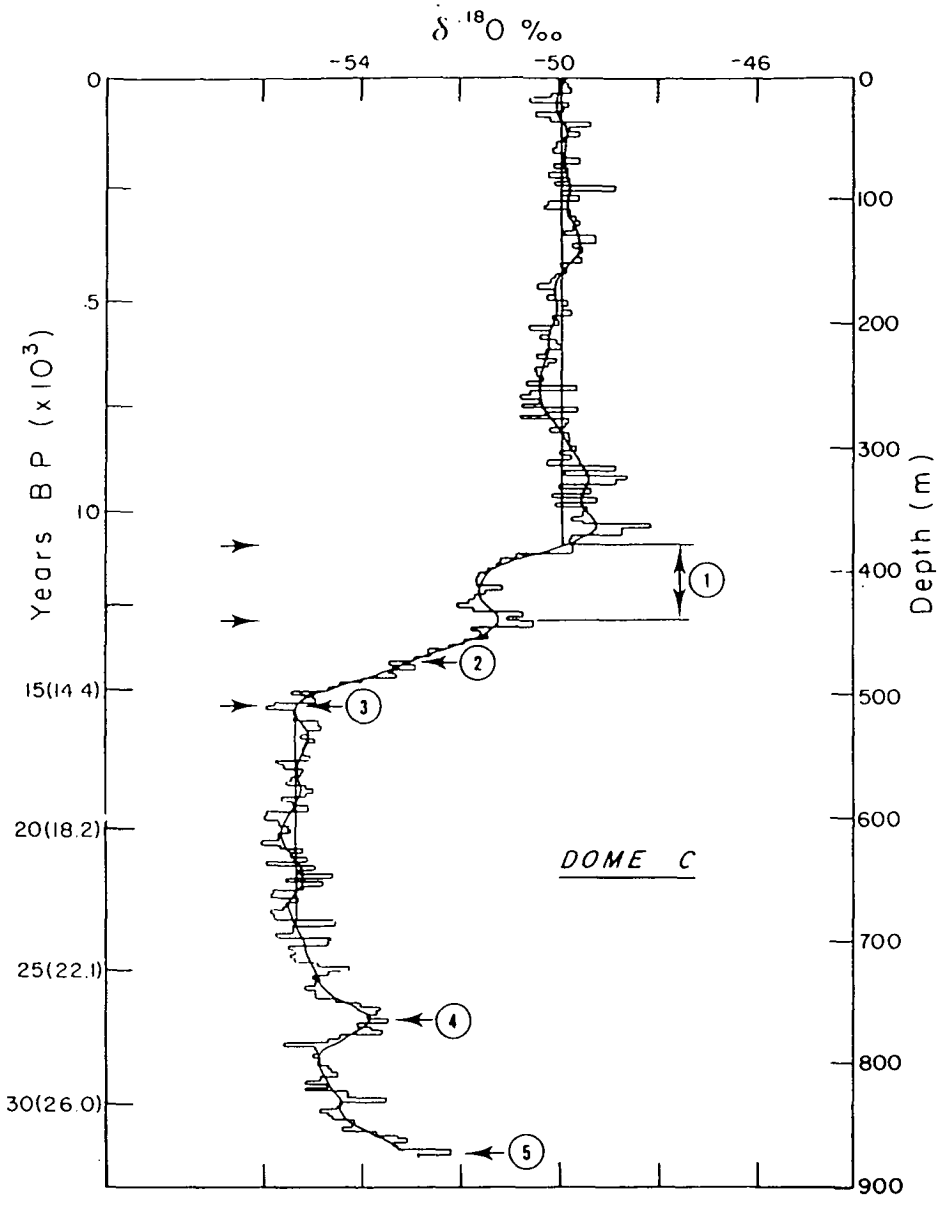

Figure 1.6 $\delta^{18}O$ time series from the Dome C ice core plotted for 4 m long increments and a smoothed curve (after Lorius et al., 1979). The straight line represents the mean value for the last 11,000 years, which is close to the mean value for the last 100 years. Note the fluctuations in the last 5,000 years which are compared to the equivalent fluctuations in the Law Dome DSS $\delta^{18}O$ record in Figure 1.7. The ages were determined from ^{14}C dates obtained from marine sediments and calibrated over the full length of the ice core to 35,000 years B.P.. The ages in brackets were estimated by a simple flow model by Lorius et al. (1979).

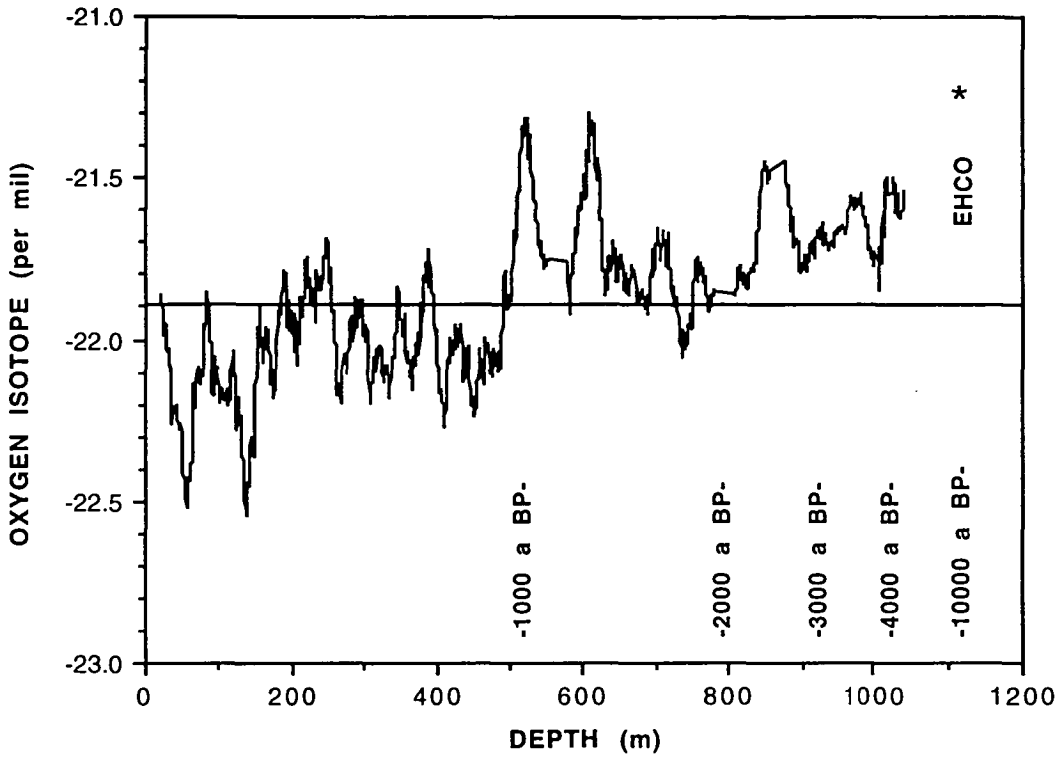

Figure 1.7 $\delta^{18}O$ time series for DSS at Law Dome Summit. The time series has been smoothed over an 80 year interval. The data are preliminary and incomplete and were provided by Vin Morgan (Antarctic CRC, Hobart, 1994). The data only include a few 80 year intervals during the Early Holocene Climatic Optimum (EHCO), which are designated by the asterisk. The chronology was calculated using a simple ice flow model and was matched to the nearby chronology at BHD using the characteristic features of the $\delta^{18}O$ records (Vin Morgan, pers. comm., 1994). The solid line represents the mean $\delta^{18}O$ value for the last 4,000 years. Note that this approximates the long-term Holocene mean value.

4,500 years B.P. with a comparable ~0.3°C increase in temperature above the present. The similarity in the temporal $\delta^{18}O$ patterns between both cores suggest that the signal in both cores can be confidently interpreted as primarily reflecting synchronous oscillations in surface temperature and regional climate at sites which are 1,000 km apart. The smaller magnitude in the short term events of 100 years in the DSS core probably indicates the effect of elevation change on the $\delta^{18}O$ value.

The temporal pattern in ^{10}Be measurements on the Vostok ice core provides support for a significant short (~1,000 yrs) warm period at approximately 4,000 yr B.P. and the Early Holocene Climatic Optimum. Raisbeck et al. (1987) and Jouzel et al. (1989) determined from ^{10}Be measurements on the Vostok ice core that accumulation rates were 30% less than the Holocene long-term mean rates at 14,000 to 15,000 yr B.P., and increased to 20-25% greater than the Holocene long-term mean rates during the EHCO, and up to 20% greater at ~3,000 yr B.P.. These periods of increased accumulation at Vostok correspond to warm periods in the $\delta^{18}O$ in the Vostok core (Jouzel et al., 1989) and imply that the fluctuations in the $\delta^{18}O$ record represent real temperature changes, since the accumulation rate is intrinsically linked to air temperature and the saturation water vapour (Jouzel et al., 1989). This topic is discussed in greater detail in Chapters 3 and 6 of this study.

Morgan (1985) previously reported a $\delta^{18}O$ record for the Law Dome summit core BHD covering the last 2,000 years, and discussed the geographically widespread Little Climatic Optimum (LCO). The mean temperature over the last 1,000 years has been close to the long-term mean for the last 11,000 years, except for during the Little Ice Age (LIA)(200-500 years B.P.) when the temperature was up to 0.5°C cooler than the long-term mean (after Morgan, 1985). The $\delta^{18}O$ records from Mizuho Station in Dronning Maud Land (Morgan, 1985), Law Dome and South Pole (Mosley-Thompson et al., 1990) indicate that temperatures were cooler at all these sites during the Little Ice Age. Alternatively, Mosley-Thompson et al. (1990) determined from the $\delta^{18}O$ record at Siple Station in Ellsworth Land that temperatures were warmer along the Antarctic Peninsula during the Little Ice Age. This is in contrast to the cooler temperatures experienced in the South American Andes (Mosley-Thompson et al., 1990). Since the end of the Little Ice Age these proxy records suggest that temperatures have generally increased to the present across Antarctica.

Supporting climatic evidence has also been reported by glacial geological studies. Baroni and Orombelli (1994a) reported that during the mid-late Holocene optimum between 3,000-4,000 years B. P. there was a proliferation of Adélie penguin rookeries along the Victoria Land coast which they attributed to extensive open water

conditions and favourable snow free coastal sites for rookery occupation during summer. Most of these penguin rookeries have been abandoned since 3,000 years B.P. possibly due to increased sea ice conditions and decreased summer snow melt. There was some penguin re-occupation of sites between 800-1,400 years B. P. which corresponds to the Late Holocene optimum. Similarly, most of the dates of penguin occupation of the presently abandoned rookeries on Bailey Peninsula, Windmill Islands are between 3,000-4,000 years B. P. (Goodwin, 1993b). This indicates that the ice core $\delta^{18}O$ records also reflect the temperature trends along the coast and can be used as proxy climate records for the ice margin.

There is also geographically widespread evidence for fluvial activity in the ice free areas including the Vestfold Hills, Larsemann Hills and Windmill Islands during the mid-late Holocene. Quilty (1993) and Goodwin (1993b) both found evidence for increased lake volumes and fluvial activity, during or since the mid Holocene in the Vestfold Hills and the Windmill Islands, respectively. Dry or partly dry, stream valleys and source lakes formed in mid-Holocene age sediments indicate that a decrease in precipitation rates or a decrease in meltwater supply has occurred in the catchment of these lakes since the mid-Holocene. The reduced lake volumes are probably the result of the progressive melting of the residual ice cover from the LGM expansion, since precipitation was most likely higher than at present between 4,500 to 2,500 yr B.P. according to the interpretation of the ice cores, presented above. Bronge (1992) described a pattern of lacustrine sedimentation in the Vestfold Hills, and attributed the fluctuations in organic matter, wet bulk density and water content in the lake sediment cores to climatic fluctuations on the time scales of a few hundred years. The overall pattern of organic sedimentation shows a continuous increase from 5,000 to 2,500 yr B.P. which corresponds to a probable decrease in the lakes meltwater supply, from the contribution of melting ice. Between 2,500 to the present the organic sedimentation has fluctuated around a stable mean value. One of these fluctuations shows a period of high organic sediment (algae) production between 2,600 to 2,300 yr B.P. which is followed by a period of low organic sediment (algae) production between 2,300 to 2,000 yr B.P.. This sedimentation pattern shows some correspondence to the fluctuation in ice sheet temperatures from warm to cold during this period (Figure 1.2). However, the smaller fluctuations in the sedimentation pattern between 4,000 to present which Bronge (1992) attributes to climate are more likely recording small local changes in meltwater drainage and winter snowfall rather than being indicative of regional climate variations.

The overall agreement between proxy climate data across Antarctica and between the deep ice core records and the marine sediment records indicates that the variation in

climate was synchronous over large regions of Antarctica and the Southern Ocean, especially in the Indian Ocean and south-west Pacific Ocean sectors. There is also well defined supporting evidence for the EHCO in Tierra del Fuego (Margraf, 1983), Alerce, Chile (Heusser and Streeter, 1980) and Kerguelen (Young and Schofield, 1973). Some evidence to the contrary from the Antarctic Peninsula and the nearby Southern Ocean Islands suggests that the climatic optimum may have occurred later during the Mid Holocene (Clapperton, 1990), although this evidence is incongruous with the nearby records from Tierra del Fuego and Southern Chile.

In summary, the Holocene climate in Antarctica can be broadly described by four periods. These are:

- Early Holocene Climatic Optimum between 11,000 and 9,000 yr B.P. when mean temperatures were ~1°C above the long-term Holocene mean values;
- Mid Holocene Cool Period between 8,000 and 6,000 yr B.P. when mean temperatures were 0.4°C less than the long-term Holocene mean values;
- A period between 4,500 and 1,000 yr B.P. when temperatures were generally above or close to the long-term mean Holocene values, possibly reaching 0.3-0.4°C warmer than the mean values at 2,500 to 4,000 yr B.P. and at 1,000 to 1,400 yr B.P., which correspond to the Second Climatic Optimum and Little Climatic Optimum, respectively of Lorius et al. (1979) and Goudie (1983), and;
- A period between 1,000 yr B.P. and the present when temperatures were generally below the long-term mean Holocene values, reaching minimum values of 0.5°C below the mean values at 200 to 500 yr B.P. during the Little Ice Age and at 700 to 900 yr B.P..

1.3 REVIEW OF FACTORS DETERMINING SEA LEVEL

In order to understand the relationship between the mass balance of Antarctica and global sea-level and the deductions made in the thesis it is important to outline all the factors which affect global sea-level.

Definition of sea-level and causes of sea-level changes

Global or eustatic sea-level is determined by a complex array of oceanographic, geophysical, geological, astronomical and meteorological variables. All of these variables combine to cause significant departures in the mean sea-level as defined by

the geoid or equipotential surface of the earth's gravity field. Pirazzoli (1991) and Devoy (1987) provide comprehensive summaries of the causes of sea-level changes, and only a brief outline is presented below.

Eustatic sea-level changes with spatial and temporal variations in:

- the volume of the ocean basins;
- the mass of ocean water; and,
- the ocean water density (steric changes) (Pirazzoli, 1991).

The volume of the ocean basins changes with continental and ocean plate tectonics, volcanism, sedimentation ,and isostatic adjustments to the earth's crust in response to ice loading on the continents and continental shelves. The mass of ocean water changes primarily by the melting and/or accumulation of ice on the continents, and the distribution and retention of groundwater and surface water on the land. The ocean water density changes according to variations in ocean temperature and salinity.

While the eustatic sea-level is defined by the instantaneous combination of the above constraints, it can only be measured relative to the land. These relative sea-level determinations are affected by:

- the vertical movement of the land, either as uplift or subsidence;
- gravitational and rotational variations in the earth's orbit; and,
- changes in atmospheric pressure, winds, ocean currents and tides (Pirazzoli, 1991).

The vertical movements of the land relative to the sea primarily result from tectonic displacements, isostatic adjustments due to changes in ice load (glacio-isostasy), changes in magma load (volcano-isostasy), changes in sediment load (sedimento-isostasy) and changes in water mass (hydro-isostasy). Subsidence movements generally occur due to compaction of sediments or interruption of sedimentation, and withdrawal of groundwater.

Eustatic sea-level has been interpreted to have been rising over the last century (Gornitz, 1993). The magnitude of the rise depends upon the methods used by researchers in the global averaging of the network of tide gauge records. These methods are summarised in Pirazzoli (1993). The estimate of the sea-level trend for this century is 1.0-2.0 mm a^{-1} with the best estimate taken as 1.5 mm a^{-1} (Warrick and Oerlemans, 1990). This trend is correlated with the observed global temperature

increase of 0.5°C over this century (Wigley and Raper, 1993) However, it is inappropriate to conclude that this trend is in response only to modern influences. Time lags and residual effects in geophysical and geological processes controlling eustatic sea-level mean that measurement of sea-level changes include long-term effects, in addition to instantaneous changes due to climatic forcings. Perhaps the most relevant past influence on the modern sea-level records is the variation in the ocean volume and the associated isostatic adjustments during the Holocene. Since 18,000 years B.P. a large volume of meltwater equivalent to a sea-level rise of 121± 5 m has been added to the global oceans (Fairbanks, 1989) through the deglaciation of the Late Pleistocene ice sheets. Approximately 70 m of this sea-level rise has occurred in the last 10,000 years (Fairbanks, 1989). This rapid sea-level rise has resulted in an equally rapid retreat of the earth's coastlines with large changes to sedimentation patterns and large continental and ocean basin isostatic adjustments. The timing and volume of the meltwater contribution from Antarctica during the Holocene is critical in understanding the eustatic and relative sea-level history of both continental margins and oceanic islands (Nakada and Lambeck,1988, 1989), and hence the modern trends and future predictions.

Climate induced present and Late Holocene sea-level changes

The main contributing factors to a climate induced sea-level rise are:

- the thermal expansion of the ocean;
- changes in the mass balance of small glaciers and ice caps;
- changes in the mass balance of the Greenland ice sheet; and,
- changes in the mass balance of the Antarctic ice sheet (Warrick and Oerlemans, 1990).

The present magnitude of these contributing factors, particularly the cryosphere related factors, have been assessed by a number of researchers including Warrick and Oerlemans (1990), Paterson (1993), Meier (1993), Wigley and Raper (1993) and the DOE (1985). The best estimate of sea-level rise due to the thermal expansion of the ocean over the last 100 years is +0.3-0.6 mm a^{-1} (Wigley and Raper, 1993). The best estimate of sea-level rise contributed by the mass balance of small glaciers and ice caps over the last 100 years is +0.4 ± 0.2 mm a^{-1} (Meier, 1984). The best estimate of the sea-level contribution of the Greenland Ice Sheet is a rise of +0.29 ± 0.15 mm a^{-1} (Paterson, 1993, Oerlemans, 1993). The present estimates of the Antarctic sea-level contribution are reviewed in the following section.

1.4 REVIEW OF THE PRESENT SEA-LEVEL CONTRIBUTION OF ANTARCTICA.

The Antarctic contribution to sea-level change is determined by imbalances between surface accumulation and losses due to iceberg calving and to a lesser extent basal meltwater runoff (Jacobs et al., 1992). There are two schools of thought on the present sea-level contribution of Antarctica. One group (Budd and Simmonds, 1990, Bentley and Giovinetto, 1990) believes that the mass balance was close to zero or slightly positive during the last 100 years, and has produced a slightly negative contribution to sea-level. They suggest that the mass balance may have become more positive in the last two decades as accumulation rates have increased in accordance with the rate of global increase in air temperature. This negative sea-level contribution has been estimated as -0.1 to -1.1 mm a^{-1} (Bentley and Giovinetto, 1990). The second group (Jacobs et al., 1992, Paterson, 1993) favours a slight negative balance or positive sea-level contribution of ~+0.45 mm a^{-1}. They included ice shelf melting and ice sheet runoff in their calculations since changes to the thickness of ice shelves directly influence the ice outflow rates from the outlet glacier drainage by changing the back-pressures at the ice shelf and outlet glacier interface. Church et al. (1991) suggest that if the present trend in sea-level rise is closer to 1.0 mm a^{-1} then this can be accounted for by ocean expansion and the melting of non-polar ice alone. This divergence of opinion on the sea-level contribution of Antarctica is primarily due to the large uncertainty in our present knowledge of its mass balance which Bentley and Giovinetto (1990) estimate as ±20%. Some studies either exclude the Antarctic Peninsula or treat its contribution in a minimal context. The Antarctic Peninsula is the warmest region of Antarctica and experiences significant summer melting and very high accumulation rates. The present state of mass balance is uncertain (Paren et al., 1993) although Drewry and Morris (1992) indicate that in the last 40 years the Antarctic Peninsula may have been contributing to sea-level rise by +0.013 mm a^{-1}.

An alternative approach in determining the present sea-level contribution of Antarctica has been to calculate the residual from the sum of the other sources. For example, Paterson (1993) suggests that the Antarctic contribution is equivalent to a sea-level rise of 0.65 mm a^{-1} using a best total estimate of 1.8 mm a^{-1} (after Tushingham and Peltier, 1991 and Trupin et al., 1992). Jacobs (1992) used a similar approach to calculate a sea-level rise contribution of 0.45 mm a^{-1} using a best total estimate of sea-level rise of 1.5 mm a^{-1}.

However, these studies have assumed that the sea-level contribution due to essentially anthropogenic changes in groundwater, lakes and reservoirs is negligible. Sahagian et al. (1994) in a detailed examination of these sources calculated that a combination of groundwater withdrawal, surface water diversion and land use changes has caused a net sea-level rise of 11.8 mm since 1930, which equates to a rate of sea-level rise of 0.2 mm a^{-1}. Gornitz et al. (1994) disputed the conclusions of Sahagian et al. (1994) and suggested that these anthropogenic processes have acted to reduce the rate of sea-level rise. Ignoring their disputed contribution from changes in irrigation practices, a reasonable estimate of the anthropogenic contribution to sea-level rise is -0.4 mm a^{-1}. Therefore the anthropogenic contribution to sea-level rise is estimated to be between -0.4 to 0.2 mm a^{-1}.

The above estimated contributions to sea-level rise can be subtracted from the measured rate of eustatic sea-level rise to determine the residual contribution which is likely to be derived from Antarctica. The sea-level rise budget is calculated as follows:

- measured rate of eustatic sea-level rise $+1.50 \pm 0.50$ mm a^{-1},
- ocean thermal expansion $+0.45 \pm 0.15$ mm a^{-1},
- small glaciers and ice caps $+0.40 \pm 0.20$ mm a^{-1},
- Greenland $+0.29 \pm 0.15$ mm a^{-1},
- groundwater, lakes and reservoirs -0.10 ± 0.30 mm a^{-1},
- residual (Antarctica) $+0.46 \pm 0.80$ mm a^{-1}

Thus the best estimate of the sea-level contribution of Antarctica from the literature review is calculated as ranging from a sea-level rise of 1.26 mm a^{-1} to a slight lowering of -0.34 mm a^{-1} using the residual approach. Alternatively, the research in this thesis on the temporal variation of accumulation rates over the last 50 years is applied to the surface mass balance estimates for the whole Antarctic ice sheet to determine the direct measurement of the recent sea-level contribution (Chapter 8).

CHAPTER 2
SPATIAL VARIATION OF SURFACE MASS BALANCE IN EAST ANTARCTICA

2.1 INTRODUCTION

Surface mass balance is defined as the difference between the net snow accumulation at a site and the loss to the atmosphere by evaporation or melt. The net accumulation at a site results initially from precipitation and subsequently from the reworking of the snow surface by surface wind redistribution (primarily down slope by katabatic winds). The term net accumulation pattern (precipitation minus evaporation) will be used throughout the discussion in place of surface mass balance since evaporative losses are small in comparison to accumulation over the ice sheet. The central core of this thesis is the examination of the temporal variation in the accumulation rate pattern and its effect on the contribution of Antarctica to global sea-level during the last 50 years and during the last 10,000 years. However, the overall spatial accumulation rate pattern is highly variable and is determined by temperature, elevation, macroscale slope and aspect, continentality (distance to moisture source), sea ice extent and concentration, and the general circulation pattern (Giovinetto et al., 1990). Accumulation rate is also spatially variable on the macroscale (100 -1000 km), mesoscale (10-100 km) and microscale (0.02 - 1 km) as a result of topographic effects (elevation, slope and aspect) on precipitation and redistribution processes. Consequently, the spatial or regional variability in the accumulation rate pattern must be defined prior to an analysis or extrapolation of temporal surface mass balance variation across the ice sheet. This study examines the spatial accumulation rate pattern of the Wilkes Land-Queen Mary Land region and the Lambert Glacier Basin region as a background study for the interpretation and discussion of the temporal variation in these regions, in Chapter 3.

Present estimates of accumulation rates across East Antarctica have been obtained mainly from oversnow traverses since the IGY in 1957-58. The current maps of accumulation rate have been compiled from Drewry (1983) and more recently by Giovinetto and Bull (1987). Accumulation rate maps for Wilkes Land-Queen Mary Land, and the Lambert Glacier Basin in MacRobertson and Kemp Lands presented in this chapter were compiled from measurements obtained by Australian National Antarctic Research Expeditions (ANARE) oversnow traverses between 1978-86 and 1989-94 respectively. The inter-annual data were collected during the austral autumn

(March-May) and the austral spring / summer (September-January). A total of 180 to 200 days per year was spent in the study areas. The periods of measurement and sources of the data are given in Table 2.1. Maps of Wilkes Land and the Lambert Glacier Basin which depict the traverse routes are shown in Figures 2.1 and 2.2 respectively. The eastern and western Wilkes Land routes approximately follow the 2000 m elevation contour ranging in elevation from 1600 to 2300 and the southern Wilkes Land route follows the 112°E longitude between 1800 m and the 3000 m contour. The route along the 2000 m elevation contour in Wilkes Land extends from longitude 95°E to 131°E a total distance of 1490 km. The southern Wilkes Land route extends for 750 km. The Lambert Glacier Basin route extends for 2000 km from inland of Mawson along the western edge of the basin to inland of Law Base at the eastern edge of the basin. The route approximately follows the 2500 m elevation contour ranging from 1500m to 2900 m elevation and traverses the flowlines at the head of the Lambert Glacier at 2250m.

TABLE 2.1 SUMMARY OF ANARE ACCUMULATION RATE MEASUREMENTS

Region	Period of measurement	Source
Eastern Wilkes Land	1981-85	Goodwin (1988a)
Southern Wilkes Land	1978-84	Thwaites (1987)
Western Wilkes Land-Queen Mary Land	1983-86	Medhurst (1984) and Hazelton (1987)
Lambert Glacier Basin	1989-95	Higham (1994)
Kemp Land	1977-79	Morgan and Jacka (1979)

These spatial accumulation rate data are used to construct a contour map of accumulation rate isopleths. The regional patterns in Wilkes Land and the Lambert Glacier Basin are then discussed with respect to the controlling climatic and physical factors. The accumulation rate pattern has been shown by a number of studies including Giovinetto and Bentley (1990) and Muszynski and Birchfield (1985) to be highly correlated to ice sheet elevation. The effect of ice sheet topography on the accumulation rate pattern is discussed for the macroscale, mesoscale and the microscale, together with the development of regional accumulation-elevation relationships. The discussion on the topographic effects on the accumulation pattern draws from a case study on eastern Wilkes Land which is documented in Goodwin

(1990). The experimental methods and data collected are published in Goodwin (1988a).

2.2 REGIONAL SETTING OF THE EAST ANTARCTIC KATABATIC ZONE

The katabatic zone is characterised by a dual surface wind system; (i) a depositional cyclonic wind (E-ESE) which accompanies snow precipitation events; and (ii) a predominant strong erosional surface katabatic wind (ESE-SSE) which drains cold air from the ice sheet's interior down-slope to the coast redistributing the precipitation (Kotlyakov 1961, Watanabe 1978).

Precipitation is generated by the direct orographic uplift and adiabatic cooling of moist cyclonic air masses below 3000 m elevation (Bromwich, 1988). Above 3000 m elevation the dominant precipitation mechanism is radiative cooling and advective transport through decreasing air temperatures. The lapse rate of the katabatic slope in Wilkes Land below 2500 m elevation is super adiabatic at 1.33° C/100 m and from 2500-3500 m it is 2.43°C/100 m (Thwaites, unpublished). Higham (1994) measured similar lapse rates of 1.01°C/100 m between 1500-2500 m, and 1.49°C/100 m between 2500-2800 m in the Lambert Glacier Basin. Above 3500 m the lapse rate is 0.5°C/100 m (Budd et al., 1984). There are strong seasonal changes in the lapse rates with the super adiabatic zone not present during the summer. These changes have been attributed to the regional and seasonal changes in the strength of the surface inversion (Allison et al., 1993). Analyses of oxygen isotope in firn cores revealed that the majority of precipitation on the ice sheet occurs during late autumn to late spring (this study, Chapter 3).

However, in the katabatic zone net snow accumulation at a point is not only a function of the precipitation received at that point, but the amount of drift snow redistributed and/or evaporated at that point. The amount of drift snow deposited or eroded by wind redistribution is controlled by the local surface roughness and its effect on wind turbulence and speed. The katabatic wind speed is controlled by the regional fall-line surface slope (Ball, 1960). The accumulated snows are deposited in the form of dunes or surface microrelief, which are topographic features with a spatial scale of 10 -100 m. These exhibit distinct characteristics indicative of; the mode of deposition (whether precipitation or drift snow), surface roughness, wind speed and accumulation rate.

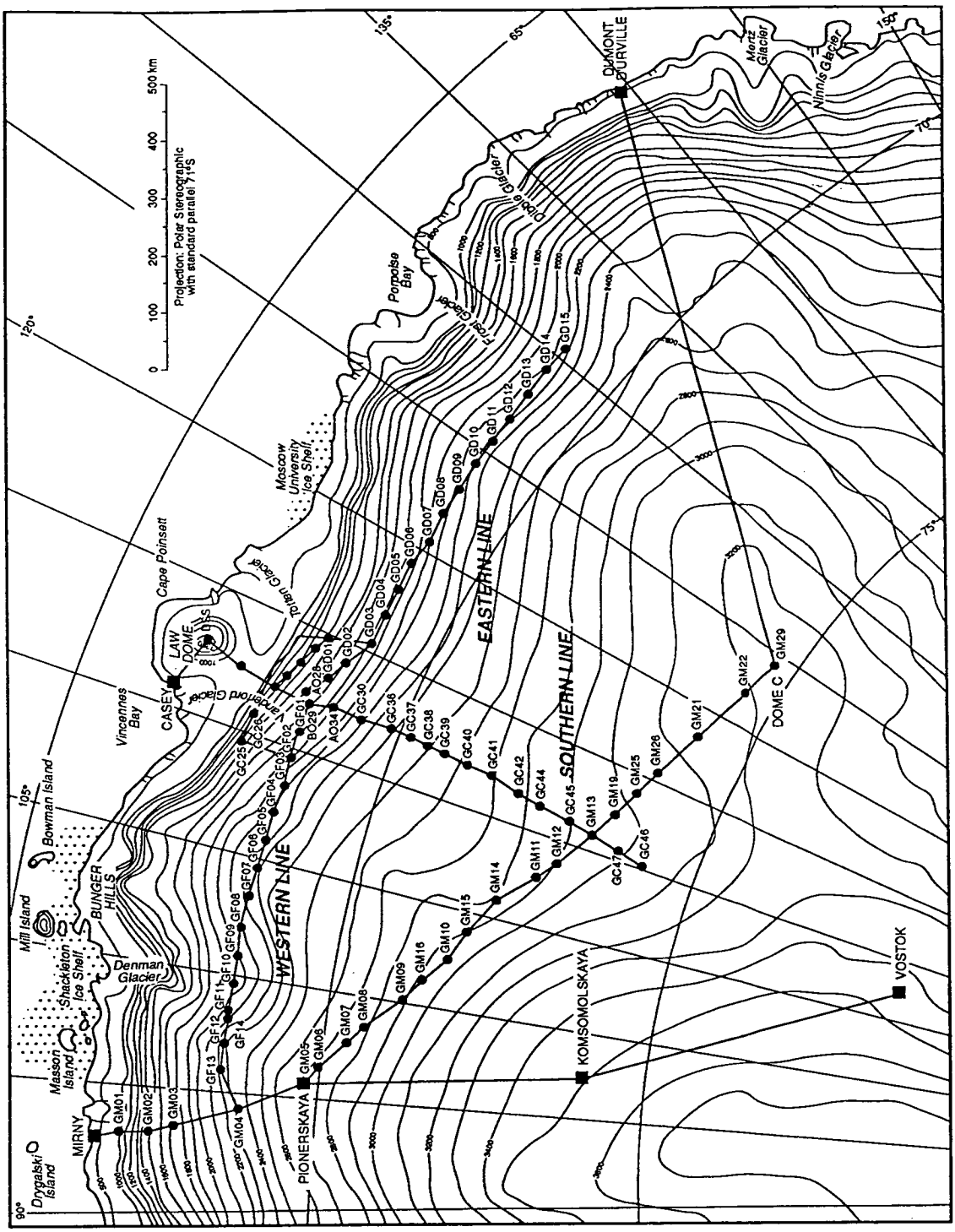

Figure 2.1 Locality map of Wilkes Land and Queen Mary Land drainage basins showing the eastern, western and southern ANARE traverse routes. Also shown is the Soviet traverse route from Mirny to Dome C. The ANARE firn core sites (discussed in chapter 3) GD15, GD06, GD03, GF01, and GF12 are also shown, together with the deep ice core sites at DSS, Vostok, Komsomolskaya and Dome C. The elevation contours are derived from ANARE field surveys, Seasat Radar Altimetry and in the interior, from the SPRI atlas by Neal Young, Antarctic CRC.

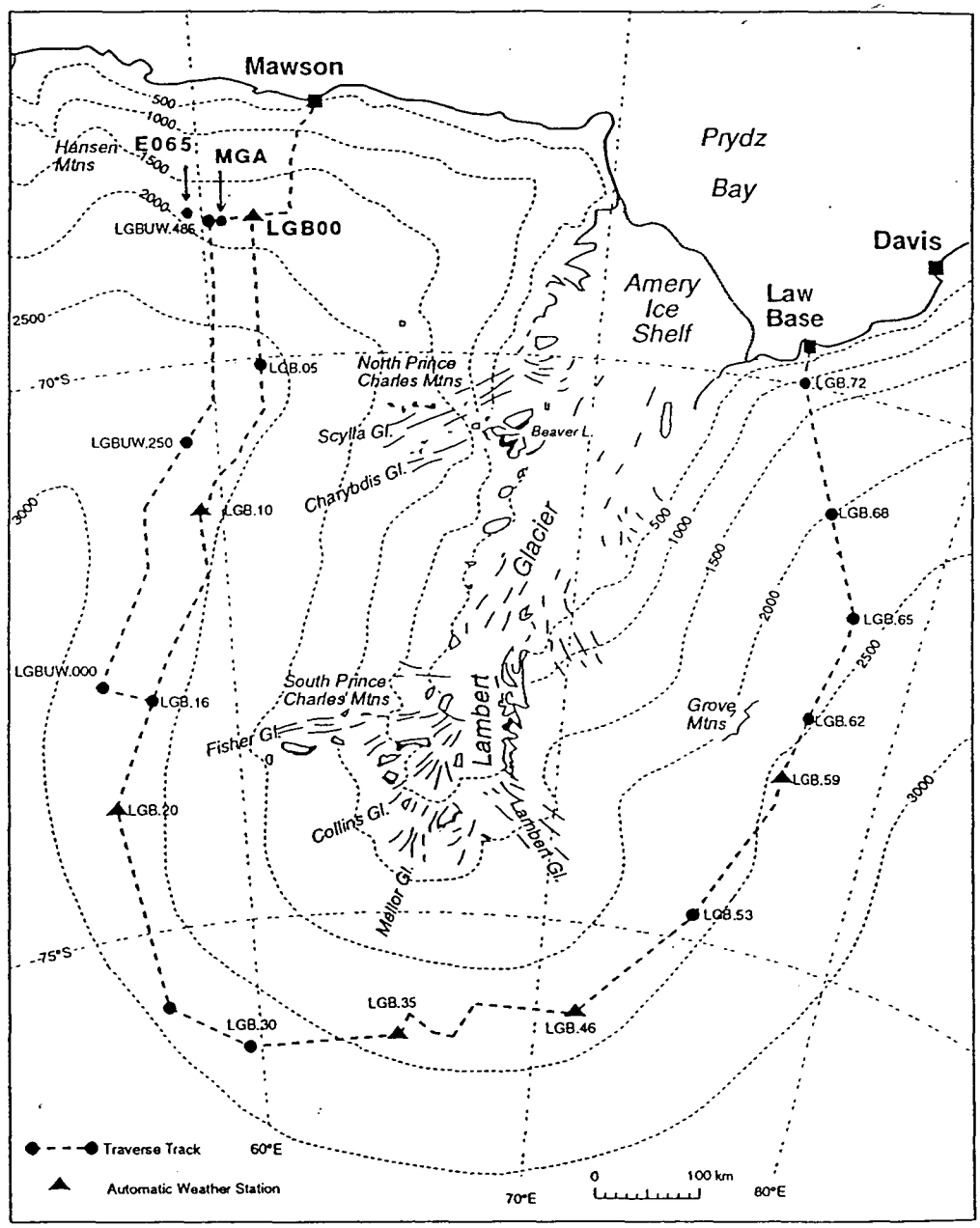

Figure 2.2 Locality map of the Lambert Glacier Basin showing the ANARE traverse route. Also shown are the ANARE firn core sites LGBOO, MGA and E065, inland of Mawson. The elevation contours were derived from ANARE field surveys and the SPRI atlas (Drewry, 1983).

2.3 SNOW ACCUMULATION AND SURFACE TOPOGRAPHY IN WILKES LAND

2.3.1 REGIONAL SURFACE TOPOGRAPHY

Surface elevation profiles were measured by barometric levelling along the traverse routes in Wilkes Land and controlled by Doppler satellite surveying, at intervals of 50 km. The east-west routes traverse along the 2000 m elevation contour and parallel to the coast, from the Queen Mary Land drainage basin inland of Mirny across the western Wilkes Land drainage divide to near the eastern Wilkes Land drainage divide (Figure 2.3a). A number of broad meridional trending depressions and ridges and north-west, north and north-east aspects with an elevation range of 1600 to 2350 m are traversed. These include the Denman Glacier Valley, the western Wilkes Land drainage divide, the Totten Depression, and a broad regional ridge which extends from Dome C (74° 34'S, 123° 10'E) to the coast west of Porpoise Bay (Figure 2.1). The southern Wilkes Land route extends between 1800 m elevation in the Totten Depression towards Vostok to 3000 m elevation, and is shown in Figure 2.4a. A break in slope at 2500 m separates the katabatic slope from the ice sheet interior.

2.3.2 SNOW ACCUMULATION RATES

2.3.2.1 EASTERN AND WESTERN WILKES LAND

Snow accumulation measurements were made on bamboo canes spaced at 2 km intervals along the routes. Net snow accumulation rates were calculated from the measurements made over a 3 year interval. The cane measurements were converted to accumulated mass using surface densities which were filtered using a 20 km running mean to minimise the effect of the variation in the snow surface due to different microrelief types. Snow surface density measurements for the upper 10 cm varied between 350 to 480 kg m^{-3} reaching a peak in the Totten Depression. These densities were scaled to produce a mean density for the upper 1 m of snow pack which corresponds to the depth of snow accumulation over the 3 year epochs. The density scaling was determined from the measured densities in firn cores drilled at intervals of 50 km along the route. The mean measured snow density of 420 ± 20 kg m^{-3} was determined for the upper 1 m of snow pack along the routes.

In eastern Wilkes Land the range of accumulation rates at markers extends from 850 kg m^{-2} a^{-1} at 1610 m elevation in the Totten Depression to 170 kg m^{-2} a^{-1} at

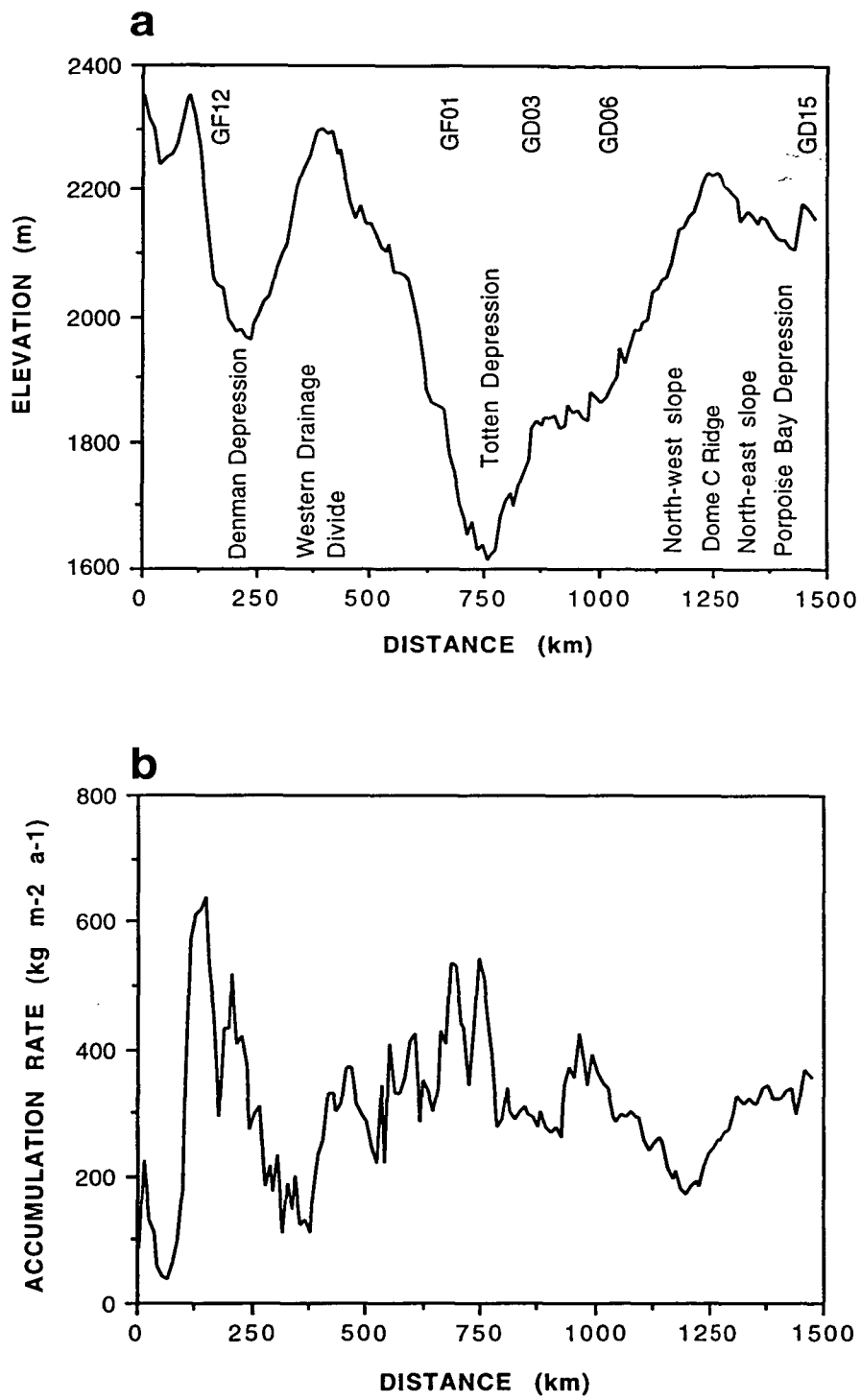

Figure 2.3 (a) The Wilkes Land elevation profile along the eastern and western Wilkes Land 2000 m contour traverse routes. The eastern and western traverse routes commence from the Totten Depression near the 750 km marker. The locations of the shallow firn cores discussed in Chapter 3 are also shown. (b) The spatial mean accumulation rate (H_2O equivalent) profile for eastern Wilkes Land (1982-85) and western Wilkes Land (1983-86), filtered using a 20 km running mean at 10 km intervals.

2010 m elevation on the north-west aspect slope of the Dome C ridge (Figure 2.3b). In western Wilkes Land the range varies from 50 kg m^{-2} a^{-1} at 2250 m elevation inland of Mirny to 735 kg m^{-2} a^{-1} at 2100 m elevation in the Denman Depression (Figure 2.3b). The accumulation rates reach 500-600 kg m^{-2} a^{-1} in the Totten Depression. The accumulation rates shown in Figure 2.3b were filtered using an overlapping 20 km running mean at 10 km intervals to minimise the variability in the rates due to mesoscale topographic roughness and surface microrelief. The combined variability ranged from 14-34% of the mean accumulation rate (calculated as the ratio of standard deviation/group mean ($s / \bar{x}$) for each 20 km cell). The accumulation rate distribution at ~2000 m elevation in eastern Wilkes Land reaches a minimum of 170 kg m^{-2} a^{-1} on the north-west aspect slope 50 km to the west of the Dome C Ridge. Similarly in western Wilkes Land the respective accumulation rate minima of 120 kg m^{-2} a^{-1} and 50 kg m^{-2} a^{-1} occur on north-west aspect slopes at 50 km west of the drainage divide and the western ridge of the Denman Depression. The peaks in the accumulation rate distribution also occur offset from the topographic features. The peak of 500 kg m^{-2} a^{-1} occurs 50-75 km to the west of the floor of the Totten Depression and the peak of 650 kg m^{-2} a^{-1} occurs 100 km to the west of the floor of the Denman Depression. The accumulation rate distribution generally displays higher rates on windward (north-east aspect) slopes than on leeward (north-west aspect) slopes for the same elevation range.

To investigate the aspect dependency of the accumulation distribution, linear regression was applied to the 20 km mean elevation data and the corresponding 20 km mean accumulation data for eastern Wilkes Land across the region where the route traverses the Dome C ridge (distance 1000-1400 km in Figure 2.3a, covering the elevation range 1870-2250 m). This region covers the gradual transition from the north-west aspect (leeward slope) to the north-east aspect (windward slope) across the north-south trending ridge. The sample size (n) for both aspect slopes is comparable 25 points (250 measurements) for the north-west slope and 16 points (160 measurements) for the north-east slope. The linear regression produced correlation co-efficients (r) of 0.93 and 0.94, for the north-west aspect and north-east aspect slopes, respectively and are significant at the 99.5% confidence level. The regression lines for the north-west slope and the north-east are as follows;

$A = -0.50\,E + 1268$ for the north-west slope between 1870 m and 2230 m;
$A = -1.03\,E + 2538$ for the north-east slope between 2119 m and 2230 m;
where A is accumulation rate in kg m^{-2} a^{-1} and E is elevation in m.

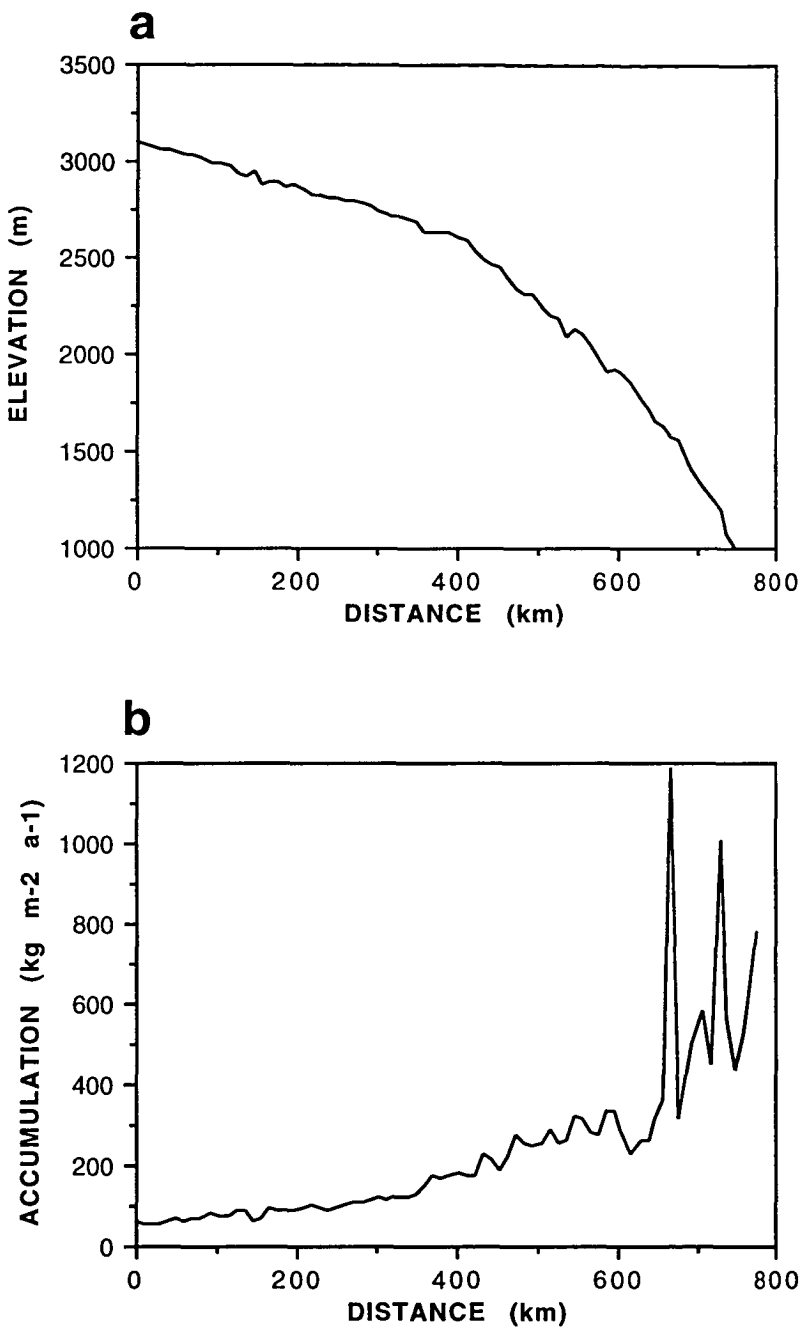

Figure 2.4 (a) The southern Wilkes Land surface elevation profile along the ANARE traverse route, from 100 km inland of the Dome C to Pionerskaya traverse route, north to the saddle between Law Dome and the East Antarctic ice sheet. The surface profile was determined from continuous barometric levelling controlled by geodetic positions from Doppler satellite measurements at 50 km intervals. (b) The spatial mean accumulation rate (H_2O equivalent) profile for southern Wilkes Land (1979-84) and western Wilkes Land (1983-86), filtered using a 20 km running mean at 10 km intervals.

The accumulation-elevation gradient is twice as steep on the north-east or windward slopes. This reflects the interaction between the topography and the snow redistribution processes with less erosion on the north-east slopes than on the north-west where the orientation of the fall-line is closer to the katabatic wind direction. The interaction between topography and snow redistribution processes is discussed in greater detail in section 2.6.

2.3.2.2 SOUTHERN WILKES LAND

The spatial accumulation rate pattern was measured along the 112°E longitude at 2 km intervals over a six year period between 1978-84 (Thwaites, 1987). These accumulation rates were also filtered using a 20 km running mean at 10 km intervals and are shown in Figure 2.4b. The rates decrease from ~600-800 kg m^{-2} a^{-1} with peaks up to 1200 kg m^{-2} a^{-1} at 700 m elevation in the Totten Depression to 50 kg m^{-2} a^{-1} at 3000 m elevation in the interior. There is considerable noise in the accumulation rate below 1800 m due to mesoscale topographic undulations where longitudinal snow dunefields occur (Goodwin and Fraser, 1987). The mean coefficient of variability for the 20 km cells changes from 26% for the elevation range 1800-2500 m, to 19% for the elevation range 2500-3000 m. The reduction in variability with elevation is due to the reduction in both the roughness of the mesoscale surface topography and in the strength of the surface windfield.

2.3.3 ACCUMULATION-ELEVATION RELATIONSHIPS

The accumulation rate distribution displays an overall negative correlation with elevation. Regression analyses of the Wilkes Land accumulation distribution determined that a third order polynomial relationship existed with elevation from 700-3000 m. The correlation coefficient r = 0.78. The accumulation-elevation bi-plot is shown in Figure 2.5 and the relationship is as follows;

$A = 943\ 45 - 0.273\ E - 4.933e^{-5}\ E^2 + 1.434e^{-8}\ E^3$,
where A is accumulation in kg m^{-2} a^{-1} and E is elevation in m.

This relationship indicates that the accumulation distribution is a combined function of ice sheet elevation and continentality, and possibly latitude or temperature, since the elevation contours are approximately parallel to the coast. The greater scatter or noise in the accumulation below 2000 m elevation is due to the interaction between the

greater relief of the ice sheet's topography together with a stronger and more complex katabatic windfield than at higher elevations on the interior plateau.

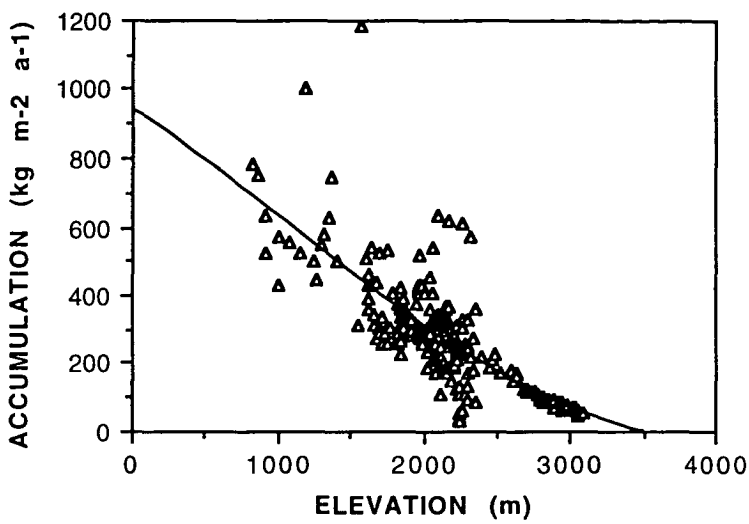

Figure 2.5 Relationship between accumulation rate and elevation in the Wilkes Land drainage basin.

2.3.4 WILKES LAND DRAINAGE BASIN ACCUMULATION DISTRIBUTION

Accumulation rate isopleths (contours) were determined using the above accumulation-elevation relationship for the area covered by the traverses together with the accumulation data reported in Young et al. (1982). They reported data averaged over 50 km intervals for the French traverse route from Dumont d'Urville to Dome C (Figure 2.1) and the Soviet traverse route from Mirny-Pionerskaya to Vostok and Pionerskaya-Dome C (Figure 2.1). The resulting map of the accumulation rate distribution for the entire Wilkes Land drainage basin and part of the Queen Mary and Terre Adélie drainage basins is shown in Figure 2.6.

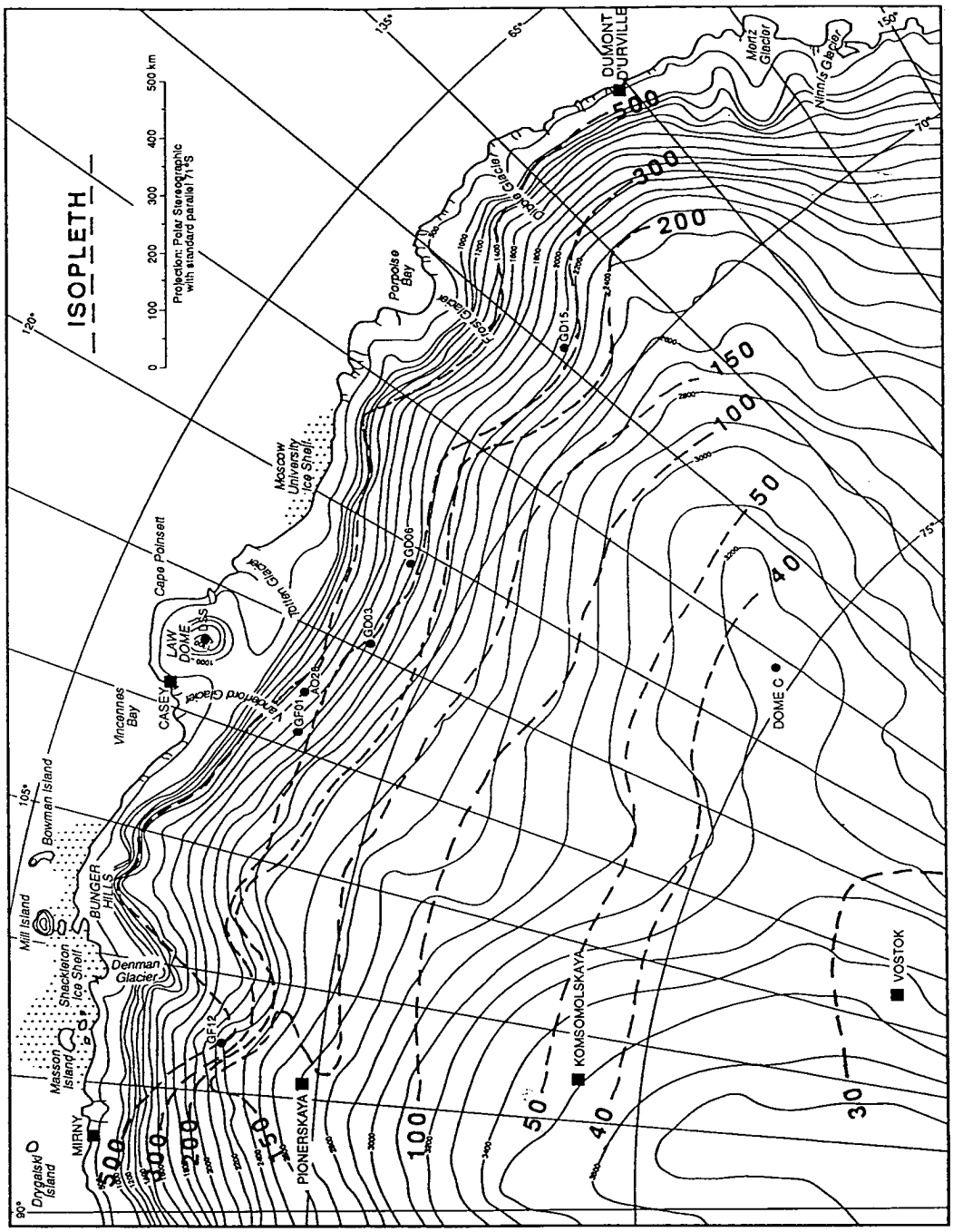

Figure 2.6 Distribution map of the mean accumulation rate in kg m^{-2} a^{-1} for the Wilkes Land basin draining to the Vanderford and Totten Glaciers and to Porpoise Bay. The Queen Mary Land basin draining to the Denman Glacier is also shown. The isopleths were constructed from the accumulation rate measurements along the ANARE eastern, western and southern Wilkes Land Routes, together with those given in Young et al. (1982) for the Soviet Mirny-Pionerskaya-Vostok route, the Soviet Mirny-Pionerskaya-Dome C route, and the French Dumont d'Urville route.

The map clearly shows the western displacement of the accumulation pattern relative to the broad topography. The accumulation pattern for the Law Dome, a separate ice cap to the north of the Totten Depression, is characterised by a large east to west gradient in accumulation rate Budd and Morgan (1977). The pattern on Law Dome results from higher precipitation on the eastern and north-eastern slopes due orographic processes and precipitation under strong east to south-east winds. This may also partly explain the higher accumulation observed on the north-east aspect slopes in the katabatic zone.

2.4 SNOW ACCUMULATION AND SURFACE TOPOGRAPHY IN THE LAMBERT GLACIER BASIN

2.4.1 REGIONAL SURFACE TOPOGRAPHY

Surface elevation profiles were measured by barometric levelling along the traverse routes in the Lambert Glacier Basin and controlled by GPS satellite surveying, at intervals of 30 km (Higham, 1994). The route approximately follows the 2500 m elevation contour and circumnavigates the basin from 150 km inland of Mawson Station at the 2000 m contour to inland of Law Base (Figure 2.2). The route descends from the 2500 m contour to the 1000 m contour near Law Base. The Lambert Glacier Basin forms a broad depression in the East Antarctic ice sheet which extends approximately 1000 km from the coast. The elevation profile of the route is shown in Figure 2.7a. The gradients of the slopes are approximately equivalent around the basin from east to west. The broadscale topography is undulating on a wavelength of approximately 400 km along the western side of the basin. On the eastern side of the basin the slopes are undulating with a shorter wavelength of approximately 150 km.

2.4.2 SNOW ACCUMULATION RATES

Accumulation rates were measured on bamboo canes at 2 km intervals along the route. The accumulation rates were measured along the entire route over a 10-11 month period between the austral summer 1993/1994 and the austral summer 1994/1995. The western half of the route was measured over a four year period from the austral summer 1990-1991 to the austral summer 1994/1995. A comparison of the one year accumulation measurements along the route with those from the four year period 1990-93 indicated that the one year period 1994 was not anomalous (Allison, pers. comm., 1995). The mean accumulation rate for the 1990-93 period was 66 kg m^{-2} a^{-1}

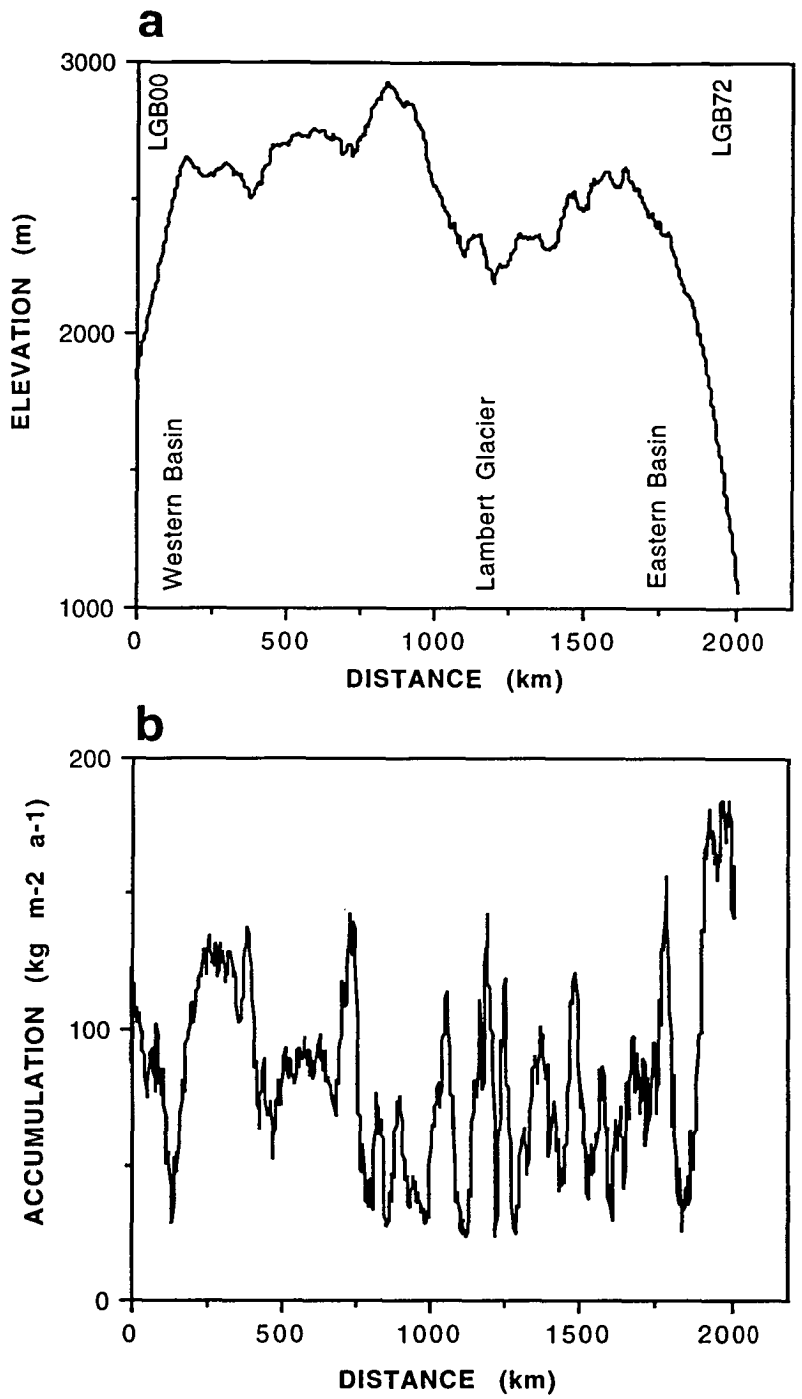

Figure 2.7 (a) The Lambert Glacier Basin surface elevation profile along the ANARE traverse route, from LGB00, ~100 km inland of Mawson to LGB72, ~30 km inland of Law Base, approximately along the 2,500 m elevation contour. The surface profile was determined from continuous barometric levelling controlled by geodetic positions from GPS satellite measurements at 30 km intervals. (b) The spatial mean accumulation rate (H_2O equivalent) profile for the Lambert Glacier Basin, filtered using a 30 km running mean (after Higham, 1994, and additional data on the eastern side of the basin from I. Allison, pers. comm. 1995).

whilst the mean accumulation rate for 1994 was 68 kg m^{-2} a^{-1}. However, the one year measurements along the eastern half of the route display high variability due to surface microrelief and local topographic roughness. The snow accumulation rates were converted to water equivalent mass using measured snow surface densities which were averaged over 30 km intervals (Higham, 1994, and Allison, pers. comm., 1995) The accumulation rate profile was filtered using a 30 km running mean to minimise the noise due to the surface microrelief and local topographic roughness. The resulting accumulation rate profile is shown in Figure 2.7b.

The accumulation rates generally fluctuate widely from 50 kg m^{-2} a^{-1} to 100-125 kg m^{-2} a^{-1}. The accumulation rate distribution displays a very high level of spatial variability calculated as 20% to 150% (the ratio of standard deviation/group mean ($s / \bar{x}$ for each 30 km cell). The significantly larger spatial variability than in Wilkes Land is due to the very low accumulation rates. There appears to be a stronger relationship between the accumulation rate distribution and the mesoscale (100-500 km) topography rather than with elevation. Accumulation rates along the western side of the basin between 200-700 km distance from LGB00, range from 85 to 130 kg m^{-2} a^{-1} where the elevation is between 2600-2800 m. In comparison, the accumulation rates along the eastern side of the basin between 1250 to 1750 km distance from LGB00, generally range from 50 to 85 kg m^{-2} a^{-1} where the corresponding elevation is between 2250-2500 m. Thus higher accumulation rates occur along the western side of the basin than along the eastern side of the basin. To investigate this pattern further a regression analysis of the accumulation rates on the two sides of the basin was conducted for the elevation range 1000-2500 m. The accumulation rates for sites with elevations between 2500-3000 m were located towards the inland edge of the basin and were spatially too variable for inclusion in the analysis. A biplot of accumulation versus elevation is shown in Figure 2.8. The accumulation rates on the western side of the basin display a linear relationship with elevation (albeit from a limited elevation range), but the eastern side accumulation rates significantly depart from such a relationship. The fluctuation is probably due to the snow redistribution processes and their interaction with the Lambert Basin and its mesoscale and local topography. This is discussed further in section 2.6.

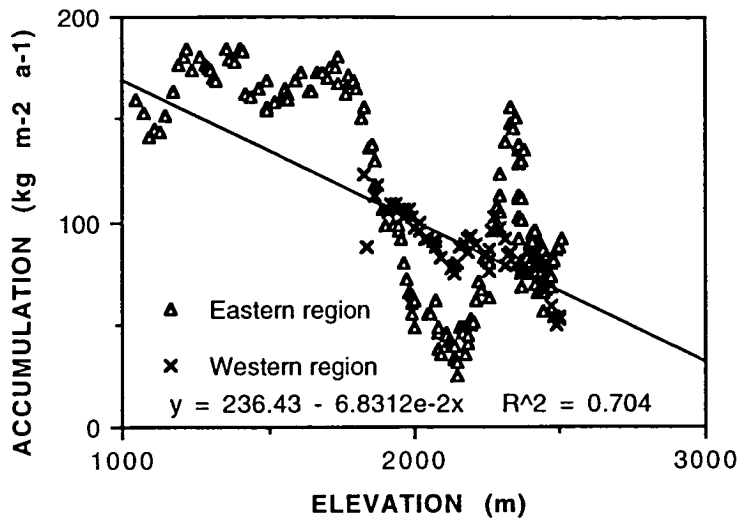

Figure 2.8 Relationship between accumulation rate and elevation in the eastern and western regions of the Lambert Glacier Basin.

2.4.3 LAMBERT GLACIER BASIN ACCUMULATION DISTRIBUTION

Accumulation rate isopleths were determined for the basin using the accumulation and topography profiles in Figure 2.7, together with the accumulation-elevation relationship. Isopleths were also compiled from those published by Allison (1979) for the basin and those published by Budd et al. (1982) for the Amery Ice Shelf. The isopleths were determined using both the 30 km mean distribution together with an accumulation distribution averaged over 200 km to smooth out some of the large fluctuations due to the local the mesoscale topography. The resulting broadscale accumulation map is shown in Figure 2.9. The distribution displays a general asymmetry with the topography. The 100 kg m^{-2} a^{-1} isopleth is located approximately along the 2700 m elevation contour in the west of the basin whilst it is located along the 1900-2000 m elevation contour in the east of the basin. This asymmetry also exists for the 50 and 75 kg m^{-2} a^{-1} isopleths. The asymmetry is discussed with respect to the surface katabatic windfield in section 2.6.

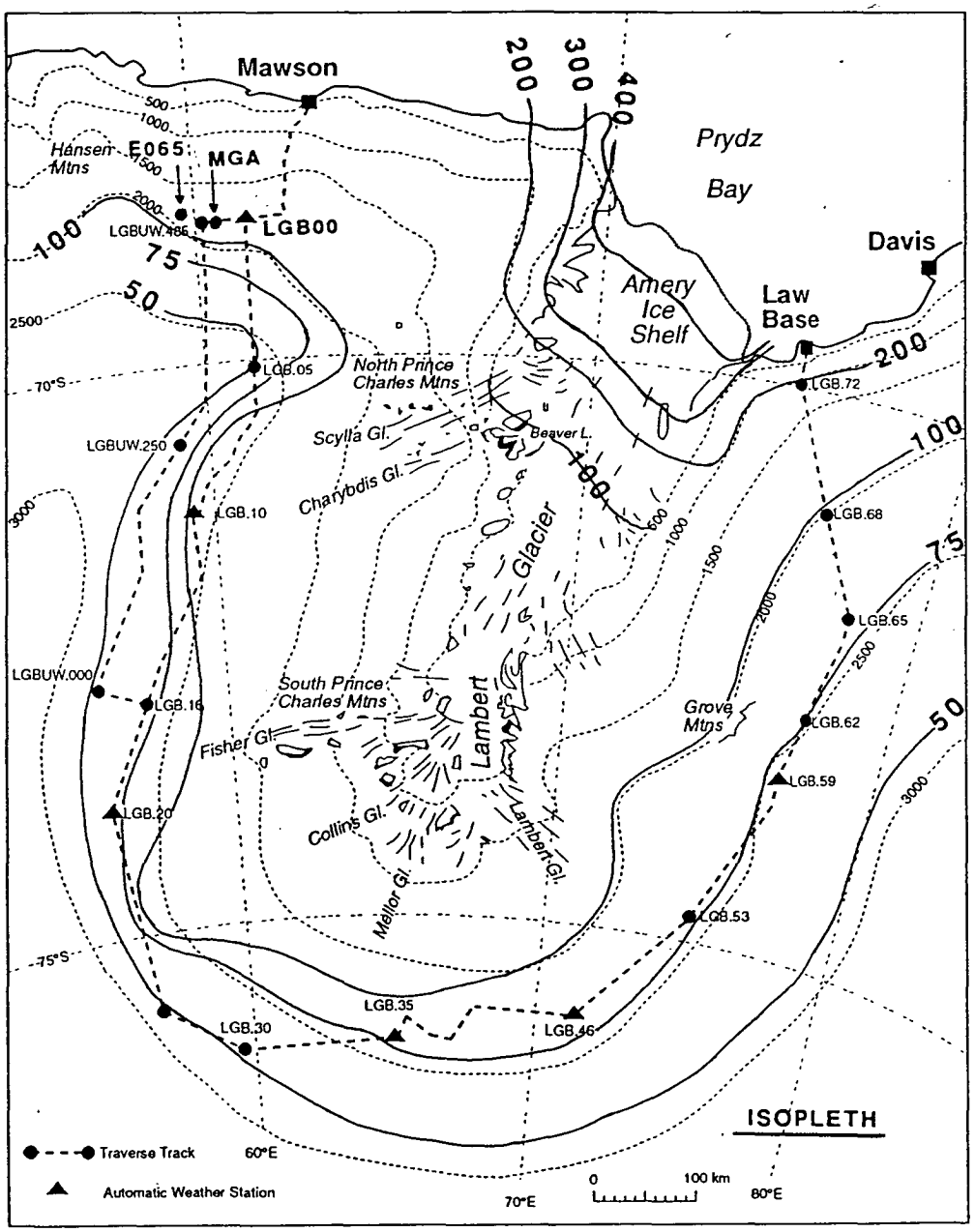

Figure 2.9 Distribution map of the mean accumulation rate in kg m^{-2} a^{-1} for the Lambert Glacier Basin. The isopleths were constructed from the accumulation rate measurements along the ANARE traverse routes reported in Higham, 1994, Allison, 1979, and Budd et al., 1982.

2.5 SNOW REDISTRIBUTION PROCESSES: A CASE STUDY OF SURFACE MICRORELIEF IN EASTERN WILKES LAND

The accumulation rate patterns in both Wilkes Land and the Lambert Basin display a significant aspect dependency and a westerly offset with higher accumulation on the windward slopes and lower accumulation on the leeward slopes. To investigate snow redistribution processes a regional study of the surface microrelief was conducted in eastern Wilkes Land over a 200 day period in 1985. The data collected during the study are published in Goodwin (1988a) and in Goodwin (1990).

The morphology and formation of snow surface microrelief in Antarctica have been well documented by numerous workers, in particular Kotlyakov (1966); Doumani (1967); Fujiwara and Endo (1971); and Watanabe (1978). These studies have classified surface microrelief into 3 types which reflect their unique mode of formation. These are; (i) stationary depositional features formed during precipitation (Figure 2.10a), (ii) erosional features formed from the long-term exposure to the katabatic winds during hiatus in precipitation (Figure 2.10b) and (iii) mobile depositional or redistribution features formed from wind transported friable snow (Figure 2.10c) .

The spatial distribution of surface microrelief type, size and orientation was determined along the eastern Wilkes Land route in the austral spring (September to December) 1985 in conjunction with spatial snow accumulation measurements. The spring season provided the best opportunity to investigate microrelief development and distribution since the observed microrelief features have formed during winter when the majority of precipitation occurs in the region (Jones 1983) and the strongest katabatic surface winds occur (Allison, Wendler and Radok, 1993). Type, size and orientation measurements were made over 500 m x 500 m quadrats at 8 km intervals along the route.

Type and size observations

The microrelief features observed in each quadrat were classified into one of the 3 type classes using a two tiered classification system (shown in Table 2.2), described by Fujiwara and Endo (1971) and applied on Japanese Antarctic Research Expeditions (JARE) traverses inland of Syowa on the Mizuho Plateau region of Queen Maud Land. The mean height of the microrelief features in each class was also recorded for each quadrat in 0.15 m size classes. The resulting spatial distribution of surface microrelief type and size for the austral spring, 1985 is shown in Figure 2.11 and represents the mean development of microrelief features from the winter precipitation

a

b

Figure 2.10 (a) Depositional surface type, showing a longitudinal dune, movement is from left to right. The marker is 1 m long and is graduated in 0.1 m intervals. (b) Erosional surface type, dominated by strong glazing accompanied by etched pits, grooves and transverse ridges. The view is downwind. A longitudinal dune of friable drift snow (0.1 m high) lies to the left.

c

Figure 2.10 (c) Redistribution surface type, showing lanceolate sastrugi developed in wind crusted and laminated snow, surrounded by low friable dunes. The view is upwind and the lanceolate sastrugi are 0.3-0.5 m in height.

at each sample location.

TABLE 2.2 MICRORELIEF TYPE CLASSES

eg	erosion surface - wind glazed and crusted, with pits and transverse ridges,
ef	erosion surface - fine split sastrugi
eb	erosion surface - mature broad sastrugi
ep	erosion surface - wind crusted, with pits and transverse ridges
el	erosion surface - lanceolate sastrugi
rb	redistribution surface - drift snow forming banks, dunes and juvenile lanceolate sastrugi
dd	deposition surface - dunes
db	deposition surface - fields, spots and strips

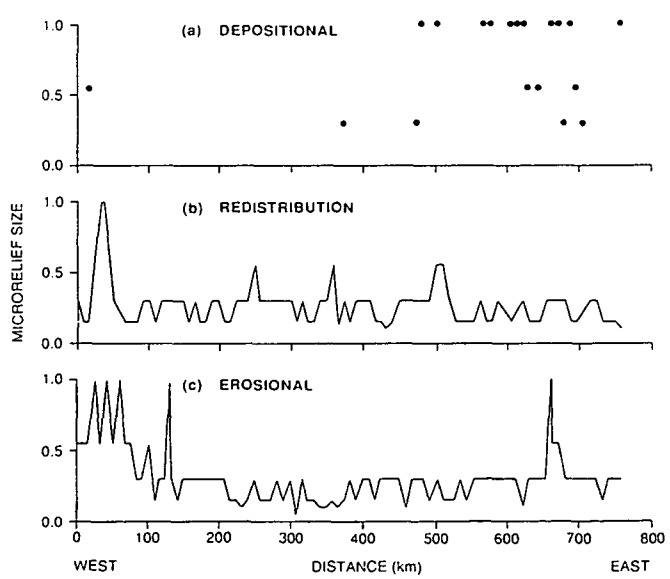

Figure 2.11 Snow surface microrelief, mean size distributions observed along the eastern Wilkes Land route for (a) depositional, (b) redistribution and (c) erosional features. The mean distribution is calculated from the observed median of each of the size classes listed in the text.

The depositional type distribution shown in Figure 2.11(a) defines the occurrence of stationary longitudinal dunes with a mean height of 1 m along the route. These dunes occur only on the north-east or windward slopes especially between 1250-1400 km and corresponding to the region above 2000 m. Kotlyakov (1966) described these dunes as forms which arise during precipitation under strong drifting snows. They are aligned in an easterly direction (105°-110° True) parallel to the prevailing cyclonic wind direction and at a 20°-40° angle to the prevailing katabatic wind direction. Longitudinal dunes were observed to form at GD15 (69°00'S, 130°49'E) during a major precipitation event which accompanied strong synoptic easterly winds in November 1985. These longitudinal dunes were typically 50-100 m long, 10-15 m wide and 1 m high.

In contrast, the redistribution type features, comprising mobile friable snow banks, longitudinal dunes and barchan dunes were observed continually throughout the study area as shown in Figure 2.11(b) with an average height of 0.3 m. These redistribution/depositional features are kept in motion by the constant katabatic winds which transport friable snow grains by saltation and in suspension. The friable snow banks/dunes are typically 20-50 m long, 2-3 m wide and 0.3-0.5 m high. They are oriented parallel to the dominant katabatic surface wind direction. Large barchan dunes were observed in isolation near GD01 (68°35'S, 113°20'E) up to 2 m high. These redistribution features were mainly observed moving on a well developed, multi-layered wind glazed erosion surface (classified as 'eg' in Table 2.1).

This wind-glazed erosion surface was one of two common erosional features observed along the route and was spatially continuous. This surface was characteristically a strongly polished wind glaze and etched/pitted surface. The strongest development of this wind glaze occurs on the north-west (leeward) slope between 1000 -1250 km. The second common erosional type is the sastrugi which have a myriad of forms dependent upon the shape and size of the parent snow dunes from which they are sculptured by the katabatic wind. They are aligned in the direction of the surface katabatic wind. Sastrugi were observed up to 2 m high on the north-east aspect slope (0-150 km) below 1800 m elevation but are generally 0.3 m in mean height as shown in Figure 2.11(c). The majority of sastrugi were observed in clusters and were developed from the erosion of friable snow banks/dunes and averaged 0.3 m in height. These friable dunes are one third the average size of the longitudinal dunes observed only on the north-east aspect slope. Sastrugi were also observed to form on the upwind apex of the longitudinal dunes and linearly along the windward exposure of the dune. These longitudinal dunes are characteristically eroded diagonally by the katabatic wind since their orientation is 20°-40° to the east of the katabatic wind.

Consequently, the depositional longitudinal dunes clearly have a morphology which is distinct from that of the redistribution friable dunes and can be consistently classified as such.

Whilst the redistribution and erosional features are spatially continuous throughout the study area, depositional microrelief only occurs on the north-east or windward slopes in conjunction with the regions of relatively high accumulation . This indicates that these regions experience relatively weaker katabatic winds and less erosion of the original precipitation occurs. It also suggests that the original precipitation rates may be higher on east and north-east aspect slopes which is best characterised by the spatial accumulation pattern on Law Dome. The spatial continuity of redistribution and erosion features indicates that the broadscale snow surface erosion and redistribution processes occur throughout the study area, above 1800 m elevation.

Orientation

The spatial continuity of the wind glazed erosion surface 'eg' provided a reliable source from which to infer the regional, surface katabatic wind direction since the micro features; pits/grooves embedded in the surface were aligned in the dominant katabatic wind direction. At the same sites as the microrelief type and size measurements (8 km spacing) the orientation of the sharp, well defined pits and grooves were measured by magnetic compass and transferred to true bearing by solar compass observations. These orientations for eastern Wilkes Land are shown in Figure 2.12a and show consistent relative alignment (ESE-SSE) at a local scale and are co-incident with the prevailing wind directions observed during the field work. Similarly, sastrugi orientations representing the dominant katabatic wind direction were also determined in western Wilkes Land and are shown in Figure 2.12b. These sastrugi orientations were found to be in good agreement with the modelled broadscale winter wind directions of Parish and Bromwich (1987) and Parish (1988) (Figure 2.13) and the mesoscale model of van Meurs (unpublished Meteorology Department Report, University of Melbourne, 1987). However, the field inferred directions show the surface wind pattern in much greater detail and reveal areas of local divergence and convergence as a result of the mesoscale topography.

2.6 KATABATIC SURFACE WIND PATTERN AND SNOW REDISTRIBUTION

Both the modelled streamlines and the inferred wind directions clearly define broadscale divergence of the windfield across the divides and crests on the upper

a

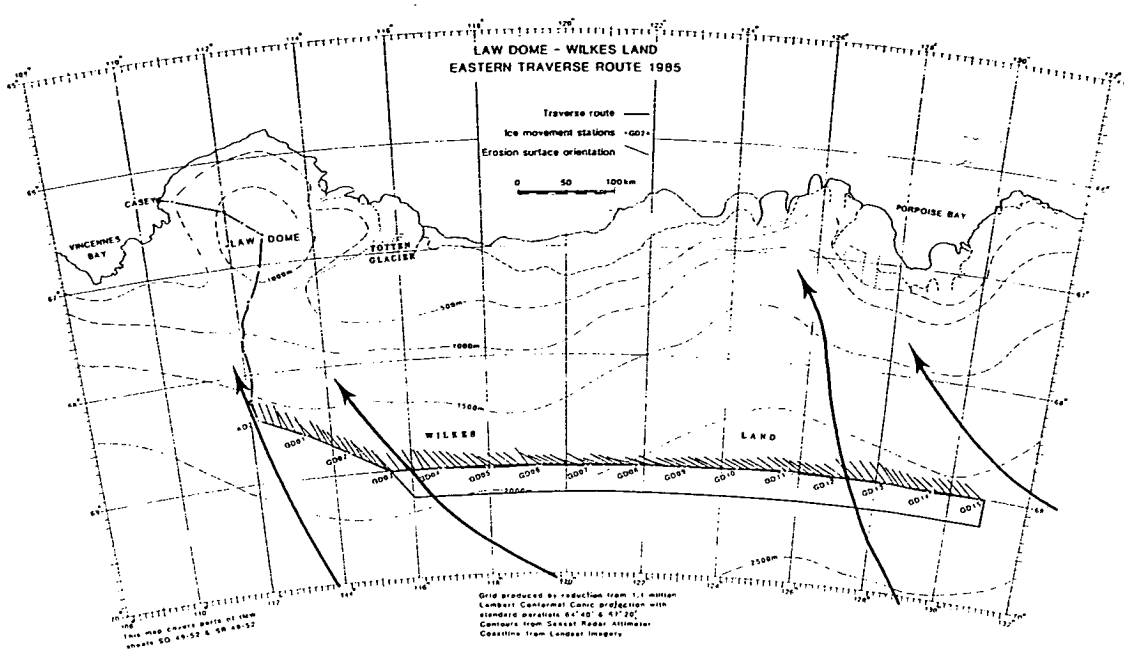

b

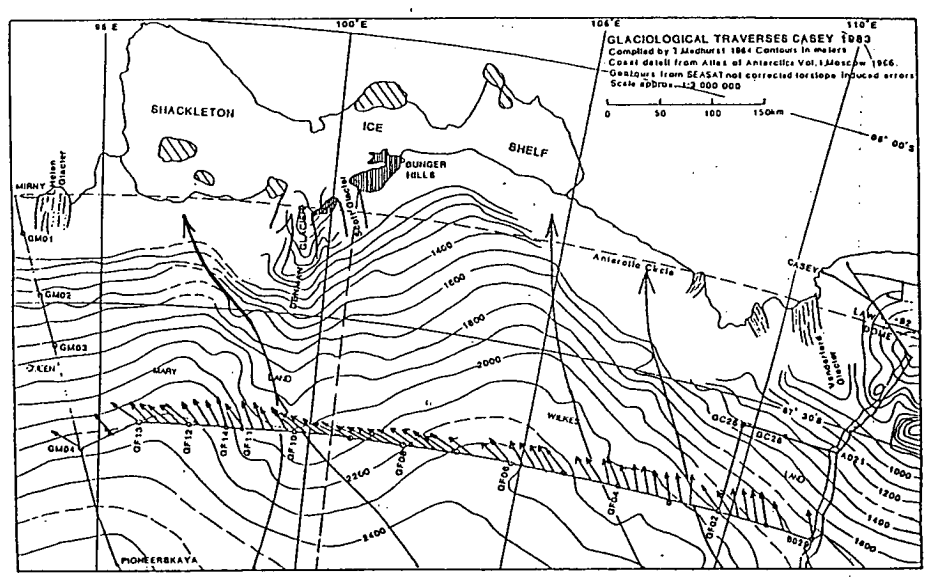

Figure 2.12 (a) Sastrugi orientations representing the dominant katabatic wind direction in eastern Wilkes Land. (b) Sastrugi orientations representing the dominant katabatic wind direction in western Wilkes Land (measurements from Hazelton, 1987). The bold arrows delineate modelled regional wind directions from Parish and Bromwich (1987).

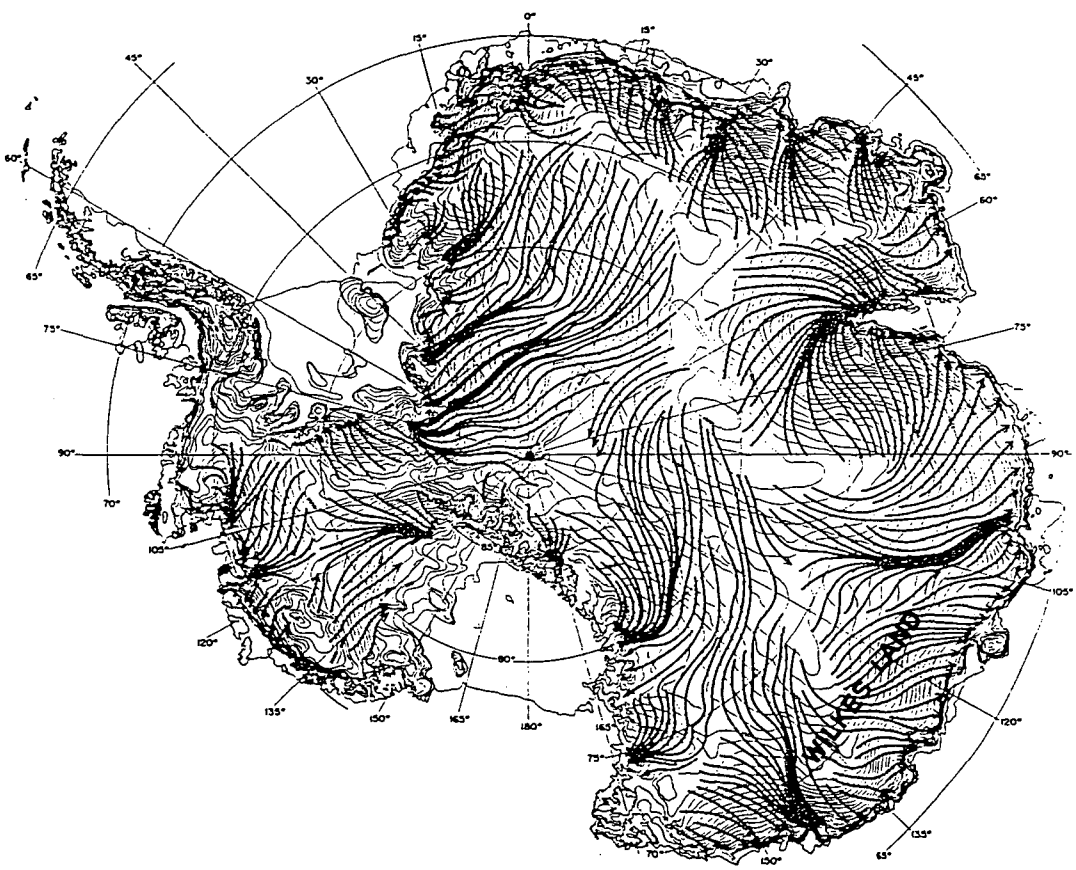

Figure 2.13 Time-averaged near-surface winter streamlines of katabatic drainage over Antarctica (after Parish and Bromwich, 1987).

north-east aspect slopes and the broadscale convergence in the Totten and Denman depressions and on the north-west aspect slopes in Wilkes Land. The broad regions of katabatic wind convergence correspond to the regions where the observed wind glazed erosion surface 'eg' was at its peak development. The modelled katabatic wind flowlines of Parish and Bromwich (1987) show that wind is funnelled into the Denman Depression from as far south as latitude 75°S. The windfield on the north-west aspect slopes has a greater deflection of the wind direction from fall-line direction of ~50° compared to ~40° on the north-east aspect slopes and indicates a relatively stronger katabatic wind flow on these slopes.(Ball, 1960). Accordingly, these slopes experience relatively higher rates of snow erosion. In contrast, the north-east slopes experience lower rates of snow erosion and hence their accumulation rates are closer to the precipitation rates at these sites. This relationship is supported by the occurrence of the depositional microrelief on the north-east aspect slopes only. The largest gradient in snow accumulation on the opposing aspect slopes occurs in the Denman Depression. Accumulation rates are between 100-200 kg m^{-2} a^{-1} on the north-west aspect slope and reach up to 650 kg m^{-2} a^{-1} on the north east aspect slopes. Near the 2000 m elevation, the strongly funnelled windflow traverses the trough and crosses the lower to middle north-east aspect slopes.(Figure 2.13). Strong convergence together with a reduction in topographic gradient occurs in this region. It is probable that this results in a slight reduction in windspeed coupled with an increase in snow deposition. The slight decreases in the wind velocity could result in substantial deposition of snow as the snow drift transport capacity decreases (Bagnold, 1941, Budd, Dingle and Radok, 1966, Radok, 1968). Radok(1968) calculated from observed snow drift data that a 1 m sec^{-1} reduction in mean wind velocity corresponds to a 150 g m^{-1} sec^{-1} or 38% reduction in snow transport. Thus the convergence of the katabatic windfield coupled with an increase in redistributed snow deposition may explain the abnormally high accumulation rates on the north-east aspect slope of the Denman Depression.

The surface katabatic windfield in the Lambert Glacier Basin was modelled by Parish and Bromwich (1987) and is shown in Figure 2.13. The major feature in the windfield is the strong funnelling of the flow into the Lambert Glacier trough from the south-east. There is a stronger convergence of the flow on the western side of the basin where the wind direction is west to south-west and is close to the fall-line (as predicted by Ball, 1960). The surface windfield is a near parallel easterly between latitudes 70°-75°S on the eastern side of the basin inland of Law Base. Similar to the Denman Depression, the stronger convergent katabatic flow on the western side of the basin is most likely transporting a higher volume of snow to these slopes. This covergent flow may partly explain the relatively higher accumulation rate pattern on the

western side of the basin than on the eastern side. In the region between LGB00 and LGB05 on the western side of the basin (Figure 2.9) the windfield changes from convergent to divergent. This change in the windfield corresponds to a reduction in snow accumulation rates which is described by the shift in the 100 kg m^{-2} a^{-1} from the 2500 m elevation contour to the 2000 m contour. This shift transforms the distribution to be equivalent to that at 2000 m elevation on the eastern side of the basin. The adjacent Kemp Land coastal slopes to the west of LGB00 also experiences a weak divergent windflow together with a short fetch. This windflow is coupled to the lowest coastal accumulation rates in East Antarctica (Giovinetto et al., 1990). Whilst the katabatic windfields are an important determinant of the accumulation pattern through their effect on snow erosion and deposition, and surface evaporation, the synoptic windfields are also important in determining the precipitation pattern.

2.7 OVERVIEW OF THE REGIONAL SURFACE MASS BALANCE PATTERN

Giovinetto et al. (1990) calculated first order linear relationships for Antarctic surface mass balance and temperature, elevation and distance to open ocean designated as 50% sea ice cover. These diagnostic relationships characterised the physical and climatological variables controlling the regional accumulation distribution together with the atmospheric circulation. These relationships show that despite modification of the precipitation by the surface katabatic windfield a strong relationship between the net accumulation distribution and elevation and continentality remains. Similarly, the above discussion has shown that the regional accumulation rate distribution is strongly related to ice sheet elevation, topographic aspect and the surface katabatic windfield in Wilkes Land, Queen Mary Land and the Lambert Glacier basin.

Bromwich (1988, 1990) and Budd et al. (1994) have modelled the atmospheric moisture fluxes over the Antarctic. Bromwich (1988) proposed that quasi-stationary cyclones form around the coast of Antarctica (after Jenne et al., 1974) which direct poleward moving meridional moisture transport with the largest amount lying to the east of the vortex centre. He stated that on the average this is consistent with the view that most cyclonic precipitation occurs in poleward moving moist air masses east of the vortex centre. Bromwich (1990) established good agreement between calculated moisture flux and accumulation rates over the interior of the ice sheet south of 80° S. Budd et al. (1994) derived net air mass and moisture fluxes over the Antarctic using global atmospheric analyses. Their pattern of net moisture flux divergence broadly fits the accumulation rate distribution for Antarctica which was compiled by Giovinetto and Bull (1987). The discrepancies between the two patterns can be largely explained

by the snow drift erosion and transport patterns determined by the interaction between the topography and the surface katabatic windfield. However, the net moisture flux divergence pattern is anomalously high with respect to the accumulation rate distribution in the Lambert Glacier Basin.

Both the spatial accumulation rate distribution and the net moisture flux divergence pattern show that Wilkes Land receives the highest precipitation and net accumulation of the coastal slope zones in East Antarctica. Kemp Land and Dronning Maud Land receive the lowest. For regional comparison purposes, the accumulation-elevation relationships for Wilkes Land and the Lambert Glacier Basin are shown in Figure 2.14. There is a large difference in the accumulation rate distributions on the coastal slopes below 2,500 m elevation. The distributions are equivalent in the interior above 3,000 m elevation. At 2,000 m elevation the distribution in Wilkes Land is twice that in the Lambert Basin and at 1,000 m elevation it is three times greater. Bromwich (1988) showed from his atmospheric moisture flux modelling that moisture transport in the western Lambert Basin is anomalously low because net air movement is northward, rather than poleward as for the remainder of East Antarctica. Thus atmospheric moisture transport together with ice sheet elevation are the primary determinants of precipitation rates on the ice sheets. These precipitation rates are modified by the surface snow redistribution processes and surface evaporation to form the net accumulation rate distribution. The surface snow redistribution of precipitation is greatest in areas where the surface katabatic windfield is strongly convergent and the slopes are steepest, such as on the north-west aspect slopes in Wilkes Land and MacRobertson Land, and in the Totten, Denman and Lambert Glacier depressions. The original precipitation is only weakly modified by the surface windfield on the ridge crests and on the upper north-east aspect slopes in Wilkes Land. The effect of the surface windfield in modifying the precipitation becomes significantly less above 3000 m on the interior plateau where the accumulation pattern is strongly related to elevation and the precipitation pattern.

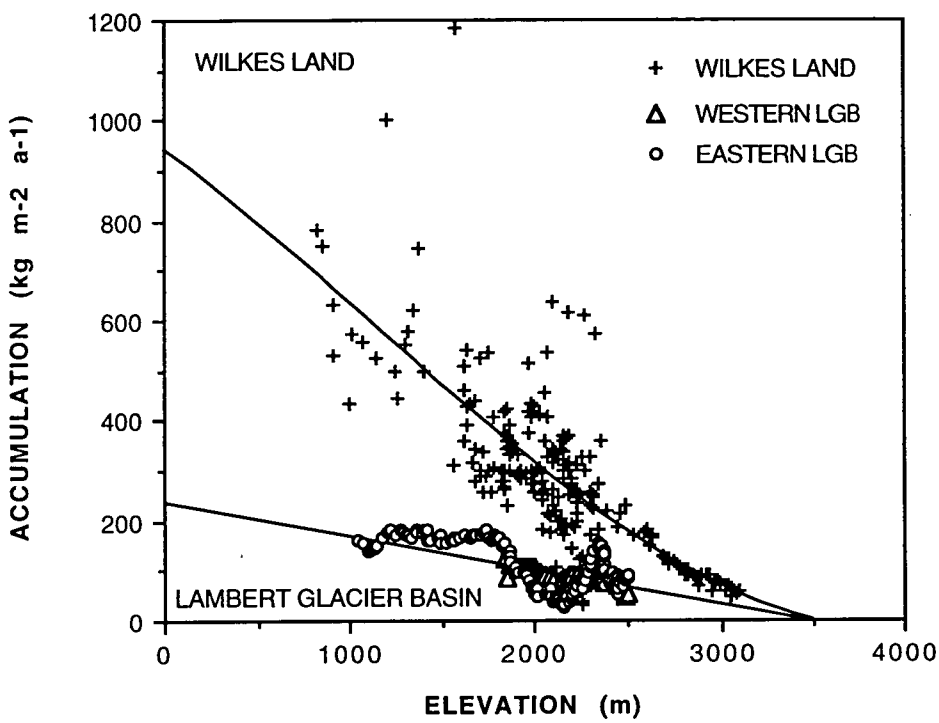

WILKES LAND Acc = 943.45 - 0.27286Elev - 4.9330e-5Elev^2 + 1.4344e-8Elev^3
R^2 = 0.601

LAMBERT GLACIER BASIN Acc = 236.43 - 6.8312e-2Elev R^2 = 0.704

Figure 2.14 Comparison of accumulation - elevation relationships for Wilkes Land and the Lambert Glacier Basin.

CHAPTER 3
TEMPORAL VARIATION OF SURFACE MASS BALANCE AND OXYGEN ISOTOPES IN EAST ANTARCTICA

3.1 INTRODUCTION

Temporal changes in surface mass balance and the oxygen isotope values ($\delta^{18}O$) of snow result from a combination of interdependent and coupled factors, such as mean air and ocean temperature fluctuations, sea ice extent and concentration changes, and general atmospheric circulation changes (Budd and Simmonds, 1991). These combined factors influence the surface mass balance by modifying:

- the available moisture transport capacity;
- the frequency, seasonality, intensity and tracks of cyclones;
- the frequency and seasonality of precipitation events;
- the intensity of the surface katabatic windfield and snow redistribution; and
- the gross ablation rate from evaporation, sublimation and melting (Giovinetto et al., 1990).

It is important to define the relationships between accumulation rate and oxygen isotope patterns with the above climatological parameters before a detailed understanding of the present mass balance of Antarctica can be developed. Similarly, these relationships are required before an understanding of Holocene mass balance fluctuations can be determined in conjunction with the interpreted Holocene climatic history.

This chapter reports the results of a regional study on the temporal variation of accumulation rate and annual oxygen isotope values. The aim of the study was to define the nature of the variations and to investigate the contribution of the above climatological parameters to the variations observed around East Antarctica. Temporal accumulation rate and oxygen isotope time-series for the period 1930-85 were determined from a number of shallow firn core stratigraphic studies.

Shallow (30 - 40 m) firn core drilling was carried out by ANARE glaciological expeditions in 1985 (Goodwin, 1988b) and 1986 (Hazelton, 1987) at sites along the 2000 m contour in Wilkes Land and Queen Mary Land, covering the katabatic zone from inland of Dumont d'Urville to inland of Mirny (Figure 2.1). Four firn core sites

were located in Wilkes Land at GD03 (69° 00'S, 115° 30'E, 1835 m), GD06 (69° 00'S, 119° 17'E, 1884 m) and GD15 (69° 00'S,130° 48'E, 2155 m), and along the western drainage divide of the Denman Glacier in Queen Mary Land at GF12 (68° 29'S, 97° 11'E, 2322 m) (Figure 2.1). In addition, a total of fifteen 10 m deep cores were drilled from GD01 to GD15 at 50 km intervals along the eastern Wilkes Land route to enable the spatial comparison of inter-annual variability.

In Kemp Land three shallow firn cores were drilled within 50 km of each other approximately along the 68°39' S latitude at sites designated LGB00 (68°39'S, 61°07'E, 1832 m), MGA (68°39'S, 60°15'E, 1850 m) and E065 (68°37'S, 59°42'E, 1870 m) (Figure 2.2). The sites were selected because they represented the highest known accumulation rates (without depth hoar in the firn) in the 1800-2000 m elevation range in eastern Kemp Land (Morgan and Jacka, 1979) accessible to the ANARE Lambert Glacier Basin Traverse. Suitable sites for the evaluation of accumulation time-series were difficult to locate in Kemp Land due to the relatively low coastal accumulation rates and the extreme spatial variability of snow accumulation. This can best be illustrated along latitude 68°39'S, at an elevation of 1850 m, where sites of extensive depth hoar with very low accumulation rates (less than 20 kg m^{-2} a^{-1} from the 1975-78 cane measurements) exist within 10 km of MGA. MGA has an average accumulation rate of 270 kg m^{-2} a^{-1} (3-year epoch 1975-78) (Goodwin et al., 1994).

Similar studies were also conducted on the Amery Ice Shelf at elevations close to sea level. The regional accumulation and oxygen isotope time-series over the last 30-50 years are compared to contemporaneous changes in sea ice extent and air temperature to determine the regional forcings of the accumulation fluctuations. The temporal changes in accumulation are discussed with respect to the regional spatial accumulation patterns identified in Chapter 2. The recent relationships between accumulation rate and oxygen isotope, and climatological parameters, are applied in Chapter 7 to the determination of the palaeo accumulation pattern during the Holocene. The results are also applied in Chapter 8 to the determination of the present mass balance of Antarctica and the contribution to sea-level.

3.2 BACKGROUND ON THE OXYGEN ISOTOPE COMPOSITION OF ANTARCTIC SNOW AND FIRN

The oxygen isotope $\delta^{18}O$ composition of snow and ice has been widely applied in stratigraphic studies since a statistical linear empirical relationship exists between mean

annual $\delta^{18}O$ and mean annual air temperature at a site (Dansgaard, 1964). The oxygen isotope ratio used for stratigraphic studies is the ratio between the heavier $H_2{}^{18}O$ molecule with the lighter $H_2{}^{16}O$ molecule. The relationship between the isotopic ratio $\delta^{18}O$ and temperature occurs because the heavier $H_2{}^{18}O$ molecules of water evaporate less rapidly than the lighter $H_2{}^{16}O$ molecules and that the heavier molecules condense more rapidly (Robin, 1983).

There are a number of factors which influence the $\delta^{18}O$ in snow. Firstly, the distance to the moisture source is important in Antarctica, since water vapour evaporated from the Southern Ocean to the north of the sea ice edge is less depleted (less negative) due to the warmer ocean water than water vapour evaporated from open water within the sea ice and closer to Antarctica (Bromwich and Weaver, 1983). The distance also affects the rate processes of evaporation and condensation during the transport of the water vapour inland over the ice sheet (Jouzel and Merlivat, 1984). As the water vapour is transported over the ice sheet it becomes progressively fractionated and more depleted in $H_2{}^{16}O$ molecules from the condensation of the water vapour. However, Lorius and Merlivat (1977) found that the water vapour is not affected by significant depletion in $\delta^{18}O$ for the first 1000 m of elevation rise over the ice sheet. This is principally determined by the height of the cloud base over the coastal margins. Above 1000 m the cloud cover generally follows the ice sheet surface whose surface temperature generally follows an adiabatic relationship with elevation. Hence snow precipitated onto the ice sheet surface from either the orographic lifting of moist air, radiative cooling or clear sky mechanisms (Bromwich, 1988) contains the $\delta^{18}O$ composition established by the air temperature at the time of the condensation. The large seasonal fluctuations in air temperature between summer to winter together with the large fluctuations in the seasonal sea ice cover results in a seasonal fluctuation in the $\delta^{18}O$ of snow equivalent to ~7-8‰. It is this seasonal fluctuation in $\delta^{18}O$ which makes it an ideal stratigraphic index. However, snow redistribution processes can significantly alter this seasonal signal in $\delta^{18}O$ by mixing surface snow and through some surface evaporation and hence fractionation. These processes are significant in areas with very low accumulation such as in the interior of the continent.

A strong relationship between $\delta^{18}O$ and surface air temperature exists for Antarctica. Robin (1983) and Morgan (1982) reported the variation in the oxygen isotope-temperature relationship between regions of Antarctica. He also showed that this relationship varied according to spatial or temporal (single site) determinations. Thus each of the observed changes in the mean oxygen isotope composition from firn cores need to be transferred to temperature changes according to the relevant regional

transfer relationship. Thwaites (1987) established a regional transfer relationship of 0.79‰/°C for Wilkes Land while Lorius and Merlivat (1977) determined a relationship 0.74‰/°C for the Terre Adélie coast to Dome C. Higham (1994) established a transfer relationship of 0.80‰/°C for MacRobertson and Kemp Lands. Isaksson and Karlen (1994a, 1994b) established a transfer relationship of 1.16‰/°C for Dronning Maud Land and Peel (1988) reported a transfer relationship of 0.66‰/°C for the Antarctic Peninsula.

3.3 DEVELOPMENT OF A FIRN STRATIGRAPHIC MODEL AND STRATIGRAPHIC METHODS FOR THE KATABATIC ZONE

3.3.1 SEASONAL DEVELOPMENT OF THE SURFACE SNOW LAYER

A cane farm comprising 100 bamboo canes was established at GD03 in eastern Wilkes Land (Figure 2.1) to define snow surface variability, the characteristics of the seasonal snow layer and the regional firn stratigraphic model for the coastal katabatic zone of East Antarctica. Two arms of 50 canes spaced at 1 m intervals were set up to intersect at right angles with one arm parallel to the prevailing katabatic surface wind direction. Surface microrelief type, size and orientation measurements, together with surface density and hardness measurements were also made. The snow surface topographic profile and the net snow accumulation at each cane were determined by optical levelling and cane measurements during autumn, spring and summer, 1985. In order to extend the measured record to cover 2 years of accumulation, a total of 21 x 2 m deep snow cores were drilled at 5 m intervals along each of the arms. These cores were measured in detail for visible stratigraphy, density and seasonal oxygen isotope $\delta^{18}O$ values. The autumn and spring 1984 surfaces together with the summer 1983/1984 surface were interpreted from the ice cores.

Three distinct, seasonal snow surfaces were observed to form in autumn, spring and summer. The characteristics of each of these surfaces are found in Table 3.1. The autumn wind - glazed ice crust forms over a wind crust during a major hiatus in snow supply and consequently, marks the end of the balance year. Jones (1983) attributed these ice crusts to surface melting which resulted from kinetic energy of snow drift under strong katabatic wind flow. Beneath the wind crust is a layer of depth hoar which forms in snow deposited as surface hoar or from light snow falls during mid - late summer (post December). Light surface winds prevail during the

summer and consequently redistribution processes are at a minimum preserving the surface hoar layer. Beneath the hoar layer is the summer surface which is characterised by a thin ice layer formed from the regelation of a surface melt film caused by solar radiation during late spring to mid summer (November - December). This ice layer or radiation glaze is spatially discontinuous and its distribution is dependent upon the spring surface roughness. A wind - glazed crust can also form on the surface during late winter and or spring whenever a hiatus in the snow supply occurs. However the winter or spring glazes are not as well developed or as thick as the autumn glaze because precipitation is more frequent. The maximum development of the autumn glazed surface is correlated to the occurrence of the strongest surface winds in autumn (Allison, 1985). Occasionally, depth hoar layers occur in the upper 100 - 300 mm of snow dunes as a result of mass transfer within the snowpack under strong temperature gradients. The oxygen isotope data show that the majority of annual accumulation is derived from early winter to late spring precipitation.

A model of firn stratigraphy was developed from the above observations which is similar to that used by Alley (1988). The firn stratigraphy model interprets the annual autumn wind - glazed ice crust overlying the summer hoar and radiation glazed surface as the annual horizon marker.

3.3.2 FIRN STRATIGRAPHIC METHODS

All firn cores were drilled to depths of between 30-42 m using the PICO (Polar Ice Coring Office) lightweight auger. The drilling methods are outlined in Goodwin (1988b). Annual accumulation layer thicknesses were primarily determined by the interpretation of annual cycles in the oxygen-isotope ($\delta^{18}O$) and ice-crust stratigraphy on all the cores. The cores at GD03, GD06 and GD15 in eastern Wilkes Land, at GF12 in Queen Mary Land (Figure 2.1) and at LGB00 and MGA in eastern Kemp Land (Figure 2.2) are located in a snow accumulation regime where strong katabatic winds redistribute the precipitation (Goodwin, 1991). Despite this mixing there is an annual cycle in $\delta^{18}O$. This is not as clear as in the coastal Law Dome cores at DSS and DE08 which are located close together (separation 18 km) near the summit of Law Dome in a high accumulation zone. On Law Dome summit, little snow redistribution occurs (strong surface winds are infrequent in the Law Dome automatic weather station data, Allison, et al. 1993) to the original precipitation and they show exceptionally well preserved annual cycles of $\delta^{18}O$ because the annual accumulation rates are high and surface melting rarely occurs (Morgan et al., 1991).

The time-series for these coastal cores which were published in Morgan et al.(1991), are used later in the discussion on the temporal variation of the accumulation pattern. The $\delta^{18}O$ data from all the inland cores were supplemented by visible stratigraphy techniques based on the firn stratigraphic model and the annual horizon marker, defined above as the "autumn ice crust and wind slab couplet". This stratigraphic interpretation was confirmed in the GD03 firn core data by stake height measurements of recent accumulation and a reference horizon (1955) determined from gross beta radioactivity profiling. In parts of the cores where the $\delta^{18}O$ data were ambiguous due to the absence of a summer snow layer, electrical conductivity profiling methods (Hammer, 1980) [DSS, DE08, MGA, E065 and LGB00 cores] and hydrogen peroxide (H_2O_2) methods (Sigg and Neftel, 1988) [DSS, DE08, GF12 cores] were applied to clarify the annual cycle. Hydrogen peroxide has a strong seasonal signal in polar snow and like $\delta^{18}O$ is a function of temperature at the time of condensation. The peak in H_2O_2 occurs in Late Summer snows which in Antarctica corresponds to February. If summer snowfalls occur late in February rather than December or January the peak summer signal in $\delta^{18}O$ is often absent in the stratigraphic record and instead a peak H_2O_2 signal is recorded. Similarly, the amount of salt or acidity of snow is seasonal and reaches a peak in late summer and can be detected by electrical conductivity profiling methods. Thus both these alternative methods can be used to clarify the interpretation of annual cycles based on the identification of a summer peak or spike in the signals. Generally the peak $\delta^{18}O$ signal occurs in snow located above the radiation glaze, whilst the peak conductivity signal occurs above the radiation glaze and often in association with the autumn wind-glazed ice crust. The cores were sampled at 0.03-0.05 m intervals which correspond to 12-20 samples per year, except for the GD03 and GD15 cores which were sampled in the field at 0.10-0.15 m intervals corresponding to a coarser sampling rate of 5-7 per year. The accuracy of annual layer interpretation using these combined techniques is approximately 3-5 ambiguities in each 50 year record. A number of shallow, 2 m deep cores were drilled on the Amery Ice Shelf and accumulation and ablation rates were determined using $\delta^{18}O$ data and visible layer stratigraphy, together with the earlier stratigraphic observations and stake measurements made during the early to mid 1960's . The $\delta^{18}O$ data were used primarily to detect areas of snow accumulation from areas dominated by ablation. Even in areas of strong melt percolation remnant cycles were apparent in the firn.

The annual accumulation thickness data from the cores were converted into annual accumulation rate records after consideration of; the densification of snow at depth, the upstream variation in snow accumulation (because the ice at depth originated upstream of the borehole, this was typically close to zero for the inland cores) and the vertical

TABLE 3.1 KATABATIC ZONE SURFACE LAYER CHARACTERISTICS

Season	Surface layer description
Autumn	Wind - glazed ice crust, strong hardness up to 1000 kg m^{-2}, spatially continuous, 0.9 - 2.0 mm thick opaque glaze, consisting of 2 - 5 layers, over wind crust up to 200 mm thick. Melt forms a cement, bonding snow grains, creating an opaque aggregate layer. Forms during the March - April hiatus in snow supply. Surface dominated by large friable, mobile snow dunes (barchan and longitudinal) up to 1 - 2 m high, consisting of early autumn snow.
Summer	Radiation glaze, weak hardness up to 100 kg m^{-2}, spatially discontinuous, 0.5 mm thick, transparent regelation ice. Forms during mid December - mid January when maximum radiation occurs, melting a thin film over wind laminated drift snow, originating from light December snowfalls / hoar frost. On microrelief high points the radiation glaze forms on top of the exposed spring wind - glazed surface. Dominant snow surface microrelief is wind laminated drift snow with weak wind ridges 100 mm high.
Spring	Wind - glazed ice crust, strong hardness up to 400 kg m^{-2}, spatially discontinuous, 0.5 mm thick glaze over wind crust. Forms during the September - November hiatus in snow supply, following large snowfalls during June - August. Surface dominated by redistributed, friable longitudinal dunes 200 - 400 mm high.

strain due to ice flow (also close to zero). Accurate corrections for the densification of firn in the upper layers were made from detailed density measurements on the cores (Goodwin, 1988b). The correction for the upstream accumulation gradient is negligible for, GD03, GD06, GD15, GF12, LGB00, MGA, E065 and DSS. At DE08 the accumulation rate was linearly corrected for the upstream gradient using a +5% correction for the deepest ice (Morgan et al, 1991). Thinning due to vertical strain in the ice is also negligible at 30-35 m depth. However, thinning was significant at DE08 and DSS because of their longer depths. Morgan et al. (1991) corrected the accumulation rates by applying corrections based on measurements of the horizontal strain rate around the boreholes.

The accumulation rate time-series are presented for eastern Wilkes Land, Queen Mary Land, MacRobertson Land and Kemp Land separately in the following sections.

3.4 WILKES LAND AND QUEEN MARY LAND TEMPORAL ACCUMULATION PATTERNS

The Wilkes Land and Queen Mary Land katabatic region experiences moderate snow accumulation rates, with recent (1978-1987) mean accumulations of 560, 355, 378, 356 and 567 kg m^{-2} a^{-1} at GD03, GD06, GD15 and GF12 respectively (Chapter 2). The GD03 and GD06 sites are located in primarily erosional and redistributional environments with mesoscale north-west aspect (leeward) slopes and convergent wind fields (Figure 2.3b). In contrast, the GF01, GD15 and GF12 sites are located in primarily depositional and redistributional environments with mesoscale north-east aspect (windward) slopes with divergent wind fields (Figure 2.3b). The temporal variability of the 55 year (1930 - 1985) annual accumulation and oxygen isotope time series for GD03, GD06, GD15 and GF12 are discussed below.

3.4.1 OXYGEN ISOTOPE STRATIGRAPHY AND ACCUMULATION RATES IN WILKES LAND, LAW DOME AND QUEEN MARY LAND

3.4.1.1 GD03 CORE

The oxygen isotope profile together with an autumn ice layer stratigraphy for the GD03 core is shown in Figure 3.1a. The majority of autumn ice crusts (approximately 80%) can be matched to clear annual cycles in $\delta^{18}O$ values despite the coarse sampling of $\delta^{18}O$ at five-seven samples per year. The accumulation rate time-series for GD03 is shown in Figure 3.2a. The mean annual accumulation rate for the interval 1930-85 at GD03 was calculated as 315 kg m^{-2} a^{-1} with an inter-annual variability of σ = 77 kg m^{-2} a^{-1}. The inter - annual variability has a slightly larger magnitude (24% of the mean) than the single year spatial accumulation variability of σ = 67 kg m^{-2} a^{-1} (18% of the mean) measured across the cane farm (Goodwin, 1991). The 6% increase in variability between the 55 year record and the single year record provides an indication of the temporal variability of accumulation rate due to fluctuations in the precipitation regime, since the accumulation rate is primarily derived from the frequency of precipitation events throughout the year. For comparison, the mean annual measured accumulation by stake for 1982-85 is 336 kg m^{-2} a^{-1} and the corresponding accumulation from the stratigraphy is 362 kg m^{-2} a^{-1}. The

discrepancy is equivalent to 0.06 m of snow and is attributed to different microrelief size between the cane and the drill hole.

3.4.1.2 GD06 CORE

An annual accumulation rate record was determined using the above methodology for a core at GD06 which is located 151 km to the east of GD03 (Figure 2.1). The GD06 core represents 57 years of annual snow accumulation increments from 1928-1985. The oxygen isotope profile together with an autumn ice layer stratigraphy for the GD06 core is shown in Figure 3.1b and the accumulation time rate series is shown in Figure 3.2b. The mean annual accumulation rate for the interval 1928 - 1985 at GD06 is 339 kg m^{-2} a^{-1} with an inter - annual variability of σ = 91 kg m^{-2} a^{-1} or 27%. The mean annual measured accumulation by stake for 1982-85 is 349 kg m^{-2} a^{-1}. The higher inter-annual variability at GD06 than that for GD03 between 1928-1985 is largely the result of the increased accumulation rate and the katabatic wind redistribution processes. The latter are a strong determinant of the accumulation rate at GD06 due to its location at the break in the mesoscale north-west slope. In this region there is a reduction in the katabatic wind speed and snow transport, with snow deposition occurring. The accumulation rate is significantly influenced by the integral of the snow transported and redistributed from upslope together with the net precipitation at the site.

3.4.1.3 GD15 CORE

An annual accumulation rate record was determined using the same methodology for a core at GD15 which is located 750 km to the east of GD03 (Figure 2.1) on the north-east aspect slope. The GD15 core represents 50 years of annual snow accumulation increments from 1935-1985. The oxygen isotope profile together with an autumn ice layer stratigraphy for the GD15 core is shown in Figure 3.1c and the accumulation time rate series is shown in Figure 3.2c. The mean annual accumulation rate for the interval 1935 - 1985 at GD15 is 299 kg m^{-2} a^{-1} with an inter - annual variability of σ = 65 kg m^{-2} a^{-1} or 21%. The mean annual measured accumulation by stake for 1982-85 is 315 kg m^{-2} a^{-1}. As described in section 2.2.7 the accumulation rate at GD15 is approximately 150 kg m^{-2} a^{-1} greater than for sites at equivalent elevations on the opposing north-west slope due to topographic influences on the precipitation regime.

3.4.1.4 GF12 CORE

An annual accumulation rate record was determined using the same methodology for a core at GF12 which is located 760 km to the west of GD03 (Figure 2.1). The GF12 core represents 45 years of annual snow accumulation increments from 1940-1985. The oxygen isotope profile together with an autumn ice layer stratigraphy for the GF12 core is shown in Figure 3.1d and the accumulation time rate series is shown in Figure 3.2d. The mean annual accumulation rate for the interval 1940 - 1985 at GF12 is 536 kg m^{-2} a^{-1} with an inter - annual variability of σ = 100 kg m^{-2} a^{-1} or 18.6% of the mean. The mean annual measured accumulation by stake for 1982-85 is 517 kg m^{-2} a^{-1}, which is equivalent to the accumulation rate at Law Dome summit at an elevation of only 1300 m. The anomalously high accumulation rates experienced by the GF12 region are largely determined by katabatic snow redistribution processes. GF12 experiences significant deposition of redistributed snow associated with the convergence of the katabatic windfield along the western drainage divide of the Denman Glacier valley.

3.4.2 TEMPORAL VARIATION OF ACCUMULATION RATE AND OXYGEN ISOTOPE IN WILKES LAND, LAW DOME AND QUEEN MARY LAND

The annual accumulation rate time-series and long-term trends determined by linear regression for the GD03, GD06, GD15 and GF12 cores are shown in Figure 3.2a, b, c and d respectively. The time-series were filtered using a five point (year) Gaussian weighted running mean to smooth the interannual variability due to surface microrelief. The three filtered records for eastern Wilkes Land display good correlation on the timescale of decades (especially since 1950) indicating that they reflect the temporal variability due to regional climatic effects across Wilkes Land rather than residual variability due to local effects at the sites. The correlation also indicates that there are no systematic errors in the independent dating of the three cores. The accumulation records for GD03 and GD15 display an overall increase from 1930 to 1985 whilst the accumulation records for GD06 and GF12 show an overall stable long-term trend with large interdecadal fluctuations. The overall increases in the long-term accumulation rate GD03 and GD15 are equivalent to overall increases of +21% and +19%. A comparable increase in accumulation rate of +18% and +19% also occurs in the DSS and DE08 cores from Law Dome summit (Morgan et al., 1991, Figures 3.2e and f) which have recent (1978-1987) mean accumulations of 570 and 1160 kg m^{-2} a^{-1} respectively.

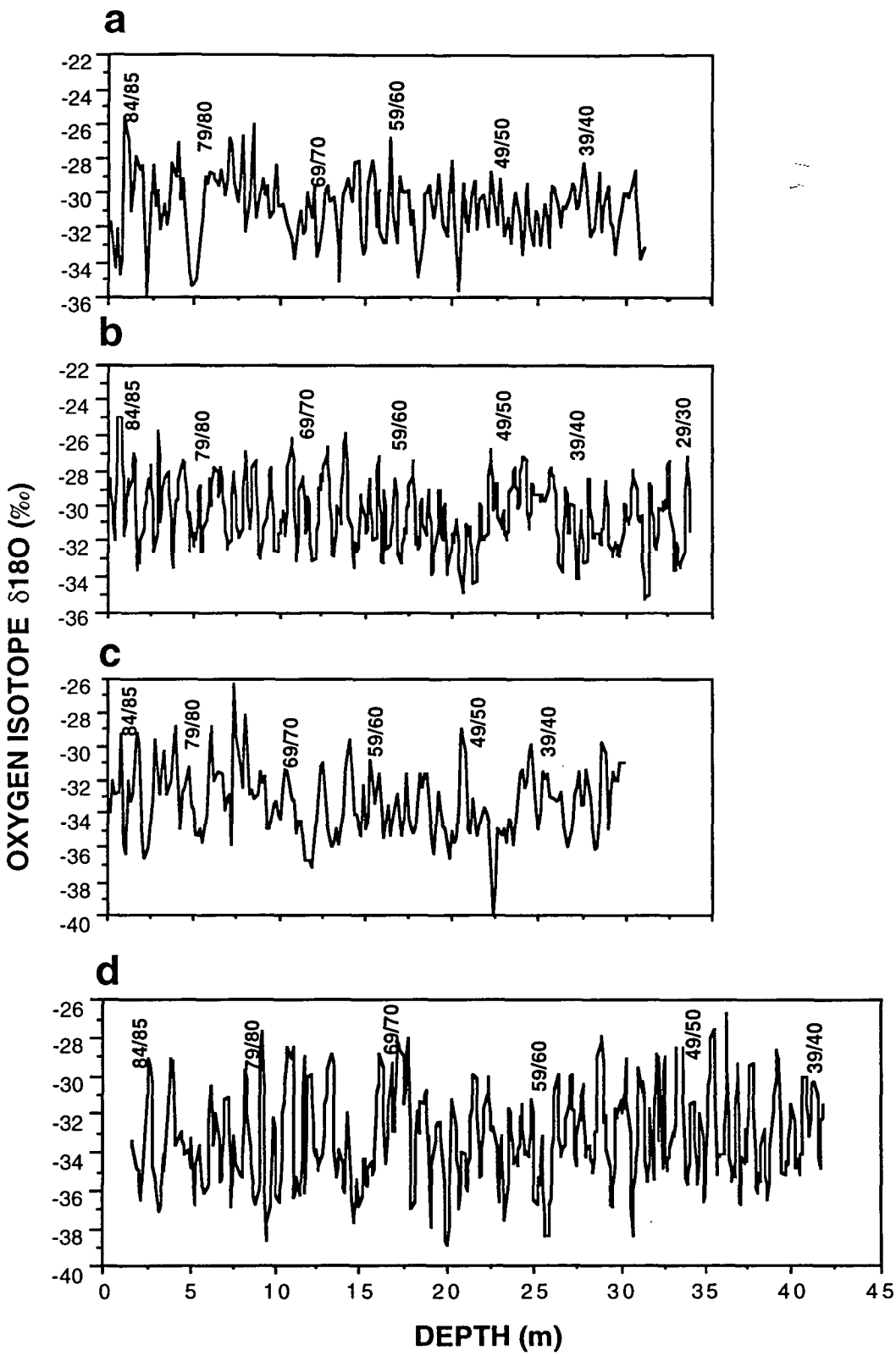

Figure 3.1 Oxygen isotope ($\delta^{18}O$) profiles for firn cores drilled at (a) GD03, (b) GD06, (c) GD15, and (d) GF12. The interpreted stratigraphy is indicated by the decadal horizon markers.

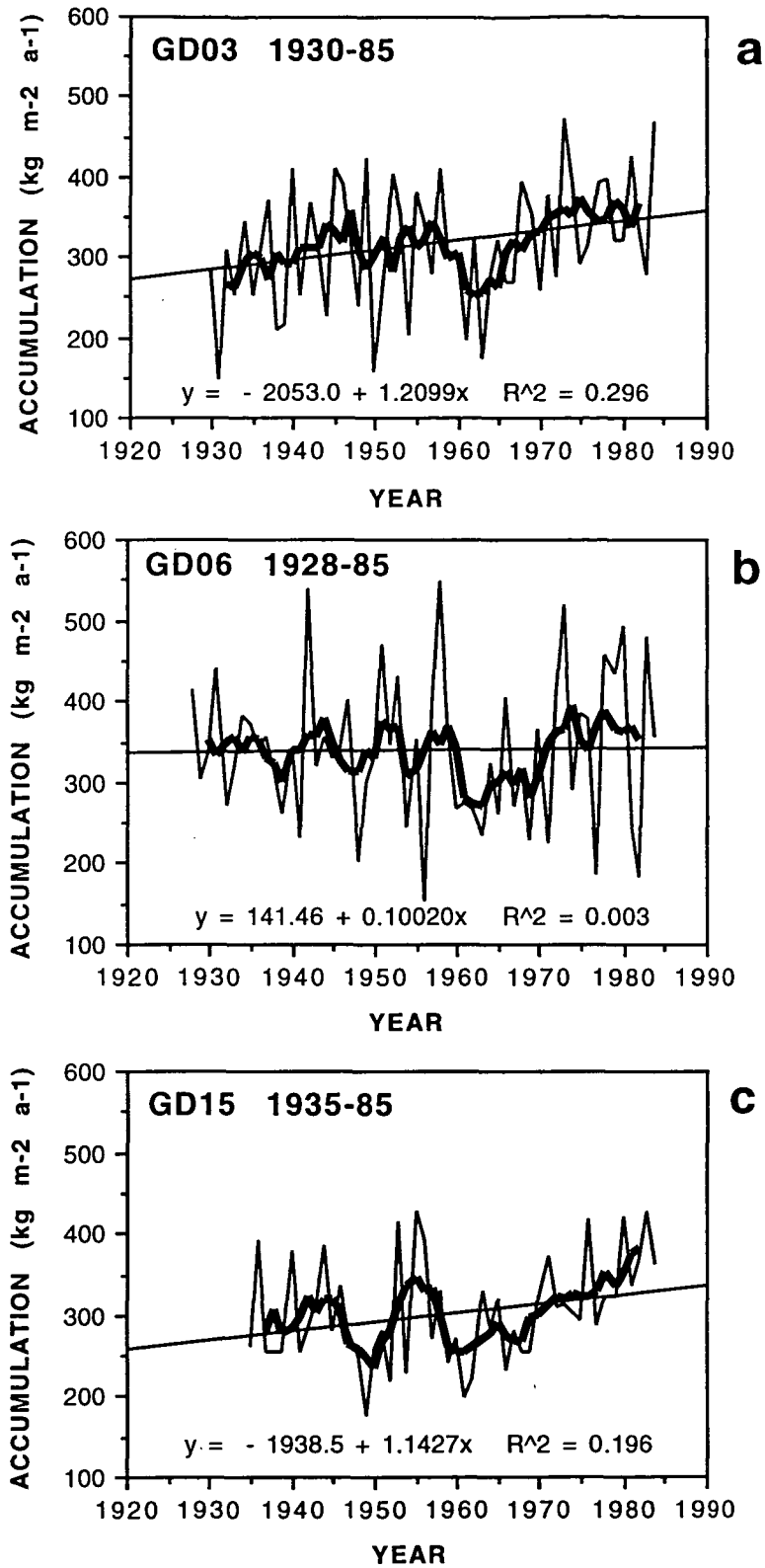

Figure 3.2a-c Eastern Wilkes Land annual accumulation rate time-series (thin line) and smoothed time-series (bold line) using a 5 year running mean to remove the noise due to surface microrelief. Figure (a) GD03, (b) GD06, and (c) GD15. Regression lines are also plotted to indicate the overall change in accumulation rate.

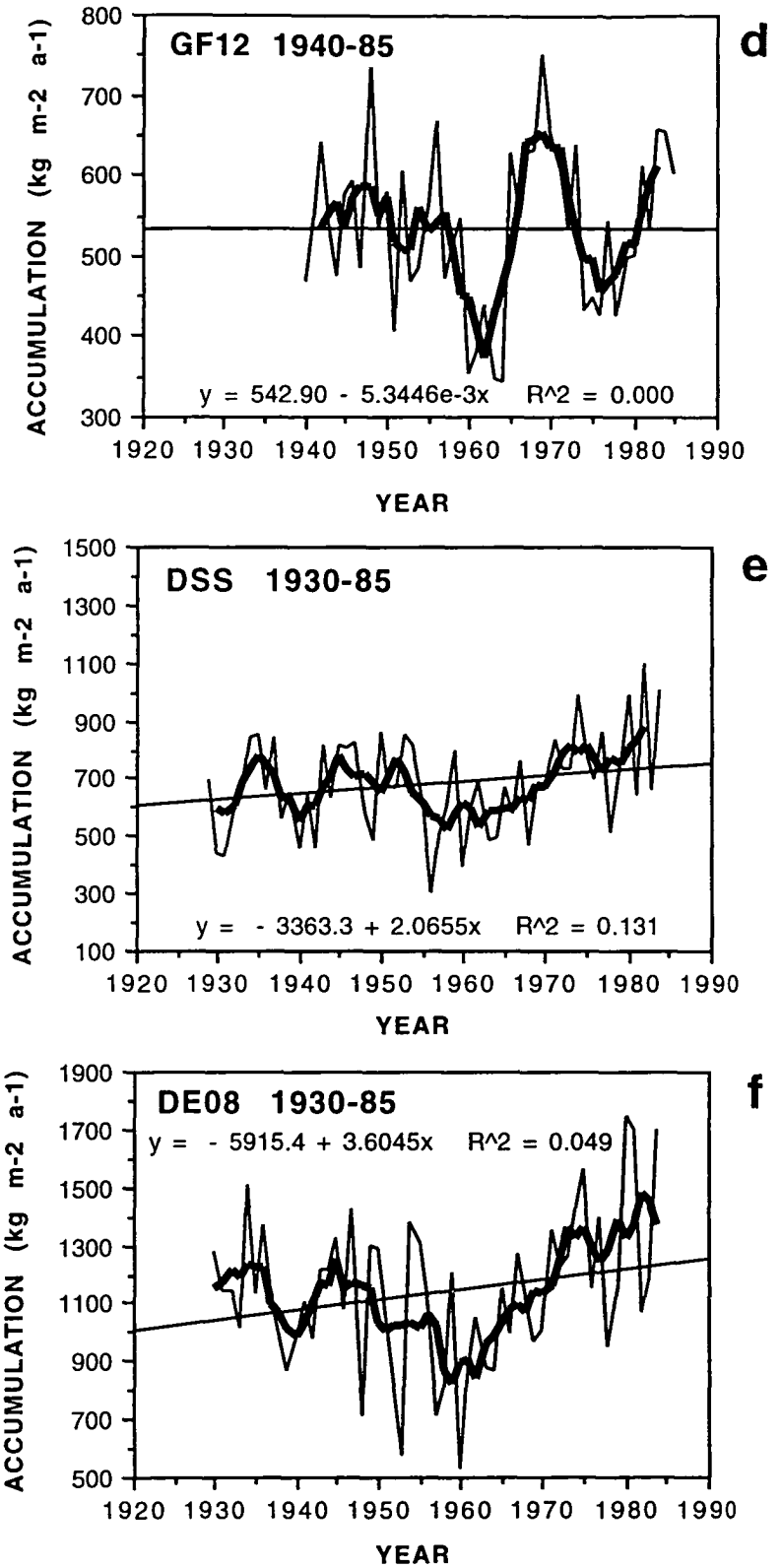

Figure 3.2d-g Queen Mary Land and Law Dome (after Morgan et al., 1991) annual accumulation rate time-series (thin line) and smoothed time-series (bold line) using a 5 year running mean to remove the noise due to surface microrelief, shown in Figure (d) GF12, (e) DSS, and (f) DE08. Regression lines are also plotted to indicate the overall change in accumulation rate.

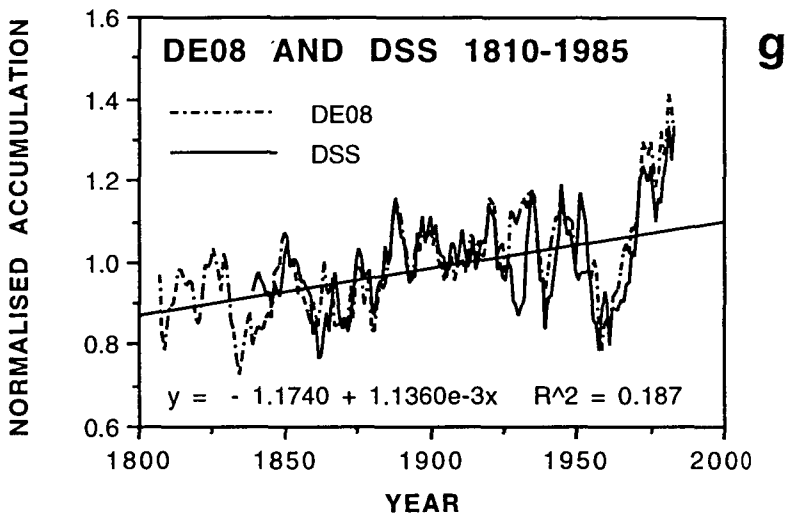

Figure 3.2g shows the accumulation rate time-series for DSS and DE08 from 1810 to 1985, which depicts an overall continuous increase in accumulation rate during this period. A regression line is also plotted to indicate the overall change in accumulation rate.

Notable in all the cores is a marked decrease in accumulation rates at 1955, reaching a low point at 1960 and increasing to 1985 for all cores except for GF12. The latter rates are the highest accumulation rates in the 50 year period for eastern Wilkes Land. In the GF12 core the accumulation rates increase rapidly from the low point at 1960, reaching the highest accumulation rates in by 1967-73, followed by a marked decrease centred on 1975 before increasing in the mid 1980's. A similar pattern occurs in the GD06 core although to a minor extent. A multiple regression of the five year filtered accumulation rates in the GD03, GD06, GD15, DSS and DE08 cores for the 1955-85 period, showed that the temporal accumulation pattern is highly correlated across eastern Wilkes Land and Law Dome with a coefficient r = 0.71 (significant at the 99.5% confidence level). Figure 3.2g (after Morgan et al., 1991) shows the long-term accumulation rate time-series for DSS and DE08 since 1800. The recent increase in accumulation rates since 1970 is up to 30% higher than the long-term mean for the last 150 years.

The corresponding (GD03, GD06, GD15, and GF12) oxygen isotope records for the period 1930-85 were smoothed over a 0.7 m increment (1 year) using a Gaussian weighted running mean. These are shown together with long-term trends determined by linear regression in Figure 3.3a, b, c and d, together with those for GF01 in 3.3e and DSS and DE08 in 3.3f and 3.3g. The four Wilkes Land cores and the Law Dome cores indicate that the mean annual oxygen isotope value has been enriched or increased by between +0.015 and +0.024 $‰a^{-1}$ which is equivalent to a total increase of +0.83 to +1.2 ‰ between 1930-85. In contrast, the mean annual oxygen isotope value has been depleted or decreased at GF12 by a similar amount, a total of -0.90 ‰ between 1940-85 equivalent to -0.020 $‰a^{-1}$. Regression analysis of the Wilkes Land cores showed that the mean annual oxygen isotope values at GD03 and GD15 were correlated with a coefficient r = 0.52 which is significant at the 95% confidence level. There was no correlation between the mean annual oxygen isotope values between GD03 and GD15 with GD06, and similarly between the GD cores with the Law Dome cores and GF12 cores. However, the mean annual DSS and DE08 oxygen isotope records which were highly correlated (as was expected from their close proximity) were moderately correlated over some decades with the GF12 core from Queen Mary Land. For the 1974-84 period DE08 oxygen isotopes were correlated (r = 0.53, n=12, significant at the 95% level) with the GF12 record. This indicates that the moisture source and precipitation patterns on Law Dome and Queen Mary Land may be teleconnected over some decades. This is analysed further in section 3.8.

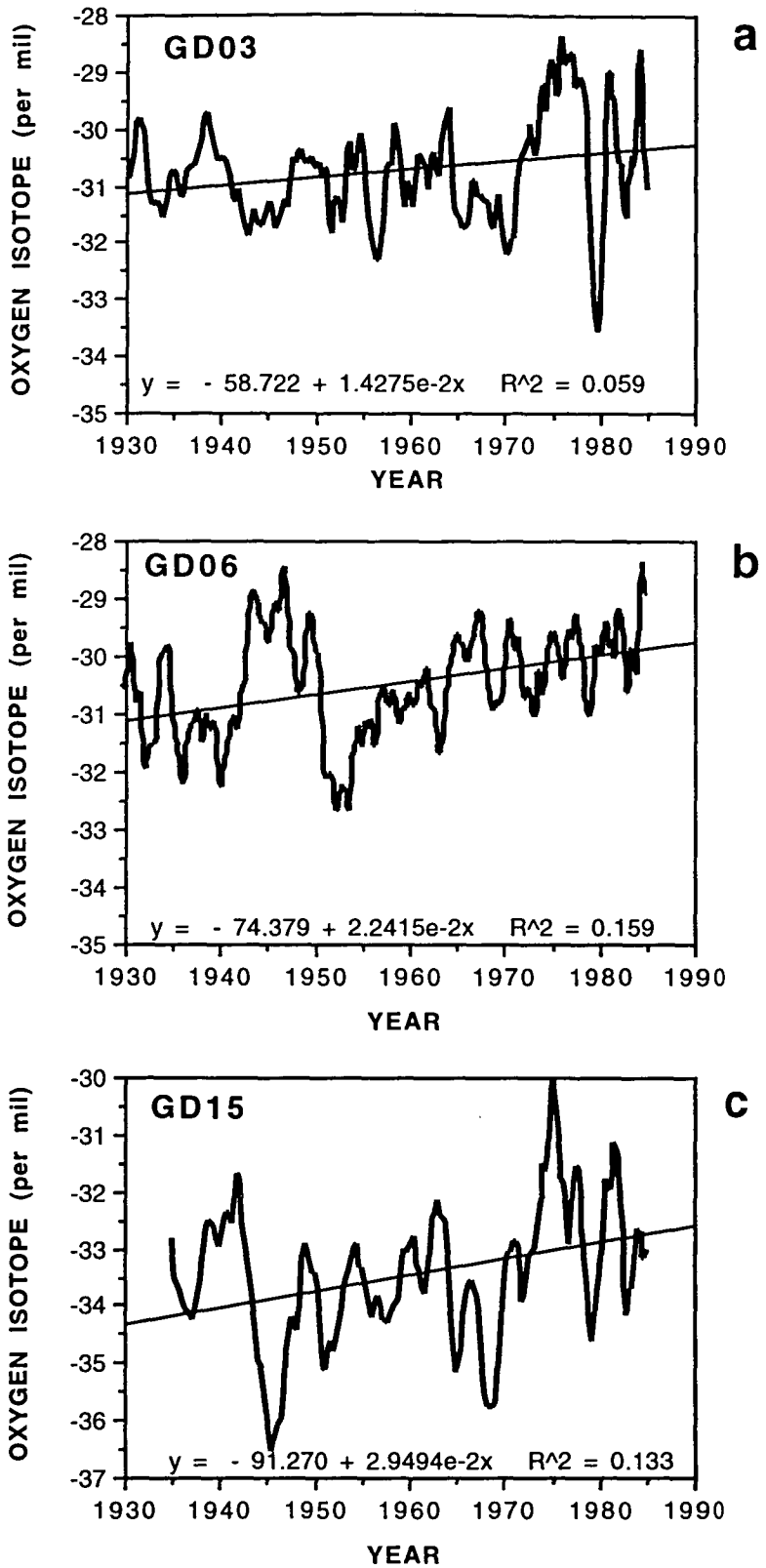

Figure 3.3a-c Eastern Wilkes Land oxygen isotope-depth time series smoothed over a 0.7 m increment equivalent to ~1-1.5 years accumulation at (a) GD03, (b) GD06, and (c) GD15. Regression lines are also plotted to indicate the long-term change.

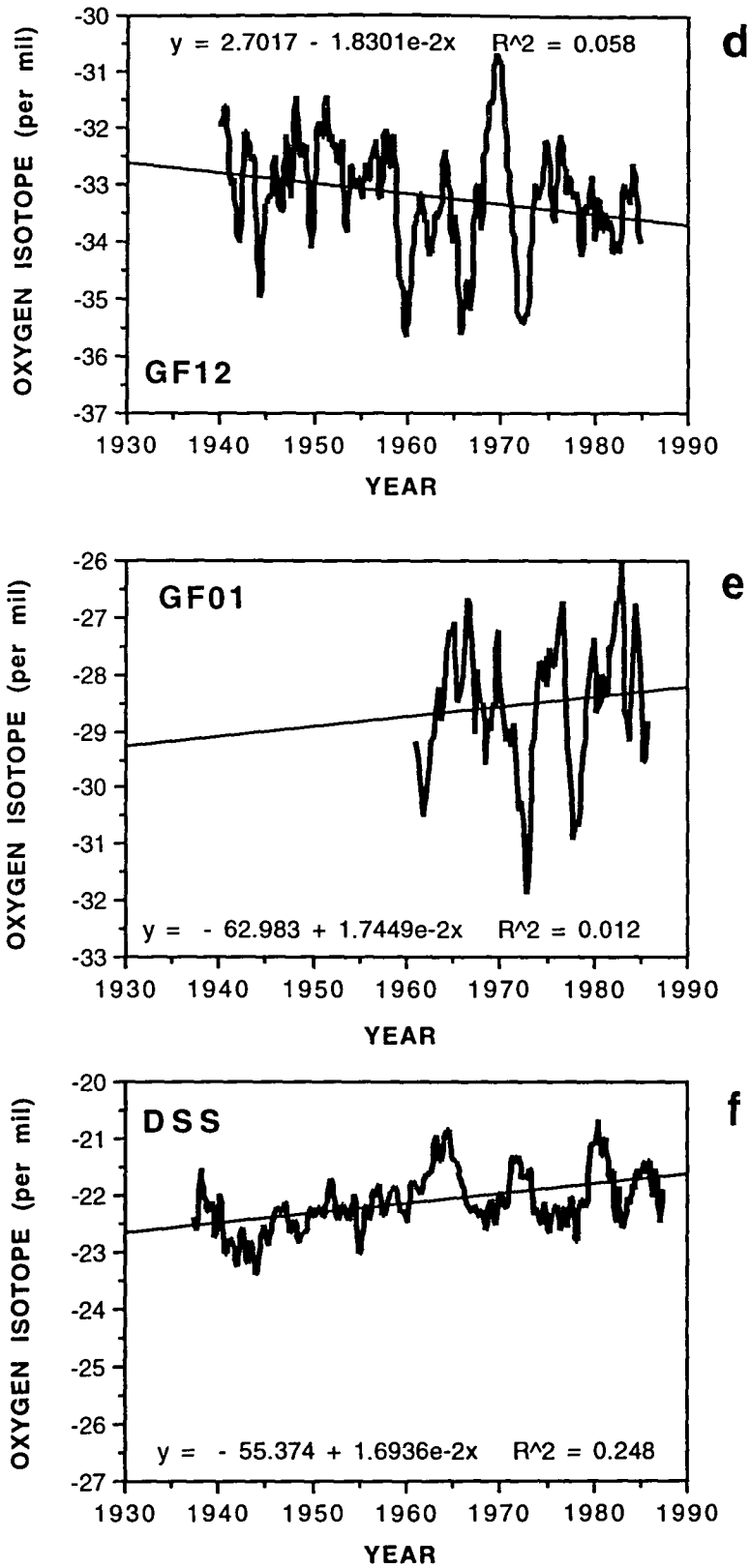

Figure 3.3d-f Queen Mary Land, Western Wilkes Land and Law Dome oxygen isotope-depth time series smoothed over a 0.7 m increment equivalent to ~1-1.5 years accumulation at (d) GF12, (e) GF01 and (f) DSS. Regression lines are also plotted to indicate the long-term change.

Thus at GD03, GD15 and DSS, the accumulation rate between 1930-85 has increased by +20% with a rise in mean annual $\delta^{18}O$ of 1.0‰. No significant trend in accumulation rate for the same period has occurred at GD06 despite a comparable increase in mean annual oxygen isotope of +1.0‰. In contrast, at GF12 no significant accumulation rate change is associated with the anomalous decrease of -0.90‰ in mean annual oxygen isotope. An additional oxygen isotope profile was obtained from the GF01 (68° 30'S, 110° 51'E, 1783 m), which is located 100 km to the west of GD03 towards GF12. The GF01 oxygen isotope values show a similar increase to those at GD03, GD15 and DSS of +0.45‰ between 1960-86. A general accumulation rate record was determined at GF01 for 1960-86 using hydrogen peroxide (H_2O_2) and oxygen isotope ($\delta^{18}O$) measurements only, since visible stratigraphy and density profiles were not obtained . The resulting long-term mean accumulation rate at GF01 is estimated as 363 kg m^{-2} a^{-1} which indicates that the measured accumulation rates of 560 kg m^{-2} a^{-1} between 1983-86 are well above the mean and are correlated to the increase in oxygen isotopes.

Other short term Antarctic accumulation records, are primarily determined from gross beta radioactivity horizons in Antarctic firn in 1955 and 1965. For comparison with these the recent trend in increasing accumulation at the Wilkes Land sites was analysed between the two epochs, 1955 - 1965 and 1975 - 1985. The results are listed below in Table 3.2. Data from GF12 were not included in the comparison due to their overall anomalous accumulation and $\delta^{18}O$ patterns during the 1940-85 period.

The results in Table 3.2 show that recent accumulation rates increased overall by 26% since 1960 across Wilkes Land and Law Dome. This increase in accumulation rate is comparable to the recent increases reported in the interior of Wilkes Land and coastal Terre Adélie. The Law Dome cores extend back to 1806 and show an overall mean increase in accumulation of 22.5% since that time (Morgan et al., 1991). Although the present day accumulation values are the highest in the Law Dome records, earlier fluctuations over time periods of 10-20 years reach ~15% above the mean and there is large variability on time scales of up to 100 years. The mean Wilkes Land and Law Dome accumulation pattern for the decade 1975-85 is 19% higher than the 1930-70 period, which is equivalent to the long-term mean for the period 1870-1970 in the Law Dome cores (after Morgan et al., 1991).

TABLE 3.2 ACCUMULATION RATE AND OXYGEN ISOTOPE COMPARISON FOR WILKES LAND, LAW DOME AND QUEEN MARY LAND

SITE	ELEV.	ACC RATE	ACC CHANGE	OXYGEN ISOTOPE CHANGE	ACC CHANGE	OXYGEN ISOTOPE CHANGE
		1975-85	[(75-85) -(55-65)]*	[(75-85) -(55-65)]*	[(70-85) -(30-70)]*	[(70-85) -(30-70)]*
	m	kg $m^{-2}a^{-1}$	%	‰	%	‰
GD03	1828	355	+23	+0.68	+18	+0.75
GD06	1884	359	+16	+1.13	+9	+0.86
GD15	2155	356	+26	+1.06	+20	+1.21
MEAN			+22%	+0.96‰	+16%	+0.94‰
DE08	1200	1160	+27	+0.58	+23	+0.02
DSS	1370	570	+37	+0.06	+25	+0.24
MEAN ALL			+26%	+0.70‰	+19%	+0.62‰

* Note the change in accumulation rate and in oxygen isotope is calculated as follows;
Change (%) = [(1975-85) - (1955-65)] / (1955-65).
Change (%) = [(1970-85) - (1930-70)] / (1930-70).

The comparisons in Table 3.2 show that there is a general coupled increase in oxygen isotope with increasing accumulation rate. However, there is considerable interannual variation and to a lesser extent interdecadal variation between sites rather than a consistent correlation. This variation is due mainly to changes in the surface temperature and seasonal precipitation regime, changes in the katabatic redistribution processes and changes in the moisture source. An analysis of the cause of the variation in oxygen isotope is discussed in section 3.8. The interdecadal comparisons in Table 3.2 suggest that a mean increase in accumulation rate of 26% can be expected to be associated with a mean increase in oxygen isotope of +0.70‰. Averaging over several decades reduces this relationship to a mean increase in accumulation rate of 19% together with a mean increase in oxygen isotope of 0.62‰.

The general trend of increasing accumulation rate in Wilkes Land is supported by the results of Pourchet et al. (1983). They made a comparative study of accumulation rates for the decades 1965 - 1975 and 1955 - 1965. The sites were mainly below 3000 m elevation in Terre Adélie, but also include Vostok (78° 28'S, 106 49E), Dome C (74° 34' S, 123° 10' E), and the South Pole. They reported a general increase in accumulation of 30% across Antarctica, and a mean increase of 36% for Wilkes Land from the coast near Dumont d'Urville to the South Pole (with a large variability from 10 - 90%). Their study used gross beta radioactivity measurements to identify the 1955 and 1965 layers for 14 sites in East Antarctica. A discussion of the parameters contributing to the accumulation fluctuations is presented in the later section 3.8.

3.5 LAMBERT GLACIER BASIN, MAC.ROBERTSON LAND AND EASTERN KEMP LAND TEMPORAL ACCUMULATION PATTERNS

The accumulation rate measured on canes at MGA is 270 kg m^{-2} a^{-1} (3-year epoch 1975-78), at LGB00 it is 153 kg $m^{-2}a^{-1}$ (9-year epoch 1983-92) and at E065 it is 135 kg $m^{-2}a^{-1}$ (3-year epoch 1975-78) (Goodwin et al., 1994). Spatial variability of snow accumulation on a local or microscale was investigated at LGB00 by a cane farm study between 1983-93, and ranged from 18-29% of the mean rate for a 3-4 year period and down to 18% for the mean rate for a 6 year period (Higham, 1994). This region experiences strong katabatic wind flow and the mean winter wind speed is in excess of 12 m/s (Allison et al., 1993), similar to those in Wilkes Land. The accumulation rates in Kemp Land are approximately 70% less than those for the same elevation range in Wilkes Land (Chapter 2). Consequently, surface microrelief are of an equivalent size to annual accumulation rates and produce significant noise in the stratigraphy (Goodwin et al., 1994). This is particularly the case at LGB00 and E065.

3.5.1 OXYGEN ISOTOPE STRATIGRAPHY AND ACCUMULATION RATES AT LGB00, MGA AND E065

The $\delta^{18}O$ profiles and decadal stratigraphy for the LGB00, MGA and E065 cores are shown in Figures 3.4a, b and c respectively. A significant proportion of $\delta^{18}O$ cycles have an amplitude less than the seasonal variation of 8-10‰ (eg. 10.5-12.5 m depth in MGA; and 9-15 m depth in LGB00). The reduced signal amplitude is often due to a lack of isotopically heavier peak summer snowfall (less negative $\delta^{18}O$ values) and, to

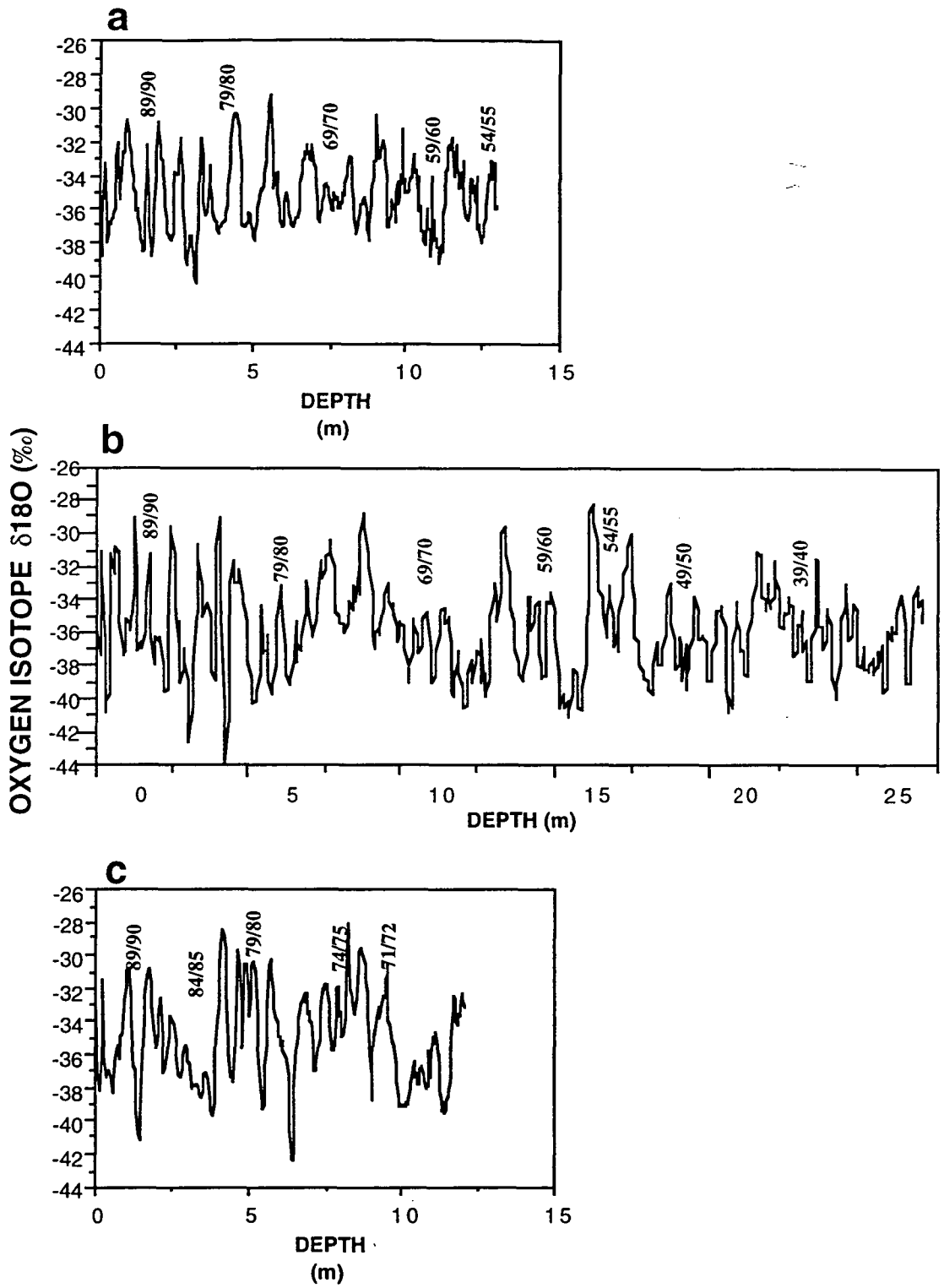

Figure 3.4 Oxygen isotope ($\delta^{18}O$) profiles for firn cores drilled at (a) LGB00, (b) MGA, and (c) E065. The interpreted stratigraphy is indicated by the decadal horizon markers.

a lesser extent, the lack of winter peak values. This would occur if the bulk of the accumulated snow for those years fell during autumn and spring together with a hiatus in snow supply over summer which is often evidenced by the development of a strong radiation/wind glaze or crust. Occasional radiation-glazed dune microrelief in the stratigraphy indicate that the microrelief highpoints do not accumulate snowfall during summer. These hiatus occur approximately once every ten years of accumulation. The higher autumn conductivity values helped to solve the inter-annual ambiguities in both cores and the resolution of the late summer-early autumn annual surface. There were considerable dating problems with the E065 record which resulted in the accurate interpretation of only the upper half of the core. This was primarily due to the large noise component due to surface microrelief and the low accumulation rates. The resulting E065 chronology was checked by matching the oxygen isotope profile with that for MGA between 1972 and 1992. The maximum error between the two chronologies at 1972 was 2 years difference.

Accumulation rate time series were derived for the period 1955-93 in the LGB00 core and the period 1939-93 in the MGA core. An accumulation rate time series was derived for the period 1972-93 in the E065 core. These time series are shown in Figure 3.5a, b and c. The mean annual accumulation rate for the interval 1955 - 1993 at LGB00 is 170 kg m^{-2} a^{-1} with an inter - annual variability of σ = 46 kg m^{-2} a^{-1} or 27% of the mean. The mean annual accumulation rate for the intervals 1939-93 and 1955 - 1993 at MGA are 259 and 263 kg m^{-2} a^{-1} respectively with an inter - annual variability of σ = 62 kg m^{-2} a^{-1} or 25% of the mean. The mean annual accumulation rate for the interval 1972 - 1993 at E065 is 232 kg m^{-2} a^{-1} with an inter - annual variability of σ = 55 kg m^{-2} a^{-1} or 24% of the mean.

3.5.2 TEMPORAL VARIATION OF ACCUMULATION RATE AND OXYGEN ISOTOPE IN EASTERN KEMP LAND

The accumulation time-series for LGB00, MGA and E065 are presented in Figure 3.5a, b and c. The time-series have been filtered using a five point (year) Gaussian running mean to reduce the effect of surface microrelief. These time-series for eastern Kemp Land show that accumulation rates were relatively constant between 1945-1982 and following that, the accumulation abruptly decreased to a low point at 1985 for all three sites. The low rates during 1980-1987 are comparable to the rates at MGA during 1940-47. Accumulation has decreased over the long-term from 1950-93 by -17% at LGB00 and by -19% at MGA (Table 3.3). Both records are correlated on decadal timescales (r = 0.67, significant at the 95% confidence level).

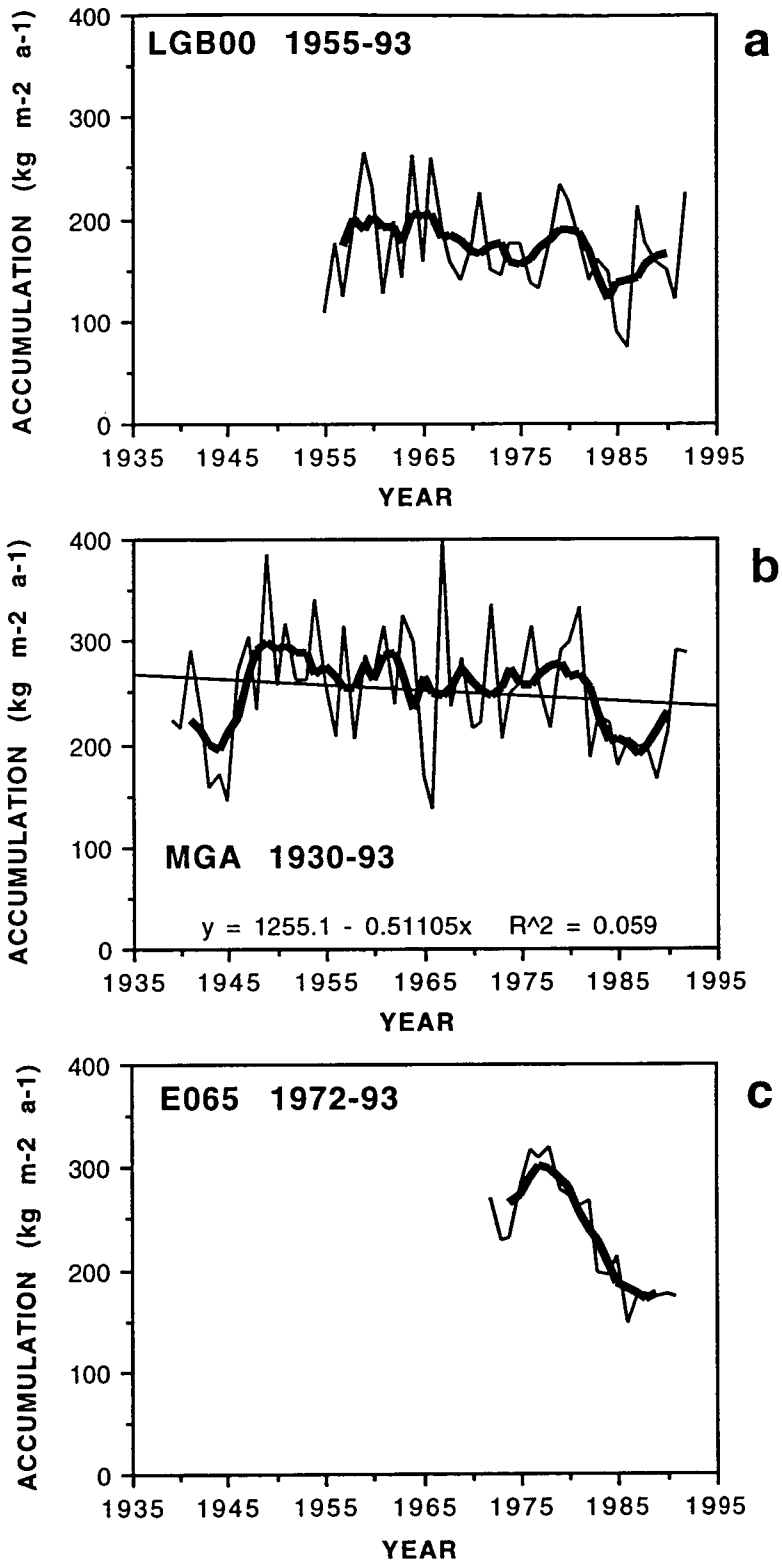

Figure 3.5 Annual accumulation rate time-series (thin line) and smoothed time-series (bold line) for (a) LGB00, (b) MGA, and (c) E065. Annual increments were smoothed over a 5 year period to minimise the noise due to surface microrelief. A regression line is also plotted to indicate the long-term change at MGA.

The decreasing accumulation trend for E065 since 1972 is consistent over the last two decades with that for the longer records. Unlike the time-series from Queen Mary Land, Law Dome and eastern Wilkes Land there is not a marked decrease in the Kemp Land accumulation centred on 1960 and there is no pattern of increasing accumulation since then. The fluctuation in accumulation rates at MGA during the 1940's also occurs in the GD15, GD06, DSS and DE08 cores and indicates a widespread change in accumulation at that time.

The oxygen isotope profiles for the LGB00, MGA and E065 cores were smoothed using a 21 point running mean equivalent to a 1 m length of core. The smoothed profiles together with the long-term change for the 1939-93 period in the MGA record are shown in Figure 3.6a, b and c. All three oxygen isotope time series display considerable variability over 5-10 year intervals, without significant long-term trends. The estimate of long-term change for 1939-93 at MGA suggests an overall enrichment or increase of +0.50‰, although this is not a significant trend. The lack of any significant trend in annual oxygen isotope ($\delta^{18}O$) values is probably a function of both the seasonal variability in the precipitation events, with some periods biased by the lack of significant summer or winter snowfalls, and changes in the moisture source. The causes of these fluctuations are investigated further in section 3.8.

TABLE 3.3 ACCUMULATION RATE COMPARISON AT LGB00 and MGA

SITE	ACC RATE	ACC CHANGE [1]	ACC CHANGE [2]
	1982-93		
	kg $m^{-2}a^{-1}$	%	%
LGB00	149	-17	NA
MGA	214	-19	-20

* Note the change in accumulation rate is calculated as follows:
Change [1] (%) = ((1982-93) - (1955-82)) / (1955-82).
Change [2] (%) = ((1982-93) - (1939-82)) / (1939-82).

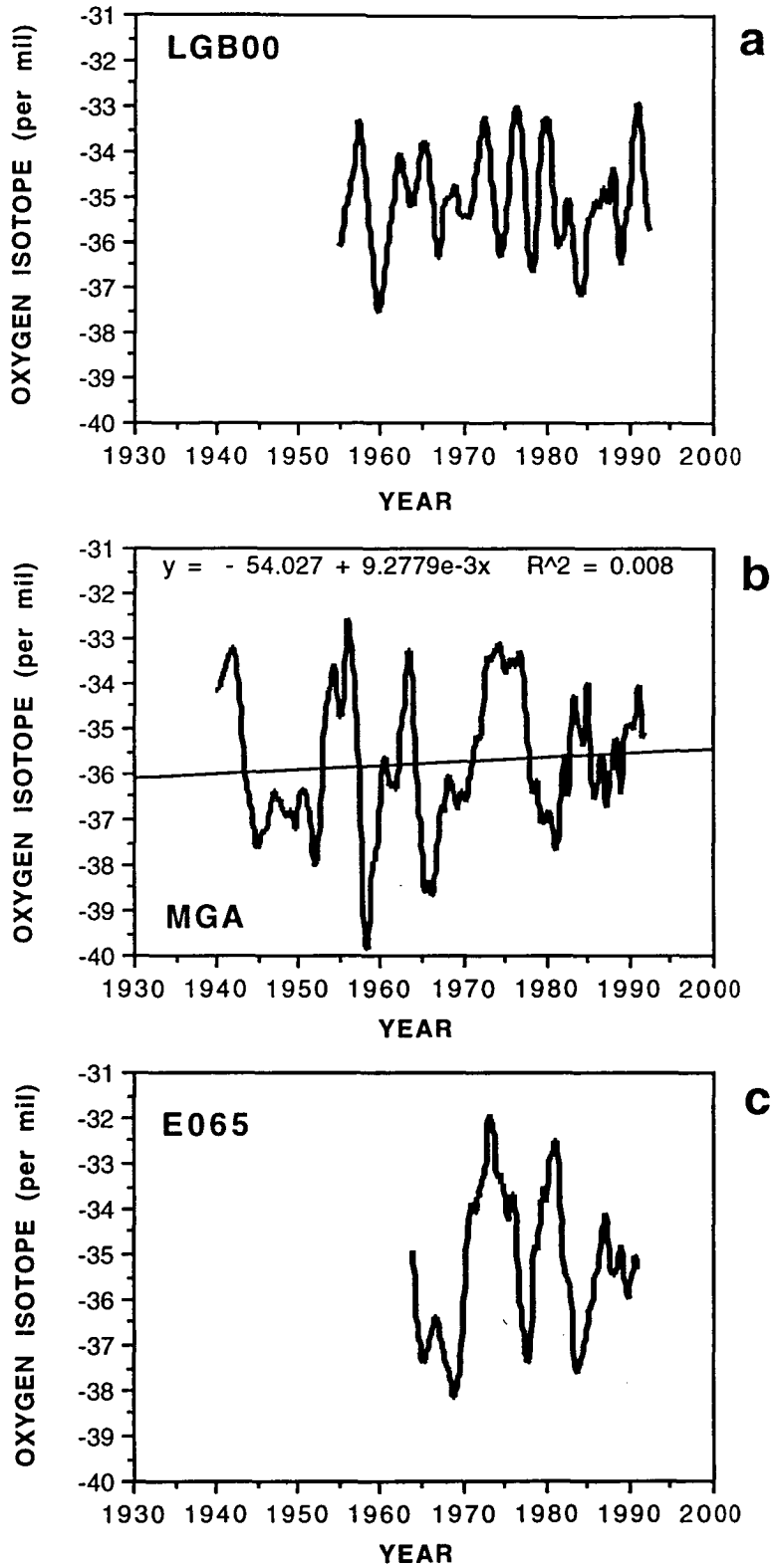

Figure 3.6 Oxygen isotope ($\delta^{18}O$) time-series smoothed over a period equivalent to 2 years accumulation for (a) LGB00, (b) MGA, and (c) E065. A regression line is also plotted to indicate the long-term change at MGA.

3.6 AMERY ICE SHELF TEMPORAL ACCUMULATION RATE PATTERNS

The Amery Ice Shelf is the third largest ice shelf in Antarctica and extends for 300 km southwards to the grounding zone with the Lambert Glacier. This outlet system drains approximately one eighth of the East Antarctic ice sheet (see Figure 2.2). The Amery Ice Shelf had previously been studied by ANARE glaciologists between 1962 to 1970 and hence, an opportunity existed to determine the nature of any change to the surface mass balance pattern during the intervening three decade period.

During the 1962-63 austral summer pit stratigraphy was carried out in eight pits along a north-south transect of the ice shelf (Budd, 1966). Annual accumulation rates were interpreted in all pits and cover the epoch 1958-62. In the following 1963-64 summer a network of stakes was set up at a spacing of 3.2 km along the north-south central region of the ice shelf. The network extended from 35 km from the ice front to 280 km from the ice front. These stakes were remeasured in the 1968-69 summer providing a 5 year net accumulation / ablation record. During the 1988-89 austral summer shallow (2m) core stratigraphy was carried out at twelve locations ranging from 180-200 km from the ice front near the confluence of the Charybdis/Scylla ice streams, to eight locations within the grounding zone, some 300 km from the ice front. Stakes were placed at each of these locations and remeasured in 1989-90 and 1990-91 producing a two year net accumulation/ablation record.

The ice shelf surface is flat with elevations varying from 40 m near the ice front to approximately 100 m , within the grounding zone some 300 km inland. The majority of the ice shelf surface is smooth with little microrelief. Surface microrelief is restricted to areas around the edge of the ice shelf where the katabatic wind dissipates as it flows down the ice sheet and glaciers onto the ice shelf. Snow accumulation rates increase away from the katabatic zones at the edge of the ice shelf (Budd et al., 1966).

The areal extent and shape of the ice shelf has changed significantly during the 1962 to 1990 period. In 1962 the ice shelf was at its maximum recent area and northerly extent with the ice front located approximately 35 km further into Prydz Bay than the ice front position in 1988. In late 1963 or early 1964, a huge iceberg (960 km^2) calved from the front of the ice shelf and caused a 60 km retreat in the position of the ice front (Budd et al, 1966). Since 1964 the ice front has advanced approximately 25 km to its present position.

Surface mass balance was found to decrease almost linearly with distance from the ice front by Budd et al (1966). Consequently, surface mass balance measurements on the Amery Ice Shelf are plotted as a function of distance from the respective ice front position for each epoch, in Figure 3.7.

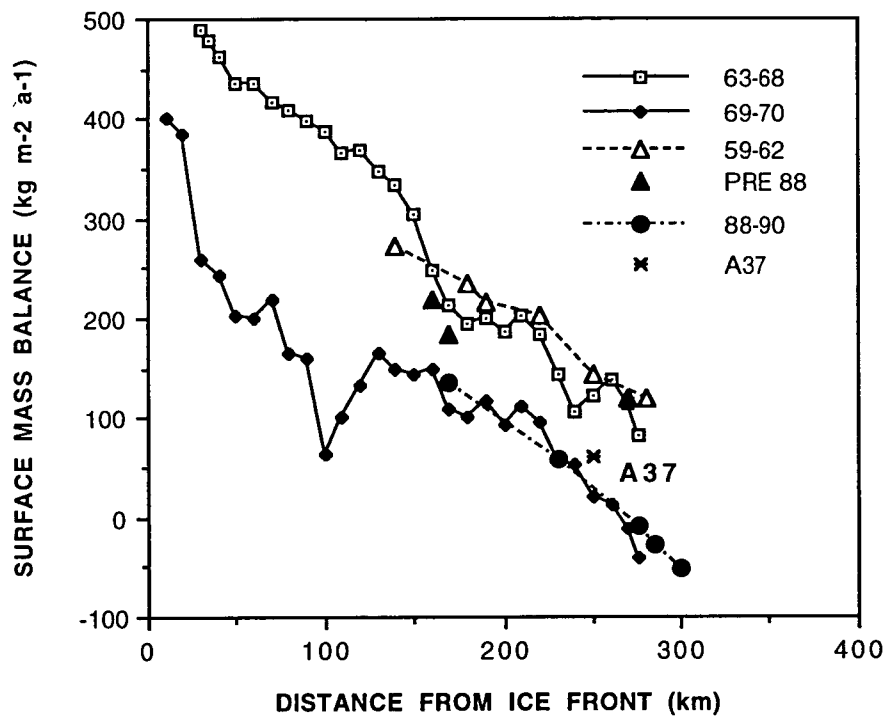

Figure 3.7 Surface mass balance is plotted as a function of distance from the respective ice shelf front position for each set of measurements, to allow comparison of the different epochs. The surface mass balance, changes from net accumulation to net ablation at ~250-300 km from the ice front. The 1964-68 and 1969-70 data are from Budd et al. (1967)and Budd et al. (1982). The 1959-62 data are from Landon Smith (1965). The 1988-90 and pre 1988 data are from stake and stratigraphy measurements made by the author. The pre 1988 data represent mean values for annual increments measured by stratigraphy within the 1988-89 ablation zone. It is assumed that they correspond to the 1960-70 period when accumulation rates were higher.

Two distinctly separate accumulation patterns are apparent in Figure 3.7. A high accumulation series is recorded for 1959-62 (pit measurements), 1963-68 (stake measurements) and pit measurements made in 1988 which were made on firn layers which unconformably lie beneath the 1988 ablation zone. These later pit measurements (designated as Pre 1988 in Figure 3.7) represent the accumulation rate prior to the recent change in the surface mass balance state to net ablation, and were plotted with respect to the pre 1964 ice front position. A second accumulation series defines a rate 100 kg m^{-2} a^{-1} lower and is recorded for 1969-70 (stake measurements), 1970-91 (stake measurement at A37) and 1988-90 (stake measurements). In the lower accumulation series the ablation zone is located 60 km further towards the ice front than for the higher series. It is implied in Figure 3.7 that the lower accumulation pattern is typical for the 21 year period between 1969-91 since the longest measured stake at A37 near G3 (1970-91) is located on the same line as both the 1969-70 and 1988-90 measurements. The 1988-90 stake measurements fall into the low accumulation pattern whilst the pit measurements made in 1988 at the same sites reflect accumulation rates which fall into the high accumulation pattern. At 270 km inland (near the grounding zone) the 1988 pit measurements indicate an accumulation rate of 120 kg m^{-2} a^{-1} whilst the 1988-90 stake measurements recorded an ablation rate of -8 kg m^{-2} a^{-1}. It was interpreted that the period of accumulation represented in the "Pre 1988" pit stratigraphy corresponded to the accumulation layers measured by Landon-Smith (1965) for the pre 1970 epoch when accumulation was higher, and ablation layers were absent. No more recent accumulation layers were interpreted at these sites due to net ablation over the last 3 decades.

Landon-Smith(1965) defined the inter annual variability of accumulation rate as 11% from pit measurements along the ice shelf. Therefore the 20% decrease in accumulation rates since 1970 indicates a significant change in the surface climatology of the Amery Ice Shelf and lower Lambert Glacier system. Analysis of the stratigraphic diagrams for snow pits measured by Landon-Smith in 1963 shows that the degree of melting from the existence of melt features in the firn was greatest in the 1956-59 period with little or no melt between 1960-63. The period of low melt corresponds to a period of relatively colder temperatures than the present across Antarctica between 1960-63 which is observed in the Mawson and Davis temperature records but not as marked as that in Wilkes Land (Jacka et al., 1984, 1992).

Thus the higher accumulation rates during 1960-63 may be partially due to a reduction in net ablation due to the colder temperatures. In contrast, the lower accumulation rates which occurred from 1969-1990 are associated with a 60 km expansion of the ablation area towards the ice front. The 1988-90 observations of the surface snows

and upper firn pack (in the same localities as Landon-Smith's observations relative to the ice shelf front) showed that free water was present throughout the upper firn. The extent of free water observed both on the surface and within the snowpack during 1988-90 indicates that net ablation since 1988 is similar to that interpreted by Landon-Smith in the late 1950's. Both periods have experienced higher ablation rates than during the 1960's. There is some evidence for higher regional summer temperatures (~1°C) during the 1970-1990 period in the incomplete Davis temperature record when compared to the early 1960's (Jacka et al., 1984, 1992). Budd (1967) measured monthly ice ablation rates at Mawson and reported a gradient in ablation of 80-100 kg m^{-2} a^{-1} per 1 degree change in temperature. Thus the variation in summer temperatures and melting may explain the 100 kg m^{-2} a^{-1} variation in surface mass balance between the higher pattern during the 1960's and the lower pattern observed since 1970.

3.7 ON THE RELATIONSHIP BETWEEN ACCUMULATION RATE, OXYGEN ISOTOPE COMPOSITION AND CLIMATE PARAMETERS

The regional firn core stratigraphic studies indicate that large temporal fluctuations in accumulation and oxygen isotope occur over interannual and interdecadal periods. They also show that the fluctuations may be regionally widespread or opposing on the decadal timescales. For example, increasing accumulation rates in Wilkes Land are coincident with decreasing accumulation rates in MacRobertson and Kemp Lands. The largest fluctuations in all the accumulation rate time-series occurs during the period since 1955-1960. The longest records from Law Dome show that the recent fluctuations since 1970 depart from perturbations about the long-term mean for the last century.

The primary climatological factors which contribute to the interpreted fluctuations in accumulation rate and oxygen isotope are air temperature, sea ice extent and concentration, and the atmospheric circulation. The relationships between accumulation and these factors are discussed below.

3.7.1 AIR TEMPERATURE

Accumulation in Antarctica is principally controlled by air temperature (moisture transport is limited by saturation vapour pressure of the cold air), distance to moisture source, topography, and, particularly in the coastal zone, by the frequency of

"precipitation" events which depend on the intensity of cyclonic activity (Pourchet et al., 1983). Empirical studies by Fortuin and Oerlemans (1990), Loewe, (1962) and Mellor (1963) do show correlation between temperature and accumulation (albeit for geographic rather than temporal variation) but the pattern of high accumulation in winter compared to summer arises from the increased intensity of cyclonic activity in winter, which overrides the accumulation signal produced by the effect of temperature and moisture transport. Therefore the total net accumulation varies in an opposite way to the total air column moisture throughout the year (Budd et al., 1995). Since precipitation events are accompanied by higher temperatures (Loewe, 1974) increased cyclonic activity leads to more frequent or long lasting events and to higher average temperatures and hence the observed correlation between accumulation and temperature (Morgan et al., 1991). The effect is most pronounced near the coast but even inland precipitation (of ice crystals from clear skies) is influenced by the advection of moist air over the continent by cyclonic activity (Bromwich, 1988). The accumulation signal has been shown to be coupled to changes in oxygen isotope value which can be applied as a proxy temperature signal. It is important to note that positive or negative fluctuations in mean oxygen isotope composition can be the result of changes in the bias of seasonal precipitation regimes or changes in the moisture source rather than solely changes in mean air temperature at the time of condensation.

Estimates of the temperature effect range from 3-4% per °C from general circulation models (Mitchell et al, 1990) to ~6-10% per °C for polar models (Huybrechts and Oerlemans, 1990, Budd and Simmonds, 1991). Estimates from the variation of the saturation vapour pressure of water over ice as suggested by Robin (1977) also give ~10% per °C. The time varying accumulation records for Wilkes Land, Law Dome and Kemp Land do show broad correlation with regional Antarctic temperatures but this cannot be a cause and effect relation with temperature alone, because the change in accumulation rates are much too large (20-25‰ per °C in Wilkes Land and Law Dome, and 40-50‰ per °C for Kemp Land).

3.7.2 SEA ICE EXTENT, CONCENTRATION AND ATMOSPHERIC CIRCULATION

Sea ice extent and concentration are highly correlated with temperature and are a major determinant in the general atmospheric circulation, especially cyclogenesis and the cyclone paths (Simmonds and Wu, 1993). Two types of cyclones have been observed in Antarctica (Schwerdtfeger, 1984). These are the coast-parallel migrating cyclones and cyclones originating in the lower to middle latitudes. The former type are strongly influenced by the sea ice extent and concentration. Sea ice characteristics

also determine the proximity of major moisture sources to the continent, and hence have a large effect on the source oxygen isotope composition of Antarctic precipitation. High sea ice concentration usually determines that the precipitation moisture source is located north of the sea ice edge whilst lower concentrations with significant open water leads provide moisture sources closer to the coast. Changes in the strength or tracks of cyclones can cause both local and mesoscale changes in the sea ice extent and concentration through the associated changes in windfields. For example, increased cyclonic activity can cause divergence in the sea ice field. This divergence causes changes in sea ice area and/or extent and allows the development of larger coastal polynyas, open water leads or thin ice within the pack, where relatively warm deep water rises and is available for moisture transport into the atmosphere (Worby and Allison, 1991, Jacobs, 1992) Simmonds and Budd (1991) in a GCM sensitivity analysis found that increased precipitation would occur over the southern sea ice regions and the coastal margins of Antarctica due to large changes in sensible heat fluxes which accompanied the growth in pack ice leads and the open water fraction. Jacka and Budd (1991) found that the annual maximum sea ice extent had been decreasing during the period 1973-89 in the Wilkes Land sector with a maximum decrease at the longitude 110°E near Casey. This decrease in sea ice extent corresponds to the period of rapid increase in accumulation rates on Law Dome and in Wilkes Land. Since the ice sheet receives the bulk of its precipitation during late autumn to late spring the maximum annual sea ice extent during August to October is the major determinant through its control on ice sheet continentality from the moisture source. The relationship between the variation in annual maximum sea ice extent and temporal accumulation patterns is investigated in detail in the following section.

3.8 REGIONAL ANALYSIS OF ACCUMULATION RATE AND OXYGEN ISOTOPE WITH AIR TEMPERATURE AND SEA ICE EXTENT VARIATIONS

An extensive data bank on coastal air temperature at each of the Antarctic stations is available for the period 1955 to 1992 (Jacka et al., 1984, 1992 and pers. comm.). Similarly, a data bank on the sea ice extent is available for the period 1973 to 1992 (Jacka, 1983, 1987 unpublished supplement) together with data on sea ice extent, area and concentration from satellite passive microwave observations (Gloersen et al., 1992). Since this data overlaps with the accumulation rate and oxygen isotope time-series for the period 1973-84 a detailed regression analysis was carried out to determine the connections between these parameters and the temporal variation in accumulation rates. The maximum annual sea ice extent was taken from the records

for the month of October. Bromwich (1983) showed that the sea ice extent and area lagged the mean coastal air temperature by one month for coastal East Antarctica. This was tested in this study for the Wilkes Land, Queen Mary Land and Kemp Land coasts and was found to be the case where a correlation between temperature and sea ice extent existed. The following discussion concentrates on the 1973-84 period but also discusses the wider implications of the regression analysis for the fifty year periods covered by the cores.

3.8.1 WILKES LAND AND LAW DOME

The Wilkes Land accumulation rates for the period 1973-84 were determined to be 15% above the mean rates for this century. Mean annual coastal air temperatures at Dumont d'Urville (Figure 3.8a) and Casey Station (Figure 3.8b) fluctuated widely during this period by up to 3.5 °C in 1980-81 with a general increase of 0.4 and 0.8°C, respectively (Jacka et al., 1984). Similarly, the sea ice extent at longitudes 110° E, 120° E and 130°E shown in Figure 3.9a have varied widely with a large fluctuation of some 400 km or 50% of the extent centred on 1978-82 (data from Jacka, 1983, 1987). Figure 3.9b shows the corresponding fluctuations in annual oxygen isotope for the GD03, GD06 and GD15 cores. Figure 3.9c shows the mean of the annual accumulation rates determined from the stratigraphic analyses of 10 m deep firn cores, located at 50 km intervals over a 750 km distance. The mean of the interannual accumulation rates in 10 spatially separated cores significantly reduces the noise due to surface microrelief. Regression analyses were applied to the data to detect correlation or connections between the populations.

A strong correlation exists between the 5 year filtered annual accumulation rates for GD03, GD06, GD15, DSS and DE08 and the five year filtered coastal air temperatures at Casey Station for the period 1958-84 (r = 0.82, 0.73, 0.90, 0.89 and 0.88, significant at the 99.5% level).

The mean annual accumulation rate pattern for the 10 eastern Wilkes Land sites is highly correlated to the interannual changes in sea ice extent at Longitude 120°E (r = 0.68, n=11, significant at the 95% confidence level). Accordingly, mean annual accumulation rates increased by 12.5 kg m^{-2} a^{-1} for a latitudinal reduction in sea ice extent of 100 km. Figure 3.10 shows the spatial accumulation pattern along 400 km of eastern Wilkes Land measured in 1981 and 1982 when a large fluctuation in sea ice extent and coastal temperature occurred. The mean annual spatial accumulation rates varied from 425 and 327 kg m^{-2} a^{-1} in 1981 and 1982 respectively, whilst coastal air temperature was ~2°C colder in 1982 than in 1981 at Casey and Dumont d'Urville .

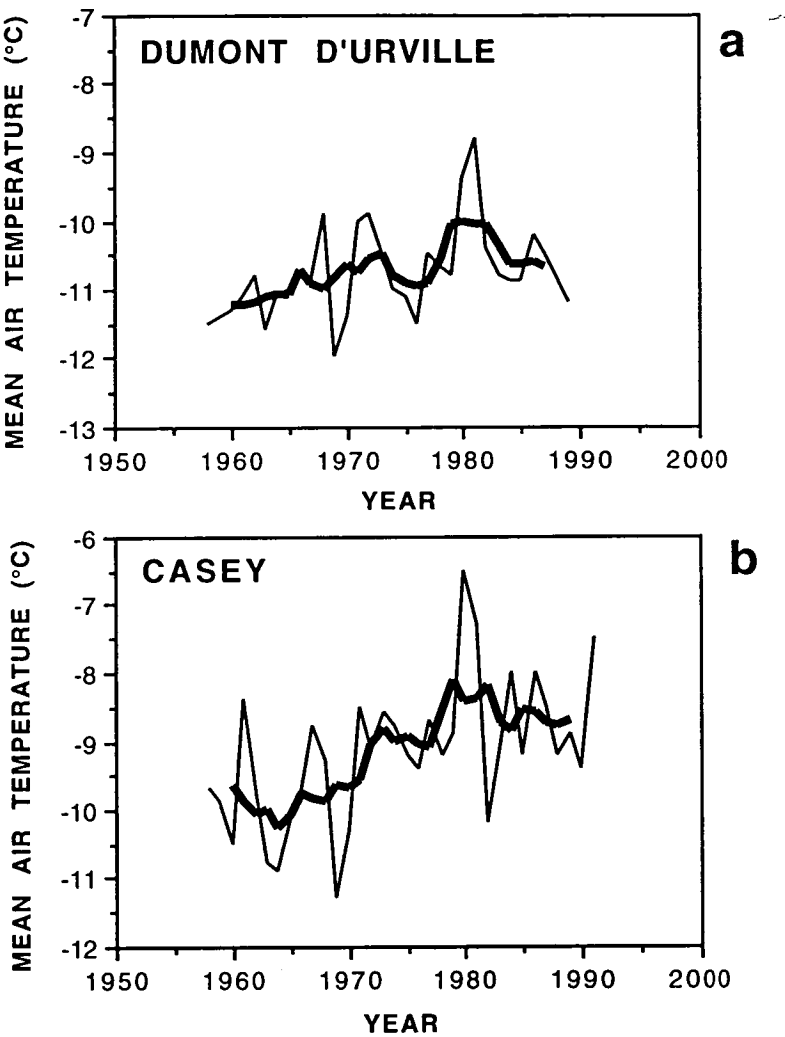

Figure 3.8 Mean annual air temperatures (after Jacka et al., 1983, 1987, unpublished data) for (a) Dumont d'Urville and (b) Casey. The bold line represents the 5 year smoothed mean temperature.

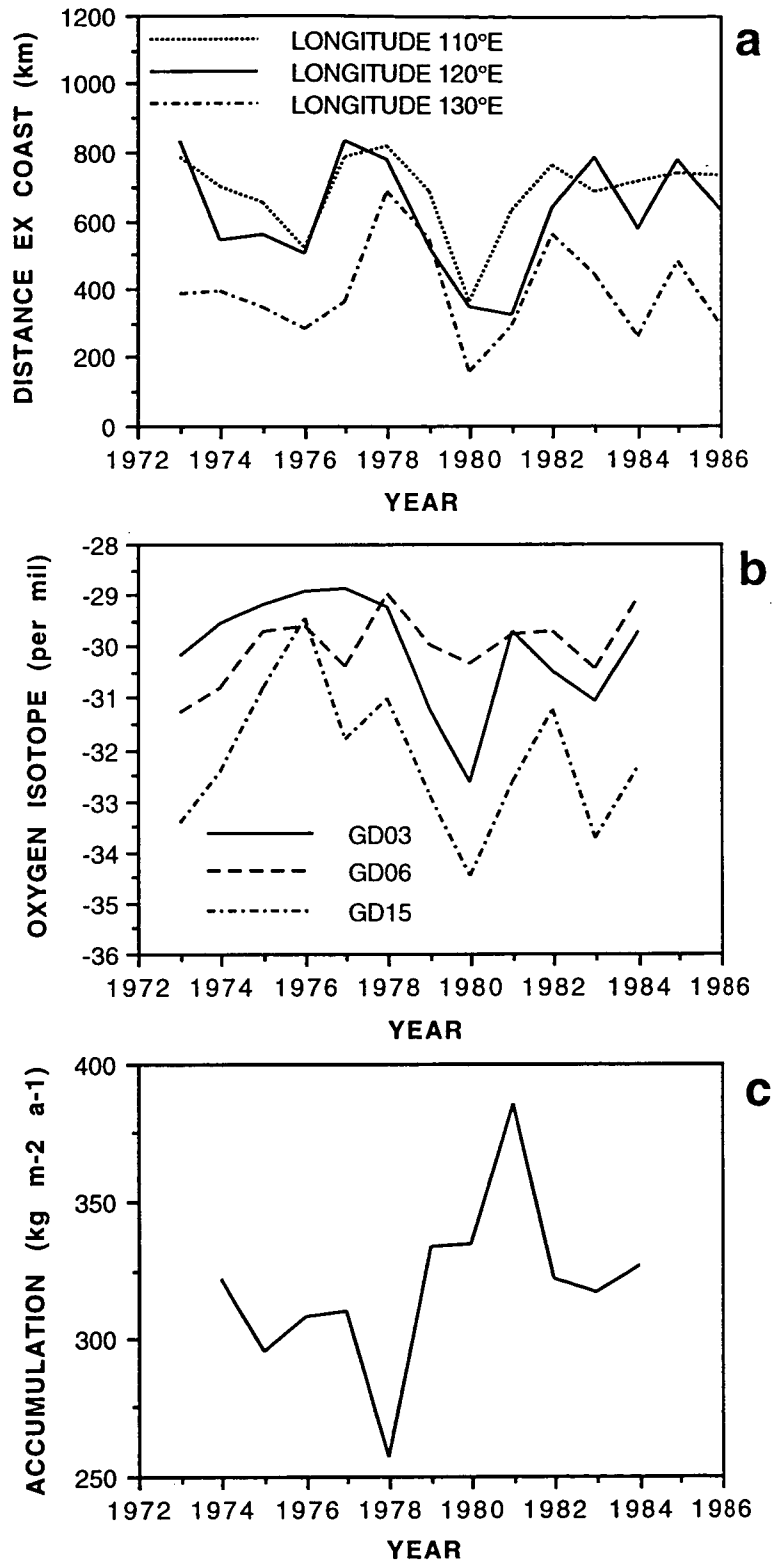

Figure 3.9 Comparison of temporal variation in eastern Wilkes Land of (a) sea ice extent, (b) mean annual oxygen isotope in the GD03 and GD06 cores, and (c) mean annual accumulation rate for the decade 1973-84. The mean accumulation rate was calculated from the decadal mean rate measured in 10 firn cores separated over a 750 km distance between longitudes 112°E and 130°E.

The 30% fall in accumulation rate from 1981-82 was associated with an 27% increase in sea ice extent from 2.05 to 2.6 millions of square km, and a 10% increase in sea ice concentration from 71% to 81% (after Gloersen et al., 1992).

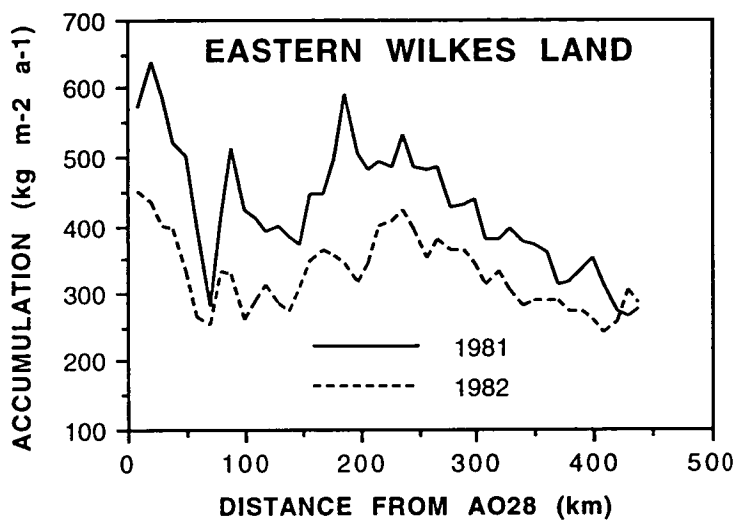

Figure 3.10 Spatial accumulation pattern measured along 400 km in eastern Wilkes Land from A028 (junction with the southern Wilkes Land Route) to GD08 for 1981 and 1982 (Goodwin, 1988a).

Mean coastal temperatures for the month of September at Casey and Dumont d'Urville and the changes in maximum sea ice extent at Longitude 110°E are significantly correlated ($r = 0.49$, $n=19$, significant at the 95% confidence level, and $r = 0.59$, $n=19$, significant at the 99% confidence level respectively). Accordingly, sea ice extent changed by 100 km/0.76°C and 100 km/0.79°C. A latitudinal isotopic gradient (change in $\delta^{18}O$ for a change in sea ice extent) of 0.0044‰/km was determined from a relationship between the September coastal air temperature, mean annual oxygen isotope at GD03 and the sea ice extent changes at Longitude 110°E ($r = 0.50$, $n=11$, significant at the 95% confidence level). This is in accordance with the bulk of the annual accumulation occurring from autumn to spring, when the sea ice extent is near its maximum.

A higher correlation between mean annual oxygen isotope in ice sheet surface snows and sea ice extent would result if the original precipitation had not been modified by

snow redistribution processes. The latter is the case for the GD06 and GD15 sites where the oxygen isotope is more strongly affected by snow redistribution processes. Since the GD03 and GD15 mean annual oxygen isotope profiles are correlated (r = 0.52, significant at the 95% level) and neither are correlated with the profile from GD06 it is suggested that the latter is the most affected by redistribution processes. It is important to note that all three profiles have the same +0.24‰ a^{-1} long-term increase in oxygen isotope for 1930-85. Thus the snow redistribution processes significantly affect the interannual comparisons but do not affect the long-term comparisons. This observation implies that neither differential moisture source changes nor differential changes in the seasonal precipitation patterns occur between the three sites. The latter is confirmed by the observed coincidence of storm events along the Eastern Wilkes Land traverse route and those recorded in the A028 automatic weather station data (Allison, 1985).

The Wilkes Land accumulation, air temperature and oxygen isotope parameters are not correlated at any other longitudes. The correlation between the mean annual oxygen isotope values in Wilkes Land and the changes in sea ice extent at Longitude 110°E suggests that the primary moisture source for precipitation falling in eastern Wilkes Land is located near the northern sea ice limit at this longitude. The correlation between the mean annual accumulation rates and the sea ice extent changes 10° further east at longitude 120°E indicates that the accumulation rates may increase as the reduction in sea ice extent at longitude 120°E triggers coast-parallel migrating cyclones to track further south and closer to the coast.

The location of the eastern Wilkes Land moisture source is just east of the centre of the quasi stationary cyclone near 100° E - 110° E in the circumpolar low - pressure trough, north-west of Casey Station (Bromwich, 1988). Analysis of mean winter monthly (JJA) sea-level pressure data (MSLP) for the circumpolar low - pressure trough over the period 1957-89 has shown that the trough has deepened at 110.5°E to the north of Casey over this period (Allan and Haylock, 1993). Figure 3.11 (after Allan and Haylock, 1993) shows that the trough has deepened below 985 hPa between 1966-71 and 1975-89, and becomes shallow with MSLP above 985 hPa between 1957-65 and to a slight extent in 1972-74. These pressure changes correspond to the recent accumulation changes in the eastern Wilkes Land cores and the Law Dome cores. The decrease in the mean sea-level pressure of 2.5 hPa between 1957-65 and 1975-85 corresponds to an accumulation rate increase of 21% in eastern Wilkes Land and 40% on Law Dome. The greater increase on Law Dome is due to its proximity to the pressure changes and reflects the increase in winter storm and precipitation events during this period. The large interannual fluctuation in accumulation rate and the

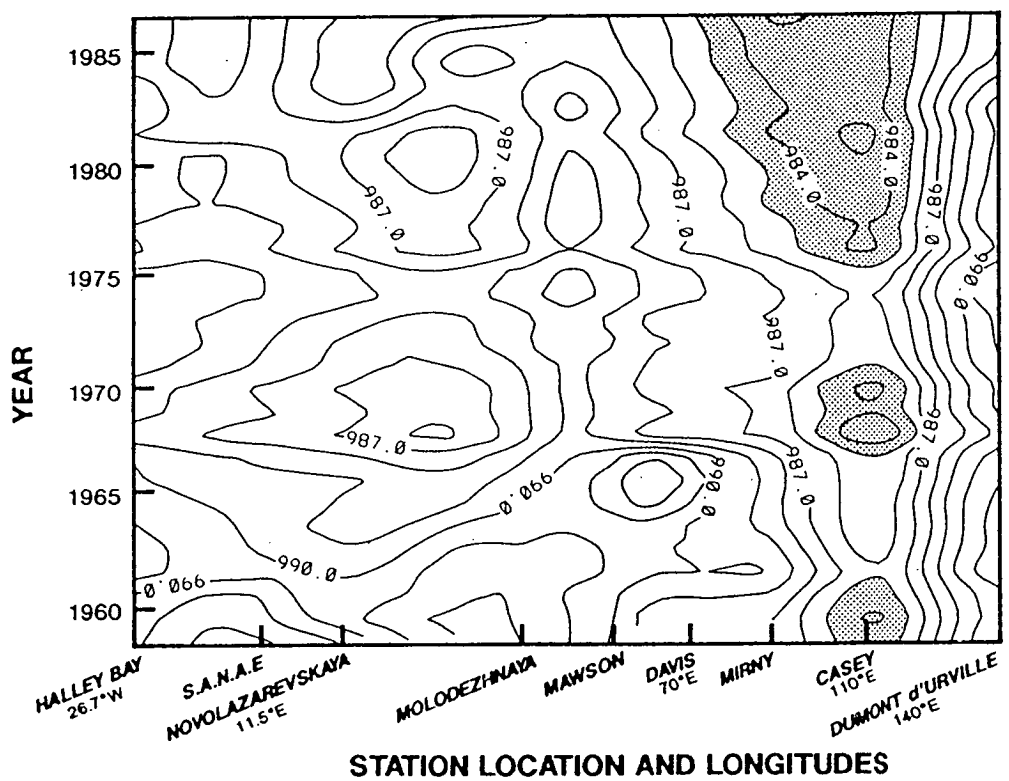

Figure 3.11 Time plot of contoured and smoothed MSLP during austral winter (JJA) at Antarctic coastal locations from Halley Bay (26.7°W, 75.5°S) to Dumont d'Urville (140.0°E, 66.7°S) from 1958 to 1987. MSLP is in hPa, with contours every 1 hPa. The shaded region is where MSLP is less than or equal to 985 hPa (after Allan and Haycock, 1993).

Casey coastal air temperature between 1980-82 is synchronous with the deepening of the trough to 983 hPa during this period. Since the mean sea-level pressure has been stable in the region east of 120°E longitude (Figure 3.11) the lesser change in accumulation rate experienced in eastern Wilkes Land can be related more to the reduction in the sea ice extent and concentration than to changes in atmospheric circulation. It is likely that the decrease in MSLP north of Casey has strengthened the surface windfield over the sea ice in the eastern Wilkes Land sector. This would have caused the divergence in the sea ice cover which is correlated to the increase in coastal air temperature at Dumont d'Urville. The overall increases in the oxygen isotope values in the Wilkes Land cores are most likely the combined result of increased air temperature, reduced sea ice extent and an increase in storm events during 1965-85 period.

Whilst the above discussion has described the probable links between the atmospheric circulation and the temporal ice sheet precipitation pattern, there remains considerable variation in the corresponding accumulation rates as shown in Table 3.2. The GD03 and GD15 sites show a similar increase of 15-21% for the 1975-85 decade over the long-term 1930-70 mean, despite being 600 km apart and 330 m different in elevation. This is not the case for GD06 (located only 150 km from GD03) which experienced a much lower increase of 6% for the same period. In contrast the oxygen isotope values have changed by +0.2-0.4‰ higher than the increases at GD03 and GD15. The GD06 site may experience a stronger katabatic flow year-round than GD03 and GD15 due to the mesoscale topographic convergence of the windfield near GD06 (Figure 2.1). Hence, it is possible that the accumulation rate at GD06 is more strongly controlled by surface snow erosion processes than at either GD03 or GD15. The higher increase in oxygen isotope at GD06 may be partly attributed to greater net erosion of winter snowfall.

3.8.2 QUEEN MARY LAND

The Queen Mary Land accumulation rates for the period 1973-84 are shown in the GF12 core. Since only one core was obtained in this region it is difficult to make a comparative analysis with the multiple core times-series in Wilkes Land. The major limitation of a single core is the level of noise due to surface microrelief in the interannual estimates, and whether the location is representative of the area. However, the former is only a minor problem at GF12 since the site experiences extremely high accumulation rates of 530 kg m^{-2} a^{-1} which are equivalent to those at coastal sites ~1000 m lower in elevation. Thus annual accumulation time-series at the GF12 site should proportionately record the annual precipitation pattern.

The accumulation rates at GF12 experienced two large oscillations during the 1955-85 period with a periodicity of about 12-13 years (Figure 3.2d) following a relatively stable period between 1940-1955. During the 1973-84 period GF12 experienced the second of these oscillations which is shown in Figure 3.12c. The rates decreased from a recent high at 1970 to a low at 1976 before increasing to 1984. The corresponding mean annual oxygen isotopes for GF12 are shown in Figure 3.12b. The interannual sea ice extents are plotted for Longitudes 60°E, 70°E and 90°E in Figure 3.12a. The most obvious feature in this plot is the large fluctuation or increase in sea ice extent at longitudes 80°E and 90°E between 1978-82 This is opposite to the large decrease observed in the sea ice extents off eastern Wilkes Land (Figure 3.9a) for the same period. Sea ice growth off Queen Mary Land is positively correlated with a decrease in coastal air temperature at Mirny of 2.8°C and 2.1°C at Davis (Jacka 1983) for 1980-82. A regression analysis was applied to this data for the 1973-84 period.

The inter-annual fluctuations in the accumulation rate pattern at GF12 (longitude 97° 11'E) are not correlated with changes in sea ice extent. In contrast, the mean annual oxygen isotope values are negatively correlated with the sea ice extent at longitude 70°E with an ($r = 0.43$, $n=12$, which is significant at the 95% confidence level). The oxygen isotopes generally decrease as the sea ice extent migrates northwards contrary to the relationship in Wilkes Land. The latitudinal gradient in oxygen isotope was calculated as 0.0037‰/km. The mean annual oxygen isotope values at GF12 are correlated with the mean annual temperatures at Davis Station (Longitude 78) ($r = 0.45$, $n=12$, significant at the 90% confidence level. No correlation was observed between Mirny temperatures (Jacka et al., 1984) and GF12 oxygen isotopes. Jacka and Budd (1990) reported that the long-term (1973-89) increase in sea ice extent at 80°E-90° E was anomalous with the long-term decrease for East Antarctica between 20°E-180°E. These characteristics indicate that the fluctuations in accumulation rate at GF12 are most likely determined by changes in atmospheric circulation rather than sea ice cover.

A quasi-stationary long-wave trough is centred at 110°E north-east of GF12 and extends from longitude 70°E to 120°E in the circum-polar circulation. The interannual variation in sea ice extent for the 1973-84 period reaches a peak in this sector of Antarctica between 80-100°E with fluctuations of 400-500 km. In contrast the sea ice extent at the longitudes 70°E and 120°E at the edges of the quasi-stationary long-wave trough has varied by 100-200 km. The time plot of mean winter MSLP in the East Antarctic circum-polar trough (Figure 3.11) shows that the MSLP north of GF12 has

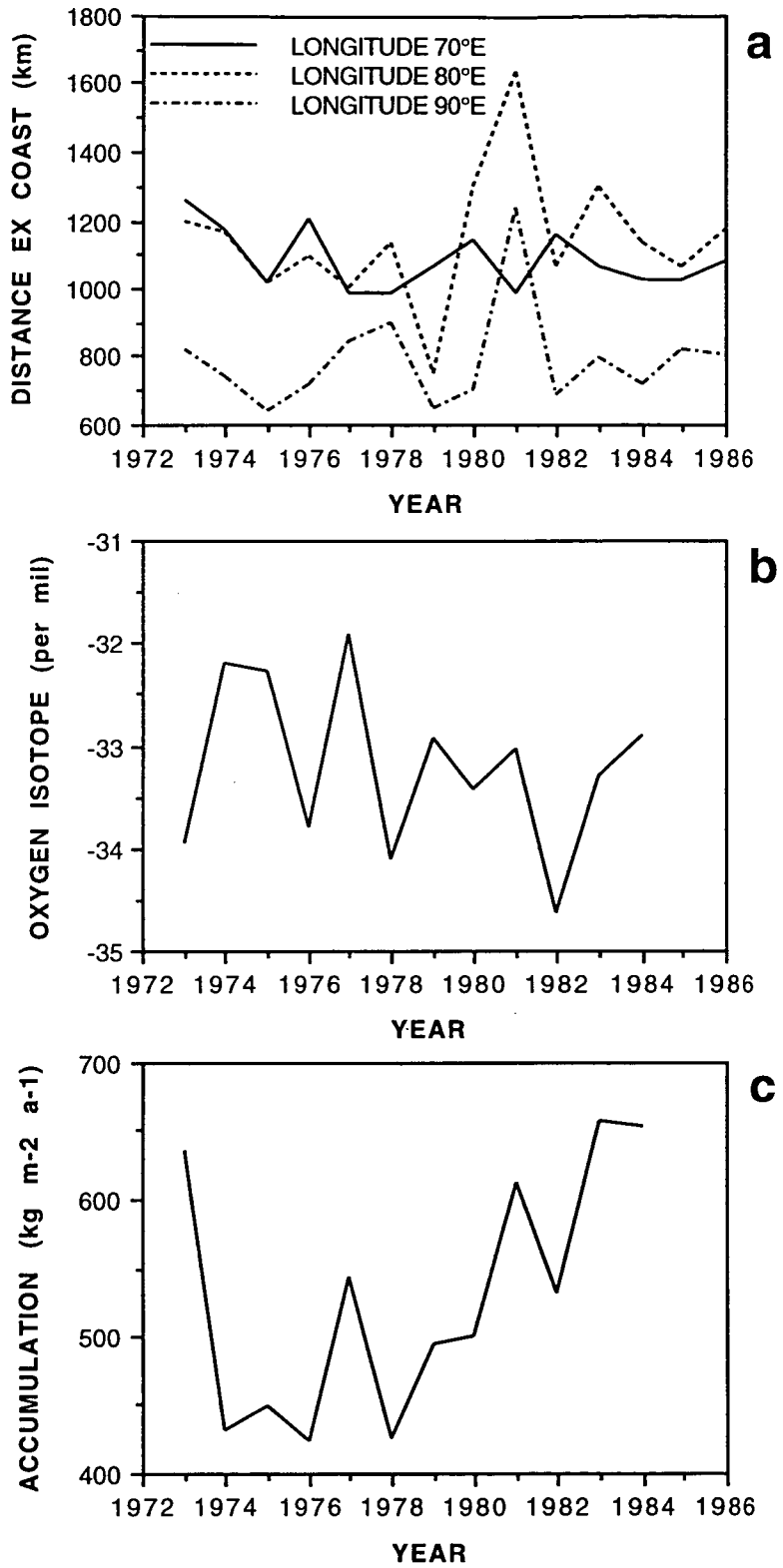

Figure 3.12 Comparison of temporal variation in Queen Mary Land of (a) sea ice extent, (b) mean annual oxygen isotope in the GF12 core, and (c) mean annual accumulation rate for the decade 1973-84. The sea-ice extent data are from Jacka (1983, 1987).

decreased by 1.5-2 hPa during 1975-89 (Allan and Haycock, 1993). It is likely that this has increased the cyclone intensity and the surface windfield, resulting in a divergence in the sea ice cover and a fluctuation in sea ice extent.

The above regression analysis suggests that the parent moisture source for GF12 is located between longitude 70°E and 80°E. The oxygen isotope composition of the sea water within the sea ice and close to the coast is more depleted than in the open ocean because of: the upwelling of ice sheet meltwater in the open water leads, and; other effects such as fractionation associated with the formation of sea ice. Thus the decreasing oxygen isotope values in the GF12 core coupled with the increased sea ice extent suggests that as the sea ice cover expands northwards the parent moisture is sourced from open water leads within the sea ice zone rather than the open ocean to the north. An increase in open water leads would result from cyclone intensification as discussed above. The overall decrease or depletion in oxygen isotopes between 1940-85 is likely to reflect the shift to a more depleted moisture source particularly since 1970. The large 30% oscillation in accumulation rates at GF12 since the late 1950's is synchronous with the fluctuations in winter MSLP at 100°E. The rapid increase in accumulation rates between 1965-71 corresponds to the ~1.5 hPa decrease in the trough MSLP. Similarly the accumulation rates rapidly fell from 1972-76 as the MSLP increased by 1.5 hPa. Since 1976 the accumulation rates have rapidly increased as the mean MSLP have fallen by ~3 hPa. It is likely that this variation in accumulation rate is the combined function of MSLP fluctuations and their effect on the circum-polar cyclone tracks and the late autumn and winter precipitation pattern.

3.8.3 MAC.ROBERTSON AND KEMP LANDS

The accumulation rates between 1973-84 at LGB00, MGA and E065 in Kemp Land are characterised by a slight increase during the 1970's before a sharp decrease to a minimum rate for the total 1955-92 period (Figure 3.5). This sharp decrease in Kemp Land accumulation rates occurs during a period when accumulation rates were increasing in Queen Mary Land, Law Dome and in Wilkes Land. Mean annual coastal air temperature at Mawson Station (longitude 63°E) cooled during this period by 1.5-2.5°C (Jacka et al., 1992). The mean annual coastal air temperatures at Mawson Station and Molodezhnaya are shown in Figure 3.13a and 3.13b respectively. The maximum sea ice extent at longitudes 60°E, 50°E and 40°E is shown in Figure 3.14a to have fluctuated between 200-400 km during the 1973-84 period. The mean annual oxygen isotope ($\delta^{18}O$) values for LGB00 and MGA are shown in Figure 3.14b and fluctuate between 2.5-4.5‰. The corresponding mean annual accumulation rates are shown in Figure 3.14c and fluctuate on the order of 100 kg m^{-2} a^{-1}.

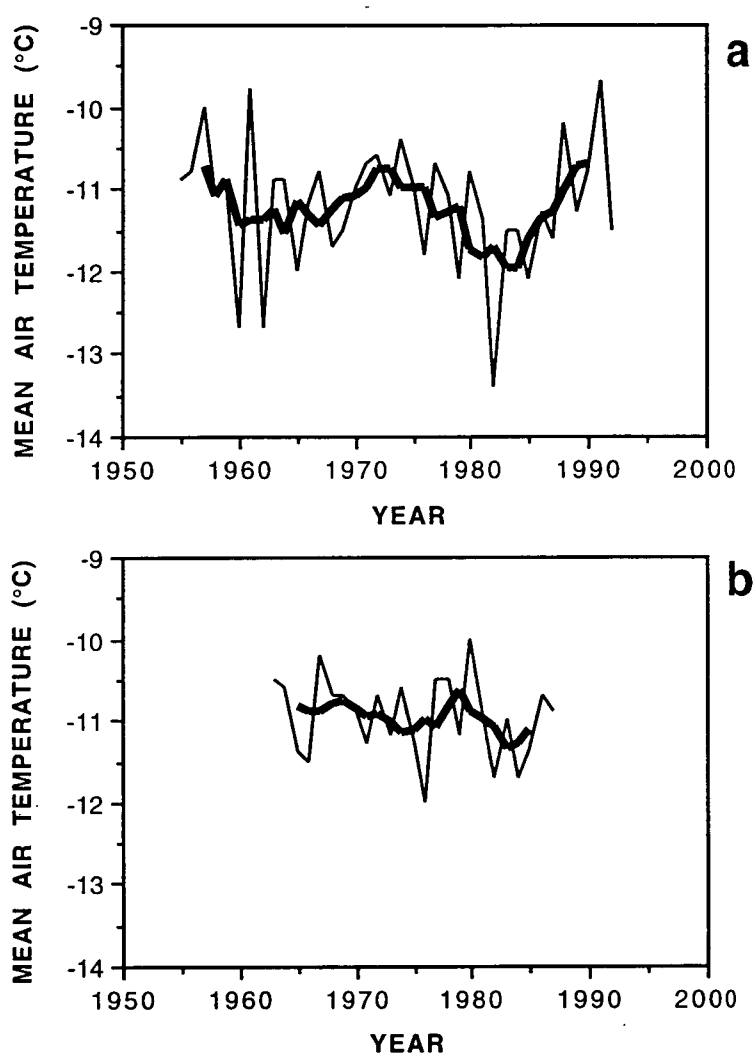

Figure 3.13 Mean annual air temperatures (after Jacka, 1984, 1992, unpublished data) for (a) Mawson and (b) Molodezhnaya. The bold line represents the 5 year smoothed mean temperature.

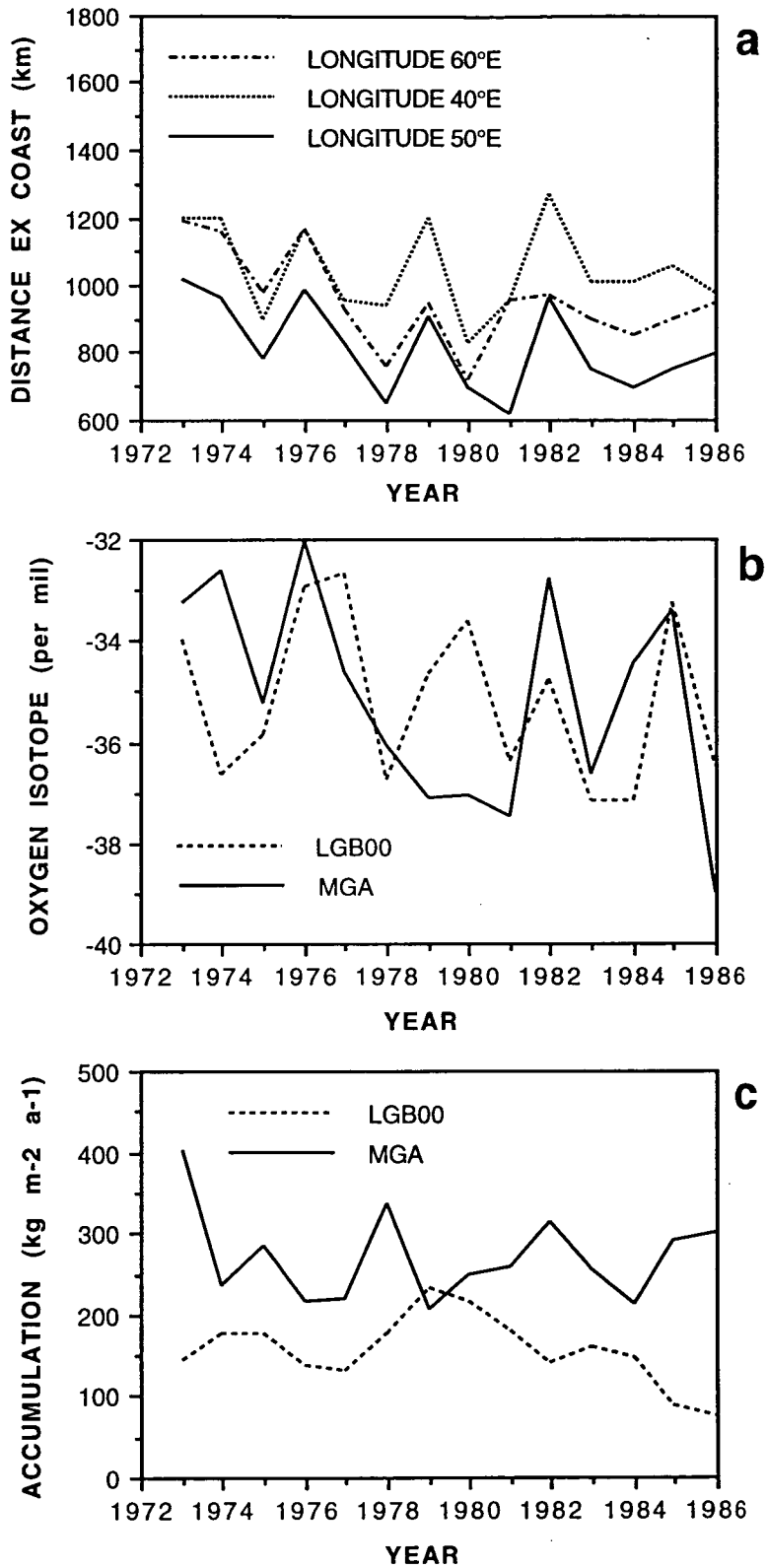

Figure 3.14 Comparison of temporal variation in MacRobertson and Kemp Lands of (a) sea ice extent, (b) mean annual oxygen isotope in the MGA and LGB00 cores, and (c) mean annual accumulation rate for MGA and LGB00 for the decade 1973-84. The sea -ice extent data are from Jacka (1983, 1987).

Regression analyses were applied to the data to detect any connections between the populations.No correlation was detected between the mean LGB00 and MGA annual accumulation rates and maximum sea ice extent. This was partly expected due to the high level of surface noise in single cores from katabatic snow redistribution processes. In comparison the mean annual oxygen isotope profiles in both cores show reasonable correlation except for 1978 where a large dune had formed during summer-early autumn at MGA. This indicates that the snow redistribution processes have less effect on modifying the mean annual oxygen isotope value than on the annual mass of snow accumulated. The mean annual oxygen isotopes for MGA and LGB00 are correlated with sea ice extent at 50°E and 60°E longitude respectively ($r = 0.758$, $n=12$, significant at the 99% confidence level, and $r= 0.484$, $n=12$, significant at the 90% confidence level). The mean annual oxygen isotope values increase (become enriched in $\delta^{18}O$) with increasing sea ice extent, similar to the pattern in Wilkes Land. The latitudinal gradient in oxygen isotope is 0.010‰ km^{-1} which is equivalent to the 0.009‰ km^{-1} gradient calculated by Bromwich (1983) for precipitation and sea ice extent in the Syowa region, further to the west (Figure 1.1).

A strong correlation exists between the five year filtered annual accumulation rates at LGB00 and MGA, with the five year filtered coastal air temperatures at Molodezhnaya approximately 600 km to the west ($r = 0.79$ and 0.65 which are significant at the 99.5% and 97.5% confidence levels). Molodezhnaya and Mawson are the only two of thirteen Antarctic stations to have experienced a temperature cooling trend between 1973-89 (Jacka and Budd, 1990). This cooling trend is synchronous with the increasing trend in sea ice extent at 80°E north of Prydz Bay. The Molodezhnaya temperatures and the Kemp Land accumulation rate pattern appears to lag the Mawson temperatures by ~5 years for this decade.

Thus both the accumulation-temperature relationships and the accumulation-sea ice extent relationships show a strong link between the ice sheet accumulation in Kemp Land and the sea ice and climate in the vicinity of Molodezhnaya. Figure 3.11 shows that the MSLP at Molodezhnaya have been reasonably stable between 1970-89. This suggests that the rapid accumulation decrease in Kemp Land between 1980-85 is likely to be in response to the air temperature decrease and changes in the local atmospheric circulation. The latter may involve a northerly shift in the cyclone tracks towards the sea ice edge.

Further east, in the Prydz Bay region an increase in sea ice extent is synchronous with the 20% (~100 kg m^{-2} a^{-1}) decrease in the accumulation rates over the Amery Ice Shelf since 1970, and the decrease in air temperature recorded at Mawson. During this time

the mean annual sea ice extent has increased by ~90 km. However, the corresponding latitudinal accumulation rate/sea ice extent gradient of 94.5 kg m^{-2} a^{-1} 100 km $^{-1}$ is far too large to be attributed to the variation in sea ice extent, alone It is more likely that the decrease in Amery Ice Shelf accumulation rates is determined principally by changes in atmospheric circulation, as suggested by the MSLP (Figure 3.11). These have remained stable from 1970-1980 with a decrease of ~1 hPa since 1980 at the location of the Amery Ice Shelf (longitude 72°E). In addition, the decrease in regional air temperatures between 1970-80 (0.7-1.0°C, Figure 3.13) may have lowered precipitation by up to 10% based on the changes in the saturation water vapour pressure. During this period of decreased air temperatures it is likely that the open water fraction within the sea ice would have been reduced. This may have significantly increased the continentality of the Amery Ice Shelf by shifting the moisture source and the cyclone tracks away from the coast towards the edge of the sea ice. Thus the effective change in the continentality may be significantly greater than the estimated ~90 km expansion in the sea ice extent.

3.9 DISCUSSION ON THE EAST ANTARCTIC TEMPORAL ACCUMULATION PATTERN

This study has shown that Wilkes Land and Law Dome have experienced an increasing trend in accumulation rates since 1930. The region affected extends from the coastal zone deep into the ice sheet interior to Dome C and Vostok (Pourchet et al., 1983). The long-term accumulation rate pattern from Law Dome (Morgan et al. 1991) indicates that this may have been occurring since 1850, although the increase has been more rapid since 1970. The increase in accumulation rates in these regions is probably due to:

- a general Antarctic wide increase in temperature measured as ~1°C since 1960, (Jacka and Budd, 1991),
- a reduction in sea ice extent ,
- a deepening of the long-wave trough at 110.5°E and,
- an intensification of circum-polar cyclones with tracks closer to the coast.

The relatively narrow zone of sea ice in the Wilkes Land sector of East Antarctica ensures that this region has a close link to open water and Southern Ocean climate. This is particularly demonstrated by the large increases in accumulation rates on Law Dome, which is located closest to the sea ice edge. A major regional determinant of this pattern is probably the deepening of MSLP trough in the circum-polar circulation

(centred at 110.5°E north west of Casey Station). The region affected by this intensification in MSLP extends from 70°E to 120°E. Bromwich (1988) described a high poleward moisture transport on the ice sheet at longitudes to the east of the quasi-stationary trough which has been verified by the high accumulation rates in eastern Wilkes Land (Goodwin, 1990). In contrast, Bromwich (1988) described a net equator-ward moisture transport in regions to the west of the trough. This is in agreement with the very low accumulation rates which were described for Kemp Land in Chapter 2. This study has also shown that the long-term accumulation rates near the centre of the trough in Queen Mary Land have experienced large oscillations with a period of ~13 years. Unlike Wilkes Land, no long-term trend in accumulation rates has occurred in Queen Mary Land since 1940. These large oscillations in accumulation rate may be linked to oscillations in the MSLP intensification within the long-wave trough. Similar large oscillations in accumulation rate occur in other firn core records. One such oscillation occurs in the Wilkes Land cores, particularly the GD15 core and the Dome C core (Petit et al., 1982) between 1945-1955. The Dome C core has experienced three such oscillations since 1900 with a period of ~20 years. The most significant oscillation in the Queen Mary Land, Wilkes Land and Terre Adélie accumulation time-series occurs between 1955-1965. This event has also been recorded in the accumulation time-series for the Antarctic Peninsula (Peel, 1992).

These fluctuations in accumulation rate are shown to influence entire drainage basins. This has important consequences for the determination of the long-term effects of climate change on the ice sheet. However, Zwally (1983) made the observation that decreased sea ice in one Southern Ocean sector is often balanced by an increase elsewhere. This has also been observed by Jacka and Budd (1991) in conjunction with the coastal air temperature pattern. This meridional alternation in the surface temperature and sea ice extents may be linked to MSLP fluctuations in the troughs centred at 110°E off western Wilkes Land and at 25°E off Dronning Maud Land.

Isaksson et al. (submitted) reported a 60 year accumulation record from Core E at 700 m elevation and longitude 12.5°W in coastal Dronning Maud Land. The Core E accumulation record shows an overall accumulation decrease of ~20% (significant at the 90% confidence level) between 1931 and 1991. The interdecadal accumulation rates have fluctuated widely with a rapid decrease in accumulation rates from 1976-1991. No trend in accumulation rates was reported from the second core in the interior of Dronning Maud Land at 2900 m elevation. The mean annual oxygen isotope ($\delta^{18}O$) value has increased by 2.2‰ between 1931-1991. Isaksson and Karlen (1994) reported that mean annual accumulation rates measured in seven firn cores between 100-1200 m elevation in Ritscherflya, Dronning Maud Land had

decreased by 50% between 1976-1988. The decrease in accumulation rates since 1976 is correlated with a temperature decrease of ~1°C at Halley Base located at 25°W some 500 km to the west of the core sites. The decreasing trend in mean annual accumulation and coastal air temperature in Dronning Maud Land are synchronous with the mean increase in maximum sea ice extent of 80-100 km. These patterns in accumulation rate, oxygen isotope, coastal air temperature and sea ice extent are comparable to those observed in Kemp Land. Both regions are located near long-wave ridges at the western edge of the quasi-stationary trough positions with a similar net seaward moisture transport and low accumulation rates (Bromwich, 1988). The respective accumulation and elevation change relationships of ~40%/°C and 50%/°C for Kemp Land and Dronning Maud Land for the 1976-88 period can not be explained by air temperature and sea ice changes alone. Therefore the large accumulation changes indicate that significant changes in atmospheric circulation have occurred in these regions. Such changes in atmospheric circulation may be forced by the fluctuation in MSLP intensity within the quasi-stationary long-wave troughs.

The ice sheet accumulation rate time-series may be applicable as proxy MSLP and sea ice extent indicators if the observed interactions between ice sheet accumulation, MSLP and sea ice extent during the 1957-89 period are typical. Accordingly, the decreased accumulation rates in Wilkes Land between 1955-65 may be correlated with increased sea ice extent coupled with the temperature cooling observed during this period. The corollary exists for Kemp Land where accumulation rates were higher during the 1955-65 period than during the 1980's both on the coastal slopes and on the Amery Ice Shelf. There are a number of decadal oscillations in the accumulation rate time-series which indicate that similar temporal patterns in accumulation rate have occurred throughout Wilkes Land to Queen Mary Land. Alan and Haylock (1993) have shown that the reversal of MSLP anomalies between Australia and Antarctica influence the precipitation trend in south-western Australia. This study has shown a similar relationship exists between MSLP anomalies in the long-wave trough at 110.5°E and ice sheet accumulation rates on Law Dome and in Wilkes Land. According to Alan and Haylock (1993) this relationship may be linked to low-frequency characteristics of the ENSO phenomenon. However, these interdecadal fluctuations are superimposed on the long-term climate trends which reflect continental and hemisphere scale changes.

3.10 ACCUMULATION-TEMPERATURE AND ACCUMULATION-SEA ICE EXTENT RELATIONSHIPS

Future and past accumulation rate patterns have often been determined as a function of temperature change. This has occurred primarily because of the relationship between air temperature and the moisture carrying capacity defined by the saturation water vapour pressure. However, in the previous sections it has been shown that the observed changes in the accumulation rate pattern are at least twice those expected due to the changes in the saturation water vapour pressure alone. The greater observed changes in accumulation rates have been attributed to changes in other parameters such as; MSLP, sea ice extent and concentration and circum-polar cyclone frequency, tracks and intensity. These changes are a function of mean air temperature change in some way and hence can be related as some function of temperature. Since the data sets are spatially and temporally limited, the changes are expressed as a single term function of temperature, either as change in sea ice extent/change in temperature or, change in accumulation rate/temperature. It should be noted that these relationships are also often derived from a proxy temperature record such as the oxygen isotope $\delta^{18}O$ record since the air temperature record is not available over the ice sheet.

Accumulation-temperature relationships

The correlation of the five year filtered accumulation rate time-series with the five year filtered coastal air temperatures enables the determination of a direct relationship between the total accumulation rate change and air temperature. The total accumulation rate change refers to the change in accumulation rates due to variations in saturation water vapour pressure, sea ice extent and concentration and atmospheric circulation changes. These parameters are not mutually exclusive but an attempt to separate out their contributions to the total observed changes in accumulation has been made.

The eastern Wilkes Land and Law Dome accumulation rate time-series were found to be correlated to the coastal air temperatures at Casey Station at the 99.5% confidence level. The resulting linear accumulation-temperature relationships are listed below in Table 3.4. The accumulation is in kg m^{-2} a^{-1} , the temperature in °C and the accumulation change is calculated as a percentage of the 50 year mean for each site.

TABLE 3.4 ACCUMULATION-TEMPERATURE RELATIONSHIPS FOR WILKES LAND AND LAW DOME

Site	Relationship	Accumulation change %/T ℃
GD03	A = 788.2 + 49.8 T (r=0.82)	16%
GD06	A = 730.0 + 42.4 T (r=0.73)	13%
GD15	A = 796.9 + 52.7 T (r=0.90)	18%
DE08	A = 3628.8 + 265.7 T (r=0.88)	25%
DSS	A = 2038.7 + 144.4 T (r=0.89)	25%

For comparison the mean change in eastern Wilkes Land accumulation rate per change in mean oxygen isotope $\delta^{18}O$ value from Table 3.2 is ~18%/°C using a transfer relationship of 0.79‰/°C (Thwaites, 1987). Similarly, the mean change in Law Dome accumulation rate per change in mean oxygen isotope $\delta^{18}O$ value from Table 3.2 is ~36%/°C. However, the $\delta^{18}O$ on Law Dome are probably affected by a change in moisture source associated with MSLP decrease and the divergence of the sea ice cover.

The Kemp Land accumulation rate time-series were found to be correlated to the coastal air temperatures at Molodezhnaya Station at the 97.5% confidence level. The resulting linear accumulation-temperature relationships are listed below in Table 3.5. The accumulation is in kg m^{-2} a^{-1} , the temperature in °C and the accumulation change is calculated as a percentage of the thirty and fifty year mean for the respective sites.

TABLE 3.5 ACCUMULATION-TEMPERATURE RELATIONSHIPS FOR KEMP LAND

Site	Relationship	Accumulation change %/T ℃
LGB00	A = 1178.1 + 91.8 T (r=0.79)	51%
MGA	A = 1177.1 + 84.5 T (r=0.65)	32%

The accumulation-temperature relationship for Kemp Land calculated from Table 3.3 is 20%/°C using a transfer function of 0.80‰/°C (Higham, 1994). The lower estimate

calculated from the corresponding mean oxygen isotope values is largely due to changes in the moisture source. The latitudinal gradient in oxygen isotope value in Kemp Land of 0.010‰/100 km is twice that calculated for Wilkes Land. Thus small changes in the location of the moisture source in the Enderby -Kemp Land sector can produce large changes in the oxygen isotope value of ice sheet precipitation. The large 32-51‰/°C relationship for Kemp Land which was calculated by linear regression with the Molodezhnaya air temperatures illustrates the effect of atmospheric circulation changes rather than the change in saturation water vapour pressure or sea ice extent and concentration. Similarly the accumulation-temperature relationship of ~50‰/°C for Dronning Maud Land (calculated after Isaksson et al, submitted) also shows the large variation in accumulation rate probably due mainly to atmospheric circulation changes.

Accumulation-sea ice extent relationships

A broad relationship between change in sea ice extent and the corresponding change in accumulation rates can be determined for the regions where the present accumulation pattern is largely controlled by the proximity to open water, such as in Wilkes Land. The latitudinal gradient in Wilkes Land accumulation for a 100 km change in the maximum sea ice extent was calculated as 12.5 kg m^{-2} a^{-1} from the linear regression of the mean annual Wilkes Land accumulation rate and the variation in sea ice extent at Longitude 120°E. This is equivalent to a latitudinal gradient of 4%/100 km by applying the gradient to the mean accumulation rate of 309 kg m^{-2} a^{-1} for eastern Wilkes Land at 2000 m elevation. This latitudinal gradient in accumulation per sea ice extent was converted to an accumulation-temperature relationship by applying the latitudinal gradient in coastal air temperature per sea ice extent changes. The latter gradient was calculated by linear regression between the variation in maximum sea ice extent at longitude 120°E with the preceding month's coastal air temperatures at Dumont d'Urville. This produces a latitudinal gradient in coastal air temperature of 0.60°C/100 km which is equivalent to the mean gradient calculated for Antarctica by Jacka and Budd (1990). Thus the variation in accumulation rates in eastern Wilkes Land with the variation in the maximum sea ice extent is 7%/°C. The interannual comparison of 1980-82 in Wilkes Land showed that the accumulation rate varied by 15%/°C with an equivalent change in sea ice extent of 110 km/°C and in sea ice concentration of 5%/°C.

Budd and Simmonds (1991) reported the results of a GCM study which determined that ice sheet accumulation rates would increase by 48% if the total Antarctic sea ice cover was removed. The increase in ice sheet accumulation is the direct result of the

increased sensible-heat flux between the ocean surface and the atmosphere. Simmonds and Budd (1991) in a companion study used a GCM to determine the sensitivity of atmospheric circulation to fractional changes in the open water leads in the sea ice cover. They found a monotonic sensitivity of precipitation and surface air temperature over the coastal margin of Antarctica with the fraction of open water leads. Since they related the precipitation increase due to fractional changes in open water it is possible to derive an estimate of the total ice sheet accumulation changes as a function of open water within the sea ice cover. Thus for a 5%, 50%, 80% and 100% fraction of open water in the sea ice, the total ice sheet accumulation rates would change by, 7%, 28%, 34% and 48% respectively. The GCM calculated variation in accumulation rates for a 5% change in open water leads is equivalent to that determined from the field data. It is not possible to test the larger changes since the field data do not exist.

Discussion

Since the variation in accumulation due to changes in the saturation water vapour pressure for polar regions is estimated as ~10%/°C (Budd and Simmonds, 1990) and the variation due to sea ice extent is 7%/°C, the total accumulation change without additional atmospheric circulation changes is 17%/°C. This is equivalent to that observed in eastern Wilkes Land. Peel (1992) also reported an increase in accumulation rate of ~15-20% since 1950 in ice core data from three sites on the Antarctic Peninsula which he attributed to an increase in air temperature and changes in the sea ice extent alone. These lower rates of change imply that the higher rate of change on Law Dome of 25%/°C contains up to ~8%/°C due to atmospheric circulation changes, such as the observed deepening of the MSLP in the quasi-stationary long-wave trough north of Casey Station. However, the 25%/°C rate for Law Dome may be typical of the variation in accumulation rate along the coastal margins of East Antarctica below ~1000 m because of their close proximity to the source of the atmospheric and oceanographic fluctuations. The higher rate of change (25%/°C) may also be a function of the higher accumulation rates which are typical for the coastal margins. This higher rate on Law Dome probably represents the best estimate of long-term change in accumulation rate with temperature since the location of the long wave trough is a permanent feature of the Southern Hemisphere circulation. In contrast, the observed variation in accumulation rate in Kemp Land and Dronning Maud Land may be affected by a component of variation in accumulation up to 20%/°C which can be attributed to changes in atmospheric circulation and changes in the seasonal moisture sources. This is consistent with the observations since these regions have recently experienced anomalous temperature and sea ice trends when compared to the whole of Antarctica.

Therefore it is probable that the ~20-25%/°C rate of accumulation change is more typical of the long-term changes (timescale of hundreds of years) which have occurred throughout the Holocene and that the higher rates are more typical of fluctuations on the timescales of decades. The lower rates are in closer agreement to those determined by the GCM studies and hence are in closer agreement to the changes predicted by the physical theory of ocean-atmosphere heat exchange. It is important to note that Simmonds and Budd (1991) found that the average surface air temperature changes over the sea ice zone were non linear in response to changes in open water within the sea ice. Hence, these accumulation-temperature relationships may be applicable only for surface air temperature changes of 1-2°C different from the present pattern. These relationships will be applied to the sensitivity studies on the response of surface mass balance to temperature increases during the Holocene, in Chapter 7.

CHAPTER 4
LATE PLEISTOCENE-MID HOLOCENE GLACIAL HISTORY, COASTAL EVOLUTION AND SEA LEVEL CHANGES AT THE EAST ANTARCTIC ICE MARGIN: A CASE STUDY OF LAW DOME

4.1 INTRODUCTION

A case study of Late Pleistocene-Mid Holocene deglaciation was undertaken to provide a baseline from which to determine fluctuations in ice sheet extent, and behaviour of the East Antarctic ice sheet margin in response to climatic and sea level changes during the Holocene (Goodwin, 1993b). The margin of the Law Dome ice cap was chosen for this study because it's morphology is reasonably well known from almost 25 years of glaciological and geological research by ANARE scientists and it is a small ice cap whose response to climatic forcings might be simpler to understand than the East Antarctic ice sheet as a whole.

The Law Dome is approximately 200 km in diameter with its summit at 1300 m above sea level. It abuts the Windmill Islands on its north-western margin forming the Clark, Bailey, Mitchell and Browning Peninsulas (Figure 4.1). Law Dome is separated from the main East Antarctic Ice Sheet to the south by a saddle at 1000 m elevation. The Windmill Islands are a group of low islands, islets and peninsulas with elevations less than 100 m forming a major ice-free 'oasis' located at the eastern edge of Vincennes Bay on the East Antarctic coast. The Windmill Islands shown in Figure 4.2 cover an area of 75 km^2 and extend up to 15 km offshore from the present margin of Law Dome. The relief of the southern islands is more rugged than the northern islands and their geology is predominantly of igneous rocks (charnockite and granite). The northern islands consist of metamorphic rocks (schist, gneiss and migmatite) (Blight and Oliver, 1977). Ice radar profiling has revealed that the islands extend inland beneath the Law Dome forming a bedrock high. The subglacial bedrock relief falls below sea level to the north and south of the islands where the majority of the ice outflow occurs. At the southern edge of the Windmill Islands, a major outlet glacier, the Vanderford Glacier, occupies a trough 1000 to 2000 m below sea level and discharges ice from western Law Dome and the main East Antarctic ice sheet.

Cameron et al. (1959) and Hollin and Cameron (1961) described the results of preliminary glacial geological investigations carried out in the Windmill Islands during the 1957-58 International Geophysical Year (I.G.Y.). Their investigations revealed

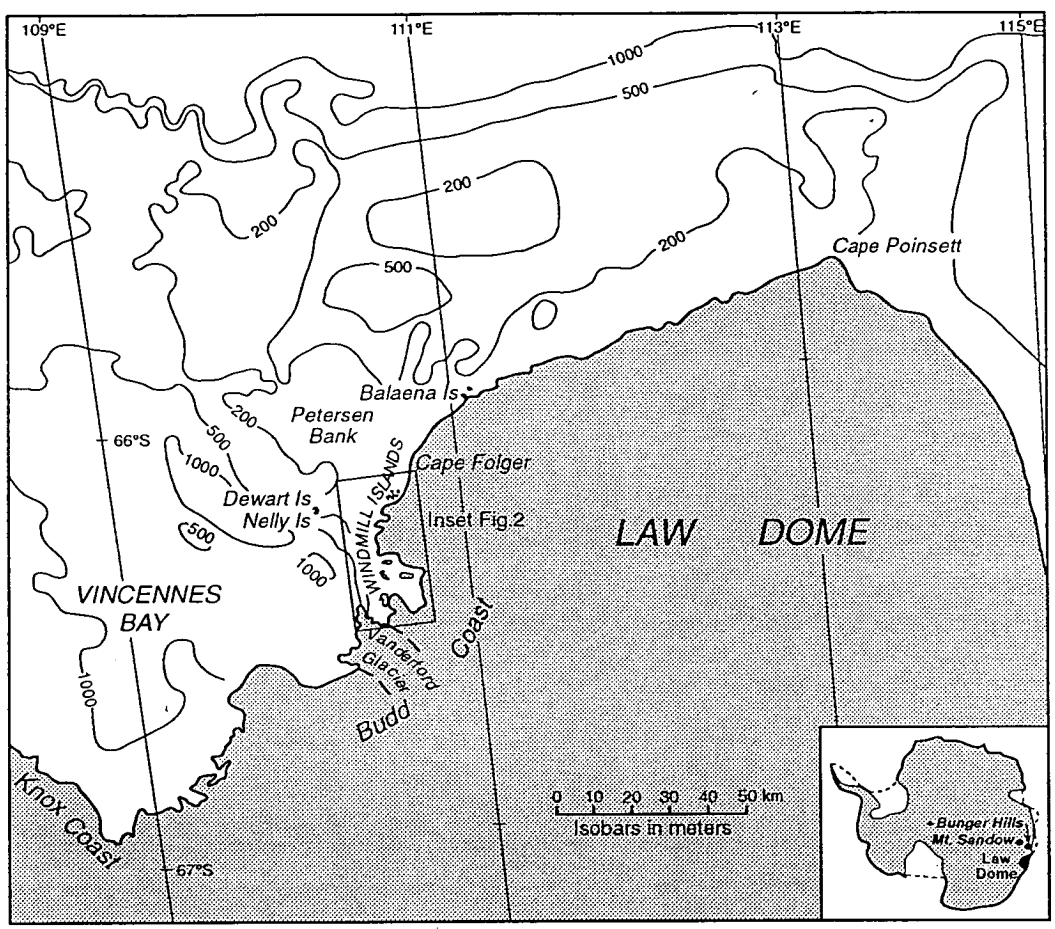

Figure 4.1 Map showing the location of Law Dome in Wilkes Land and the location of the Windmill Islands, Nelly Island and Dewart Island at the western margin of Law Dome, bordering Vincennes Bay. Bathymetric contours (isobaths) which were compiled from GEBCO Charts 542 and 558 and AUS 601, are shown to the north and west of the Law Dome margin.

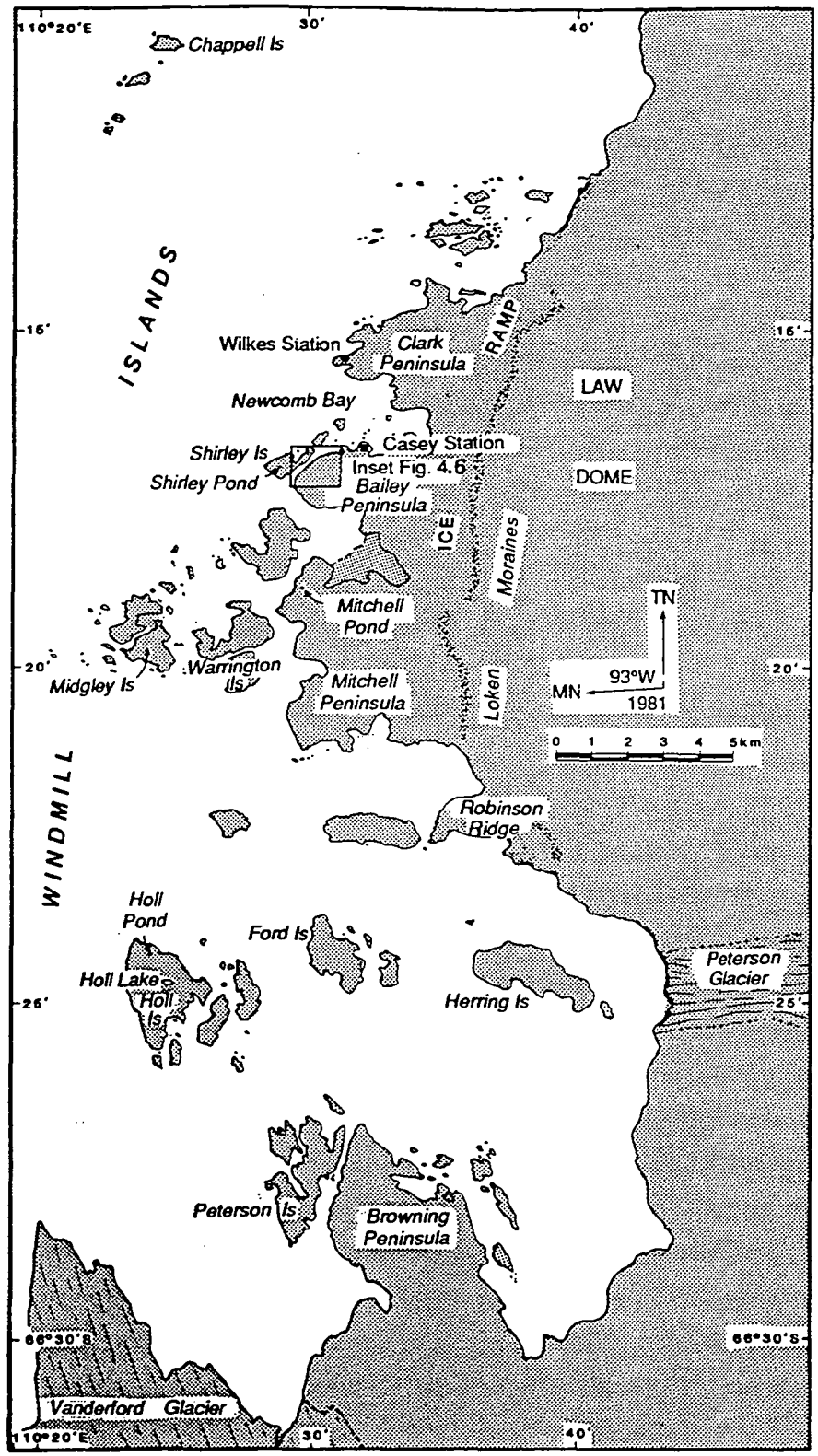

Figure 4.2 Map showing the location of the Windmill Islands and the Law Dome western margin. The arbitrary north-south delineation between the northern Windmill Islands and the southern Windmill Islands referred to in the text is located at Robinson Ridge. Detailed sites of sedimentological study are shown on Holl Island, Mitchell Peninsula, Shirley Island, and Bailey Peninsula.

that the entire Windmill Islands had been glaciated and that the weak to moderate stage of bedrock and surficial sediment weathering indicated recent glaciation during the Late Pleistocene/Early Holocene. Løken (1959) reported the existence of raised marine features throughout the islands which defined an elevated upper marine limit at approximately 30 m elevation.

During the 1985/86 and 1987/88 summers the author conducted fieldwork in the Windmill Islands. The surficial sediment cover, lake sediments and raised marine features were surveyed and sampled to determine a chronology for deglaciation and emergence. The fieldwork was largely concentrated on the northern peninsulas and adjacent islands with brief visits to some outer islands, and to Browning Peninsula.

4.2 EVIDENCE OF LATE PLEISTOCENE GLACIATION

Glacial striae and chatter marks are found on bedrock exposures throughout the Windmill Islands, indicating that the islands had been recently glaciated. The glacial striae and chatter marks indicate that the palaeo-ice flow direction over the northern Windmill Islands was between 265° to 280° (Cameron et al., 1959) which is consistent with the present ice flow abutting the Windmill Islands. The striae are best preserved on the northern peninsulas and islands where the gneiss bedrock is highly polished and weakly weathered as indicated by the relatively fresh grey exposures. In contrast, the rusty-orange charnockite bedrock high knolls on Browning Peninsula, Peterson Island and Holl Island are moderately to extensively weathered by granular disintegration, cavernous etching and scalloping. The charnockite bedrock is deeply weathered to a depth of 50 cm with well-developed tafoni in places. Deposits of grey freshly weathered melt-out till, granite and charnockite boulders occur on the bedrock knolls and in the valleys and depressions, which indicates recent glaciation. The deeply weathered charnockite and evidence of oxidised and manganese stains on some sheltered knolls on Browning Peninsula (Robertson, 1959) may indicate a prolonged exposure prior to the most recent glaciation. The low rounded knolls and hills across the archipelago display the asymmetry characteristic of roche moutonnée and other features of glacial erosion.

High relief and broad U-shaped valleys have formed on Holl and Peterson Islands and Browning Peninsula, and on Nelly Island and Dewart Island in the Frazier Group some 16 km offshore. These are all located adjacent to the inner shelf break and the 1000 to 1500 m deep trough in Vincennes Bay (Figure 4.1). The orientation of the U-shaped valleys (300° to 325°) corresponds to the current direction and probable

direction of an expanded Vanderford Glacier during the Late Pleistocene, as indicated by the strike of the inner shelf break. During this time an expanded Vanderford Glacier would have occupied the deep trough in Vincennes Bay and discharged an increased volume of ice from the main East Antarctic ice sheet occupying the Aurora subglacial basin (Cameron, 1964).

Robertson (1959) reported the occurrence of only three rare red sandstone erratics in the abundant distribution of igneous and metamorphic erratics across the Windmill Islands. These were located on the north-western section of Browning Peninsula, Nelly Island in the Frazier Group and on the western half of Clark Peninsula. These were all located below the 30 m contour and the erratic on Nelly Island is located in the U-shaped valley. The author sampled these erratics in 1987-88 and found that their lithology is similar to that reported in bedrock exposures on Mt. Sandow (67° 22' S, 100° 22' E) a nunatak inland of the Bunger Hills, in the ground moraine in the Bunger Hills and in moraines along the Knox Coast to the west of the present Vanderford glacier drainage basin (Korotkevich and Timofeev, 1964). Red sandstone erratics have not been observed in the Løken Moraines on Law Dome and are likely to be from the Aurora subglacial basin. These erratics were almost certainly transported in the basal zone of the expanded Vanderford Glacier and later transported by ice rafting in Vincennes Bay to their present locations prior to relative sea level lowering. The distribution of the erratics further supports the northerly expansion of the Vanderford Glacier during the Late Pleistocene.

4.3 SURFICIAL SEDIMENT COVER

A shallow veneer of unconsolidated sediment covers the bedrock across the islands and was classified broadly into three types by Cameron et al. (1959); (i) marine reworked till which is located below the 30 m elevation and is confined to gravelly sand textured pocket beach deposits and sorted pebble/boulder sea ice push ridges; (ii) periglacially sorted till cover which is located above the 30 m elevation; and (iii) periglacially derived sediment (felsenmeer). All three classes have been further sorted to a minor extent by fluvial processes during summer melt periods. Glacial erratics were observed throughout the islands at all elevations. A marked difference in the texture of the sediment cover above the 30 m elevation from that below was observed between the northern and southern islands. The delineation occurs south of Robinson Ridge on Mitchell Peninsula. The southern islands including Browning Peninsula are covered with coarse grained gravelly sediment primarily derived from the extensive weathering of the charnockite bedrock at the upper elevations, and with a grey, freshly

weathered, coarse sand in the valleys and depressions, and sandy deposits on small pocket beaches. By comparison, in the northern Windmill Islands, particularly on the larger Clark, Bailey and Mitchell Peninsulas the sediment cover is dominated by gravelly fine sand deposits which occur at all elevations in bedrock depressions, and medium sand deposits on the beaches.

Micropalaeontological analyses of the fine sand deposits has revealed that they contain rare shallow (< 50 m deep) marine benthic diatoms and sponge spicules (Quilty, 1993) and even rarer Mollusc shell fragments. These fossiliferous deposits occur within the elevation range of 15-70 m. The diatom species are indicative of warmer waters than the present ice marginal waters. Their age is suggested as between 1 to 2 Myr in the Early Pleistocene to Late Pliocene (Quilty, 1993), or much younger in the Late Quaternary (Burkle pers. comm., 1994). The interpretation that the northern sediment cover was dominated by Early Pleistocene to Late Pliocene marine deposits posed many questions as to their survival beneath a Late Pleistocene ice expansion. A possible explanation is that the deposits were preserved by permafrost and that the grounded ice over the northern Windmill Islands was relatively slow moving (<5 m/yr) similar to the present configuration.

In the southern Windmill Islands, the absence of these deposits suggests that the unconsolidated sediment was eroded by the faster moving and expanded Vanderford Glacier stream. This is supported by the greater relief of the southern islands and the presence of the incised U-shaped valleys. The rarity of microfossils in the unconsolidated deposits is the combined result of subsequent reworking by glacial and marine processes. The relative lack of subglacially derived fine sediment as opposed to the abundant glacial erratic boulders can be explained by the very low debris concentrations carried englacially in the basal ice layers which have been measured as less than 4% by volume in the present basal ice at the Law Dome margin abutting the islands (Goodwin, 1993a).

4.4 RAISED MARINE SHORELINE FEATURES

Raised marine shoreline features in the Windmill Islands were first reported by Løken (1959). These features are well defined and scattered throughout the islands within a range of elevations extending from present sea level to around 30 m, indicating relative sea level lowering and the emergence of the islands. Raised beaches occur mainly as pocket beaches (Figure 4.3a), generally < 75 m in length, in bedrock coves along low cliffed coastlines and as strandlines along islands with lower relief. These raised beaches have been formed by wave action and are characterised by medium

a

b

Figure 4.3 Photographs showing; (a) The largest and most well developed raised beach on the north east coastline of central Clark Peninsula, with a maximum elevation of 18.6 m. The particle size of the beach sediment is well sorted medium sand. (b) Boulder strandlines forming a continuous beach from 8 m to 26 m on the eastern side of Shirley Island. Modern boulder strandlines are forming at the present ice foot in the adjacent channel between Shirley Island and Bailey Peninsula (visible in the upper right hand corner).

sands and well rounded cobbles and pebbles. Strandlines of well rounded boulders also occur where sea ice has been active, particularly in former narrow channels (Figure 4.3b). These boulder lines were interpreted as sea ice-push ridges and are generally 1 m high although their height is controlled by the thickness of the ice foot and the tidal range. The most extensive occurrence of ice-push ridges occurs on the eastern shore of Shirley Island and directly across the channel on the western shore of Bailey Peninsula where they extend in continuous rows from present sea level to 30 m elevation.

Distinct raised shorelines are also apparent on bedrock exposures where the sand, cobble and boulder sediment has been washed off leaving a clear bedrock surface. Small lakes and ponds were observed in bedrock depressions and are relict from small marine inlets stranded by relative sea level lowering following the transgression of the post glacial sea into low lying areas. Many of these small lakes and ponds are dammed on their seaward shore by ice pushed boulder ridges, forming barriers and are located at or just below the marine limit. On the steeper coastlines evidence of raised shorelines is restricted to rare bedrock niches and breaks in slope. This study concentrated on raised beaches, ice pushed boulder ridges and lakes and ponds.

Løken (1959) and J. Hollin (unpublished 1958 field notes) conducted surveys of raised shorelines to determine the vertical distribution of the marine limit, and the magnitude of the relative lowering of sea level, across the Windmill Islands. The author resurveyed some of these features in addition to extending the survey coverage in 1987. The elevation of each of the raised features was measured by optical levelling techniques with the survey based on sea level / tide gauge measurements as a height datum (1957 and 1958 surveys) or the elevation of survey trigonometric points as a height datum (1987 survey).

Table 4.1 lists the marine limit for a total of fourteen islands. These are compiled from the most reliable measurements available from the three surveys based on the accuracy in defining the feature due to local topographical variability and the reduced height above the datum. Table 4.1 shows that the elevation of the marine limit is spatially variable with an increase from north to south across the islands The highest marine limits of 31.3 to 32.0 m occur on Holl Island, Herring Island, and Browning Peninsula (measurements on Peterson Island were not as reliable) which are located on the edge of the Vincennes Bay inner shelf deep zone, near the present terminus of the Vanderford Glacier. Dewart Island and Nelly Island in the Frazier Group, which lie 15 km offshore to the west of Bailey Peninsula have equivalent marine limits (29 m)

to that on Bailey Peninsula (29.5 m) which is connected to the present Law Dome margin.

TABLE 4.1 MEASURED MARINE LIMITS ON THE WINDMILL ISLANDS

Area	Elevation (m)	Landform	Source	Method
Chappell Is	27.8 ± 1.3	beach	Løken 1957	optical level
N Clark Pen	26.7 ± 0.5	beach	Goodwin 1987	optical level
Nelly Is	29.0 ± 1.3	wave washed bedrock	Hollin 1958	hand level
Dewart Is	29.0 ± 1.3	beach	Goodwin 1987	hand level
Bailey Pen	29.5 ± 0.5	ice push ridge	Goodwin 1987	optical level
Shirley Is	29.3 ± 0.5	beach	Goodwin 1987	optical level
Mitchell Pen	28.1 ± 1.0	wave washed bedrock	Løken 1957	optical level
Warrington Is	27.5 ± 1.0	beach	Løken 1957	optical level
Midgeley Is	28.1 ± 1.0	beach	Løken 1957	optical level
Robinson Ridge	28.5 ± 1.0	beach	Løken 1957	optical level
Ford Is	28.9 ± 1.0	wave washed bedrock	Løken 1957	optical level
Holl Is	31.5 ± 1.5	wave washed bedrock	Hollin 1958	optical level
Herring Is	32.0 ± 1.0	beach	Hollin 1958	optical level
Browning Pen	31.3 ± 1.0	wave washed bedrock	Hollin 1958	optical level

Marine macrofossils, which have been found extensively in raised beaches from other coastal oases in East Antarctica eg. Vestfold Hills (Adamson and Pickard, 1986), Bunger Hills (Colhoun and Adamson, 1991), and Syowa (Yoshida and Moriwaki, 1979, Hayashi and Yoshida, 1994) were not found in the Windmill Island sediments, probably due to the higher energy coastline and lack of shallow embayments. In addition the raised beach material and ice push ridge material was too coarse having

been sorted by wave action, to contain suitable marine microfossils such as foraminifera. The microfossils in the raised beach sediments are restricted to recent and Late Pliocene - Early Pleistocene diatom assemblages and sponge spicules (P. Quilty, pers. comm.) However, Cameron (1964) reported a ^{14}C date of 6040 ± 250 yr B.P. (M-1052) for *Archaeolithothamnion* a coralline algae found in a raised beach at Eyres Bay on Browning Peninsula at 23 m above present sea level. This is the only date available for in situ marine microfossils in raised beaches in the Windmill Islands.

4.5 RADIOCARBON AGE DETERMINATION AND RESERVOIR EFFECTS

To determine minimum dates for deglaciation, emergence, and landscape development, the search for organic material which could be dated by ^{14}C techniques was concentrated on lake and pond bottom sediments, both above and below the marine limit. In addition, sediments from abandoned penguin rookeries located above the marine limit were sampled to determine minimum dates for penguin occupation. Although ^{14}C radiocarbon dating is the most suitable method, in Antarctica it is subject to large variability in reservoir corrections which are specific to both the freshwater or marine origin, and the species of organism or material. Marine organisms and ocean surface waters are depleted in ^{14}C, and yield ^{14}C dates older than terrestrial sediments. This is known as the Antarctic reservoir effect caused by the release of ancient ^{14}C depleted CO_2 from the melting of glacial ice (Omoto, 1983). The reservoir effect on ^{14}C dates on marine shell material has been reported as between 850-1312 yr B.P. by Harkness (1979), Yoshida and Moriwaki (1979) and Adamson and Pickard (1983, 1986), and Stuiver and Braziunas (1985) with the 1300 yr correction the most consistently applied. Alternatively the reservoir effect on ^{14}C dates obtained from seals and penguins of known age at the beginning of this century ranges from 915 to 1760 yr B.P. (Mabin, 1986; Whitehouse, 1988, 1989; Baroni and Orombelli, 1991). Baroni and Orombelli (1991) and Whitehouse et al. (1988,1989) reported an average reservoir effect for Adélie penguins as 946 ± 60 and 1091 yr, respectively. The correction for Antarctic reservoir effects in freshwater algae is between 450-700 yr B.P. (Adamson and Pickard, 1986; D. Gillieson, pers. comm. 1990; Stuiver et al., 1981). Bird et al. (1991) reported that a reservoir correction may not be required in lacustrine sediments where lakes are small and/or shallow since there is a greater equilibration with atmospheric CO_2.

For comparison between ^{14}C ages obtained from Adélie penguin remains and terrestrial organic sediments the respective reservoir correction factors were applied to the conventional ^{14}C ages. These are 1090 yr B.P. for Adélie penguin remains and 450 to 700 yr B.P. for terrestrial organic sediments.

4.6 LAKE AND POND SEDIMENTS

Cold monomictic lakes exist throughout the Windmill Islands in bedrock depressions and are generally ice free during January and February. The majority of lakes are less than 20 m in diameter and less than 1-1.5 m deep and are more appropriately referred to as ponds. Larger lakes up to 200 m in diameter occur on some of the outer southern islands such as Holl Island where the bedrock relief is greatest (Figure 4.4a). Generally the lakes and ponds can be classified as either nutrient-rich or sterile.

The nutrient-rich lakes are restricted to those coastal lakes which have penguin rookeries or abandoned rookeries located within their catchment areas. Each of these lakes experiences annual summer algal growth and their shallow sediments are composed of olive grey colour algal mats over black algal muds together with fine aeolian clastic particles throughout the profiles. All of the closed basin lakes show evidence of previously higher lake shorelines and expanded volumes defined by orange/red oxidised weathering stains on the surrounding bedrock and boulders together with areas of dry and desiccated lake beds. The present low lake levels indicate that the volume has been significantly reduced by an excess loss due to evaporation or by permafrost decay. Lichen and moss vegetation only occurs above the high water marks which may indicate that higher freshwater lake levels occurred during the Late Holocene or the oxidised bedrock is not a suitable substrate for colonisation. Some of these lakes lie in bedrock depressions below the marine limit and were previously occupied by marine inlets when the post glacial marine transgression occurred. They are now occupied by freshwater reservoirs following the evaporation of the seawater and the subsequent in-flux of snowmelt runoff.

The sterile lakes are located further inland and are fed by meltwater from snowbanks and local precipitation. Their shallow sediments are predominantly clastic and are derived from both aeolian and fluvial sources. The oxygen isotope ($\delta^{18}O$) values for bulk lake waters are generally in the range from -13‰ to -16‰. These lakes are filled with water whose source is local snowmelt. Two lakes were found to be significantly

a

b

Figure 4.4 (a) Photograph of Holl Lake, central Holl Island in Late January, 1987. The shoreline consists of an algal stained and flattened, gravelly pavement. The base of the sediment layers above permafrost yielded the carbon date 6000 ± 260 ^{14}C yr B.P. (ANU 6507) in a core obtained from the pavement in the foreground. (b) Holl Pond A, northern Holl Island. A shallow depression fed by snowmelt from the upper catchment. The bottom sediments situated above permafrost yielded the carbon date 8160 ± 300 ^{14}C yr B.P. (ANU 6401). The Law Dome and the Mitchell Peninsula are visible in the background. Both the outlets of Holl Lake and Holl Pond A are determined by bedrock sills, which control the maximum water levels.

enriched in $\delta^{18}O$. These are Holl Pond A (elevation 28 m) which has an average $\delta^{18}O$ value of -5.8‰ and a pond at Blakeney Point on Clark Peninsula (elevation 5 m) which has an average $\delta^{18}O$ value of -9.6‰. The likely source of the water in these lakes is a mixture of seawater and local precipitation since there is little evidence for high marine aerosol transport (De Decker et al., 1991). It is likely that the seawater was trapped in these shallow depressions during isostatic uplift and that evaporation has significantly reduced their volume. The Holl Pond A is discussed in more detail in the subsequent section. A total of 16 lakes was examined on Clark, Bailey , Mitchell, and Browning Peninsulas, together with Shirley, Beal, Peterson and Holl Islands. Five nutrient-rich lakes were studied in greater detail and their bottom sediments were ^{14}C dated.

4.6.1 HOLL LAKE, CENTRAL HOLL ISLAND

This is the largest lake on Holl Island which is an outer island located at the southern edge of the Windmill Islands adjacent to the Vincennes Bay inner shelf deep zone (Figures 4.2, 4.4a). Holl Lake is located at 41 m elevation in the central part of the island. It is a deep freshwater lake, 400 m long with a $\delta^{18}O$ value of -15.1‰ for the bulk surface waters and was ice covered even in January/February except for a 10-m wide peripheral moat of water. It has a large catchment with extensive snow drifts. The lake level is determined by an outlet at the eastern edge. The shoreline is covered by a flattened gravel/cobble pavement with some salt encrustations which probably are derived from the evaporation of seawater which previously filled the lake basin. The majority of the lake is sterile with only clastic sediments. However, localised green algae accumulations were observed along the shoreline of a shallow indentation of the northern shoreline. A 30-cm deep sediment core was obtained at this site (Figure 4.5a). There is a sharp transition from olive grey algal mat on the surface and a 10 cm thick unit of algal material interbedded with grey coarse sand to a 20 cm thick unit of black gravelly mud. The bottom 5 cm of the core was dated at 6000 ± 260 ^{14}C yr B.P. (ANU 6507) which corresponds to a corrected age range of 5300 to 5550 corr. yr B.P..

4.6.2 HOLL POND A, NORTHERN HOLL ISLAND

This is a small shallow (<1 m deep) pond approximately 50 m in diameter located slightly below the marine limit at 28 m in a saucer shaped bedrock depression in a broad saddle above the northern coastline of the island (Figures 4.2, 4.4b). The pond is brackish water with an average $\delta^{18}O$ value of -5.8‰ for the bulk waters. The

Figure 4.5 Lake and pond sediment profiles, investigated in this study, showing the location and uncorrected age of ^{14}C samples for: (a) Holl Lake, central Holl Island (41 m elevation); (b) Holl Pond A, northern Holl Island (28 m elevation); and (c) Bailey Pond, northwestern Bailey Peninsula (31 m elevation).

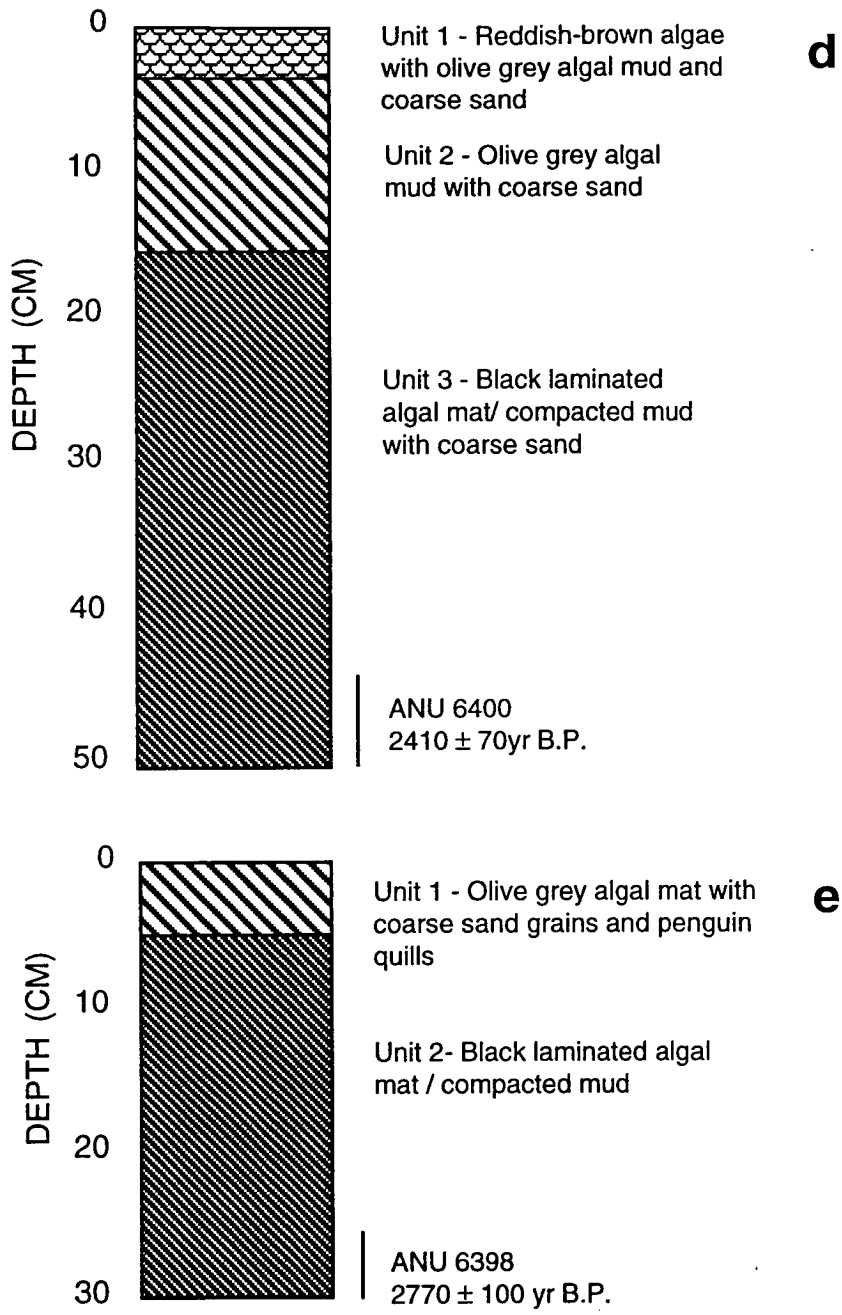

Figure 4.5 Lake and pond sediment profiles, investigated in this study, showing the location and uncorrected age of ^{14}C samples for: (d) Mitchell Pond B, western Mitchell Peninsula (23.7 m elevation); and (e) Shirley Pond, Shirley Island (25.5 m elevation).

catchment is devoid of snow drifts or meltwater streams and is closed with a previous outlet approximately 1 m above the present lake surface. There is evidence from the extent of flattened pavement for a previously higher lake level equivalent to the outlet elevation. This pond is a remnant of a much larger lake which occupied the bedrock depression. This depression was filled with seawater and became isolated from the sea through isostatic uplift and relative sea-level lowering. Continuing net evaporation has reduced the lake to a small pond. The maximum pond depth is less than 2 m ensuring warm temperatures during summer for algae production. The shoreline is salt encrusted from the seawater evaporation and is covered by a flattened gravel pavement and olive grey algal mat similar to Holl Lake together with small patches of reddish brown algae in surface micro-depressions. Above the shoreline the catchment surface cover is characterised by shallow coarse sands and some rounded beach boulders. A 30 cm-deep sediment core was obtained at the shoreline (Figure 4.5b). The core is similar to that for Holl Lake except for the lenses of reddish brown algae in unit 2. The bottom 5 cm of the core was dated at 8160 ± 300 ^{14}C yr B.P. (ANU 6401) which corresponds to a corrected age range of 7460 to 7710 corr. yr B.P. This is the oldest date obtained from the Windmill Islands.

4.6.3 BAILEY POND, NORTHWESTERN BAILEY PENINSULA

Bailey Pond is less than 50 m in length and 0.5 to 1 m deep. It is located in a narrow gully just above the marine limit at 31 m elevation between two bedrock knolls along the northwestern coast of Bailey Peninsula (Figure 4.4). There are numerous small abandoned penguin rookeries on the knolls above the pond which lies on an ancient penguin access route to the sea. The pond is freshwater with an average $\delta^{18}O$ value of -15.8‰ for the bulk waters and is fed by the summer melt from snow drifts. Higher lake levels are defined up to 3 m above the present level by an orange weathering stain. The shoreline and desiccated pond bed which extends for at least 100 m to the southeast are littered with severely frost shattered angular bedrock and small boulders. Between the boulders are deep accumulations of olive grey algal mats. A sediment profile was dug adjacent to a number of angular boulders along the shoreline. The deepest core was 30 cm (Figure 4.5c). There is a sharp transition from the medium to coarse sandy textured unit 2 to the underlying laminated black algal mud with dispersed coarse sand. The bottom 5 cm of unit 3 were dated at 5930 ± 120 ^{14}C yr B.P. (ANU 6399) which corresponds to a corrected age range of 5230 to 5480 corr. yr B.P..

4.6.4 MITCHELL POND B, WESTERN MITCHELL PENINSULA

Mitchell Pond B is located in a bedrock depression at 23.7 m with a raised beach berm forming its western shore. It is freshwater with an average $\delta^{18}O$ value of -15.5‰ for the bulk waters and is 150 m long by 40 m wide and less than 1.5 m deep. There are only small snow drifts within the catchment. The pond is located within 500 m of the ice covered interior of Mitchell Peninsula which is connected to the Law Dome (Figure 4.2). Higher lake levels were defined by an orange algal stain on bedrock and boulders up to 0.8 m above the present lake level. A deep 50 cm sediment core was obtained at the eastern shoreline (Figure 4.5d). There is an abrupt transition from the olive grey algal mud in unit 2 to the rich laminated black algal mud with dispersed coarse sand in unit 3. The bottom 7 cm of unit 3 were dated at 2410 ± 70 ^{14}C yr B.P.(ANU 6400) which corresponds to a corrected age range of 1710 to 1960 corr. yr B.P..

4.6.5 SHIRLEY POND, SHIRLEY ISLAND

Shirley Pond is located at the northwestern end of Shirley Island at 25.5 m (Figure 4.2). It is a shallow freshwater pond < 1 m deep with an average $\delta^{18}O$ value of -14.5‰ for the bulk waters. Higher shorelines were observed up to 1 m above the present level. The pond lies in a shallow depression dammed by ice-pushed ridges on the eastern and western shores. There were few snow patches within the catchment which include numerous penguin rookeries. The shoreline is covered by a flattened pebble/cobble pavement with mottled green algae in patches. A 30 cm sediment core was obtained from the eastern shore (Figure 4.5e). The core consists of a very shallow surface unit of olive grey algal mud over a homogeneous unit of black algal compacted mud. The bottom 5 cm of the core was dated at 2770 ± 100 ^{14}C yr B.P. (ANU 6398) which corresponds to a corrected age range of 2070 to 2320 corr. yr B.P..

4.7 ABANDONED ADELIE PENGUIN ROOKERIES

Abandoned Adélie penguin rookeries form conspicuous oblate mounds of pink, guano, stained pebbles and friable soil which are often nestled on bedrock ledges and flat areas near the highest relief bordering the coast. They are particularly clustered on Peterson Island and western and central Bailey and Clark Peninsulas. Adélie penguins chose their rookery sites based on; the proximity to a direct access route to open water; their high elevation which makes the sites free from deep snow accumulation and

summer meltwater flooding and the occurrence of suitable pebbles for nest building. Consequently, a chronology of penguin occupation of these rookeries would provide a useful indication of the time of minimum deglaciation and emergence of the islands.

Northwestern Bailey Peninsula (Figure 4.6) was found to have the most concentrated distribution of abandoned penguin rookeries and became the focus of detailed study. There are no currently populated penguin rookeries on Bailey Peninsula. All the abandoned rookeries are located at elevations of 45 m to 60 m and overlook the channel between Bailey Peninsula and Shirley Island (Figure 4.6). Shirley Island which has a maximum elevation of 30 m has a concentrated current population of Adélie Penguins which would be an equivalent population to that which the Bailey abandoned rookeries could accommodate. The majority of the Shirley rookeries are located in the elevation range of 10 to 20 m. The Bailey population probably abandoned the rookery and moved to the seaward sites on Shirley Island after the eastern lobe of Shirley Island (maximum elevation 15 m) emerged from the sea obstructing the direct access route to the open sea from Bailey Peninsula.

A gully (Figure 4.6) which connects a number of small abandoned penguin rookeries with an access ramp to the sea on Bailey Peninsula revealed an extensive accumulation of Adélie Penguin skeletons, bones and frozen flesh including flippers and feet at an elevation range of 26 to 33 m. The penguin remains were surrounded by an organic rich peaty sediment which had been recently eroded by snowmelt runoff down the gully. An Adélie Penguin skull found at a depth of 20 cm overlying permafrost in the gully was dated at 4380 ± 250 ^{14}C yr B.P. (ANU 6403) which corresponds to a corrected age of 3290 corr. yr B.P.. Peaty sediment surrounding the skull was dated at 3800 ± 370 ^{14}C yr B.P.(ANU 6404) which would correspond to a corrected age range of 3100 to 3350 corr. yr B.P.. It is likely that both the skull and peat have been fluvially transported a short distance from the original deposition site A small dry rock pool was discovered at 23.1 m elevation 100 m south of the gully on Bailey Peninsula. A 20 cm deep sample of dark brown compacted peat with penguin quills and bones dispersed throughout the sample was obtained from the pool. The bottom 3 cm of the peat was dated at 4980 ± 80 ^{14}C yr B.P. (ANU 6402) which corresponds to a corrected age range of 4280 to 4530 corr. yr B.P.. This range is comparable to the 6040 ±250 ^{14}C yr B.P. (M-1052), 4740 corr. yr B.P. date obtained from the raised beach at the same 23 m elevation. Consequently this is the minimum age for Adélie Penguin occupation of the Bailey abandoned rookeries which must be at least 500-1000 yr older since the rock pool site was submerged by 7 m when the relative sea level was at its Holocene marine limit and deglaciation had exposed the rookery sites.

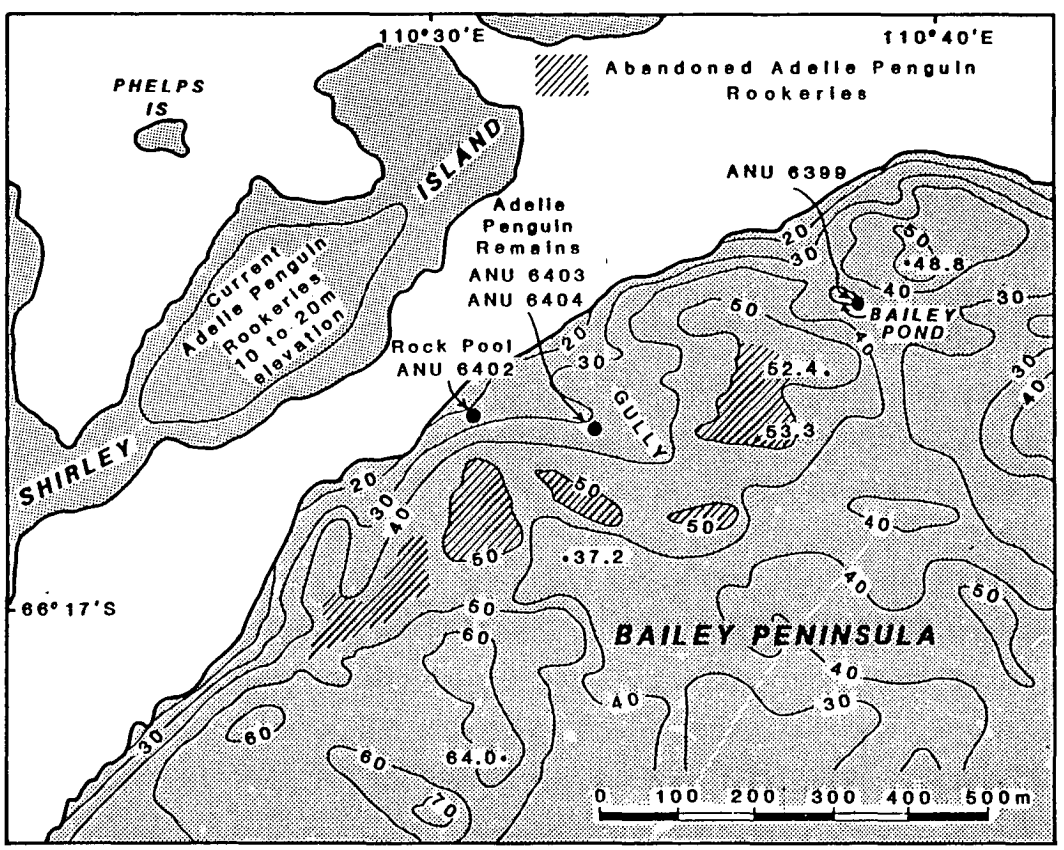

Figure 4.6 Detailed map of northwestern Bailey Peninsula showing the location and age of ^{14}C samples collected from abandoned Adélie Penguin rookeries and Bailey Pond. The contour interval is in meters. The 30 m contour approximately defines the Holocene marine limit.

4.8 ^{14}C CHRONOLOGY OF DEGLACIATION AND GLACIO-ISOSTATIC UPLIFT

Since the Holl Pond A and Bailey Pond sites are located close to the marine limits for each island the ^{14}C dates of their bottom sediments provide a suitable minimum estimate for deglaciation. Since the Holl Pond A site is located approximately 2 - 3.5 m below the measured marine limit for Holl Island the minimum date for deglaciation of Holl Island and the southern Windmill Islands must be interpreted as around 8000 yr B.P. based on the age range of 7460 to 7710 corr. yr B.P. for Holl Pond A. In comparison the later 5230 to 5480 corr. yr B.P. range of dates for Bailey Pond provides a minimum estimate for deglaciation of Bailey Peninsula and the northern Windmill Islands, which are presently connected to the Law Dome margin . The earlier emergence of the southern Windmill Islands is consistent with the higher marine limits found on the southern islands and their greater distance offshore from the present Law Dome margin.

An estimate of the Holocene post-glacial uplift of Holl Island and Bailey Peninsula was determined using the methods described in Andrews (1970) by combining the elevation of the marine limit with the amount of eustatic change since the dates of deglaciation, 8000 and 5500 corr. yr B.P., respectively. The eustatic change was determined as ~12 and ~3 m, respectively, from the modelled sea level curves of Nakada and Lambeck (1988) and Peltier (1988) for the tectonically stable site at Moruya, NSW, Australia, since a relative sea level curve for Antarctica has yet to be determined. Consequently, the total post-glacial uplift for Holl Island and Bailey Peninsula was estimated as 43 m and 33 m respectively. This equates to uplift rates of approximately 5 to 6 mm/yr. These rates are consistent with the rate of 5.5 mm/yr obtained from the ^{14}C dated shell in the raised beach at 23 m elevation. The greater uplift on Holl Island, which is located 12 km from Bailey Peninsula at the edge of the Vincennes Bay inner shelf deep zone near the probable grounding line of the expanded ice sheet and Vanderford Glacier, may reflect the comparative unloading response to greater ice thicknesses which probably occurred in the Vincennes Bay inner shelf deep zone than on the Petersen Bank.

These uplift rates, however, can only serve as a preliminary estimate since the reservoir corrections are not well known and it is not possible to determine when algal growth was initiated following deglaciation. In addition, the relationship between algal growth and the supply of nutrients from penguin activities is not known, but the available dates for the Bailey Peninsula indicate that algal production was initiated by

5500 corr. yr B.P. approximately 1000 yr before the earliest evidence for occupation of the Bailey penguin rookeries.

To determine an estimate of ice thickness at the Last Glacial Maximum (LGM) prior to deglaciation, the total isostatic uplift including the component of residual uplift remaining at the present needs to be calculated since the commencement of deglaciation. It was not possible to construct an emergence curve from the Windmill Islands since only one raised beach has been dated, and the bulk of the ^{14}C dates record environmental changes subsequent to emergence. Therefore, data from a range of sites in Arctic Canada published by Andrews (1970) was used to provide a rough estimate of residual uplift remaining after 8000 corr. yr. The residual uplift was estimated at less than 10 m since little residual uplift remains 10,000 yr after deglaciation (Andrews, 1970). It is important to note that the estimates of glacio-isostatic uplift determined from one island or one small site reflect the changes not only at that site but over a large regional area. Consequently the estimates of LGM ice thicknesses determined from isostatic uplift should be viewed as average additional ice thicknesses to the present surface topography (Hollin, 1962). Assuming that deglaciation occurred by 8000 corr. yr B.P., the maximum total uplift of the Windmill Islands since emergence was estimated at 53 m (Holl Is) which implies a Late Pleistocene-Early Holocene minimum ice thickness of ~200 m over the region of the Windmill Islands (assuming an equilibrium depression), based on the ratio between the mantle density (3.3×10^3 kg m^{-3}) and the ice density (0.9×10^3 kg m^{-3}). Such an ice thickness over the islands would result in minimum regional ice thicknesses up to 400 m thick over the adjacent Petersen Bank on the inner continental shelf. This ice mass over the present coastline requires a seaward expansion of the ice sheet by 8 to 15 km if the present ice sheet profile is maintained. Such an expansion is coincident with the location of the 200 m isobath to the west of Holl Island, Peterson Island, Browning Peninsula, Nelly Island, and Dewart Island.

However, the estimated ice thicknesses produced by the Andrews (1970) method are too low when compared to the ice thicknesses interpreted on the inner continental shelf from diamicton facies in marine sediment cores indicating the presence of grounded ice during the Late Pleistocene off the Wilkes Land coast (Domack, 1991b) and in Prydz Bay (Hambrey et al., 1991), and off the Dronning Maud Land coast (Grobe et al., 1993). This under-estimation of ice thicknesses from raised beach elevations using the Andrews (1970) method is probably due to the deglaciation process being well under way by as early as 11,000-12,000 yr B.P as interpreted in the Bunger Hills (11,600 yr B.P., Bolshiyanov et al., 1991) and in Prydz Bay (10,700 yr B.P., Domack et al., 1991a). Rapid eustatic sea level rise was occurring during this period

with the deglaciation of the Northern Hemisphere ice sheets well under way (Nakada and Lambeck, 1988). Consequently, emergence of the islands by isostatic uplift was occurring at a slower rate than the eustatic sea level rise. In addition, the isostatic response times may be significantly longer in Antarctica than in the Northern Hemisphere (Andrews, 1970) since only a small part of the margin of Antarctica was deglaciated during the Holocene.

Alternatively, estimates of maximum LGM ice thicknesses can be determined from the methods outlined by Colhoun et al.(1992) from the total uplift since LGM based on the summation of the maximum raised beach height and the eustatic sea level rise since LGM, proportioned by the ratio of mantle density to ice density (3.3/0.9). These methods are also based on the estimation of the difference between the relative sea-level during the LGM and at present. In the absence of an interpreted sea level curve from Antarctica these methods are based on the modelling of Clark and Lingle (1979). They calculated an ice thickness of 500 m over the Windmill Islands and that relative sea level at the Windmill Islands was only 1.5 m lower than present at 16,000 yr B.P., using an isostatic depression calculated for the CLIMAP scenario of maximum ice sheet expansion in Stuiver et al. (1981). However, Clark and Lingle (1979) used a maximum sea level rise of only 100 m since LGM. Since the best current estimate of eustatic sea level rise since LGM is 121 m (Fairbanks, 1989) then the relative sea-level in the Windmill Islands at 16,000 yr B.P. would be equivalent to 22.5 m below the present sea-level. Clark and Lingle (1979) also predicted that approximately 3-4 m of emergence occurred along the Antarctic continental margin since 5000 yr B.P. due to crustal tilting and loss of ocean water to the Northern Hemisphere due to rapidly collapsing proglacial forebulge depressions. There is some evidence to support crustal tilting around the East Antarctic margin, in the Lutzow-Holm Bay region, where Hayashi and Yoshida (1994) observed *Laternulla elliptica* in the growth position at higher elevations between 4,000 to 5,000 yr B.P. than at 5,500 to 6,500 yr B.P.. Thus, in the absence of an observed sea-level curve, a maximum estimate of LGM ice thickness over the Windmill Islands was calculated as 468 m, using the following formula;

Estimated ice thickness = ((LGM sea level fall (121m) - LGM relative sea-level difference (22.5m) + (maximum raised beach height (32m) - crustal tilting (3m)) x ratio of mantle density/ice density (3.3/0.9)

Colhoun et al.(1992) estimated 561 m for maximum ice thicknesses over the Windmill Islands but they did not take into account the factors due to LGM relative sea-level

differences or that due to crustal tilting at the margin. To attain an ice thickness of 500 m over the inner Windmill Islands, Law Dome would have needed to expand seaward by ~15 km onto the Petersen Bank, if the ice sheet maintained its present profile (Figure 4.7). Grootes and Stuiver (1987) examined the $\delta^{18}O$ isostope profile from three ice cores on Law Dome located at BHF, BHC-1 and BHC-2 near the 400 m elevation at Cape Folger. They concluded that the Law Dome was an independent ice sheet from the East Antarctic ice sheet similar to its present configuration during the LGM, except that the ice sheet between 40-50 km inland of the BHF ice core, has thinned by ~530 m during the Late Pleistocene-Holocene. This corresponds to a thinning at the ice margin at Cape Folger of ~750 m. They suggest that this is a slight overestimate due to ice flow, elevation and continentality changes which have not been accounted for in the oxygen isotope analysis. Nevertheless, a thinning of this order would result in an ice sheet retreat of the margin by 25 km and a poleward shift in the Law Dome summit by 40 km if the current profile is extrapolated (Figure 4.7). Alternatively, a post-glacial thinning at the ice margin of ~500 m as calculated above, would be consistent with a 15 km retreat of the LGM ice sheet margin to the present location (Figure 4.7). The Frazier Islands (Dewart and Nelly Island) are located some 16 km offshore from Clark and Bailey Peninsulas (Figure 4.2). A broad u-shaped valley dissects the islands and is oriented east-west along the present flow direction of the Law Dome ice margin. The surface of the Frazier Islands exhibits a comparable state of weathering to the Late Pleistocene-Holocene landforms on the peninsulas and suggests that contemporaneous glacial erosion occurred. This morphology of the Frazier Islands supports the estimated 15 km expansion of the Law Dome ice sheet at LGM. It also suggests that LGM ice extended further than the Frazier Islands. Analysis of the bathymetry offshore from the Windmill Islands indicates that the Law Dome ice sheet would have expanded to the north-east across the Petersen Bank from Cape Folger. Alternatively, the Frazier Islands are located on the edge of the Vincennes Bay inner shelf deep zone and a more extensive LGM ice expansion in the vicinity of the Frazier Islands is likely to be associated with the expanded Vanderford Glacier. The ~500 m estimate of ice sheet thinning at the margin is about half that suggested by Hollin (1962) for the Balaena Islets (marine limit = 30 m), north of Cape Folger, which was based on a 100 km seaward expansion of the present Law Dome ice sheet profile across the Petersen Bank to the edge of the continental shelf, and the maintenance of the present ice sheet profile.

The 8000 corr. yr B.P. minimum date for deglaciation of the southern Windmill Islands agrees with the 7700 yr B.P. minimum age for deglaciation of the northern Bunger Hills to the west of the Windmill Islands (Colhoun and Adamson, 1991, 1992), the 8,600 corr. yr B.P. minimum age for deglaciation of the Sørsdal Glacier,

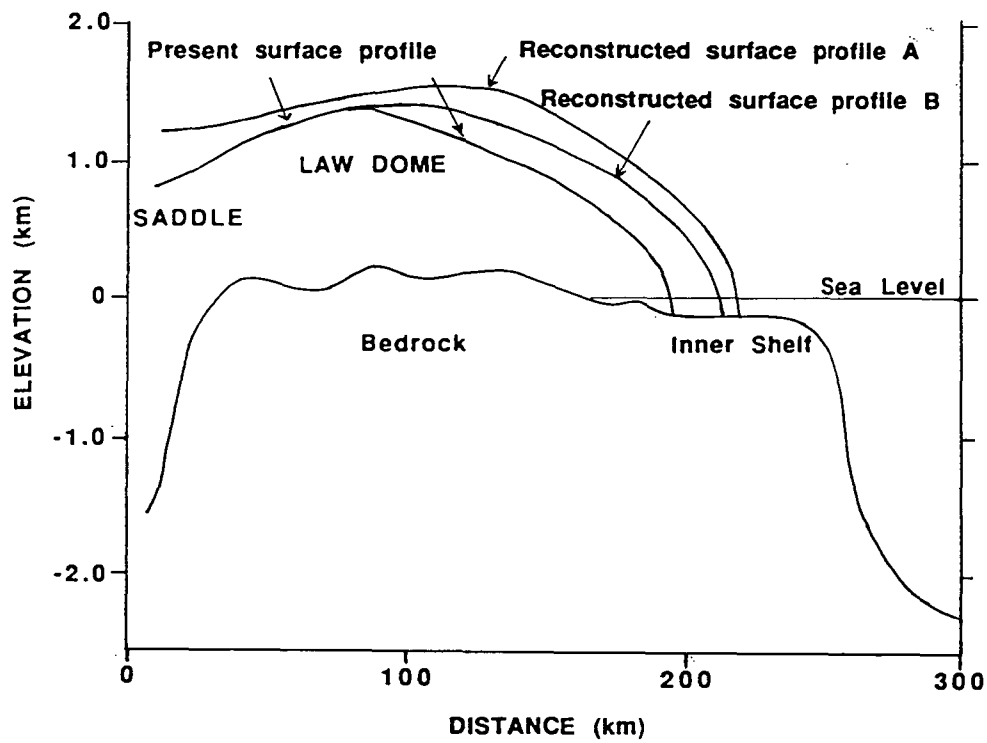

Figure 4.7 The surface and bedrock profile for the present ice sheet over Law Dome between Law Dome Summit and Cape Folger is shown after Budd and Morgan (1977). The reconstructed ice sheet surface profiles for Law Dome at LGM are also plotted. Profile A is reconstructed for an estimated 25 km expansion (after Grootes and Stuiver, 1987) with ~730 m of ice cover over the Windmill Islands. Profile B is reconstructed for an estimated 15 km expansion (this study) with ~500 m of ice cover over the Windmill Islands. The 15 km expansion would have placed the margin in the vicinity of the Frazier Islands.

Vestfold Hills (Fitzsimmons, 1990), the 9,000 corr. yr. B.P. minimum age for deglaciation of the Larsemann Hills from lake sediment production (Gillieson et al., 1990), the 8000 to 9000 yr B. P. date reported by Domack et al. (1991b) for ice sheet recession of the Wilkes Land coast, and to the 7000 to 8000 yr B.P. date for thinning in the D10 ice core on the Adélie Land coast (Raynaud et al.,1979) when eustatic sea level was rising rapidly. These dates also agree with the Clark and Lingle (1979) prediction from their sea level modelling that emergent shorelines in Antarctica should be younger than 11,000 yr B. P.. Since the southern Windmill Islands are located on the edge of the Vincennes inner shelf deep zone, close to the probable grounding zone of the expanded Vanderford Glacier, it is expected that they would be deglaciated first as rising eustatic sea level during the Late Pleistocene would have initiated the decoupling of the grounding line and retreat of the Vanderford Glacier. Since rising eustatic sea-level is the likely mechanism for deglaciation of the Antarctic marine based ice sheets (Hollin, 1962, and Thomas and Bentley, 1978), it is consistent to expect that the Vincennes Bay inner shelf deep zone was ice free by at least 10,000 yr B.P. which is comparable with the evidence reported from other major outlet glaciers such as that reported for the Lambert Glacier/ Amery Depression in Prydz Bay which was free from grounded and floating ice by 10,700 yr B.P.(Domack et al., 1991a). Because the marine limit decreases northwards across the islands it is suggested that the grounded ice over the northern Windmill Islands was much slower to retreat, by as much as 2000 yr later, as the Bailey Peninsula deglaciation date indicates. This may be supported by the abutment of the present ice margin to the northern Windmill Islands, irrespective of whether it has advanced or retreated to this position.

4.9 COMPARISON OF GLACIO-ISOSTATIC UPLIFT AT THE WINDMILL ISLANDS WITH THAT DETERMINED FROM EAST ANTARCTIC RAISED BEACHES

Colhoun et al. (1992) presented a compilation of published maximum heights and locations of Holocene raised beaches in coastal East Antarctica. The raised beach heights are extremely variable from location to location due to the different ice load in place during the Late Pleistocene glaciation. No complete relative sea level curves have been produced for Antarctic locations, except for those modelled by Clark and Lingle (1979) and Tushingham and Peltier (1991). The latter was based on the far field relative sea level history in the Wairau Valley, New Zealand. Consequently, it is extremely important to interpret the glacial geological data carefully when extrapolating isostatic uplift and LGM ice thicknesses and subsequently determining the amount of total isostatic uplift during the Holocene and its control on the grounding line of the ice

sheet and outlet glaciers. A second problem with raised beach data is that the major sites where reported raised beaches occur are located within present day 'oases' (Bunger Hills and Vestfold Hills) which may have also had an anomalous regional climate with low precipitation similar to present or lower coupled to the colder temperatures, producing a thin locally derived ice cover during the LGM expansion. In the case of Queen Mary Land most of the ice flow from the interior is discharged by the Denman and Scott Glaciers to the west of the Bunger Hills. In addition, these 'oases' are also located inland from present ice shelves which would have grounded and expanded seaward, possibly blocking flow from the ice sheet to the south and restricting the expansion of the ice sheet seaward. Any expansion of these ice shelves would have increased the distance to the local moisture source possibly resulting in decreased precipitation. Any of these factors may have contributed to relatively small increases in LGM ice sheet elevation and subsequently to the relatively low elevation raised beaches; up to 7.5 m in the Bunger Hills and up to 10 m in the Vestfold Hills. If these regions experienced anomalous climates during the LGM then neither region is suitable to draw wider implications for ice sheet extent during the LGM.

Raised beaches suitable for the determination of LGM ice thicknesses and Holocene uplift have also been observed at the margin of the East Antarctic ice sheet at 30 m elevation on the Balaena Islets (longitude 110° 10' E), and on Lewis Island (longitude 134° E) in Wilkes Land (Hollin and Cameron, 1961), at 12 m at Cape Denison, Commonwealth Bay, George V Land (Stillwell, 1918), and along the MacRobertson Land and Kemp Land coasts up to 15 m elevation (Trail, 1961), but have not been surveyed and dated. They have also been observed in the Lutzow-Holm Bay region along the Soya and Prince Olav Coast, with a reliable Holocene marine limit between 20-25 m (Hayashi and Yoshida, 1994). A second set of raised beaches occur at elevations up to 39 m along the Soya Coast and yielded ^{14}C dates between 35,000 to 40,000 years (Omoto, 1977). However, these may be much older, even Pliocene age as was found in the Vestfold Hills with molluscs dated older than 30,000 years B.P. (Zhang and Peterson, 1985). Thus, the highest known Holocene raised beaches are located on islands and peninsulas in the Windmill Islands and along the Wilkes Land coast (32.0 m) and along the Soya Coast up to 20-25 m, all of which have an open water exposure to produce consistent storm swell for beach forming. In contrast, no raised marine features have been recorded in the Larsemann Hills (Gillieson et al., 1990) despite being deglaciated by 9,000 corr. yr B.P. and probably earlier at 12,000 corr. yr B.P. which indicates that open water was not present as suitable surface moraine occurs as potential beach material.

Whilst all these sites are located largely at the margin of the grounded ice sheet there is little field data close to the major outlet glaciers where the majority of ice expansion during the LGM would be expected. This is illustrated in the southern Windmill Islands where the highest raised marine features are located adjacent to the Vanderford Glacier. Evidence of ice sheet expansion during the LGM to the outer edge of the continental shelf would provide a maximum extent and a suitable indicator to evaluate the range of estimated ice thicknesses from the coastal geological evidence.

Two sediment cores sampled from the upper continental shelf off Dronning Maud Land in the eastern Weddell Sea have been analysed by Grobe et al.(1993). The sedimentary record from these cores provides the first marine evidence that a sector of the Antarctic ice sheet extended to the shelf edge during the last glacial. The inner continental shelf in Prydz Bay also contains massive diamicton deposits from the LGM expansion of the Lambert Glacier/Amery Ice Shelf system (Hambrey et al. 1991) although the geographical extent of these deposits has not been determined.

In George V Land, Domack (1982) and Domack et al. (1991b) concluded from their interpretation of compacted massive diamicton in marine sediment cores from the continental shelf, that grounded ice had occurred during the LGM in the Mertz and Ninnis Troughs on the middle to outer shelf some 60-80 km off the George V Land coasts, as a result of an expansion of the Mertz and Ninnis Glaciers (Figure 4.8b). In comparison, Domack et al. (1991b) also concluded from their interpretation of glacio marine sediments on the continental shelf off the Terre Adélie coast that the ice sheet had advanced only 20-25 km onto the inner continental shelf (Figure 4.8a). An advance of these dimensions has also been modelled by Young et al.(1984) which showed that the ice sheet 250 km inland from D10 was 200-400 m higher than the present elevation.

The observations of Stillwell (1918) revealed that beach terraces and ice-push boulder strandlines had formed up to the marine limit of 12 m at Cape Denison and the Mackellar Islands in George V Land. This would imply an estimated ice thickness over Cape Denison at LGM of 400 m (using the methods outlined above in section 4.8). Such a thickening would have resulted in an expansion of the grounded ice sheet margin by 8-10 km which is consistent with the expansion of the nearby Terre Adélie coastline in Figure 4.8b.

Grootes and Stuiver (1987) deduced from the $\delta^{18}O$ record in the D10 core (elevation 270 m, 5 km inland from the coastal ice margin in Terre Adélie) that the ice sheet at this location was 1320 m higher during the LGM. Such a thickening would

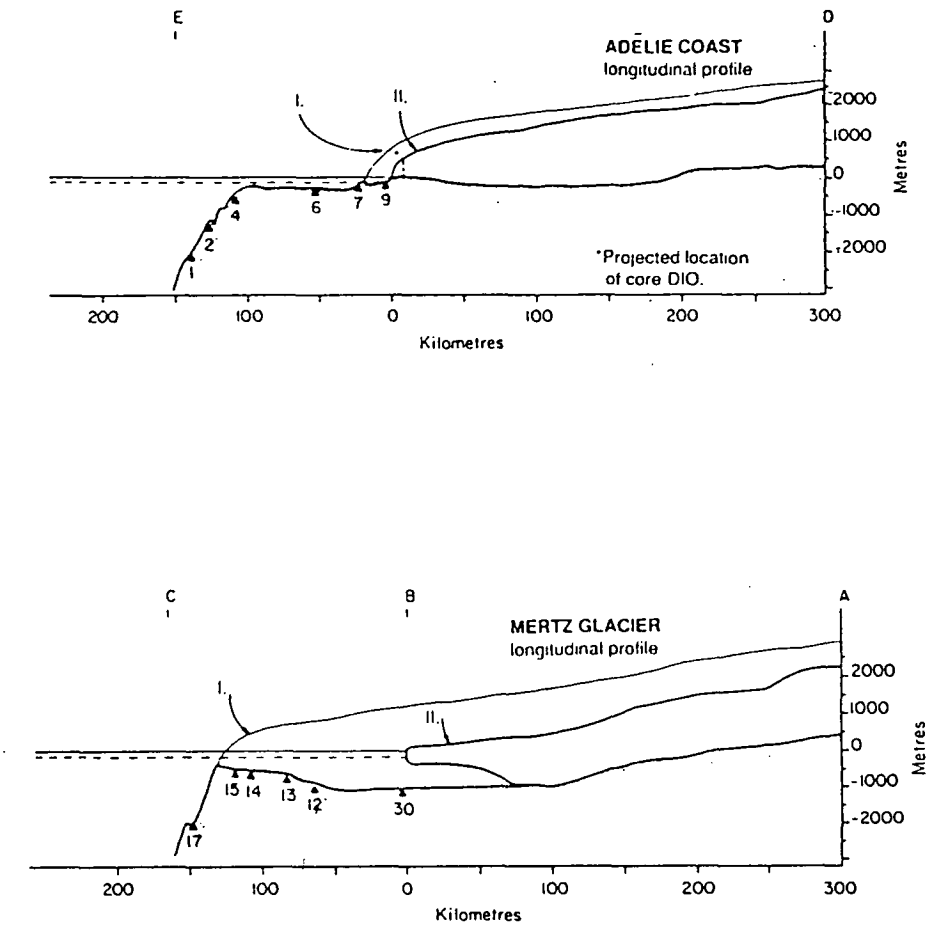

Figure 4.8 After Domack et al. (1991b). Glacial and bedrock profiles for (a) George V Land margin, and; (b) Terre Adélie margin. Glacial maximum reconstruction is shown by profile I and the present position by profile II. Present and 18,000 yr B.P. (pecked) are also shown. Isostatic depression for maximum reconstruction was not included by Domack et al. (1991b). Also plotted is the location of seafloor sediment cores from which they determined the glacial extent, and the location of the D10 ice core.

correspond to a 100 km expansion onto the outer continental shelf if the present day profile is extended to fit the elevation increase. However, on the basis of the marine sedimentary evidence (Domack et al. 1991b) the grounded ice sheet would have attained an elevation of less than 800 m in the vicinity of D10, and any thickening at D10 resulting in an elevation greater than 500 m would need to drain to the expanded Mertz-Ninnis Glacier system. Consequently, the ice sheet elevation changes estimated by Grootes and Stuiver (1987) are significantly overestimated for D10, probably due to errors in the estimation of ice flow on the D10 core, and due to their conclusion that ice sheet elevations on the interior plateau were 100 m higher than at present during the LGM.

The sedimentary records from the continental shelf indicate that significant expansion of the East Antarctic ice sheet occurred during the LGM, especially in the vicinity of the major outlet glaciers in Wilkes Land, Terre Adélie and George V Land. The marine limits and the corresponding isostatic uplift values for the 'oases' such as the Vestfold Hills and the Bunger Hills, are considered to be minimum indicators of Holocene isostatic uplift and LGM ice thicknesses in East Antarctica, since ice sheet growth in these regions may have been small due to the probable anomalously low precipitation patterns similar to the present. Accordingly the total estimate of the Antarctic ice sheet expansion (<30 km) during the LGM by Colhoun et al.(1992) must also be considered a minimum estimate. It is suggested from the marine glacial geological evidence that a significant expansion (>30 km) of the major outlet glaciers onto the middle-outer continental shelf occurred during the LGM. These outlet glaciers deliver significantly greater ice volumes to the coast than the slower moving grounded ice sheet. Accordingly, it is probable that as sea-level fell during the Last Glacial, ice sheet expansion on the inner and middle continental shelf would have been largely centred on the progressive grounding of the outlet glaciers and adjacent ice shelves, rather than the ice sheet margins.

4.10 ON THE CONTRIBUTION OF EAST ANTARCTICA TO EUSTATIC SEA-LEVEL LOWERING AT LGM

Colhoun et al. (1992) estimate that the LGM ice expansion was equivalent to less than 2.5 m of estimated eustatic sea level rise, which clearly leaves at least another 20 m of the 121 m of LGM eustatic sea level changes unaccounted for and required to have been stored in the Northern Hemisphere ice sheets. Alternatively, Huybrechts (1992) modelled the Antarctic contribution to the total eustatic sea level rise from the ice increase at 16,000 yr B. P. to be equivalent to 12 m of estimated eustatic sea level rise,

which is still half that estimated by the CLIMAP reconstruction of Stuiver et al. (1981). The former modelling indicated the majority of the LGM expansion was restricted to the advance of grounded ice in the Ross and Weddell Seas which is supported by the geological evidence in Grobe et al. (1993) for the Weddell Sea and by Denton et al. (1989) for the Ross Sea. The Huybrechts (1992) model also includes a negligible increase in ice sheet elevation over the interior of East Antarctica. Drewry (1979) estimated a sea-level contribution of 8 m which he determined from geological evidence, primarily in the Ross Embayment.

I suggest that the estimates of isostatic uplift and LGM ice thicknesses from the Windmill Islands are more typical of the response of the coastal margin of the East Antarctic ice sheet during the Late Pleistocene/Holocene, since they reflect the significant expansion of both the Vanderford Glacier and the Law Dome ice sheet. In addition, the relatively higher raised beaches and marine limits along the Wilkes Land coast (32 m in the Windmill Islands and 30 m at Lewis Island) than the Princess Elizabeth and Queen Mary Land coasts (<10 m) may indicate that greater ice sheet expansion occurred off the Wilkes Land coast. This proposition is consistent with the significantly higher accumulation rates recently observed in the Wilkes Land sector than in the Princess Elizabeth Land sector (Chapter 2). It is clear that the expansion of the ice sheet in response to relative sea level lowering during the Late Pleistocene was regionally distinct (Colhoun, 1991), not only due to the bathymetry of the continental shelf but also due to the strong regional differences in precipitation and the general circulation pattern as observed for the present East Antarctic ice sheet over the last 50 years (presented in Chapter 3).

A re-assessment of the LGM ice volume and equivalent global sea-level fall estimates of Colhoun et al. (1992) for the coastal margin of the East Antarctic ice sheet between longitude 170° E and 30° W (Southern Ocean sector) was made, based on the Wilkes Land studies. Their estimate of an average ice sheet grounding line advance of 30 km with an average thickness of 500 m (decreasing to 0 m at 2000 m elevation) due primarily to relative sea-level lowering is supported by this study. This ice sheet volume contributed 0.73 m (Colhoun et al., 1992) to global sea-level between LGM and 5,000 years (Chapter 5) as the ice sheet retreated. In addition, Colhoun et al. (1992) estimated that the interior of the ice sheet above 2000 m elevation experienced average surface lowering of 150 m during the LGM on the basis of elevation changes at Dome C and Vostok determined from ice core gas analysis by Jouzel et al. (1989). This surface lowering was equivalent to 1.5 m of eustatic sea-level which Colhoun et al. (1992) proposed would partially offset the contribution of the coastal advance. However, Martinerie et al. (1994) found that palaeo ice sheet elevations deduced from

the atmospheric pressure in air content variations in the Vostok ice core were probably overestimated since the latter were a function of non thermal parameters as well as atmospheric pressure changes. The other major parameter was the wind influence on the ice porous volume. This recent work indicates that surface lowering of the order of 150-200 m may not have occurred in the ice sheet interior during the LGM, which is also supported by the glacial geological observations of Denton et al. (1989). However, the palaeo-accumulation rates calculated by Raisbeck et al. (1987) from ^{10}Be measurements on the Dome C and Vostok ice cores indicate that LGM accumulation rates in the interior (above 2,000 m) were ~40-50% less than the mean Holocene rates. Thus the component of ice sheet lowering (above 2,000 m) during the LGM for a site with an average present accumulation rate of 0.03 m ice per year, is likely to have been ~100-125 m if a progressive change in accumulation rates occurred over a 10,000 year period, without dynamical adjustment to the ice sheet. Consequently, the net sea-level rise contribution of interior surface lowering was probably ~1.2 m if a lowering of 100 m occurred over the entire interior of the ice sheet (area estimated by Colhoun et al., 1992) as 4×10^6 km^2).

The contribution of the Lambert Glacier-Amery Ice Shelf system to sea-level was determined from the elevation of lateral moraines on Fisher Massif in the Northern Prince Charles Mountains (Mabin, 1992) and from the location of terminal moraine features on the middle continental shelf in Prydz Bay interpreted by O'Brien (1994) from radio-echo sounding data. The LGM expansion of the Lambert Glacier is constrained by a maximum elevation change of 300 m in the vicinity of Jetty Peninsula, since the weathering stage and the periglacial development of the surface sediments would indicate a significantly longer-term ice free exposure than the Holocene (field observations made by the author in 1989). Therefore a maximum elevation increase of 300 m was applied to the drainage area of the Lambert Basin below 2000 m (2.5×10^5 km^2). The resulting contribution of the Lambert Glacier-Amery Ice Shelf system to sea-level change was proportioned according to the Colhoun et al. (1992) estimate for a 200 m elevation increase below the 2000 m elevation contour and was estimated as of the order of 0.20 m. An estimate of the LGM sea-level contribution of the major East Antarctic (Southern Ocean sector) outlet glaciers is difficult, since the inner shelf bathymetry and the individual glacier morphology is poorly known. However, as an indicator of the likely sea-level contribution of major outlet glaciers, the sea-level contribution for the minimum 60 km expansion of the combined Mertz and Ninnis Glaciers was estimated from the geological and bathymetric data in Domack (1991b). This was estimated as of the order of ~0.015 m of sea-level with limits of $\pm$ 0.005 m due to uncertainties in the bathymetry and the scant geological evidence. If this was typical for the LGM extent

onto the inner shelf of the 20-25 major East Antarctic (Southern Ocean sector) glaciers, then the total sea-level contribution from these glaciers is estimated as ~0.2 to 0.25 m (assuming a typical glacier width at the grounding line of 30 km). It is not possible to estimate any associated fan shaped expansion onto the inner-middle continental shelf since the bathymetry and extent of the shelf deep zones is poorly mapped.

Thus an estimate of the total LGM sea-level lowering contribution of the Southern Ocean sector of East Antarctica between longitude 170° E and 30° W was calculated as ~0 to 1.2 m, depending on the extent of surface lowering in the interior of the ice sheet. Colhoun et al. (1992) estimate a corresponding sea-level rise contribution of 0.64 m for the same period using the greater estimate of surface lowering (150 m). However, the sea-level contribution of the East Antarctic margin is relatively small compared to the maximum sea-level contributions estimated for ice shelf grounding in the Ross and Weddell Embayments. There continues to be great debate over the magnitude of ice shelf grounding within these embayments during the LGM which may account for between 1.0 m (Colhoun et al. (1992), to 11.0 m Huybrechts (1992) of sea-level equivalent. For the Antarctic Peninsula, Payne et al. (1989) estimated an equivalent sea-level rise of 1.7 m between LGM and 6,000 yr B.P. from modelling and glacial geological observations. Alternatively, Colhoun et al. (1992) estimated a sea-level contribution of only 0.48 m for the Antarctic Peninsula and marginal West Antarctica combined.

A complete investigation of the Antarctic contribution to sea-level fall at LGM is beyond the scope of this study which is focused primarily on Mid-Late Holocene sea-level contributions, as discussed in Chapter 8. However, it is concluded that the Southern Ocean sector of coastal East Antarctica probably contributed ~1.0 m to the LGM sea-level fall, which is relatively small compared to the possible contributions from ice shelf grounding in the Ross and Weddell Embayments, and from expansion of the West Antarctic coastal margins. In addition, it is also concluded that the inner shelf bathymetry, the regional differences in ice sheet accumulation rates and outlet glacier dynamics, are the primary factors which controlled the variation in the LGM expansion of marginal East Antarctica.

The relative sea-level history and isostatic estimates for Law Dome are applied to the sensitivity analysis of the coastal East Antarctic margin in Chapter 7, to determine the contribution of relative sea-level changes on the palaeo-geography of the East Antarctic ice sheet margin during the Holocene, particularly the Mid-Late Holocene.

CHAPTER 5
THE MID-LATE HOLOCENE GLACIAL HISTORY OF THE LAW DOME ICE MARGIN

5.1 INTRODUCTION

The Law Dome ice margin at the Windmill Islands is one of only a few localities along the East Antarctic coast where the ice sheet terminus abuts terrestrial outcrops above sea level. The majority of the ice sheet terminates in marine ice cliffs whose bases are well below sea level. These terrestrial exposures provide the only accessible localities to investigate ice sheet fluctuations during the Holocene. The other major coastal terrestrial exposures which occur in the Wilkes Land to Princess Elizabeth Land sector between Commonwealth Bay and Prydz Bay, are the Bunger Hills, Vestfold Hills, and Larsemann Hills.

Hollin and Cameron (1961) first described the terrestrial exposure of the basal ice zone forming the Løken Moraines at the Law Dome ice margin (Figure 5.1). The present ice margin abutting the Windmill Islands is characterised by a concave ice ramp rising from 20 m elevation at the coastal ice cliffs, to 150-170 m elevation, some 1-2 km inland at the crest of the continuous Løken Moraines, which outcrop parallel to the coast and intersect the marine ice cliffs at the northern edge of the Windmill Islands.

The ice sheet rises with a convex profile from the inland edge of the Løken Moraines for a distance of 100 km to the Law Dome summit (Figure 4.7). The present ice margin is located within 1 km of Mid Holocene raised beaches on Clark, Bailey, Mitchell and Browning Peninsulas (Hollin, 1962, Goodwin, 1993 b). This indicates that the ice sheet may have advanced during the Mid-Late Holocene from its state of maximum post-glacial contraction during the Early-Mid Holocene. This chapter investigates the morphology and characteristics of the Løken Moraines and basal ice zone to determine the Holocene evolution of the present ice margin, and the implications for the mass balance state of the Wilkes Land coast.

5.2 MORPHOLOGY OF THE ICE RAMP

The ice ramp presently forms a stagnant and rigid ice wedge blocking the ice discharged from the interior of Law Dome and forcing a basal shear zone to form in

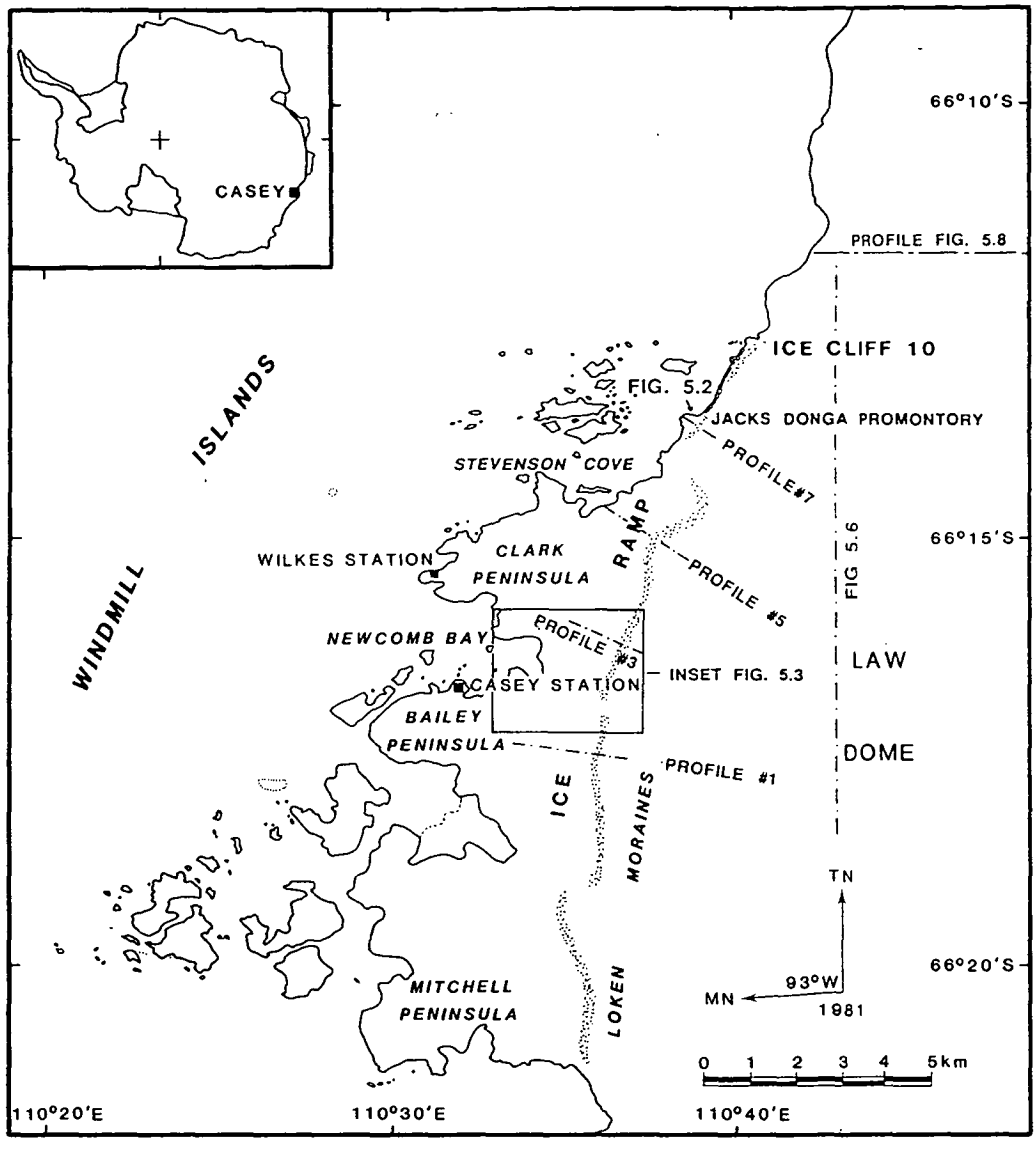

Figure 5.1 Location map of the northern Windmill Islands and the Law Dome ice margin. The Løken Moraines are shown parallel to the margin, and inland of the ice ramp. Also shown are the location of topographic profiles which are plotted in Figures 5.2, 5.5, 5.6 and 5.8, together with the inset Figure 5.3.

the base of the active ice some 1-3 km from the edge of the ramp which is expressed at the surface by the formation of the Løken Moraines. The ramp has a typical ice thickness of 100-170 m at its inland edge and forms an ablation zone during summer. The ramp has its widest zone inland of Bailey and Mitchell Peninsulas.

The internal structure of the ramp and its boundary with the basal shear zone is apparent in the longitudinal exposure in the ice cliffs along the northern side of the Jacks Donga promontory, which is shown in Figure 5.2. Oxygen isotope measurements made on samples in the ramp section of the Jacks Donga promontory exposure (this study) and shallow cores on the ramp inland of Clark and Bailey Peninsulas (Cameron et al., 1959) show that the upper few metres of the ramp consists of superimposed ice formed from the accumulation of local precipitation with an average $\delta^{18}O$ of -15‰ to -18.5‰ (V. Morgan, pers comm.). Below the superimposed ice is a wedge shaped ice tongue of glacial ice which thickens vertically towards the shear zone which has an $\delta^{18}O$ of -21‰ to -26‰.

An ice cored moraine ridge is located at an elevation of 42 m at the base of the ice ramp on Bailey Peninsula near Brown Bay. It is referred to as Bailey Moraine in Figure 5.3 and forms an end moraine, marking the most seaward terminus of the Law Dome ice sheet's advance onto the northern peninsulas of the Windmill Islands. Ice thickness measurements (determined by gravity survey) on the ice ramp inland of Bailey Peninsula and Clark Peninsula (Goodwin, 1988c) revealed that the Bailey Moraine was located at the seaward edge of a subglacial valley which is oriented parallel to the ice flow. The subglacial valley extends inland of the ice margin and is one arm of a subglacial valley which separates the Clark and Bailey Peninsulas. Two gaps in the continuous Løken Moraines delineate the location of the subglacial valley beneath the ice margin. This was confirmed by the gravity survey (Goodwin, 1988c). From the edge of the ramp to the coast, a local ice plateau extends across much of the northern peninsulas and terminates in coastal ice cliffs. The local ice plateau is composed of superimposed ice derived from the accumulation of local precipitation.

5.3 MORPHOLOGY OF THE LØKEN MORAINES

The Løken Moraines are a complex of ice-cored ridges and flats which have formed perpendicular to the ice flow and have been termed generically as either 'shear moraines' or 'inner moraines' depending upon the suggested mechanism used to describe sediment entrainment into the basal ice zone at the margin of polar ice caps. The 'shear moraine' mechanism involves the entrainment of sediment by differential

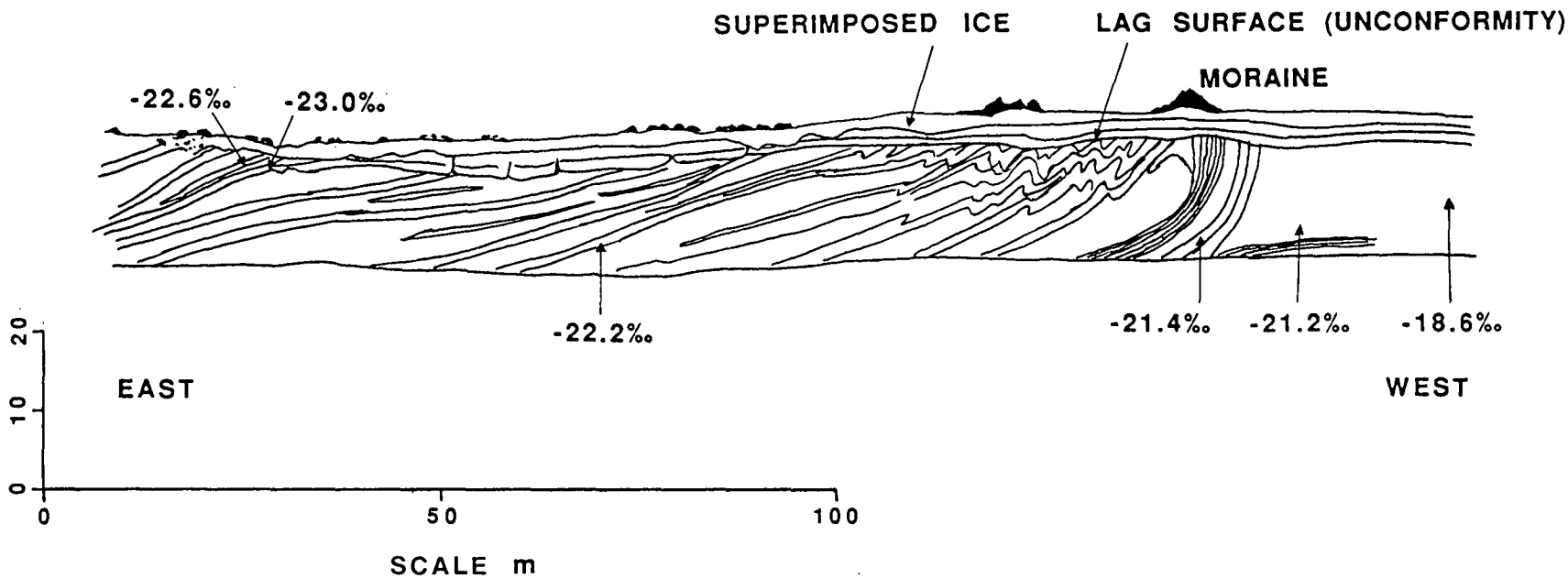

Figure 5.2 Longitudinal ice cliff exposure at Jacks Donga promontory, showing the basal debris bands and ice structure and the horizontal superimposed ice layers above. The boundary between the overlying superimposed ice and the basal ice zone is marked by an unconformity, which consists of a surface moraine lag deposit. The superimposed ice has formed from net snow accumulation, subsequent to the earlier exposure of the moraine from melting of the underlying debris band ice. Note the increase in dip of the basal ice towards the margin (to the west). The numbers refer to the measured $\delta^{18}O$ of the basal ice layers. Note the progressive depletion in the $\delta^{18}O$ away from the margin (to the east).

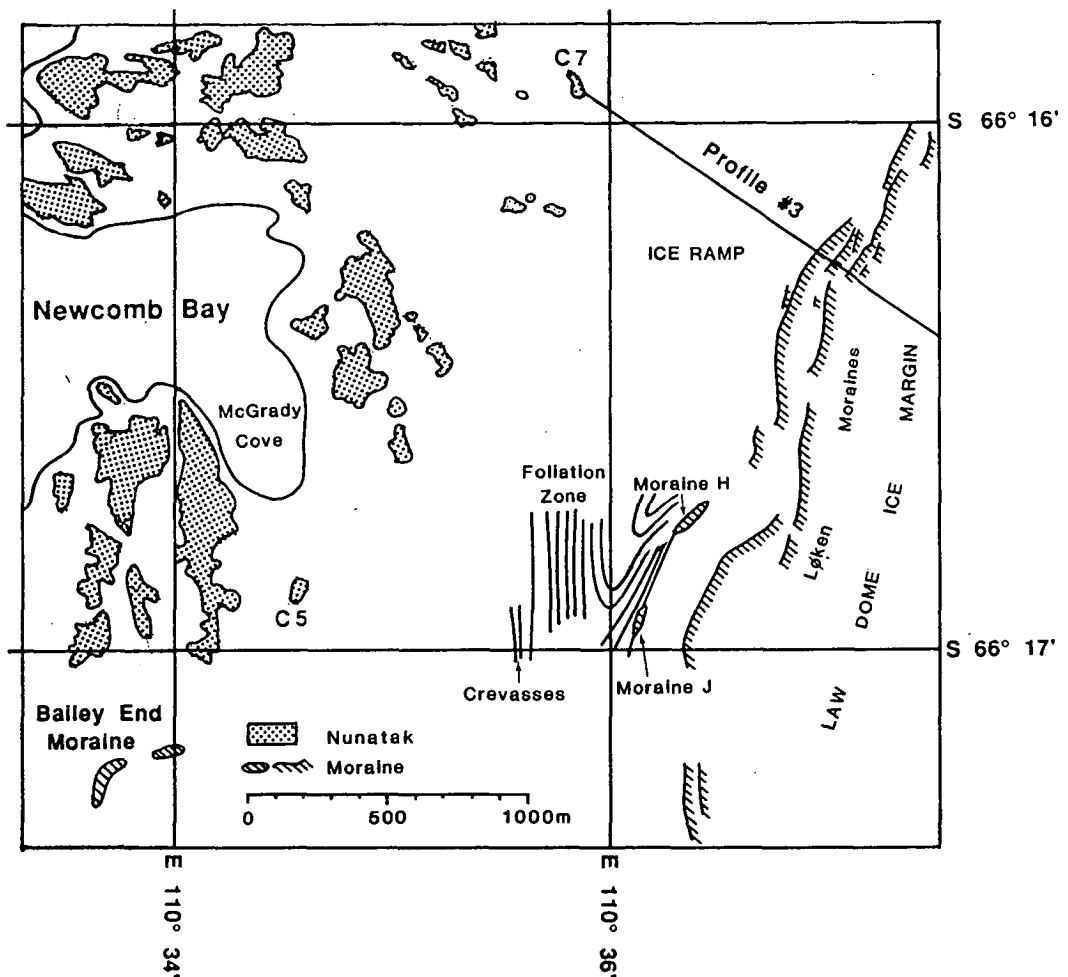

Figure 5.3 Location map of the Newcomb Bay section of the ice ramp and the Løken Moraines. The Bailey end moraine marks the seaward edge of the Law Dome ice margin's re-advance. Moraines J and H are located along a foliation within the upper limb on an isoclinal fold sequence. Also shown is the topographic profile 3 (Figure 5.5c) which was measured in 1958 and 1985 to determine surface elevation changes.

shear along basal ice planes in essentially dry based glaciers (Bishop, 1957). Alternatively,the 'inner moraine' mechanism involves the sediment entrainment by the freezing on of layers or slabs of permafrosted sediment, or within regelation ice layers where water is present at the glacier bed (Weertman, 1961). The term inner moraine will be used in the discussion since it does not imply a generic process but rather reflects the morphology.

Inner moraines are common terminal features of polar ice caps and have been previously described in Antarctica by Hollin and Cameron (1961), Souchez (1967), Chinn (1986) and Tison et al., (1993). Inner moraines generally form close to the margins of dry based polar glaciers where the flow is obstructed by bedrock high-points and the thinner more rigid ice at the margin which is frozen to the underlying sediment and bedrock (Chinn, 1987b). Their location is often at the transition from a wet base to a dry base, which is determined by the ice thickness and the mean surface temperature of the ice sheet. Figure 5.2 shows that the Løken Moraines are the surface expression of emergent basal ice debris bands which have been deformed by complex glaci-tectonics near the margin.

The ridge, swale and flat surface topography of the Løken Moraines has developed from the initially, differential ablation rates of clean ice, debris-rich ice and debris-poor ice. The ablation rates are greatest for the debris rich ice until a debris cap melts out of the ice over succesive ablation seasons and then insulates the underlying ice from rapid ablation. Consequently, after the establishment of ice-cored moraines the topography is inverted by the relatively greater ablation rates of the clean glacier ice (Hooke, 1970). Thus the elevated relief of the moraine ridges develops above the general surface of the ice margin. The form of the moraines, as either sharp or broad crested ridges, narrow or wide swales or flats depends upon the dip and thickness of the underlying debris ice layers or bands. The strongest morphological differences in the Løken Moraines occurs between the moraine topography inland of Clark Peninsula, Jacks Donga promontory and the northern ice cliffs, with the moraine topography inland of Bailey and Mitchell Peninsulas (shown in Figure 5.4). The former moraine topography consists of 3-4 distinct broad and sharp crested moraines and an extensive inland flat, whist the latter moraine topography consists of typically one or two sharp crested moraines and an extensive moraine flat.

The charactersitic moraine profiles for each segment are shown in Figure 5.5, together with the ramp profile at each location. Whilst the bedrock is below sea level at approximately -60 m elevation beneath the moraines at profiles no. 1 and no. 3 on Bailey and Clark Peninsula, the bedrock rises up to 40 m above sea level within 2 km

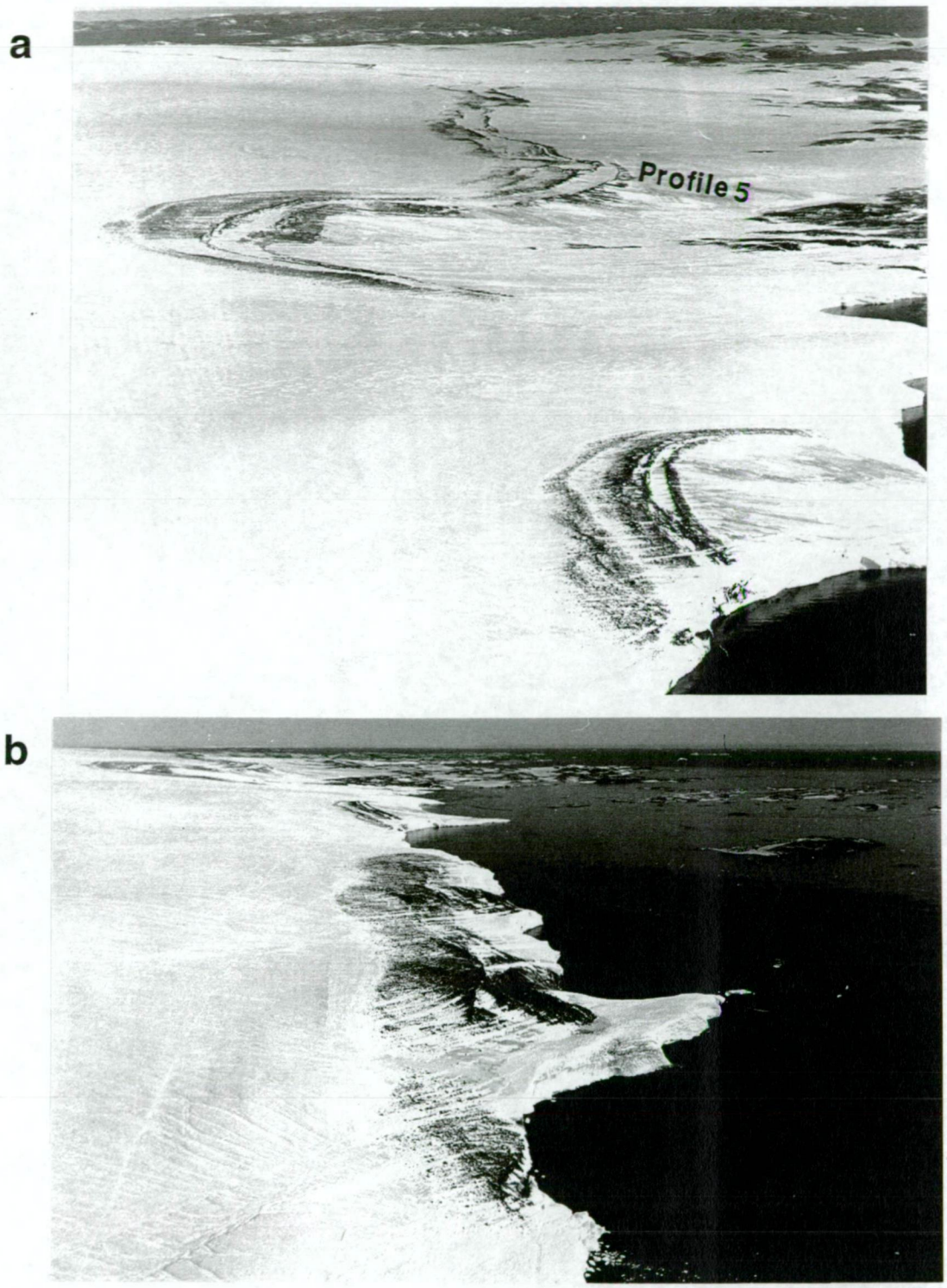

Figure 5.4 Oblique aerial photographs looking south along the Løken Moraines. (a) Note the multiple moraine ridges at Jacks Donga promontory in the foreground and in the Clark Peninsula moraine segment in the middle distance, and a single ridge on Bailey Peninsula, in the distance. The moraines on Clark Peninsula (profile #5, Figure 5.5b) are in close proximity (~0.5 km) to the raised beaches at 18-27 m elevation near Stevenson Cove. (b) The ice cliff moraines with the ice cliff 10 study site in the foreground. Photographs taken by the author in January 1986.

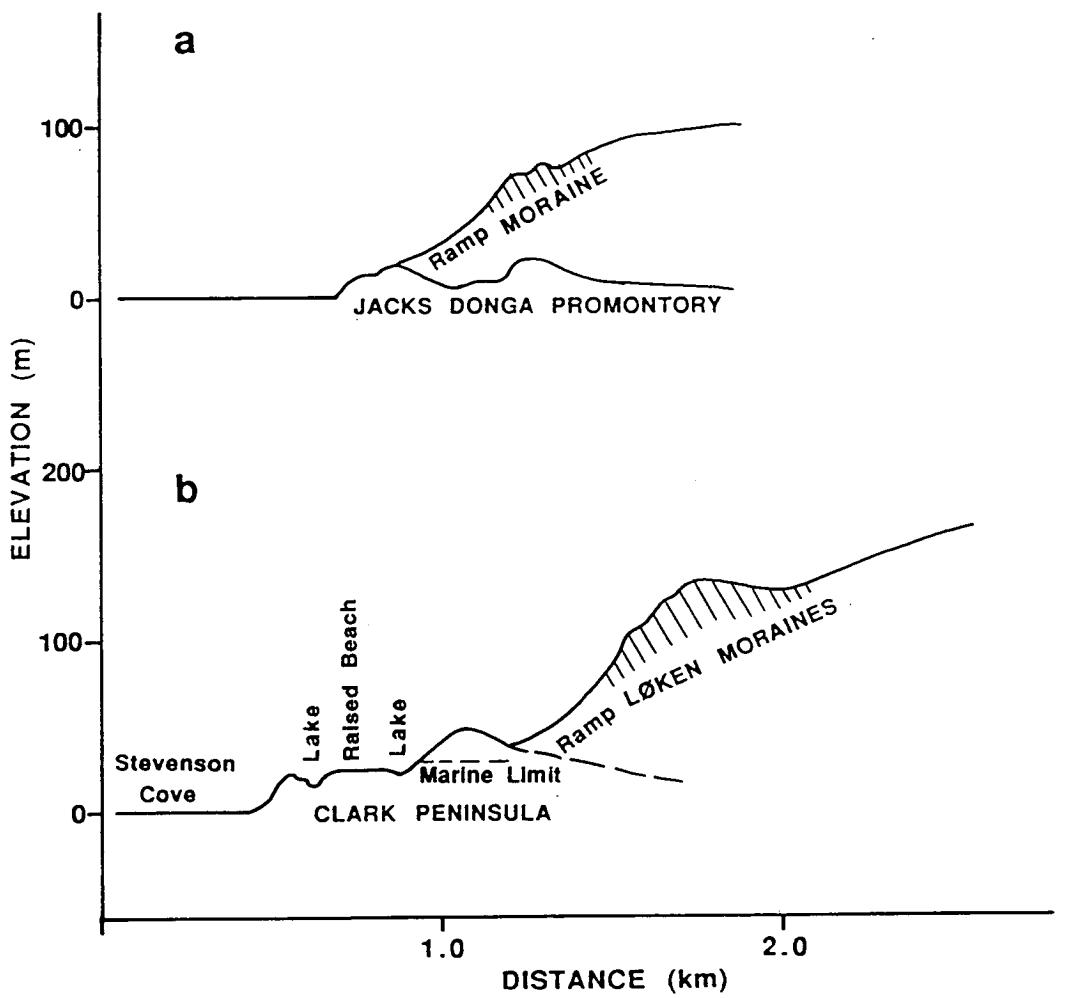

Figure 5.5 Longitudinal surface and bedrock profiles of the ice-ramp and the Løken Moraines at: (a) Jacks Donga Promontory, profile #7; and (b) inland of Stevenson Cove and Clark Peninsula, profile #5. Also shown is the marine limit on Clark Peninsula and the location of raised beaches and lakes. The surface profiles were surveyed by optical level, and the bedrock profiles are interpolated from ice thicknesses calculated from spot gravity measurements.

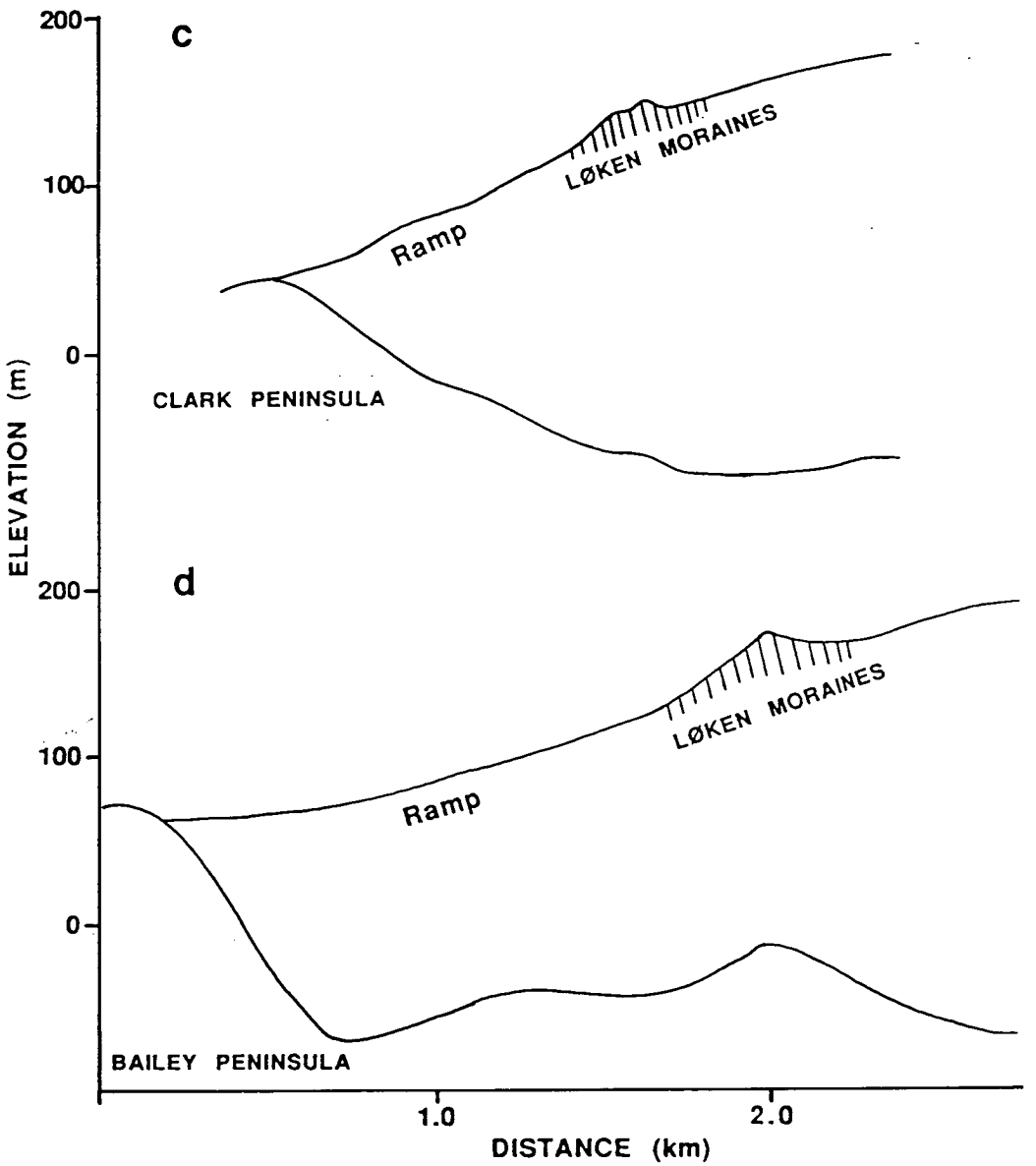

Figure 5.5 Longitudinal surface and bedrock profiles of the ice ramp and the Løken Moraines at: (c) central Clark Peninsula, inland of nunatak C7, profile #3; and (d) inland of central Bailey Peninsula, profile #1. The surface profiles were surveyed by optical level, and the bedrock profiles are interpolated from ice thicknesses calculated from spot gravity measurements.

further inland (as determined from gravity and ice radar profiling). These multi-ridged and arcuate moraines also outcrop at the inland flank of Williams, Longs and Campbell Nunataks between Robinson's Ridge and Browning Peninsula (Figure 4.1) and surrounding Haupt Nunatak on the eastern margin of the Vanderford Glacier. The total width of the moraines varies markedly with their physiography; for example the multi-ridged moraines and flats in the Clark Peninsula section vary from 200-400 m in width, whilst the single ridge and flat moraines which comprise the majority of the remainder of the Løken Moraines vary from 100-200 m in width. The inland ridge and moraine flat are the most extensive and well developed features along the entire Løken Moraines.

These morphological characteristics are important clues in the evolution of the present ice margin, since they reflect differences in glacial bedrock elevations, ice velocities and the extent of ice deformation and the range of glaci-tectonics, together with the fluctuations in mass balance near the margin. There is a marked increase in the elevation of the bedrock inland of the ice sheet margin from Cape Folger, north of IC10 southwards to inland of Mitchell Peninsula. Figure 5.6 shows that the bedrock elevation is at or below sea level from Cape Folger to inland of the Clark Peninsula. The Windmill Is extend inland beneath the Law Dome in a south-westerly direction from Bailey and Mitchell Peninsulas with undulating topography ranging in elevation from 40-70 m. The ice velocities measured on Law Dome inland of the margin directly reflect the trend in bedrock elevation. Inland of Bailey Peninsula, where the ice base is above sea level, the ice velocity is less than 1m a^{-1} (observed 2 km inland of Clark Peninsula). Inland of the northern marine ice cliffs and Cape Folger where the ice base is below sea level the ice velocities are significantly greater at 5-11 m a^{-1}. The greater development of moraine width and topography inland of Clark Peninsula and along the ice cliffs is a function of the faster ice velocities and associated strain rates, which result in the complex ice deformation within the ice margin. The ice flow directions are approximately orthogonal to the ice margin shown in Figure 5.1. The majority of ice is discharged to the north and south of the Windmill Islands.

Since the Løken Moraines are the surface expression of the basal ice zone, a detailed study of the isotope and chemical characteristics of the basal ice and sediment in the moraines was undertaken to yield information on the origin of the basal zone and hence the present ice sheet marginal morphology. Similar basal ice studies had been conducted by numerous workers in the Arctic, sub-Arctic and temperate regions (Hubbard and Sharp, 1989). However, there have been few rigorous studies of basal debris ice sequences at the margin of the East Antarctic ice sheet largely because of their inaccessibility. Souchez and Lorrain (1992) provide a comprehensive treatment

of basal ice composition and basal processes with reference to Antarctica. The second part of this Chapter investigates the sequence of ice margin evolution during the Holocene, by examining the morphology and glacio-tectonic structure of the Løken Moraines and the ice margin.

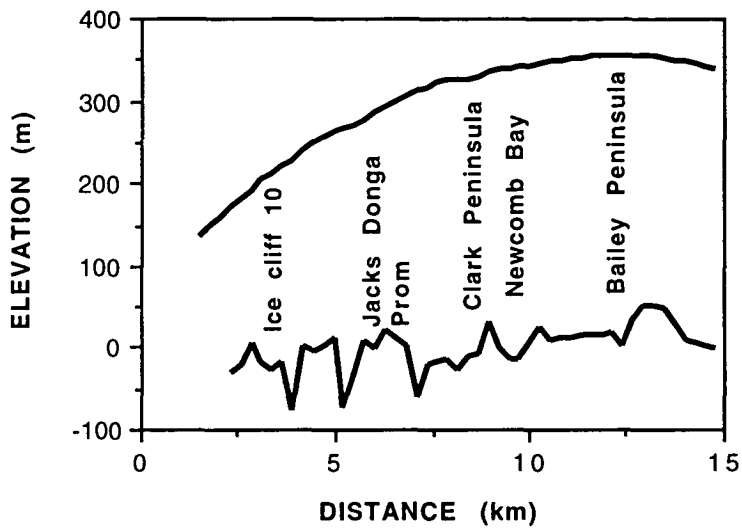

Figure 5.6 Transverse section through the Law Dome ice sheet inland of the ice margin, between Cape Folger and inland of Mitchell Peninsula. The surface elevation profile was surveyed by optical level and the bedrock by ice radar. The data are from unpublished ANARE glaciological surveys (N. Young pers. comm., 1994). The location of the profile is shown in Figure 5.1.

5.4 A STUDY ON THE EVOLUTION OF THE BASAL ICE ZONE

5.4.1 GEOGRAPHIC SETTING

A site designated as ice cliff 10 (IC10) shown in Figure 5.1, was selected for the basal ice study at the northern edge of the Løken Moraines where the basal debris bearing ice is exposed in marine cliffs. These marine ice cliffs reveal both transverse and longitudinal exposures (Jacks Donga ice cliffs) of the basal debris bands and adjacent basal zone ice providing a complete basal sequence, since the cliffs are grounded at or near sea level. IC10 is 28 m high and is grounded just below sea level (Figures 5.7).

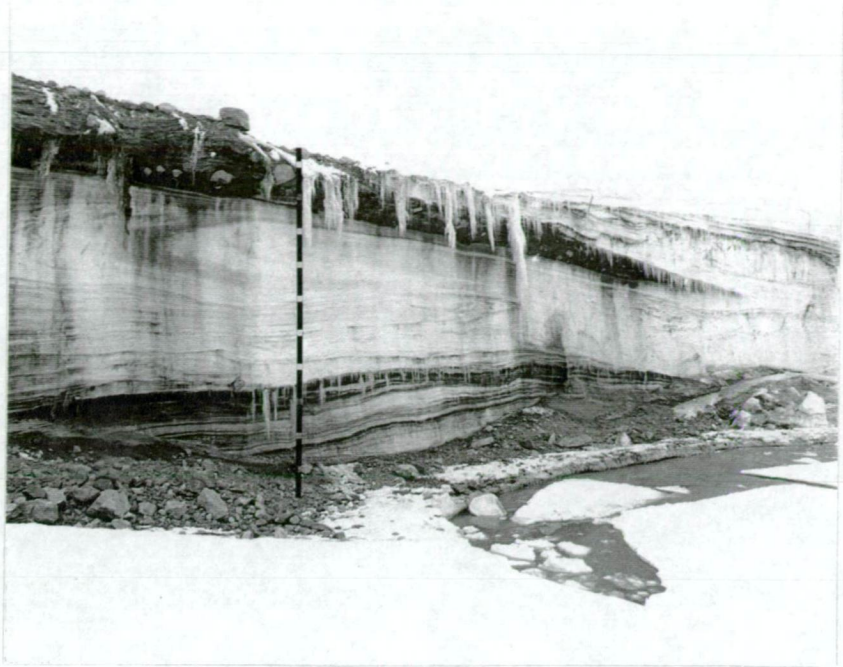

Figure 5.7 The ice cliff 10 (IC10) exposure perpendicular to the ice flow direction showing the upper and lower debris bands and folded ice of marine origin, between the bands. The upper debris band is enclosed by a single isoclinal fold. A proglacial talus fan lies on the multi-year sea-ice foot. The sample profile is also shown.

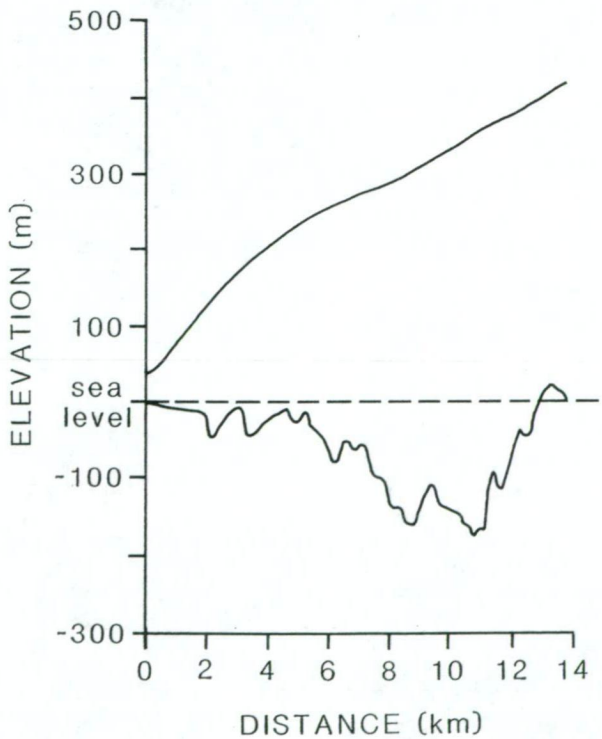

Figure 5.8 Surface and bedrock profiles inland of ice cliff 10 (IC10) showing deep bedrock troughs below present sea-level. The surface elevation profile was surveyed by optical level and the bedrock by ice radar. The data are from unpublished ANARE glaciological surveys (N. Young pers. comm., 1994).

The exposure reveals an upper and lower, stacked debris-rich ice sequence separated by a folded green translucent ice and light-green bubbly ice sequence. Above the upper debris-rich sequence, a third stacked debris-rich ice sequence emerges beneath a boulder strewn supraglacial moraine. The curious green ice sequence was also observed outcropping in adjacent ice cliffs over a distance of 3 km and resembles the green icebergs which have been observed on occasions in Antarctic waters (Warren et al., 1992).

To the north of IC10, the Law Dome ice margin is grounded below sea level and to the south it is grounded mainly above sea level where the elevation of the subglacial bedrock is in the vicinity of 50-100 m above present sea level. A profile of the ice surface and subglacial bedrock topography at the ice cliff and inland of IC10 is shown in Figure 5.8. The profiles show that the bedrock is at or below present sea level for approximately 12 km inland of the margin.

5.4.2 ICE CLIFF SAMPLING

A continuous stratigraphic sequence through the basal ice and debris zone was sampled down the entire ice cliff face using a chainsaw and a 100 mm diameter ice drill. The sequence was cut into two 5 m long cores which corresponded to the upper and lower debris band sequences, respectively. The samples were transported frozen (below -10 $^{\circ}$C) to Australia for laboratory analysis which included: (i) co-isotopic analysis for $\delta^{18}O$ and δD, (ii) electrical conductivity of melted ice, (iii) ice crystallography, (iv) solute chemistry including; Na, Ca, Mg, K, HCO_3, Cl and SO_4, (v) debris concentration by volume, (vi) debris particle size analysis, and (vii) micropalaeontological analysis. Melted ice samples were obtained primarily from interstitial debris poor ice lenses and layers (less than 1% debris by volume) within the debris-rich ice. All the ice samples were melted in sealed jars at room temperature (18°C) over a constant period of twenty-four hours to ensure particle settling. Debris concentrations were measured by weight and converted to volume after the separate debris-rich ice samples were melted and the water fraction evaporated. Debris particle size analysis was conducted using a dry sieving method for the sediment coarser than 5 phi (63 microns) and by Coulter Counter for material finer than 5 phi.

5.4.3 BASAL ICE TYPES AND STRATIGRAPHY

An oxygen isotope ($\delta^{18}O$) stratigraphy is shown in Figure 5.9 for IC10. Detailed debris concentrations (by volume), bulk layer stratigraphy and $\delta^{18}O$ stratigraphies are

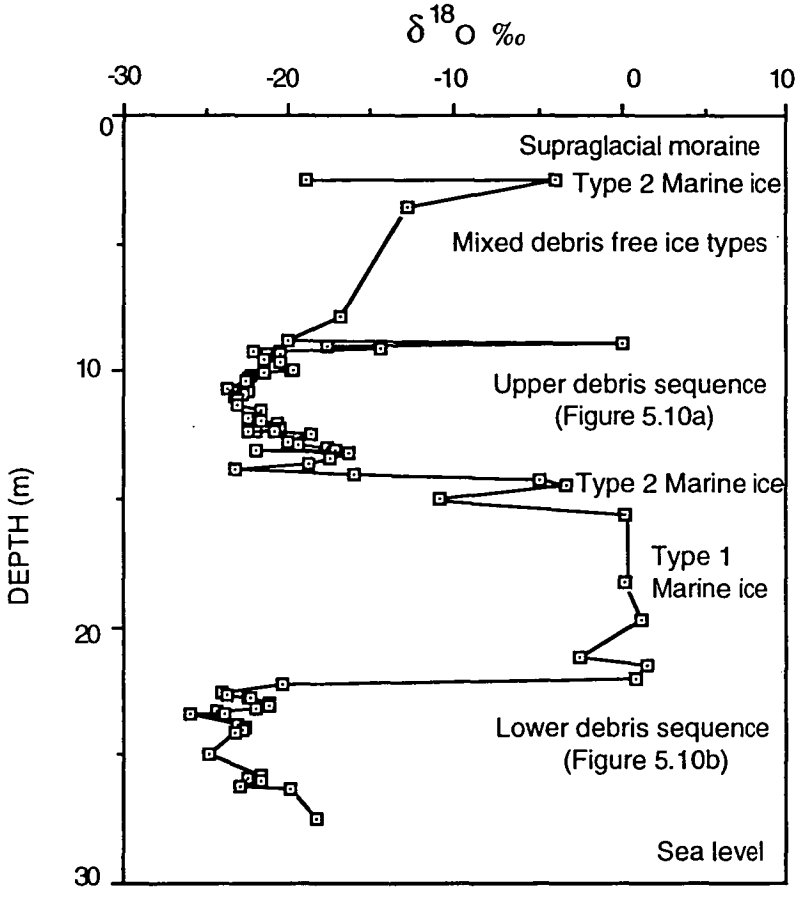

Figure 5.9 Oxygen isotope depth profile for ice cliff 10 (IC10) together with the four interpreted basal ice zones.

shown in Figures 5.10a and 5.10b respectively, for the upper and lower debris-rich sequences . The $\delta^{18}O$ range for the unaltered glacier ice interbedded in the lower basal sequence and below the upper basal sequence by folding is -26.0 to -23.2‰ which corresponds to the range for Pleistocene / Holocene transition ice near the Law Dome margin (Goodwin, 1988). The $\delta^{18}O$ range for the unaltered glacier ice immediately above the upper debris band is in the range of -23.0‰ to -21.0‰. Six basal ice types were interpreted from the stratigraphy and are described below. Similar ice crystallographic characteristics were displayed by all ice types due to the high degree of deformation in the basal zone. This has resulted in large crystals, elongated bubbles and combined shear and compression fabrics displaying multi maxima patterns. Fault planes occur in the lower basal sequence whilst boudinage (from subsequent extensive flow) occurs in the upper debris sequence with the presence of debris free glacier ice interlayered with the type 6 laminated debris ice. There is also extensive intra-folia folding of the type 6 ice in the thickened upper debris sequence. The upper and lower debris bands are enclosed by isoclinal folds. Type 1 ice forms the bulk of the 10 m exposure of folded ice separating the upper and lower debris band sequences. Type 2 ice outcrops along the isoclinal folds enclosing the upper debris band and between upper debris band and the overlying supraglacial moraine (Figure 5.9).

5.4.3.1 DEBRIS-FREE ICE TYPES

Type 1 Green bubble-poor ice

This ice has a $\delta^{18}O$ range of + 0.26 to +1.56 ‰ which is similar to that for sea ice (Souchez et al., 1991) indicating a marine origin. This is confirmed by the inclusion of some biogenic material, mainly marine benthic diatoms and sponge spicules. It is bubble-free to bubble-poor, with a crystalline, optically clear appearance and conchoidal fractures through some layers. It has a green colour in situ and is formed in a layered or banded sequence with light green bubbly ice (Type 2).

Type 2 Light green bubbly ice

This ice has a $\delta^{18}O$ range of -16.9 to -2.6 ‰ with samples clustered in two groups with $\delta^{18}O$ ranges of -2.57‰ to -4.9‰ and -10.86‰ to -16.93‰. These groups correspond to ice formed from the mixture of glacial meltwater and seawater. It has a whitish-green colour and is optically opaque, consisting of primarily bubble rich ice with strong bubble elongation. In the enriched $\delta^{18}O$ group layers or lenses of optically clear bubble-poor ice similar to type 1 ice predominate.

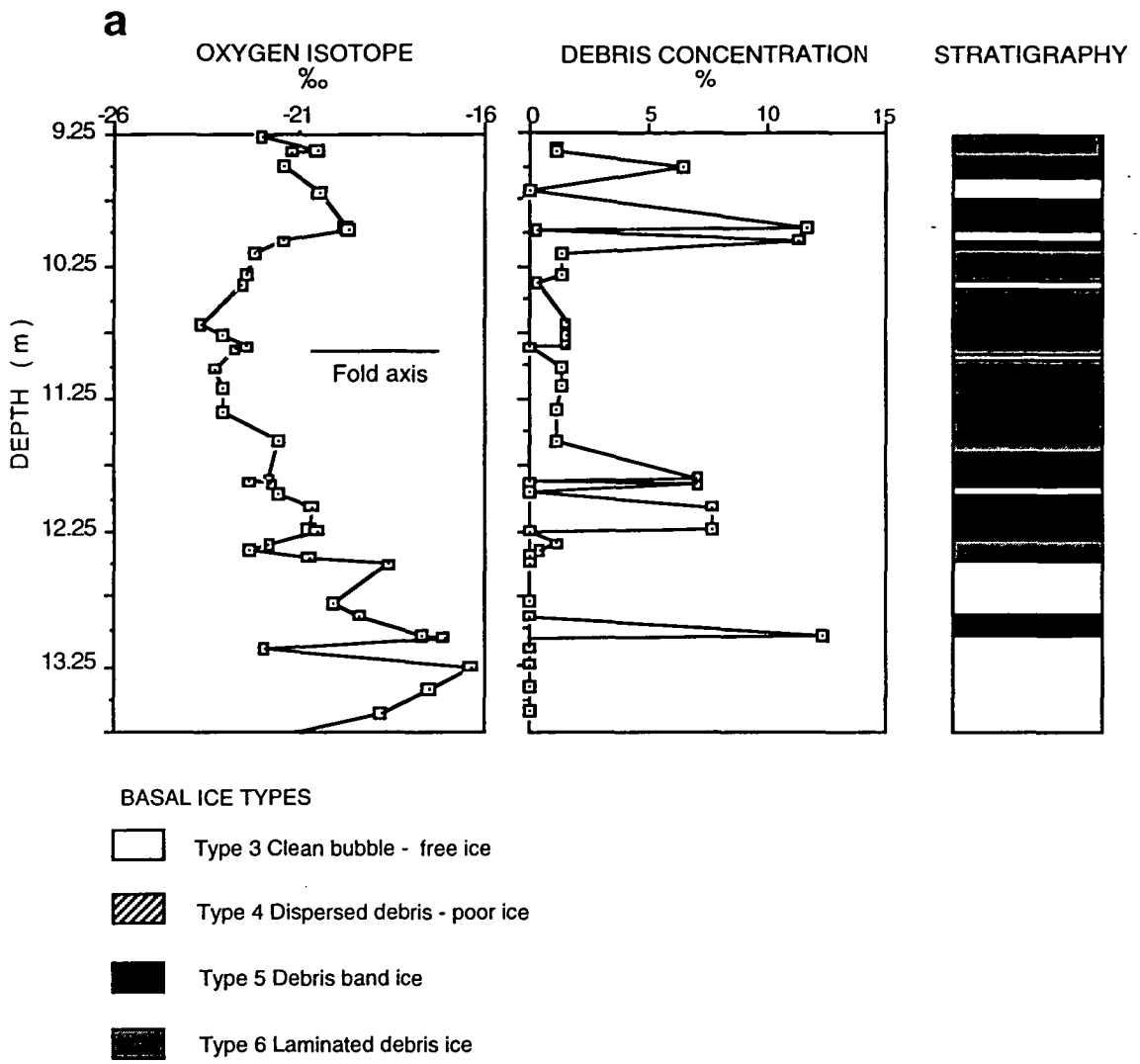

Figure 5.10a Detailed oxygen isotope, debris concentration (by volume) and visible bulk layer stratigraphies for the upper debris band, together with the basal ice types occurring in each band. The individual layering within the basal ice types is not shown.

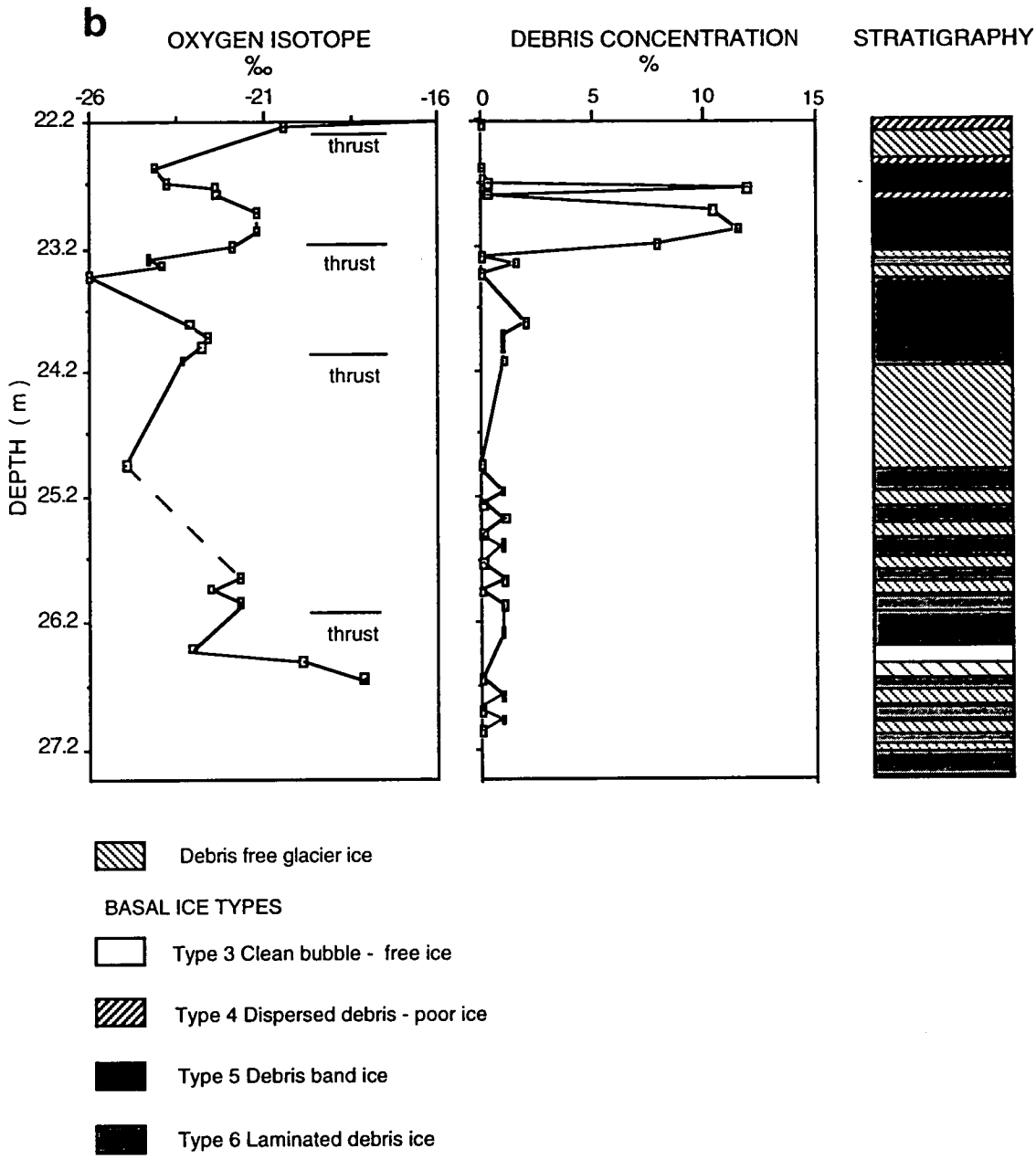

Figure 5.10b Detailed oxygen isotope, debris concentration (by volume) and visible bulk layer stratigraphies for the lower debris band; together with the basal ice types occurring in each band. The individual layering within the basal ice types is not shown.

Type 3 Clean bubble-free ice

This ice has a $\delta^{18}O$ range of -23.3 to -16.4 ‰. It is crystalline, optically clear and colourless,with very rare bubbles. It is usually found intercalated with type 5 and type 6 debris ice forming distinct couplets in the stacked debris sequences. Typically the clear ice occurs in thin laminae 10 mm thick but can occur in massive layers up to 1 m thick displaying a similar crystalline appearance to type 1 ice. Very rarely it contains small rock chips.

5.4.3.2 DEBRIS-BEARING ICE TYPES

Type 4 Dispersed debris-poor ice

This ice has a $\delta^{18}O$ range of -23.8 to -17.3 ‰. It has a whitish grey or dirty glacier ice appearance. It is bubbly ice with lenses of optically clear bubble-poor ice (type 3 ice) containing dispersed debris inclusions comprising fine debris aggregates (in concentrations less than 0.3% by volume), together with gravel and rare striated, cobble and boulder clasts. It is characterised by a strong bubble elongation.

Type 5 Debris band ice

This ice has a $\delta^{18}O$ range of -21.9 to -17.7 ‰. It consists of bubble free, debris- rich ice bands which are stratified with type 3 clear bubble-free ice as intercalated couplets. The debris concentration (< 2 phi size, 250 microns) ranges from 6.3 to 13% by volume. In an adjacent cliff the debris concentration was as high as 33% by volume. In the higher debris concentration ice, type 3 clean bubble-free interstitial ice lenses replace the alternating laminae of type 3 ice. The debris -rich ice generally occurs in bands 0.2 to 0.3 m thick, but can be up to 1 m thick The thickest debris bands are intercalated with similar thickness type 3 bubble-free ice layers. The debris contains fine sandy gravel sediment similar in texture and lithology to the surficial sediment cover over the northern Windmill Islands.

Type 6 Laminated debris ice

This ice has a $\delta^{18}O$ range of -23.9 to -20.6 ‰ which overlaps with the range for unaltered glacier ice within and adjacent to the debris sequences. It is slightly bubbly to bubble-free ice and is typically stratified with type 3 clean bubble-free ice and type 4 dispersed debris-poor ice. The debris concentration (< 2 phi size) ranges from 0.9% to 1.9% by volume. The debris has a gravelly fine sand texture and rarely contains sediment up to cobble clasts. It occurs as discrete thin (mm) laminae ranging up to massive bulk layers 2 m thick. Generally the layers are 0.3 to 0.4 m thick. This ice has a muddy appearance with sand particles in suspension. The debris also occur in

aggregates rather than laminae in the lowest concentrations where they fade into type 4 dispersed debris-poor ice.

Based on the range of oxygen isotope values measured for each of the above types it was possible to discriminate between four different sample populations. These are; marine origin type 1 ($\delta^{18}O$ range of + 0.26 to +1.56 ‰); mixed meltwater and marine origin type 2 ($\delta^{18}O$ range of -16.9 to -2.6 ‰); clean and debris-bearing types 3, 4, 5 and 6 (overlapping $\delta^{18}O$ range of -23.9 to -16.4 ‰) and glacier ice ($\delta^{18}O$ range of -26.0 to -23.2 ‰).

5.4.4 CO-ISOTOPIC COMPOSITION OF BASAL ICE

Co-isotopic linear regression analyses of deuterium (δD) and oxygen ($\delta^{18}O$) isotopes were applied separately to each of the four sample populations and are shown in Figures 5.11a and 5.11b. In this study, thirty-seven of the eighty-nine ice samples measured for $\delta^{18}O$ content were also measured for δD content. The precision of the isotope measurements was +/- 0.17‰ in $\delta^{18}O$ and +/- 0.60‰ in δD. The unaltered glacier ice samples (n=7) lie along the line with a slope of 8.2 ($\delta D = 8.2\ \delta^{18}O + 13.4$, with a correlation coefficient of 0.965). The marine origin type 1 ice samples (n=4) lie along a line with a slope of 8.1 ($\delta D = 8.1\ \delta^{18}O + 5.8$, with a correlation co-efficient of 0.988) whilst the mixed origin type 2 ice (n=9) lie along a line with a slope of 7.8 ($\delta D = 7.8\ \delta^{18}O + 4.9$, with a correlation co-efficient of 0.996). The debris-bearing ice and clean types (n=17) lie along the same line with a slope of 8.0 ($\delta D = 8.0\ \delta^{18}O + 4.8$, with a correlation co-efficient of 0.991).

Co-isotopic analysis has been used by numerous researchers into basal ice accretion processes, since the technique was first applied to this problem by Jouzel and Souchez (1982). They showed that basal ice which has undergone fractionation during refreezing, displays a distinct co-isotopic freezing slope which is less steep than the slope of S = 8 (meteoric slope) for unaltered glacier ice or precipitation (Craig, 1961). All the four sample populations have co-isotopic slopes equivalent to the meteoric slope S = 8 for precipitation. The slight variation in slope is probably due to the small sample populations and the measurement error. Since these ice types display characteristics which can only be attributed to ice formed from the freezing of water in the basal zone, the lack of a co-isotopic freezing slope required investigation. It is possible that the fractionation effects were not detected if the individual refrozen increments were thinner than the composite ice layers sampled (Souchez et al., 1988).

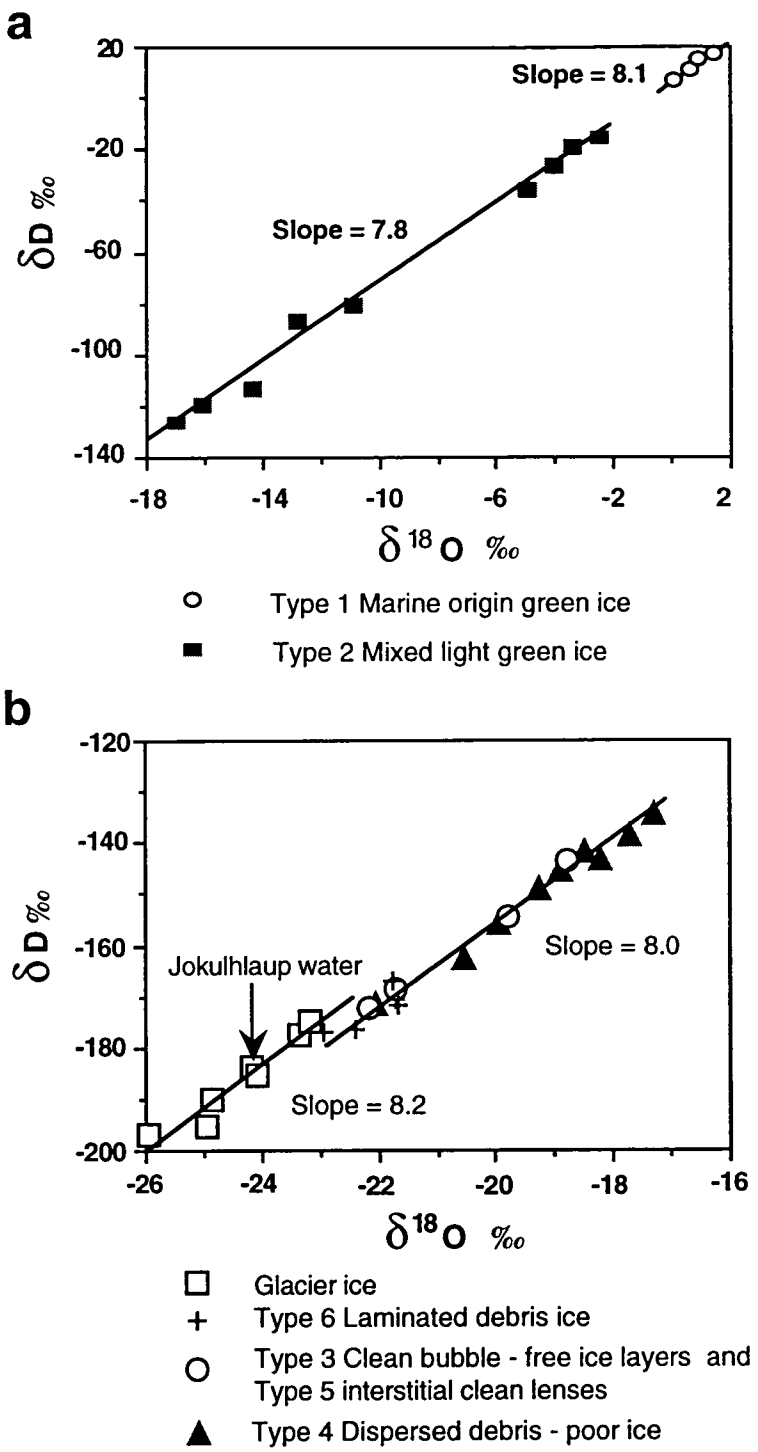

Figure 5.11 Co-isotopic plot of oxygen isotope and deuterium isotope values for: (a) type 1 marine origin and type 2 mixed glacial/marine origin ice, and; (b) glacier ice, type 3 clean ice and types 4, 5 and 6 debris bearing ice together with the jökulhlaup basal meltwater.

Alternatively, it is suggested that they were formed from a range of initial waters rather than an isotopically uniform water source and that the water input during freezing was isotopically lighter or more depleted than the initial meltwater reservoir (Souchez and De Groote, 1985). At the Law Dome margin three water sources which are isotopically distinct from basal meltwater and a variety of possible mixtures exist. These are small proglacial freshwater and brackish lakes with a range in $\delta^{18}O$ of -15.8 ‰to -5.8 ‰, permafrost and meltwater from local precipitation with $\delta^{18}O$ of -16 ‰ to -13 ‰ and seawater in adjacent embayments with $\delta^{18}O$ close to 0 ‰.

An estimate of the isotopic characteristics of subglacially produced meltwater near the Law Dome margin was obtained when water samples were collected from a major jökulhlaup event at the margin in 1985 (Goodwin, 1988). The jökulhlaup occurred approximately 7 km along the margin from IC10 (near Newcomb Bay) discharging meltwater to the ice surface. The meltwater had a mean $\delta^{18}O$ value of -24.2‰ and a δD value of -184.0‰ which are equivalent to the mean values for the Late Pleistocene-Holocene transition period (11-13, 000 y BP age) glacier ice in IC10. Consequently, the jökulhlaup water was considered to be representative of subglacially produced meltwater.

Whilst all the ice types lie along lines with the same slope, there is considerable variation in the deuterium excess value d (calculated from, $d = \delta D - 8\ \delta^{18}O$ (Dansgaard, 1964)) between the unaltered glacier ice and the basal and marine ice samples. The average d value for the unaltered glacier ice was calculated as 10.8‰ from both ice samples in IC10 and from ice of the same age in a nearby borehole at BHF near Cape Folger (N. Young and J. Jouzel pers. comm.) This d value for the Late Pleistocene-Holocene transition age ice is approximately 4-5‰ greater than the d for Holocene precipitation on Law Dome which is close to 6‰. The basal meltwater lies along the same line as that for the unaltered glacier ice in Figure 5.11a with a d value of 9.6‰ which is within the measurement precision for the unaltered glacier ice. However the basal ice types 3, 4, 5 and 6, the marine type 1 and mixed origin type 2 have average d values of 4.9‰, 6‰ and 6.7‰ respectively, which are close to the value for Holocene precipitation. This suggests that the basal ice types have formed from the mixture of marginal Holocene water bodies with the more $\delta^{18}O$ and δD depleted basal meltwaters during an ice margin advance.

5.4.5 MARINE ICE CHARACTERISTICS AND ACCRETION

As outlined above the type 1 marine ice samples are clustered in a small $\delta^{18}O$ range of +0.26‰ to +1.56‰ with a corresponding range in δD of +8.03‰ to +18.31‰.

They are interlayered with more depleted type 2 ice of mixed freshwater and seawater origin. The type 1 and type 2 ice layers have conductivities in the range 22 to 198 µS/cm which correspond to salinities of 0.008 to 0.076 ppt. Since the ice has recrystallised due to deformation it is not possible to determine its genesis from crystallography. However, the type 1 ice is distinctive in its bubble-free, optically clear and crystalline appearance.

The enriched $\delta^{18}O$ range for the Type 1 ice corresponds to the range for frozen seawater close to VSMOW (Vienna Standard Mean Ocean Water) since the freezing of seawater results in an enrichment in $\delta^{18}O$ of up to 2‰ for a single freezing event (Souchez et al., 1991). Morgan (1972 and pers. comm) reported a 158 m thickness of basally accreted frozen sea water in the Amery Ice Shelf which had a similar optically transparent appearance to the Law Dome type 1 ice together with a similar $\delta^{18}O$ range of 0‰ to +2.3 ‰ and very low salinities of 0.015 to 0.020 ppt. The $\delta^{18}O$ range and δD range for the type 1 ice is also similar to that for congelation ice and frazil ice forming beneath the Hell's Gate Ice Shelf in Victoria Land (Souchez et al., 1991).

Whilst the $\delta^{18}O$ range is comparable between the different geographic locations there is considerable geographic variation in the Na content which reflects the relative mixing of glacial meltwater with the parent seawater mixture and the rate of freezing. The Na content of type 1 ice is very dilute in the range 0.003 - 0.033 ppt which is similar to that for the Amery Ice Shelf (0.005 ppt). These concentrations are comparable to those reported by Souchez et al. (1991) for frazil ice formed from multiple freezing and melting events of congelation ice beneath the Hell's Gate Ice Shelf (0.005 - 0.15 ppt) and much lower than those for congelation ice (0.5 - 0.8 ppt) in the same study. On the basis of the isotopic ranges and the very low Na content the Type 1 ice was interpreted to be derived from frazil ice formed from the freezing of seawater.

Interlayered with the type 1 ice in IC10 is the type 2 ice with a clustered $\delta^{18}O$ range of -2.57‰ to -4.9‰, a δD range of -15.31‰ to -36.23‰, and a similar Na content to type 1 ice. This $\delta^{18}O$ range corresponds to the $\delta^{18}O$ ranges of; +1.5‰ to -4.9‰ for desalinated sea ice formed from the cyclic melting and refreezing of marine ice in the Koettlitz Glacier Tongue, in McMurdo Sound (Gow and Epstein, 1972) and; -2.5‰ to -4.9‰ for marine ice forming part of the Strand Moraines' ice core on the west coast of McMurdo Sound (Currie, unpublished). This type 2 ice is more bubbly than type 1 ice and is interpreted also as frazil marine ice (Gow et al., 1987) formed from

parent seawater with a mixture of glacial meltwater in small quantities. The second clustered type 2 ice has a more depleted $\delta^{18}O$ range of -10.86‰ to -16.93‰ and most likely formed from a greater input of glacial meltwater with the parent seawater. Similar marine ice with an equivalent δD range -20‰ to -100 ‰ which corresponds to a $\delta^{18}O$ range of -3.75‰ to -13.75‰, and a Na concentration of 0.020 ppt, was found by Lorius (1968) in the basal zone 500 m inland of supraglacial moraines near Dumont d'Urville in Terre Adélie.

The Law Dome type 1 ice and type 2 ice do not display a freezing slope unlike the marine ice samples from the Hell's Gate Ice Shelf which lie on a co-isotopic freezing slope S = 6.6 (Souchez et al., 1991). The lack of a displayed freezing slope may be due to the mixing of small amounts of glacial meltwater with the dilute seawater. This would imply that water heavier or more enriched in $\delta^{18}O$ than type 1 ice was present prior to refreezing. Such water could only have formed from seawater which had originated from multiple melting-refreezing events since its $\delta^{18}O$ range is greater than the 2‰ enrichment due to a single freezing event of sea water. Multiple freezing events of seawater would also be required to explain the very low Na concentrations measured in the type 1 and type 2 ice. Souchez et al. (1991) concluded that frazil ice like the type 1 and enriched type 2 ice formed near the front of ice shelves and glacier tongues from marine ice transfer processes, especially where the water depth shoals and the water temperature contrast decreases.

Prior to the Holocene re-advance of Law Dome it is probable that the subglacial bedrock troughs just inland of IC10 would have been marine embayments (Figure 5.8b). It is proposed that as the ice sheet advanced marine ice was accreted in these marine embayments since their orientation is roughly parallel to the ice margin where the green ice outcrops in the cliffs. The interlayering of the type 1 and the type 2 marine ice with its large $\delta^{18}O$ range suggests that the accretion process involved the episodic input of glacial meltwater to the parent seawater. The accretion of the marine ice most probably occurred beneath either fast sea ice or a small ice shelf in a marine embayment near the grounding line. Structural analysis of IC10 (Figure 5.7) showed that the debris rich sequences are enclosed by recumbent isoclinal folds whose axes intersect the sheath folded and overturned marine ice layers. It was interpreted from this sequence that the marine ice had been partially overridden by the upper folded debris rich ice sequence, and had been accreted prior to the entrainment of the debris bands.

5.4.6 MODES OF SUBGLACIAL DEBRIS ENTRAINMENT AND ICE ACCRETION

Borehole temperature measurements define a temperature gradient of 3.8°C/ 100 m at S1 (ice thickness 250 m) approximately 2 km inland of the Løken Moraines on Clark Peninsula and indicate that the basal ice is at the pressure melting point. This is supported by the presence of basal water 2.5 km downstream at the jökulhlaup site near the margin. However there is the capacity for freezing at the bed since there is twice the heat loss upwards through the ice than the estimated geothermal heat gradient (2.2°C/ 100 m) can maintain (N. Young, pers. comm.). Consequently, as the ice thins towards the margin the bed is in a zone of progressive freezing where extensive basal ice accretion may take place (Weertman, 1961), . However, the co-isotopic analysis, although on a limited data set, showed that neither the clean or debris bearing basal ice types displayed isotopic alteration and hence any clear evidence for the mode of accretion by bulk adfreezing of water and debris, as defined by Weertman (1961). A similar case was reported for the clean and dispersed debris layers in the Russell Glacier in West Greenland by Sugden et al. (1987), Knight (1987, 1989) and Souchez et al. (1988). Whilst they found co-isotopic evidence for a freezing origin for the debris band ice (similar to type 5 in this study) they attributed the un-fractionated clean and dispersed debris ice (similar to types 3, 4 and 6 in this study) to a localised small scale pressure-melting mechanism where water loss and fractionation did not occur. This process may be responsible for the Law Dome type 3 clean ice and type 6 laminated debris ice types since their typical layer thicknesses of 0.1 m and 0.3 m, respectively correspond to the local bedrock roughness. However the following discussion presents evidence for another related regelation process.

The debris sequences in IC10 significantly thicken upwards. This thickening was also observed in a longitudinal exposure of the ice cliffs together with both faulting and complex folding. The tectonics are the result of longitudinal compression of the basal ice as the flow was blocked by the relatively high bedrock elevation of the Windmill Islands. Robin (1976) proposed the pressure melting mechanism known as the"heat pump" effect within the basal ice mass, where excess water is formed in such high pressure zones upstream of obstacles. The basal ice is cooled by the heat pump effect following the squeezing of the excess water and air from the ice by the high pressure. In the downstream areas where low pressures exist, cold patches form which allow the refreezing and accretion of the squeezed water together with any other local water body. The similar large and overlapping $\delta^{18}O$ range for both type 3 (-23.3 to -16.4 ‰) and type 4 (-23.8 to -17.3 ‰) ice corresponds to the $\delta^{18}O$ range between basal meltwater (-24.2‰) and proglacial / marginal water (-16‰). This indicates that

mixtures of basal meltwater and proglacial / marginal water bodies existed prior to refreezing. Souchez and Lorrain (1978) reported that selective flushing out of ions is expected to accompany the expulsion of air and water from the basal ice by the heat pump effect, due to a more rapid migration of the alkalis (Na + K) into the squeezed water. This would lead to a characteristic chemistry in both the basal ice and squeezed water as described by the molar ratio [(Na + K) / (Ca + Mg)].

Figure 5.12 shows the separation of ice types on the basis of the molar ratio [(Na + K) / (Ca + Mg)]. The molar ratio [(Na + K) / (Ca + Mg)] for unaltered glacier ice is 3.8 which reflects the marine origin of Antarctic precipitation. Type 4 dispersed debris-poor ice is less bubbly than glacier ice and contains lenses of type 3 clean and debris-bearing bubble-poor ice. These characteristics suggest that the type 4 ice has been exposed to basal squeezing processes with the subsequent migration and refreezing of small pockets of squeezed water. This is supported by the low molar ratio [(Na + K) / (Ca + Mg)] for the bubbly type 4 ice which ranges from 0.4 to 1.2, a significant decrease from the glacier ice value and reflects the selective flushing out of ions (alkalis) due to water expulsion or squeezing (Souchez and Lorrain, 1978). The debris in the type 4 ice includes freshly eroded fine sands and rock fragments together with striated and faceted cobbles and boulders which have been carried in traction over the bed.

Lawson (1979) and Knight (1987) suggested that fine debris such as occurs in the type 4 ice may be entrained by a migration of dirty basal water into the squeezed ice away from the pressurized interface. An increase in the molar ratio [(Na + K) / (Ca + Mg)] to a range of 1.2 to 3.4 is shown for type 3 clean bubble-poor ice from the type 4 ice values. This is consistent with an origin as refrozen squeezed water relatively enriched in the alkalis when compared to the squeezed ice. The lower ratio values for the type 3 ice correspond to ice layers with sparse bedrock chips and angular bedrock clasts as a result of the preferential contribution of the alkaline-earths (Ca + Mg) as observed by Souchez and Tison (1981) in subglacial meltwater. Unweathered extremely angular and homogenous blocks of plucked local bedrock were found incorporated in the 1-2 m thick type 3 layers (Goodwin 1988c). Consequently the type 3 ice was interpreted to form over a "hard" substrate (bedrock). However, since the northern Windmill Islands are dominated by acid rocks, mainly granite gneisses (Blight and Oliver, 1977) with a high Na + K and low Ca + Mg content, it was expected that chemical weathering of the bedrock would produce a higher molar ratio in the basal meltwater. The lower than expected molar ratio in the type 3 ice may be attributed to a limited circulation of the squeezed water prior to refreezing.

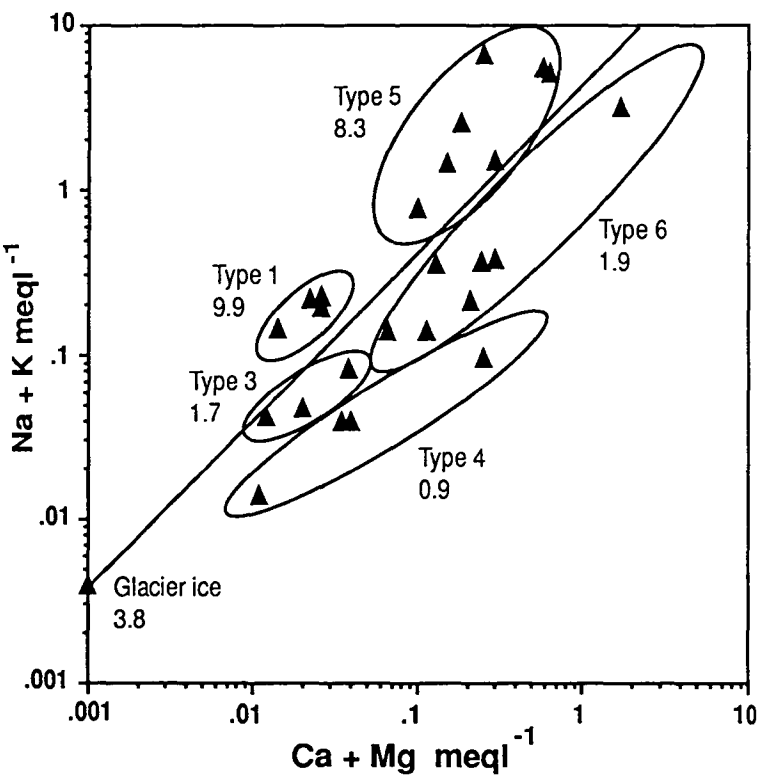

Figure 5.12 Plot of alkalis (Na + K) vs alkaline earths (Ca + Mg) for glacier ice and the basal ice types. The molar ratio (Na + K)/(Ca + Mg) value is shown for each basal ice type, and as a solid line for unaltered glacier ice.

The type 6 laminated debris ice has a similar molar ratio [(Na + K) / (Ca + Mg)] of 1.0 to 2.7 to that for type 3 ice and was interpreted to form from refrozen squeezed water transporting fine sands in suspension and angular rock fragments. These fine sands and rock fragments indicate that they are the product of freshly eroded bedrock by glacial crushing processes and that the type 6 ice probably accreted immediately downstream of the bedrock obstacles. The small $\delta^{18}O$ range of -23.9‰ to -20.6‰ for the type 6 ice overlaps with the range for glacier ice and indicates that this ice type was accreted from basal meltwater only which suggests an origin inland from the margin. The existence of both bubble-poor type 3 ice and bubbly type 4 ice intercalated and within the type 6 layers supports the origin of type 6 ice as dirty refrozen squeezed water

The type 5 ice displays a molar ratio [(Na + K) / (Ca + Mg)] which is significantly enriched in alkalis (Na + K) and ranges from 5.1 to 13.7. This enrichment in alkalis is comparable to that for type 1 congelation ice which has a molar ratio [(Na + K) / (Ca + Mg)] ranging from 7.4 to 10.2. The alkali enrichment in the type 5 ice is probably derived from saturated marine sediment with a high concentration of soluble marine salts NaCl and Na_2SO_4 rather than from meltwater cation exchange processes since less than 4% of the debris is silt and less than 1% clay. This is further supported by the comparative $\Sigma+$ (total solute load) range for type 5 ice (0.9-6.1 $meql^{-1}$) and for the jökulhlaup water (7.0 $meql^{-1}$) with its massive alkali enrichment (molar ratio [(Na + K) / (Ca + Mg)] = 26). Rare localised evaporite deposits were observed on the Windmill Islands around the shores of previously saline / brackish lakes having precipitated from trapped seawater as the islands emerged and relative sea level lowered. Since the intercalated type 3 clean ice layers and interstitial clean ice lenses in the type 5 debris band ice do not display a freezing slope the accretion of type 5 ice cannot be attributed to bulk freezing on. As the large $\delta^{18}O$ range of -21.9‰ to -17.7‰ for the type 5 ice indicates a mixed water source of glacial and pro-glacial origin, similar to that from which type 3 and type 4 ice formed, it is likely that a freezing slope would not be detected. The interstitial type 3 ice lenses indicate that the sandy substrate was saturated and permafrosted prior to or during incorporation at the sole. The intercalated type 3 clean ice layers in the type 5 ice represent refrozen meltwater formed on the surface of the impermeable permafrosted sediment. Tison et al. (1989) discussed the entrainment of similar permafrosted near shore and raised beach deposits into debris bands during a recent advance of glaciers in Southeastern Ellesmere Island. They suggested that freezing of the upper layers of proglacial wet marginal sediment allows the sediment to be incorporated by over-riding as the glacier advanced and displaced and transported in an englacial position. The high molar ratio (Na + K / Ca + Mg) and the similar

sediment characteristics of the type 5 debris band ice and the surficial sediment cover of the northern Windmill Islands indicate that the type 5 debris ice was accreted by over-riding proglacial sediment and water bodies close to the present ice margin

The over-riding of proglacial sediment is further supported by the synchronous 20 km near continuous outcrop of this ice type (exposed in the Løken Moraines) along the northern Windmill Islands margin, and that there is a significant proportion of sediment which was highly weathered prior to incorporation in the basal ice and Løken Moraines. Knight (1989) reported a similar stacking of basal debris layers in West Greenland without bulk freezing on, which he attributed to an unknown process. In an area of primarily compressive flow such as the Windmill Island section of the Law Dome margin it is likely that the stacking of basal clean and debris rich ice layers results primarily from deformation and over-riding of the basal ice rather than bulk freezing on.

5.4.7 SEDIMENT CHARACTERISTICS OF THE TYPE 5 DEBRIS BAND ICE

The basal ice study indicates that type 5 debris band ice, with debris concentrations up to 33% by volume, consists of reworked and weathered proglacial sediment which has been accreted near the ice margin by over-riding. Co-isotopic analysis has shown that this ice is indistinguishable from glacier ice primarily because small amounts of subglacial meltwater have been mixed with permafrost and proglacial water bodies near the margin.

Micropalaeontological analysis of both the type 5 debris band ice and the presently exposed surficial sediment samples across the Windmill Islands has revealed that they both contain shallow marine benthic diatoms of Pliocene or Early Pleistocene age together with sponge spicules and Mollusc shell fragments (Quilty, 1993). The type 5 debris also contains gravel to boulder sized clasts which are also found outcropping in the overlying supraglacial moraines. These clasts are predominantly sub-angular to subrounded and are indicative of subglacial erosion processes. Large (2-3 m diameter) subrounded to subangular subglacial erratics in the Løken Moraines, are striated, faceted and of a comparable weathering stage to those found over the surface of the northern Windmill Islands (Figure 5.13a). They also comprise sub-aerially weathered boulders exhibiting tafoni and honeycomb surfaces (Figure 5.13b) and rare boulders with a strong iron oxide weathering crust, predominantly in the Bailey and Mitchell Peninsula sections. The existance of sub-aerially weathered boulders of similar weathering stage to those on the peninsulas, within the type 5 debris, indicates

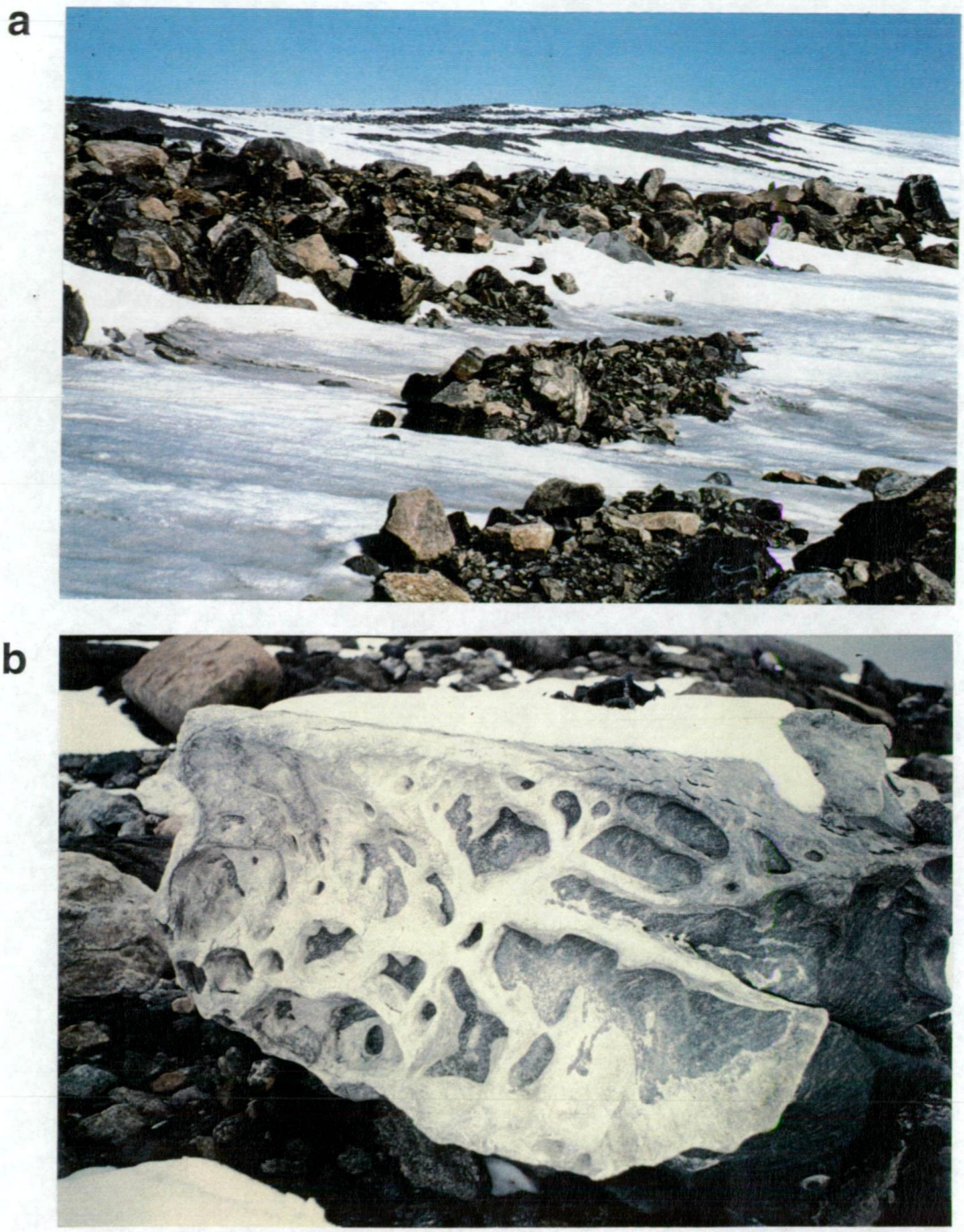

Figure 5.13 Characteristics of boulder clasts in the type 5 debris and the Løken Moraines. (a) Photograph showing the Clark Peninsula section comprised of typical sub-rounded to sub-angular boulder and cobble sized clasts, of equivalent weathering age to those glacial erratics and surface till on the northern Windmill Islands. The profile #3 is located along the skyline. (b) Photograph showing a sub-aerial (aeolian) weathered diorite boulder with characteristic pitting known as tafoni, which develop from prolonged wind exposure. It is interpreted from the weathering stage and the relatively recent exposure in the moraines, that the tafoni were eroded prior to incorporation in the ice sheet's re-advance.

that the ice sheet retreated during the early-mid Holocene to a position further inland than at present, exposing these clasts to periglacial and coastal processes. This is further supported by the occurence of highly polished and rounded beach boulders and pebbles in the Clark Peninsula section of the Løken Moraines, where the ice margin is closest to the coast. The sedimentological charactersitics of the type 5 debris and in the Løken Moraines were investigated further to determine their provenance prior to incorporation by the ice sheet.

5.4.7.1 PROGLACIAL SEDIMENTS

The type 5 debris has a strikingly similar colour, weathering condition and apparent size distribution to its parent proglacial sediments observed in situ. To examine these similarities in greater detail particle size analysis was conducted on both the type 5 debris and proglacial sediment samples from sites at elevations between 45-70 m in shallow bedrock niches at the top of small nunataks on Clark, Bailey and Mitchell Peninsulas. The latter were situated above the Holocene marine limit and were reworked slightly by periglacial processes. These samples were typical of the surficial sediment across the northern Windmill Islands above the marine limit and contained rare Pliocene-Early Pleistocene marine microfossils. The cumulative and frequency percentage particle size distributions of the type 5 debris and the proglacial sediments are shown in Figures 5.14a and 5.14b, respectively. The two distributions show that the type 5 debris and the proglacial sediments are poorly sorted sandy, fine gravels with near identical characteristics. The Type 5 debris has a slightly coarser distribution than that for the proglacial sediment, which is probably due to the partial erosion of the fines by meltout processes. These particle size measurements suggest that the origin of the type 5 debris is proglacial sediment prior to incorporation. The lack of reworking of the proglacial sediment by basal processes, supports the co-isotopic and solute evidence that the type 5 debris was incorporated into the basal ice by glacial over-riding rather than by basal meltwater and regelation processes.

5.4.7.2 BEACH SEDIMENTS

Numerous outcrops of rounded to sub-rounded, smooth polished pebbles and boulders together with sandy gravel deposits (Figure 5.15a) occur within the type 5 debris along the 20 km length of the Løken Moraines, although the greatest concentration is found in the section inland of Clark Peninsula, where the ice ramp is steepest and the ice margin abuts closest to the islands and raised beaches (Figure 5.15b and c), with its base below sea level further inland. These deposits outcrop continuously for distances of 50-100 m in the Løken Moraines.

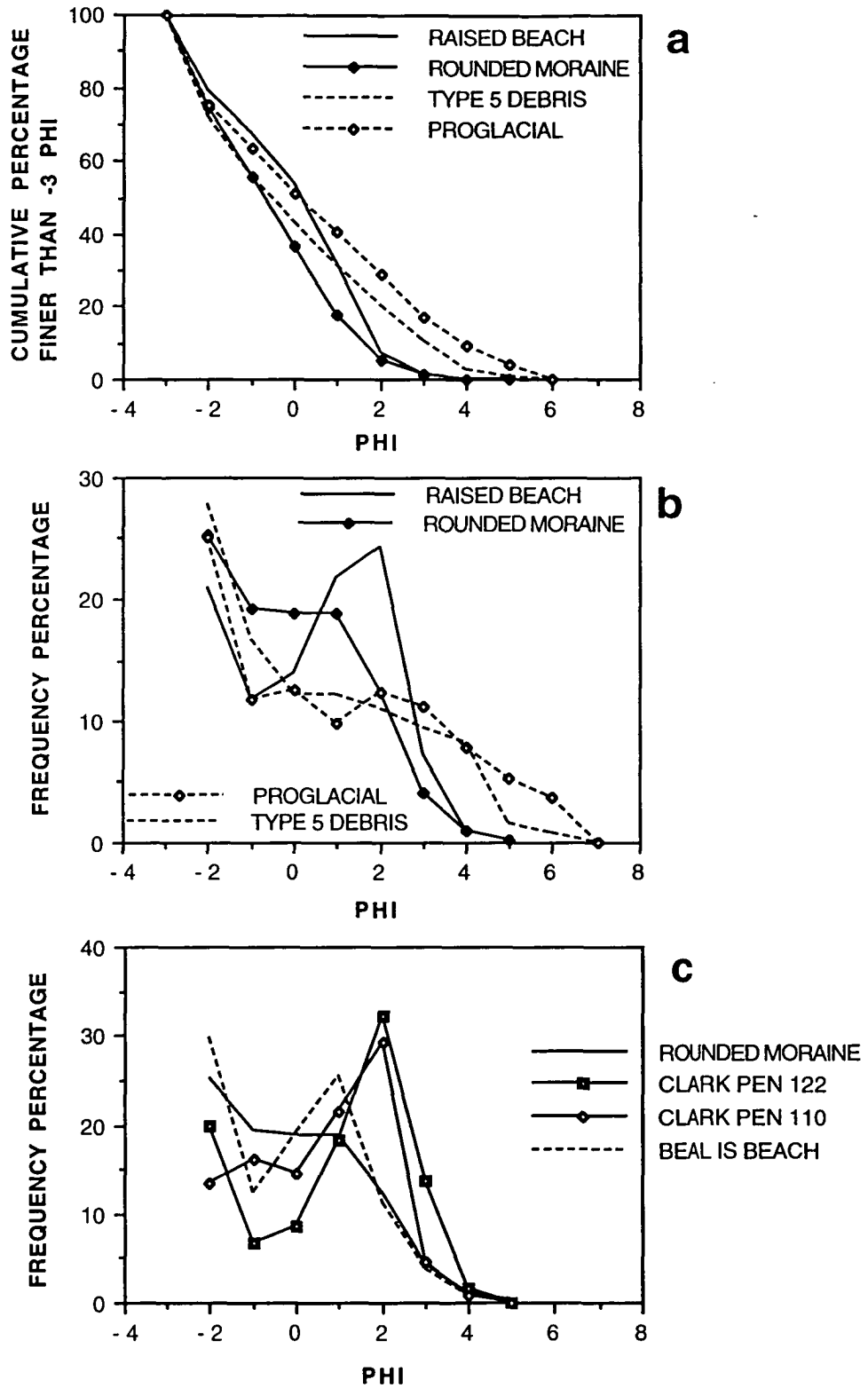

Figure 5.14 Sediment particle size distributions for raised beach (n=5), rounded moraine (n=2), type 5 debris (n=5) and proglacial (n=5) environments. (a) cumulative percentage distribution, (b) frequency percentage distribution, and (c) comparison of rounded moraine sediment with the closest raised beach samples (122, 110) from nearby Clark Peninsula (Stevenson Cove area), and Beal Island.

a

b

Figure 5.15 (a) Photograph of an outcrop of rounded and polished pebbles in the front ridge of the Clark Peninsula section of the Løken Moraines (500 m south of profile #5 in Figure 5.1). (b) For comparison with (a), a photograph of raised beach pebbles of similar size, shape and polish, on Clark Peninsula, near Stevenson Cove.

c

d

Figure 5.15 (c) Photograph of the raised beach (122) at 26 m elevation in the Stevenson Cove area of Clark Peninsula. Note that the present ice margin is close to the inland edge of the raised beach, with the Løken Moraine ridges (profile# 5) on the skyline, which is less than 1 km from the raised beach. (d) Photograph showing a massive outcrop of fine (with rare marine microfossils) silt sediment which is typical of the meltout sediment forming the supraglacial moraines between IC10 and Jacks Donga.

The most distinct and homogeneous of these deposits outcrop 80 m downslope from the front ridge of the Løken Moraines, immediately inland of the northern Clark Peninsula. To investigate the provenance of these sediments particle size analysis was conducted and compared to particle size distributions measured for Mid-Holocene raised beaches from the 18-30 m elevation range on Clark Peninsula (Figure 15c), Beal Island and Shirley Island. The cumulative and frequency percentage particle size distributions for both mean raised beach samples and the Løken Moraines samples are shown in Figure 5.14a and 5.14b, respectively.

Whilst the raised beach samples are slightly better sorted, both distributions tend towards bimodality and can be described as gravelly medium sands. These distributions are distinctly different from the sandy gravel distributions for the type 5 debris and the proglacial sediments, both in the greater degree of sorting and the lack of finer sediment. The particle size distributions for the raised beach and rounded moraine sediments are typical for coarse sediment, polar, pocket beaches (Nichols, 1961) where the degree of sorting and roundness are a function of the length of seasonal exposure to open water and waves, sea ice action, and the rate of isostatic uplift. The lesser degree of sorting in the rounded moraine samples is likely to be due to their limited temporal exposure to coastal processes prior to incorporation in the ice margin. Thus the rounded moraine sample was interpreted to be reworked beach sediment. The frequency percentage distribution of the reworked beach sediment is shown in Figure 5.14c, together with typical distributions for raised beaches on Clark Peninsula and Beal Island, near Mitchell Peninsula (Figure 4.2). The reworked beach sediment distribution is closest to that for the Beal Island raised beach sediment. Both of these distributions are coarser than those for the Clark Peninsula raised beaches. The Beal Island sample was collected from a steep raised beach which was exposed to wave action, whilst the Clark Peninsula samples were collected from gently sloping raised beaches, within small sheltered palaeo embayments. The coarser distribution of the reworked beach sediment in the Løken Moraines, indicates that its provenance is probably from a beach exposed to the relatively strong wave action. Prior to the re-advance of the Law Dome ice margin, the inland edge of the Clark Peninsula probably formed a shoreline along a large embayment, according to the bedrock profiles in Figures 5.6 and 5.8. This shoreline would have been exposed to the full force of strong easterly winds and storm waves which accompany blizzards in this area. The coarser particle size distribution of the reworked beach sediments is consistent with a provenance along such a shoreline.

By far the greatest volume of fine sediment in the moraines (Figure 5.15d), occurs along the ice cliff moraines from Jacks Donga promontory to IC10 where they outcrop

in beds up to 0.5 m thick and contain Pliocene-Early Pleistocene marine microfossils (Quilty, 1993). Since these have been incorporated into the basal zone where the ice sheet's base is below sea level (Figure 5.6 and 5.8), it is consistent to interpret their provenance as shallow marine.

On the basis of the above sediment characteristics, the type 5 debris facies was interpreted to comprise, reworked Holocene raised beach, shallow marine and proglacial sediment. It is concluded that these sediments were incorporated by an over-riding advance of the Law Dome ice margin onto part of the Windmill Islands. It is probable that the advance has occurred since maximum deglaciation occurred during the Mid-Holocene, after which beaches have been forming along the shorelines of the northern Windmill Islands, and isostatic uplift of the bedrock has occurred.

5.5 GLACIO-TECTONIC STRUCTURE AND MORPHOLOGY OF THE LØKEN MORAINES AS INDICATORS OF GLACIAL ADVANCE

The structure of the ice margin was investigated in the longitudinal ice cliff exposures at Jacks Donga promontory (Figure 5.2) and in IC10 (Figure 5.7), and along the ice ramp inland of Clark Peninsula. Field observations along the Jacks Donga promontory exposure showed that the front moraine ridge which is typically sharp crested along the entire Løken Moraines dips at 80-90° which was also measured at several sites along the length of the front ridges of the Løken Moraine. In comparison the basal ice layers forming the inland most broad ridge and moraine flat dip at a much shallower angles of 30-40° The basal ice becomes progressively more deformed with distance down-glacier from the innermost debris band to the outermost debris band. The basal ice emerging in the front moraine ridges has been deformed under longitudinal compression resulting in rounded and convolute folding with dips approaching 70-90°.

These debris bands are enclosed by isoclinal single folds (Figure 5.7) whose fold hinges are typically perpendicular to the ice flow direction. The $\delta^{18}O$ stratigraphy of IC10 in Figure 5.9 shows that the layers above and below the upper and lower debris band sequences are repeated but inverted as a result of the folding. Figure 5.3 shows similar single folds but on a larger scale outcropping in the surface of the ramp inland of Clark Peninsula and plunging vertically, enclosing along one limb, the discontinuous inner moraines J, Y and H which outcrop 170-200 metres downslope of the main front ridge of the Løken Moraines.

Huddleston (1976) first reviewed and investigated the importance of similar single folds in the ice margin as indicators of glacial advance, whilst Chinn (1987b) found that they can be used to indicate a glacial advance and expansion of the ice margin in polar glaciers, from his studies of small dry-based cirque glaciers in the Dry Valleys area of Victoria Land. Chinn (1987b) determined that single folds enclosing inner moraines are initiated by a thickening wave of ice arriving at the glacier margin as an advance proceeds. He concluded that an ice margin in equilibrium will have a fixed position inner moraine with an outer ice ramp covered by a surface veneer of meltout debris. Alternatively he found that during an advance the position of the inner moraine will migrate outward with some overriding of the outer ice ramp, coupled with a positive snow balance concealing the bulk of the debris cover on the ice ramp. Chinn (1987a) also observed a number of coastal glaciers in the Terra Nova Bay area of Northern Victoria Land which have been expanding for at least the last century to their greatest extent during the Holocene. He observed twin inner moraine ridges similar to the multi-ridged Løken Moraines. He demonstrated that as the ice sheet or glacier thickens, the position of the critical ice thickness where the shear zone forms at the plastic/rigid ice boundary will migrate outward towards the margin, forming a second inner moraine down-glacier. Complex deformation of the Law Dome basal ice from longitudinal compression and the significant increase in the dip of the shear zone from 30-90° towards the margin, indicates the seaward migration of the inner moraine ridges in the Løken Moraines in response to the thickening and expansion of the margin. The interpretation that the moraine ridges are progressively younger towards the coast is consistent with the observed decrease in the stability and periglacial sorting of the moraine sediment, and a decrease in the extent and diameter of lichen thalli on the surface of boulders. There is also a general trend for increasing sediment angularity coupled with increasing fine material from the inland ridge to the outer moraine ridge.

The clastic debris in these front or most seaward inner moraines, especially Moraines J and H, Jacks Donga and O'Briens end moraines, is composed of predominantly large, angular, and unweathered boulders (Figure 5.16a), often composed of slabs of rock of the same lithology which were determined to have been plucked from the bed by the ice bed under water pressure variations by Goodwin (1988c). In comparison, the clastic sediment in the inland ridges is composed of the type 5 debris found in the majority of the Løken Moraines, which are predominantly moderately weathered sub-angular -rounded clasts of mixed lithologies. This is especially the case inland of Clark Peninsula where the clasts are the most rounded and polished, including homogeneous sections of beach sediments. Thus the angular and fine sediment in the

a

b

Figure 5.16 (a) Photograph of supraglacial moraine J in profile, showing the angularity of the diorite and granite boulders, together with the possible matching of adjacent boulders. Each division on the markers is 10 cm long. (b) Photograph showing the summer exposure of the surface moraine veneer covering the ice ramp, 500 m seawards of the main Løken Moraine ridge at Profile #1 (Figure 5.5d).

front ridges was derived from recently eroded subglacial bedrock by glacial plucking, crushing and abrasion processes, and was entrained close to the margin by the final phase of glacial expansion of the ice margin.

Along the Clark Peninsula, Bailey Peninsula and Mitchell Peninsula sections of the Løken Moraines where the ice thicknesses are between 150-300 m thick, there has been an extensive overriding of the rigid ice ramp. This has formed the single fold enclosed inner moraines which outcrop down the ice ramp from the front moraine ridge by a distance equivalent to the ice thickness (150-200 m) . These inner moraines are probably continuous linear outcrops but are partially buried by the accumulation of superimposed ice from local precipitation in the depressions of the ice ramp surface.

There is a layer of sediment over the surface of the ice ramp which developed during the outward migration of the moraine formation and slope mass-wasting processes. This veneer is now almost totally buried by a significant thickness of superimposed ice and snow (Figure 5.16b). This is evident in the ice cliffs where this debris layer outcrops as an unconformity. During summer in late January-early February, depending upon the extent of remaining winter snow accumulations, extensive sheets of this sediment are exposed on the surface of the ramp.

In 1985, the author re-surveyed a topographic profile, designated as Profile 3 in Figure 5.5c, between a bedrock outcrop at the edge of the ramp on Clark Peninsula (C7) and the seaward edge of front ridge of the Løken Moraine, which was marked by a cane established in 1958, when the profile was initially surveyed. The results showed that a surface lowering of 3.3 m had occurred between 1958-85, which represents a lowering or net ablation rate of 0.11 m/a. Budd (1967) observed at Mawson, that the total ablation from the ice sheet surface at 200 m elevation is approximately 0.40 m/a. A similar total ablation rate on the ramp is expected given an annual winter snow accumulation of 0.3-0.5 m/a which is ablated during summer.

A retreat of the ice edge of between 50-100 m between Jacks Donga promontory and Cape Folger was determined from a comparison of the geographic position and morphology of the ice cliff terminus on aerial photographs taken between 1962 and 1987. This area includes the ice cliffs with surface moraines at Jacks Donga promontory, and ice cliffs C, 254 and 10. These indicators suggest that the present ice margin is in a state of negative balance. Xie (1983) reported that ice dipping at 30-40° and containing sediment layers was outcropping approximately 300 m inland of the Trail Gaps area. The $\delta^{18}O$ value of this ice was -25 ‰ which is equivalent to the most negative basal ice outcropping in the marine ice cliffs. Xie (1983) also measured

the fabric of these ice layers which showed that they were indicative of ice undergoing pure shear. These characteristics indicate that the active basal shearing zone has migrated inland to at least 300 m inland of the moraines in conjunction with the downwasting of the ramp and a general thinning of the ice margin.

5.6 A RELATIVE CHRONOLOGY OF THE RETREAT AND ADVANCE OF THE LAW DOME ICE MARGIN

Sediments suitable for ^{14}C dating dating were searched for in the Løken Moraines to provide an absolute minimum age constraint on the advance and expansion of the Law Dome ice margin. However, no suitable sediments were discovered. The only absolute age constraint for the advance can be based on the entrainment of Holocene age (determined by comparative weathering stages) raised beach sediments in the Clark Peninsula section of the Løken Moraines and the observed close proximity (<400 m) of the ice margin at Profile 5 to Holocene raised beaches (Figure 5.4b, 5.15c). The age of these 18-27 m elevation raised beaches is taken as contemporary with the raised beach at 23 m on Browning Peninsula at Eyres Bay, ^{14}C dated at 6040 yr B.P (Cameron, 1964) which equates to 4740 corr. yr B.P. Since the elevation of the higher bedrock knolls are generally lower on Clark Peninsula than any of the other peninsulas, and that the maximum elevation of raised beaches on Clark Peninsula is 27 m, it is unlikely that the height of the raised beach from which the basal sediment was incorporated would be significantly higher, and hence older than 5,500 corr. yr B.P. given the uplift rate of 5 m per 1000 yr for the Browning Peninsula beach. The age of the Bailey Pond sediments suggests that the outer coast of Clark and Bailey Peninsulas was deglaciated before 5,500 corr. yr B.P.. It is likely that the Mid Holocene contraction of the ice margin across the 3-4 km wide central Clark and Bailey Peninsulas to inland of the present margin, would have occurred at similar rates of retreat to those calculated for the Vestfold Hills by Adamson and Pickard (1986), since the contraction was in response to sea-level rise and climate amelioration. Adamson and Pickard (1986) calculated rates of 2-3 km per 1000 years. Hence, it is most probable that open water existed inland of Clark and Bailey Peninsulas by 4,500 yr B.P. given the exposure of the coastline by 5,500 yr B.P., and that the re-advance of the ice margin did not achieve the inland edge of the Clark Peninsula until after 4,500 yr B.P..

To compensate for the lack of absolute chronological control, the method of relative lichenometry dating was employed which was previously described by Lock et al. (1979). The field survey involved extensive searching along; north-south and east-

west transects at each of the moraine profile sites, and; at control sites on the closest nunataks at the base of the ramp, to determine the maximum discrete lichen thallus diameter. This survey was also conducted along the coast of the peninsulas where the earliest deglaciation occurred. The lichen species chosen for this study was *Buellia frigida* (Filson, 1974) a crustose lichen which was suggested as the most suitable species for lichenometry by Professor Ludger Kappen from the Polar Botanical Institute at the University of Kiel, whilst he was conducting physiological research on lichens in the Windmill Islands. *Buellia frigida* can survive snow drift burial, draws its moisture from the snow for photosynthesis, and can be found in the most exposed zonations (Rod Seppelt, Australian Antarctic Division, pers. comm.). This makes *Buellia frigida* ideal for lichenometric dating of moraines. Maximum lichen growth occurs at sites with mild microclimates, maximum sun exposure and shelter from the extreme winds (L. Kappen, pers. comm.). Thus the measurement sites were chosen with west to north-west aspects, which were sheltered from the prevailing easterly winds and were wind scoured preventing their burial by wind drifts. The resulting lichen thallus measurements are listed in the following Table 5.1.

There are two lichenometric methods used to determine a relative chronology for the moraine development. The first is to determine the initial exposure age of the bedrock substrate of the nunatak, that is the age of deglaciation or its emergence from the sea, and hence determine the growth rate of the lichen thallus and apply this rate to the meaured lichen thalli on the moraine ridges. This produces a maximum age estimate for the moraine lichens. Alternatively, if a lichen growth rate is known from physiological studies it can be applied to the measured lichen thalli to determine their age. The most significant determinant of the growth rate of *Buellia frigida* is the available moisture supply (Rod Seppelt, pers. comm.). The only known growth rate for *Buellia frigida* in Antarctica is 10 mm/1000 yr, which was determined by Rod Seppelt (pers. comm.) from a site at 800 m elevation on Mt Falconer, Taylor Valley in the Dry Valleys area of Northern Victoria Land. At this arid alpine site, the lichens derive their moisture primarily from contact with daily cloud cover, rather than precipitation. In contrast, the coastal sites in the Windmill Islands at elevations less than 170 m would have a significantly greater moisture supply from snowfall, summer melt and ocean spray, and would be expected to yield proportionally higher growth rates (R. Seppelt, pers. comm., 1994).

TABLE 5.1 LICHEN THALLUS MEASUREMENTS ON COASTAL NUNATAKS AND THE LØKEN MORAINES

OUTCROP	MAXIMUM LICHEN THALLUS DIAMETER
NUNATAKS	
Bailey Peninsula coast	195 mm
Nunatak at base of Jacks Donga promontory ramp	105 mm
Nunatak C7 at base of Ramp, Clarks Peninsula	105 mm
Nunatak C5 at base of Ramp, Bailey Peninsula	110 mm
Robinson Ridge coast	140 mm
LØKEN MORAINES	
Robinson's Ridge moraines	44 mm front ridge, 80 mm inland ridge
Mitchell profile # 12	20 mm inland ridge
Bailey profile # 1a	52 mm single ridge
Bailey profile # 1b	15 mm single ridge, 11 mm flat
O'Brien's end moraine	51 mm single ridge
Moraine E	43 mm inland ridge
Moraine J, H and Cone	Nil
Moraine profile # 3	32 mm front ridge, 65 mm inland ridge
Moraine profile #3-4	59 mm inland ridge
Moraine profile # 4	50 mm inland ridge
Moraine profile # 5	40 mm inland ridge
Jacks Donga moraine	55 mm front ridge, 50 mm inland ridge
Ice Cliff C	58 mm front ridge, 55 mm inland ridge

Assuming that the maximum measured lichen thallus (195 mm) which was found at 35 m elevation on Bailey Peninsula began growing shortly after deglaciation or at the same time as the algal production began in the adjacent Bailey Pond (5,500 yr B.P) a minimum growth rate of 35 mm/1000 yr was determined. Similarly, a growth rate of 25mm/1000 yr was determined for the 140 mm diameter thallus at 45 m elevation on the Robinson Ridge coast. Using this method, the growth rates can also be determined for the three nunataks at Jacks Donga, C7 and C5 whose elevations are 22 m, 44 m and 47 m respectively. By applying isostatic uplift rates of 5 m /1000 yr, the Jacks Donga site would have been above sea level by 4,400 yr B. P. and the C7 and C5 nunataks (Figure 5.3) would have been deglaciated by 5,500 yr B.P.. Consequently, the minimum lichen growth rates determined for Jacks Donga, C7 and C5 are; 24 mm/1000 yr B.P, 19 mm/1000 yr and 20 mm/1000 yr. The significantly more rapid growth rate for the Bailey Peninsula coastal site is probably due to the increased moisture supply, sun exposure and snowdrift free exposure at this location. Similarly, but to a lesser extent the Jacks Donga site is more protected from wind and snow drift exposure than the other two nunatak sites, which are more representative of the boulder microclimates within the moraines. On the basis of these site comparisons the most appropriate growth rate to apply to the lichen thallus measurements in the Løken Moraines was determined as 20 mm/1000 yr. This rate also compares well with that for the Mt Falconer site, since the precipitation rate in the Windmill Islands would be at least twice that for the arid Dry Valleys (R. Seppelt, pers. comm, 1994). The resulting chronology of maximum dates for the formation of the Løken Moraines and the final stage of the advance of the Law Dome ice margin is listed in Table 5.2 below.

This maximum age chronology for the establishment of the inland ridge of the Løken Moraines indicates that the Law Dome ice margin had advanced to approximately its present position by 3,250 to 2,000 yr. B. P.. The oldest date of 4,000 yr B. P. for the Robinsons Ridge inland moraine indicates that the advance reached this locality earlier than inland of the Clark, Bailey and Mitchell Peninsulas. This is in accordance with the location of the Robinson's Ridge moraine adjacent to the deeper ice in the subglacial valley occupied by the Peterson Glacier. The ice margin advance and the formation of the Bailey end moraine was contemporaneous with the advance and formation of the main Løken Moraines inland ridge. The subsequent development of additional Løken Moraine ridges seawards of the main inland ridge has occurred since 2, 000 yr B.P. as the ice margin continued thickening.

TABLE 5.2 LØKEN MORAINE CHRONOLOGY

LØKEN MORAINES	DATE OF INLAND RIDGE FORMATION
Robinson Ridge moraines	4,000 yr B. P.
Mitchell profile # 12	1,000 yr B. P.
Bailey profile # 1a	2,600 yr B. P.
Bailey profile # 1b	750 yr B. P.
O'Brien's end moraine	2,550 yr B. P.
Moraine E	2,150 yr B. P.
Clark profile # 3	3,250 yr B. P.
Clark profile #3-4	2,950 yr B. P.
Clark profile # 4	2,500 yr B. P.
Clark profile # 5	2,000 yr B. P.
Jacks Donga moraine	2,500 yr B. P.
Ice Cliff C	2,750 yr B. P.

However, observations of the present morphology of the ice margin, including the concave ramp profiles and the elevated relief (up to 40 m) of the moraines above the general ice sheet profile, indicate that the ice margin has been thinning for at least the last 400-500 years, given the measured net ablation rate of 0.11 m/a between 1958-85.

The period of thickening since 2,000 years B.P. may have been forced by an increase in surface mass balance during the Little Climatic Optimum which is evident in the DSS and BHD $\delta^{18}O$ profiles (Chapter 1) between 1,000 to 1,500 years B.P.. The subsequent thinning of the ice margin is coincident with the Little Ice Age which occurred between 200-500 years B.P.. The surface mass balance at the ice margin is a strong function of winter snow accumulation and summer melting. The winter snow accumulation melts during December and January and the underlying glacier ice is exposed to surface melting during February. It is likely that a 0.5°C fall in mean annual temperatures during the Litte Ice Age was associated with a decrease in winter snow accumulation and a decrease in summer temperatures. A decrease in snow accumulation would have resulted in a more rapid exposure of the underlying glacier ice earlier in summer, and despite lower summer temperatures may have resulted in the thinning of the ice margin through the sustained melting during January and February.

CHAPTER 6
REGIONAL EVIDENCE AND MECHANISMS FOR MID TO LATE HOLOCENE GLACIAL FLUCTUATIONS IN EAST ANTARCTICA

6.1 INTRODUCTION

The ice margin investigations in the previous chapter, revealed that an advance of the Law Dome ice sheet occurred after 4,500 yr B.P. and most likely reached its maximum extent between 3,250 to 2,000 yr B.P., with a subsequent thickening of the margin up to 1,000 yr B.P.. Supporting evidence for a widespread advance of the East Antarctic outlet glaciers and ice sheet, from both the marine sedimentary record and the terrestrial glacial geologic record is presented in this Chapter. In addition a theory on possible mechanisms for the advance and the temporal response of ice sheets to environmental changes is outlined.

6.2 MARINE GEOLOGICAL EVIDENCE

The terrestrial evidence of Late Pleistocene-Holocene ice sheet fluctuations is sporadic due to the geographically limited terrestrial exposures and the nature of ice sheet fluctuations in overriding geological evidence of prior glaciation. Also, since the majority of the East Antarctic ice sheet terminates below sea level, the probable greatest source of geological evidence for ice sheet extent and fluctuations in extent is in the sedimentary record on the inner and middle continental shelf areas. The most suitable sites within the continental shelf are the shelf deep troughs previously eroded by glacial expansion (Domack et al., 1991a). These shelf deep troughs are below 500 m depth. This is below the depth where iceberg keels rework continental shelf sediments by scouring and gouging, forming poorly stratified diamicton deposits known as ice-keel turbate which are unrelated to glacial proximity (Barnes and Lien, 1988). Consequently, the marine sediments from the shelf deep troughs should provide a high resolution record of the transition from terrigenous (glacial or ice proximal) to biogenic (open marine)sedimentation. Domack et al. (1991a) presented the first circum-Antarctic chronology from ^{14}C dated particulate organic carbon in shelf deep trough sediments. Their evidence came from 3 cores: core 12 (at 804 m depth, Operation Deep Freeze, 1979) in the Mertz-Ninnis Trough 60 km north-west of the Mertz Ice Tongue in George V Land, core 302 (at approximately 900 m depth, Japanese National Oil Corporation) in the Dumont d'Urville Trough, 33 km from the

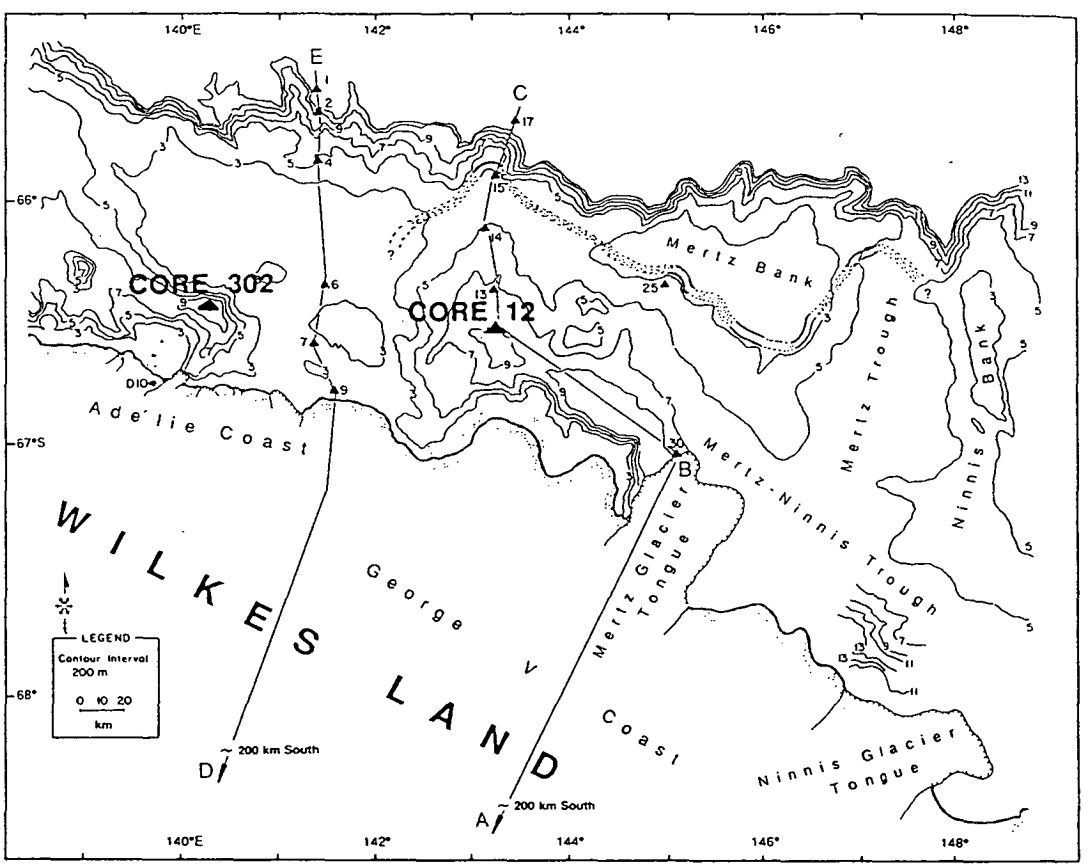

Figure 6.1 Bathymetric contours and coastal physiography for the George V and Adélie continental margin of Wilkes Land, East Antarctica. Numbers refer to core locations on the shelf. The locations of core 302 off the Adélie coast and core 12 off the George V Coast are denoted by the triangles (after Domack et al., 1991b). The location of the ice core D10 is also shown. The Moraine Prudhomme and the ice cores G1 and G2 are located 250 m and 500 m respectively, from the ice margin near D10.

Astrolabe Glacier tongue in Terre Adélie; and core 740A (56 km west of Davis Station, 68° 41' S, 76° 43' E, at a depth of 810 m, Ocean Drilling Program, Leg 119) in the Amery Depression, Prydz Bay, 130 km north-east of the present edge of the Amery Ice Shelf and the Princess Elizabeth Land coast. The locations of the cores together with the bathymetry of the continental shelf for the Terre Adélie/George V Land, and the Prydz Bay sites are shown in Figures 6.1 and 6.2 respectively.

The marine sediment cores show a transition from terrigenous (ice proximal) sedimentation to biogenic (open marine) sedimentation at 4,300 yr B.P. (Terre Adélie/George V Land) and 3,800 yr B.P. (site 740A, Prydz Bay). Only the Prydz Bay core provides a chronology of conditions prior to this mid-Holocene transition. This core shows that the period of terrigenous (ice proximal) sedimentation existed until 7,300 yr B.P.. Domack et al. (1991a) interpreted this facies as being deposited close to the respective grounding line of the expanded outlet glaciers. The facies is described as a weakly stratified to moderately well-stratified silty clay (pebbly mud) diamictite which typically is deposited beneath ice shelves and floating glacier tongues. The silty clay/pebbly mud consists of a well-sorted fine component and a poorly-sorted ice-rafted component (Domack et al., 1991a).

Budd et al. (1982) reported from flow-line mass balance calculations which were confirmed by oxygen isostope analysis at the G3 core location, that a significant amount of basal melting occurs at the grounding line of the Amery Ice Shelf. Approximately one-third of this mass loss is replaced by the basal freeze-on of seawater which results in a maximum freeze-on thickness of 200 m. Consequently, debris carried in the basal zone will be deposited close to the grounding line before the basal freeze-on zone. The remaining basal and englacial debris is transported to the ice shelf front where it is deposited from icebergs following calving and from basal meltout (Hambrey, 1991). Silty clays are presently being deposited in deep water close to the front of the Amery Ice Shelf (Quilty, 1985). In addition, the majority of icebergs from the Amery Ice Shelf drift westwards in the coastal current away from the ODP drill sites (Hambrey, 1991). Consequently, the silty clays deposited in the ODP 740 site must have been deposited close to the front of the expanded Amery Ice Shelf, which implies an advance on the order of 120-150 km during the Mid-Holocene.

The Prydz Bay core also extends back to the Late Pleistocene and shows that prior to the Mid-Holocene glacial advance, open marine conditions prevailed between 7,300 -10,700 yr B.P.. Prior to 10,700 yr B.P. ice proximal sedimentation was occurring in concert with an expanded Late Pleistocene Amery Ice Shelf/Lambert Glacier

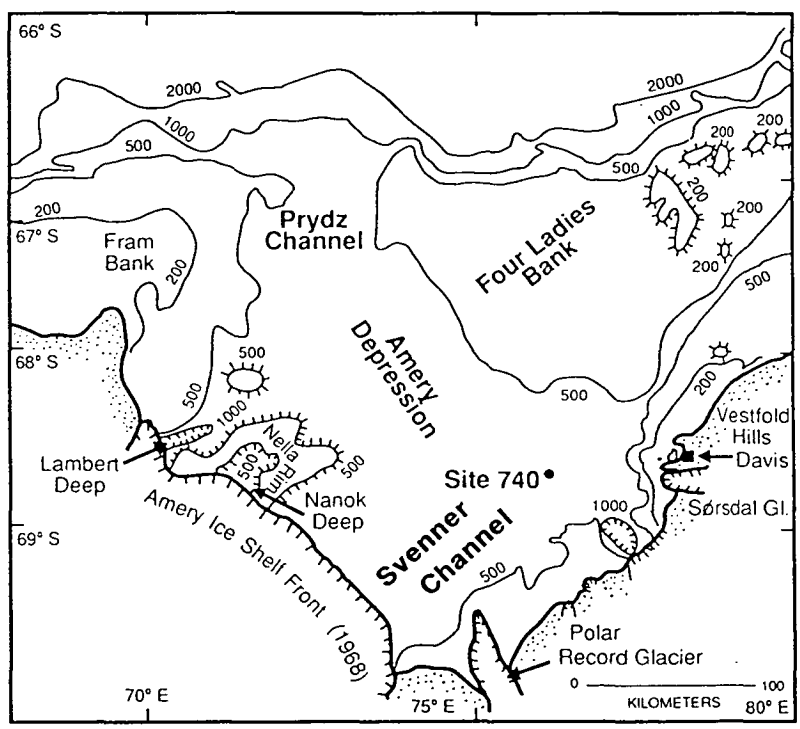

Figure 6.2 Location, bathymetry, and geographic features of Prydz Bay, East Antarctica. The location of ODP 740 is shown in the Amery Depression (after Domack et al., 1991c).

system. Since, terrestrial evidence from the Vestfold Hills (Adamson and Pickard, 1986), Bunger Hills (Bolshiyanov et al., 1991) and the Windmill Islands (Goodwin, 1993) indicates that these areas were deglaciated by 8,600, 11,600 and 8,000 yr B.P., respectively, it is consistent to interpret that the Late Pleistocene expanded ice sheet had also retreated across the inner and middle continental shelf areas off Wilkes Land and George V Land, by the early Holocene. Accordingly, the synchronous evidence during the Mid-Holocene (4,000-7,000 yr B.P.), for terrestrial (ice-proximal) sedimentation from shelf sediments off the Terre Adélie/George V Land coast and in Prydz Bay, suggests that a geographically widespread advance of the East Antarctic outlet glaciers occurred during this period.

6.3 ADDITIONAL TERRESTRIAL EVIDENCE

6.3.1 TERRE ADELIE

Nougier and Lorius (1969) and Tison et al. (1993) reported the characteristics of the basal ice zone in the vicinity of D10 within the coastal ice margin of Terre Adélie (Figure 6.1). Three ice cores, G1, G2 and D10, were drilled to bedrock, within the ice margin at 0.5 km, 0.8 km and 5 km from the coast respectively. In addition, shallow (10 m deep) ice cores were drilled in the supraglacial Moraine Prudhomme, located 0.25 km from the coast. The subglacial bedrock undulates between 5 m below sea level and 15 m above sea level near the base of the G1 and G2 cores, and decreases to 15 m below sea level near D10. The geographical setting and ice thicknesses are similar to those at the Løken Moraines and the Law Dome ice margin. Nougier and Lorius (1969) found that marine ice was formed at the base of the basal ice zone in core G1 which is situated in a subglacial valley. They also observed that the marine ice was underlain by soft sediments consisting of reworked sands typical of shallow marine or beach deposits. Tison et al. (1993) reported that debris in the basal ice zone of all the cores and the Moraine Prudhomme described a pattern of increasing degree of weathering and a lower proportion of fresh fracturing together with increasing autochthonous minerals from local bedrock, in a progression from D10 to the coast. Tison et al. (1993) also found from scanning electron microscopy (SEM) that 30-35% of quartz grains showed dissolution effects followed by renewed crushing, thus indicating weathering prior to entrainment and crushing by ice. These characteristics indicate that the ice sheet has advanced over ice marginal bedrock and nearshore marine sediments, and has incorporated previously weathered proglacial sediment, similar to the scenario presented in Chapter 5 for the Law Dome ice margin. Since this ice drains into the Astrolabe Glacier, which had advanced during

the mid-Holocene (Domack et al., 1991a) it is likely that the debris and marine ice in the basal ice zone was entrained during the mid-Holocene advance. No data on absolute dating of the entrainment or moraine formation have been recorded to allow confirmation of this conclusion.

6.3.2 EASTERN WILKES LAND AND GEORGE V LAND

Hollin and Cameron (1961) reported that the ice margin at Lewis Island (long 134° E) on the coast of eastern Wilkes Land, just west of the Dibble Ice Tongue, is located only a few metres away from completely intact raised shorelines sequences from 30 m down to sea level. They concluded from this observation that the ice margin had re-advanced during the Holocene and subsequent to isostatic uplift. Evidence for a re-advance of the ice margin at Commonwealth Bay was reported by Stillwell (1918). The margin of the East Antarctic ice sheet is located approximately 500 m inland of the raised shoreline sequence at Cape Denison, Commonwealth Bay (Stillwell, 1918), which indicates a re-advance since the isostatic uplift of the shoreline sequence.

6.3.3 BUNGER HILLS

The Bunger Hills were deglaciated prior to 10,000 yr B.P. and probably as early as 11,600 yr B.P. from ^{14}C dates on sediments in Lake Figurnoe close to the inland edge of the Bunger Hills (Bolshiyanov et al., 1991). The evidence for a Holocene re-advance of the Antarctic Ice Sheet on the periphery of the Bunger Hills comes from two sources; the Edisto Moraines which are terminal features of the Edisto Ice Tongue (Figure 6.3), and the Antarctic Ice Sheet itself. Colhoun and Adamson (1991) recorded a date of 8,950 ± 490 yr B.P. (Beta 15828), or 7,700 yr B.P. corrected years, from fragments of *Laternula elliptica* in beach sands at the head of the Edisto Inlet, which showed that marine transgression had occurred before development of both sets of moraines. Adamson and Colhoun (1992) described the Older and Younger Edisto Moraines on Geographers Island, Thomas Island, Seryi Island and on the promontory at the southern edge of Transkriptsii Inlet (Figure 6.4). In Southern Inlet at least three ridges of the Older Edisto Moraines occur and ^{14}C dates from transported shell fragments gave the minimum age of formation as 7,540 +/- 100 yr B.P. (Beta 17529) or 6,300 yr B.P. corrected years. The Older Edisto Moraines were formed when the Edisto Ice Tongue reached its maximum Holocene extent on Thomas Island, after 6,300 corr. yr B.P.. The Younger Edisto Moraines are ice-cored remnant inner moraines and have formed between the Older Edisto Moraines and the present front of the Edisto Ice Tongue. Dates obtained from transported shell fragments within these moraines gave a radiocarbon age of 1510± 110 yr B.P. (Beta 17528),

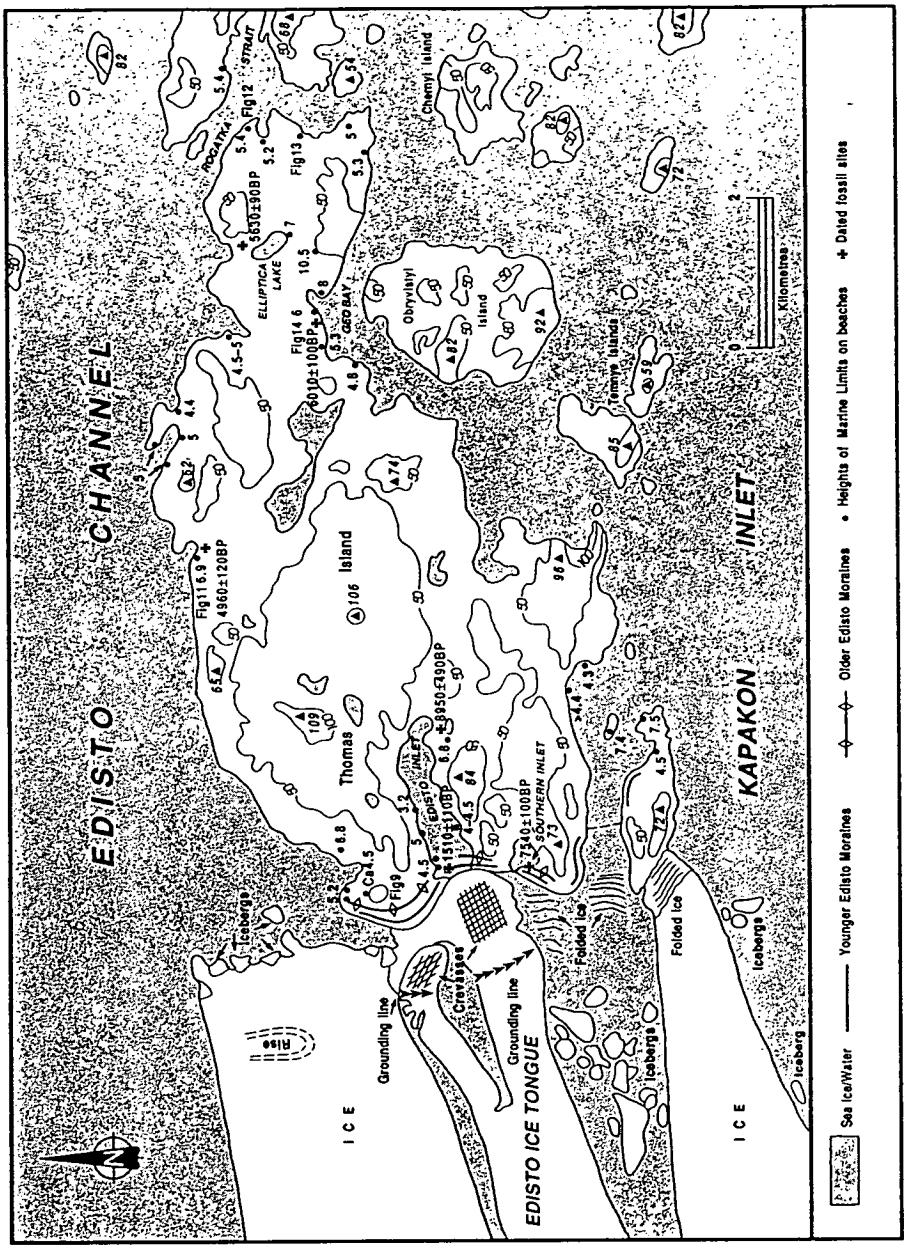

Figure 6.3 Map showing the location of the Edisto Ice Tongue and Thomas Island, Bunger Hills. Also shown are the Younger and Older Edisto Moraines and the maximum heights of raised beaches (after Colhoun and Adamson, 1992).

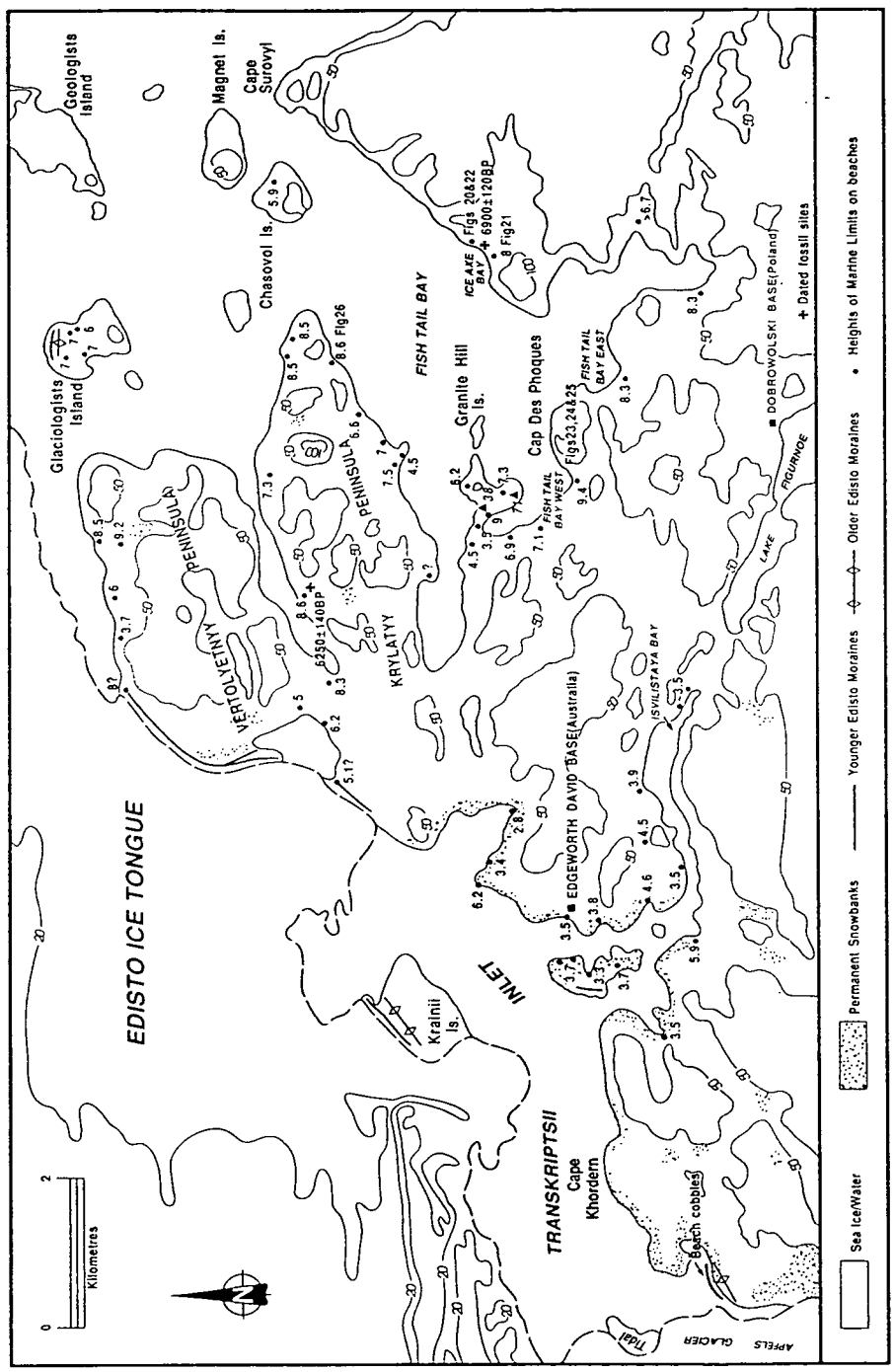

Figure 6.4 Map showing the location of Transkriptsii Inlet, southern Edisto Ice Tongue and the Apfels Glacier, Bunger Hills. Also shown are the heights of marine limits on raised beaches (after Colhoun and Adamson, 1992).

indicating formation by 200 corr. yr B.P. Colhoun and Adamson (1992) described very clear relationships between raised beaches cut into the Older and Younger Edisto Moraines on Glaciologists Island. Beaches are cut into moraine deposited by the Edisto Ice Tongue on the western, northern and eastern sides of the island up to 6-7 m above present sea level. This field evidence also shows that marine transgression and partial uplift preceded the maximum expansion of the Older Edisto ice advance as also observed on Thomas Island. Adamson and Colhoun (1992) observed that the Edisto Moraines which have formed on the promontory in the south-eastern corner of Transkriptsii Inlet, adjacent to the Apfels Glacier, contained rounded beach cobbles up to elevations of 3.7 m (Figure 6.4). These beach cobbles indicated that beaches may occur further inland under the Apfels Glacier and that these beach cobbles have been transported by a glacial re-advance during the Holocene.

Adamson and Colhoun (1992) also described the characteristics of an inner moraine complex which has formed at the ice margin of the main Antarctic Ice Sheet along the southern and south-eastern edge of the Bunger Hills, and in particular a supraglacial ice-cored moraine which occurs 3 km east of the head of Lake Figurnoe. These unweathered moraines are enclosed by recumbent folds, similar to the Løken Moraines in the Windmill Islands, and at several locations, the ice margin was observed to overly sub-aerially weathered gneiss bedrock that had been strongly altered by iron hydrolysis. In addition, tafoni (complex aeolian weathering hollows) were also observed extending into the ice margin. The degrees of oxidation and tafoni development are equal to those on deflated moraine and raised beach surfaces throughout most of the Bunger Hills.

This comprehensive field evidence and the radiocarbon dates indicate that the ice sheet and the Edisto Ice Tongue have re-advanced during the Holocene after 6,300 corr. yr B.P. following the Late Pleistocene-Early Holocene marine transgression which extended further inland than the present position of the ice margin. The ^{14}C dated shell fragments in the Younger Edisto Moraines indicate a second slight advance of the Edisto Ice Tongue occurred at ~200 corr. years B.P. during the Little Ice Age.

6.3.4 VESTFOLD HILLS

Fitzsimmons (1991) reported the earliest date for deglaciation of the Vestfold Hills at 9,900 ± 100 yr B.P. (SUA 2924) which corresponds to 8,600 corr. yr. B.P., from marine worm tubes in a layer of shell in a lateral moraine ridge, 9 m above sea level and less than 20 m from the edge of the Sørsdal Glacier near Marine Plain (Figure 6.5). Two other dates from shell and worm tubes in separate lateral moraine ridges up

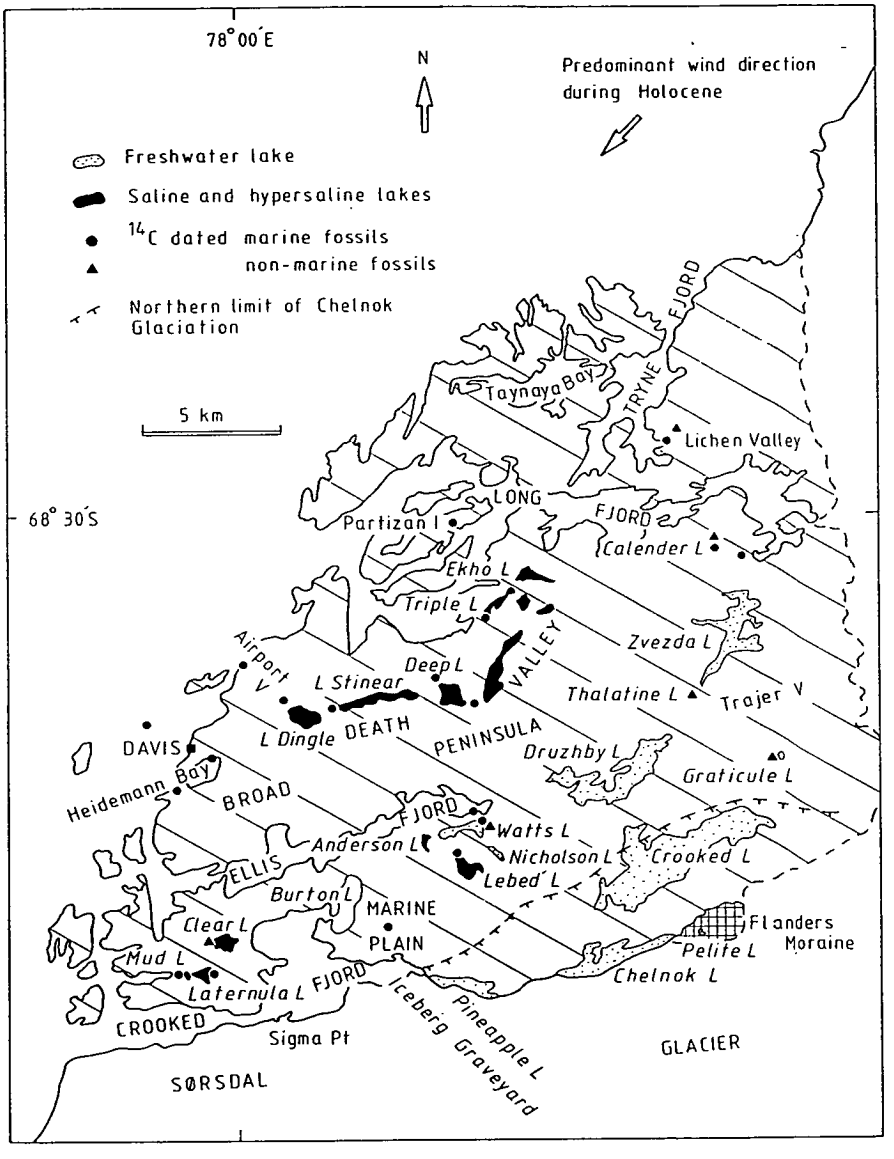

Figure 6.5 Map of the Vestfold Hills showing the location of the Sørsdal Glacier, Crooked Fjord and Marine Plain (after Adamson and Pickard, 1986).

to 500 m from the margin of the Sørsdal Glacier at the same locality, gave 5070 ± 80 yr B.P. (SUA 2923) and 2010 ± 60 yr B.P. (SUA 2922), which correspond to corrected dates of 3,770 and 710 yr B.P. respectively. The abundant marine material in the moraine ridges indicates a provenance as glaciomarine or marine sediment prior to transportation to these positions by an expanded Sørsdal Glacier. These dates represent the age of marine deposition in the Crooked Fjord rather than the age of moraine formation and thus indicate that the expansion of the Sørsdal Glacier occurred at or after 710 yr B.P. They also indicate that the Sørsdal Glacier probably retreated further inland than the present position during the Early-Holocene marine transgression. The oldest date of 8,600 corr. yr. B.P. adjacent to the deep fjord is consistent with the other oldest dates in the Vestfold Hills which are also adjacent to marine inlets (Adamson and Pickard, 1986). Fitzsimmons (1991) attributed this pattern to the Early-Holocene deglaciation in response to rapidly rising sea level. Adamson and Pickard (1986) also presented evidence for a Late Holocene advance of the Sørsdal Glacier (named the Chelnok Glaciation) on the basis of local striae directions in localities adjacent to the glacier. Fitzsimmons (1991) re-analysed the striae directions and did not find conclusive evidence for a separate glaciation other than local expansion of the Sørsdal Glacier.

The above glacial geological evidence in the Vestfold Hills and that from Adamson and Pickard (1986) suggests that adjacent to the deep marine inlets the ice tongues and in particular the Sørsdal Glacier had retreated by 8,600 corr. yr B.P., during the Early-Holocene marine transgression to a position further inland than today. The ^{14}C dates and the geomorphological evidence in Adamson and Pickard (1986) suggests that the grounded margin of the East Antarctic Ice Sheet retreated much slower during the Mid-Holocene. Both Adamson and Pickard (1986) and Fitzsimmons (1991) speculated that the moraine ridges on Broad Peninsula were deposited during a Mid-Holocene re-advance of the Sørsdal Glacier, probably synchronous with the interpreted re-advance of the Prydz Bay outlet glaciers by Domack et al. (1991). However, the dated evidence of Fitzsimmons (1991) above suggests that the Sørsdal Glacier retreated and re-advanced during the Late-Holocene with the most recent advance occurring since ~700 corr. yr B.P..

6.3.5 LARSEMANN HILLS

Gillieson (1991a) and Gillieson et al. (1990) reported that the nearshore islands (Figure 6.6) were deglaciated by 9,400 ± 180 (SUA 2749) from algal bottom sediments in Krisjes Pond on Kolloy Island, which corresponds to 9,000 corr. yr

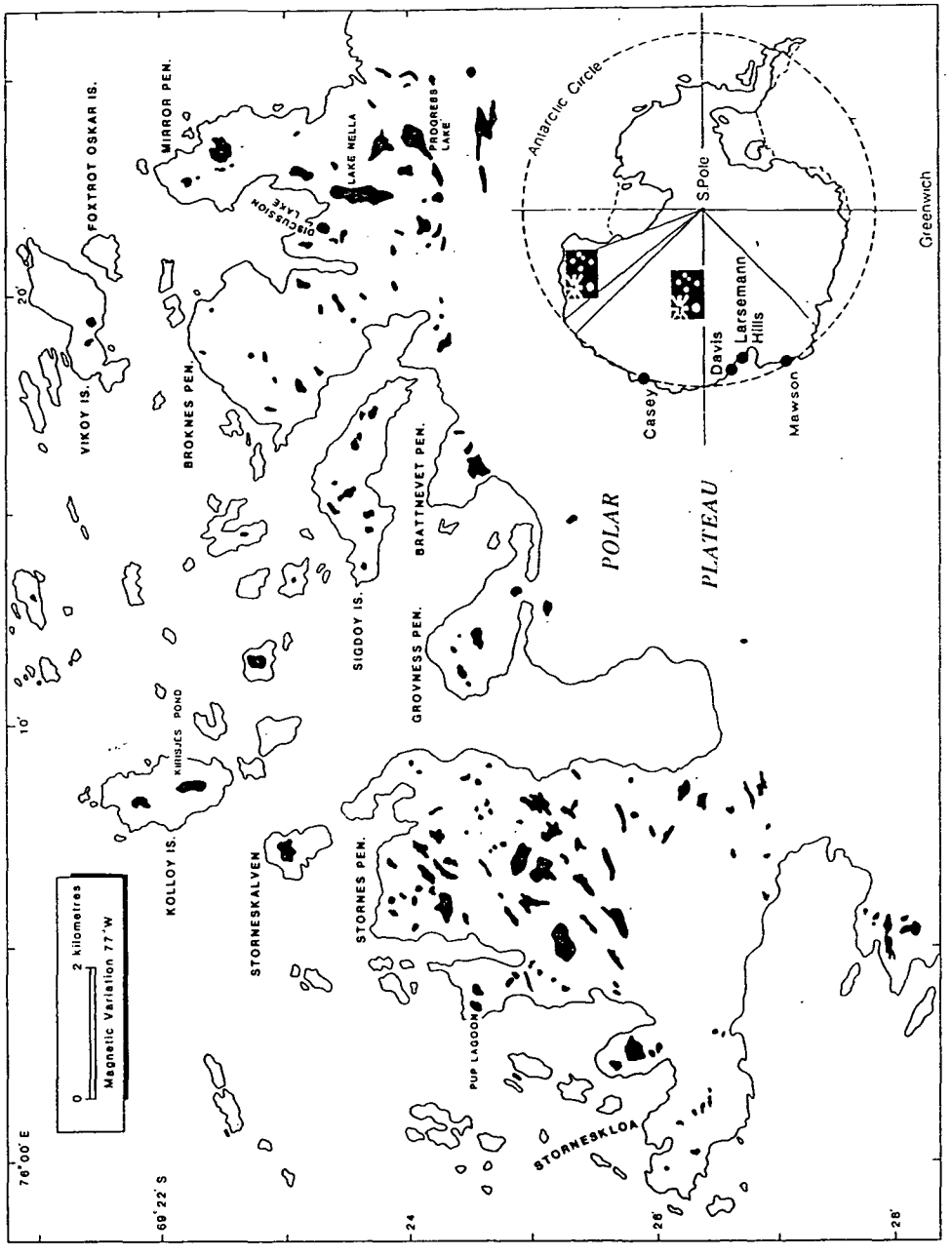

Figure 6.6 Map showing the location of the lakes and peninsulas of the Larsemann Hills (after Gillieson et al., 1990).

yr.B.P.. The present coastline of the Larsemann Hills was deglaciated by 4,500 corr. yr.B.P. (from Pup Lagoon on Stornes Peninsula) and the large glacial troughs of the Progress and Nella Lakes were probably ice free by 3,500-4,500 corr. yr. B.P.. Gillieson (1991b) later revised the deglaciation of the outer islands to ~12,000 corr. yr B.P.. A recent study by Burgess et al. (1994) dated moss in its growth position in a lake sediment core at Lake Nella, to be 24, 950 ± 710 yr B.P. This date probably provides an estimate for the onset of glaciation in the Larsemann Hills rather than an estimate of the onset of deglaciation as suggested by Burgess et al. (1994). This period in the Dome C oxygen isotope core (Lorius et al., 1979).represents a warmer interval within the last glacial and would indicate that the potential for Larsemann Hills glaciation is restricted to between 24,000 years B.P. and 14,000 years B.P..

No discrete Holocene age raised beaches were observed in the Larsemann Hills except for a few boulder strandlines on the outer islands and Dork Peninsula, which are considered to have been produced by a single set of surge waves originating from inshore catastrophic iceberg calving or roll-over events (Andy Spate, pers. comm. 1994). These iceberg calving and surge wave events have been observed by several workers in the Larsemann Hills. The lack of raised beaches in the Larsemann Hills is not due to a lack of suitable sediment, which mainly consists of sand and gravel deposits. However, the lack of raised beaches may be explained by, and give support to the interpreted advance of the Amery Ice Shelf-Lambert Glacier system into Prydz Bay between 7,300 and 3,800 ka B.P. (Domack et al., 1991), immediately offshore from the Larsemann Hills. During this period, open water conditions would not have existed along the coast of the Larsemann Hills, and hence coastal features would have been restricted to ice push ridges which may form from the tidal range of sea ice along the shoreline. However, observations of ice-push ridges have not been reported for the Larsemann Hills either, and may indicate the existence of an extensive fast, ice foot along the shoreline in the inlets. Increased fast ice activity has also been interpreted in the Bunger Hills (Adamson and Colhoun, 1992) and in the Windmill Islands between 3,500-4,500 yr B.P. In addition, the lack of evidence for isostatic uplift of the Larsemann Hills may in fact reflect a minimal ice cover during the Late Pleistocene.

6.3.6 KEMP LAND

Trail (1970) reported the location of raised beaches along the Kemp Land coast which attain elevations of between 3-15 m. They are mainly located at the margin of the grounded ice sheet in the vicinity of the Taylor Glacier, the Dovers Glacier and the Hoseason Glacier (Figure 6.7). The close proximity of the raised beaches to the present ice margin could possibly indicate that the Kemp Land ice margin has also

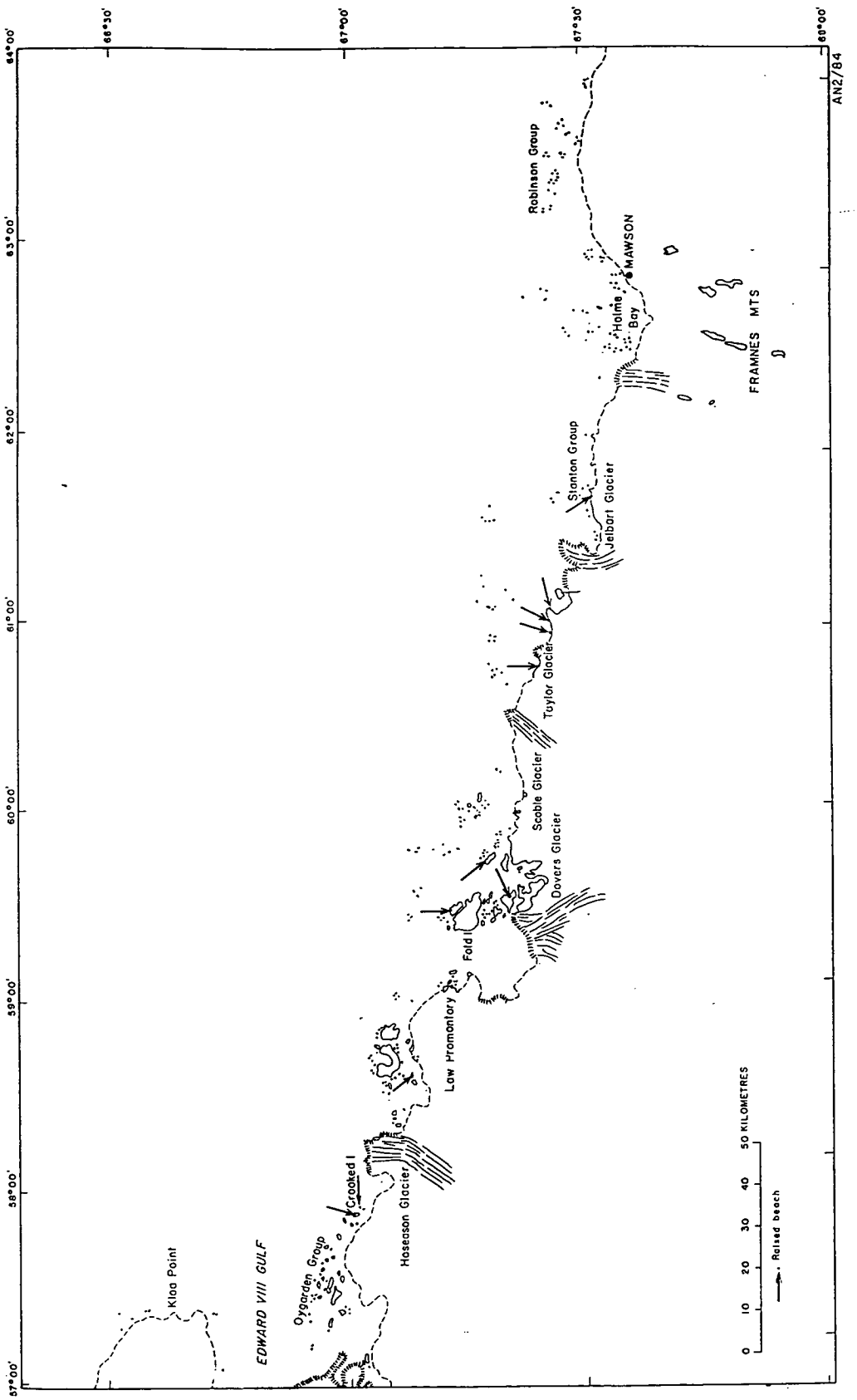

Figure 6.7 Map showing the location of raised beaches (arrows) in the vicinity of the Taylor Glacier, the Dovers Glacier and the Hoseason Glacier, along the MacRobertson and Kemp Land coasts (after Trail, 1970).

advanced during the Holocene. However, these observation were made at a reconnaissance level and no detail maps or chronologies are available to confirm this.

6.3.7 NORTHERN PRINCE CHARLES MOUNTAINS

Mabin (1992) reported the characteristics of lateral moraines of the Lambert Glacier in the vicinity of Fisher Massif and of alpine glaciers on Fisher Massif (Figure 6.8a). He described a sequence of three groups of lateral moraines of the Lambert Glacier on the south-eastern side of Fisher Massif. The oldest and uppermost belt are 1 km wide and extend from 600-800 m elevation, and the middle group extend from 200-600 m elevation. The lowest and youngest group are ice-cored and extend from the present glacier surface at 100 m elevation to 200 m elevation. The author observed these moraines from the air in 1989 and a similar set bordering Nilsson Rocks some ~25 km further inland in the Lambert Glacier valley, and both younger sets show comparatively recent weathering. There are no contemporary moraines down glacier in the vicinity of the grounding zone at Beaver Lake and Jetty Peninsula. There is no chronological control of formation of these moraines. However, Mabin (1992) suggests that the lowest are of Late Glacial Maximum age (18,000-21,000 yr B.P.) on the basis of the age of other similar lateral moraine sequences (albeit significantly higher, eg 500 m above the present surface) in the Transantarctic Mountains (Denton et al., 1989a). However, since these younger moraines at Fisher Massif remain ice-cored it is unlikely that they are of LGM age since they are located within an ablation zone. It is more likely that they were produced by the postulated Mid-Holocene advance of the Amery Ice Shelf-Lambert Glacier recorded in the marine sedimentary record at site 740A in Prydz Bay (Domack et al. 1991a). If this was the case then the Lambert Glacier thickened by between 100-200 m within 20 km of the present grounding line during the period 7,300 to 3,800 yr B.P. and subsequently thinned to the present morphology.

Mabin (1992) also described the distribution of lateral moraines of the numerous alpine glaciers on Fisher Massif. They generally are incised into the upper Lambert Glacier moraines and indicate an out of phase advance regime with the Lambert Glacier outlet system. At the north-eastern end of Fisher Massif, two alpine glaciers extend out of their valleys and down across the Lambert Moraine complexes to within a few metres of the Lambert Glacier (Figure 6.8b). Mabin (1992) observed that these glaciers are close to their maximum extents and have recently retreated slightly forming moraine complexes that cross all three of the Lambert Moraines. This succession in morphology shows that the advance of the alpine glaciers occurred after the Lambert Glacier had retreated from its most recent thickening equivalent to the elevation of the

a

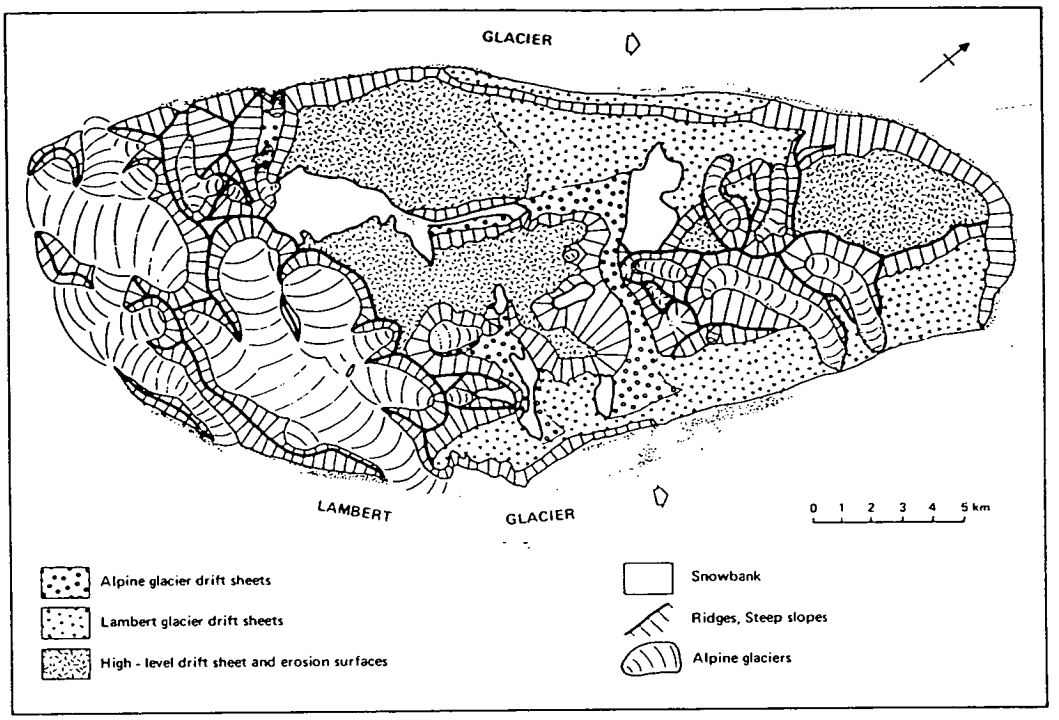

b

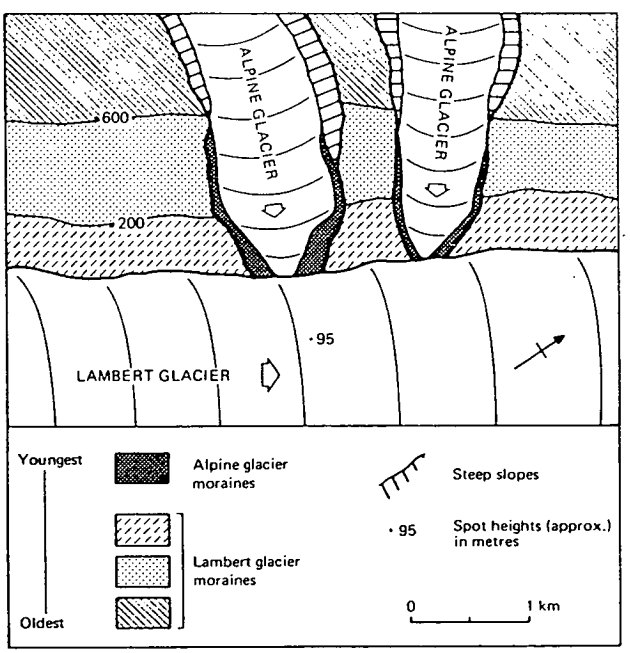

Figure 6.8 (a) Map showing the glacial landforms of Fisher Massif. (b) Map showing the expanded north-east alpine glaciers incised into the lateral moraine sequence of the Lambert Glacier (after Mabin, 1992).

lowest Lambert Moraines. Clearly, the alpine glaciers are responding asynchronously to the Lambert Glacier and other outlet glaciers in the region. The out of phase response was identified by Mabin (1992) and can be explained as follows: the alpine glaciers terminate on land and require an increase in surface mass balance to advance whilst the outlet glaciers primarily require a relative sea level lowering to advance. An expansion of the Lambert Glacier-Amery Ice Shelf system would result in a drastic retreat of the alpine glaciers due to a substantial reduction of the accumulation because of the increased continentality. The converse would result in increased accumulation which would lead to an advance of the small glaciers. In addition, the alpine glaciers are cold, dry based and very slow moving in contrast to the warmer wet based and fast moving outlet glaciers. Consequently, the advance of the alpine glaciers on Fisher Massif is most likely in response to increased precipitation during either the Early Holocene Climatic Optimum or the Late Holocene warm period between 4,000 to 3,000 years B.P..

6.3.8 TRANSANTARCTIC MOUNTAINS

Denton et al. (1989b) and Bockheim et al. (1989) reported the late Quaternary ice-surface fluctuations of the Transantarctic Mountains outlet glaciers. They examined the extensive glacial drift deposits in the Reedy, Beardmore, Darwin, and Hatherton outlet glacier valleys, and in the Taylor alpine glacier valley (Figure 6.9). They concluded that the Reedy, Beardmore, Darwin and Hatherton Glaciers which drain the East Antarctic ice sheet to the Ross Sea had fluctuated in thickness over the Late Quaternary. Mayewski (1975) reported similar lateral moraine sequences for the Scott, Amundsen, Shackleton and Beardmore Glaciers. The Plunket Drift and the Hatherton Drift typify the youngest drift deposits in each of these outlet glaciers and are found up to 15-20 m and 20-70 m above and parallel to the present ice surfaces of the Beardmore and Hatherton Glaciers respectively. The parallel ice-surfaces indicate that they represent a thickening of the glaciers due to increased ice drainage from the East Antarctic drainage basin coupled with a grounded ice margin, in the Ross Embayment, which would have partially restricted glacier flow. The eventual decoupling of the Ross Embayment grounded ice would have allowed increased flow and hence ice-surface lowering. The latter may also have occurred through a reduction in ice outflow. Radiocarbon dates on blue-green algae within the youngest drifts placed their minimum age at 5270 years B.P. Since then these glaciers have receded to their present surface levels. Such an expansion of these western Ross Embayment outlet glaciers between ~5,300 and 7,400 years (Bockheim et al., 1989) is synchronous with the expansion of the Lambert Glacier-Amery Ice Shelf system and indicates that the expansions may have been in response to similar forcings.

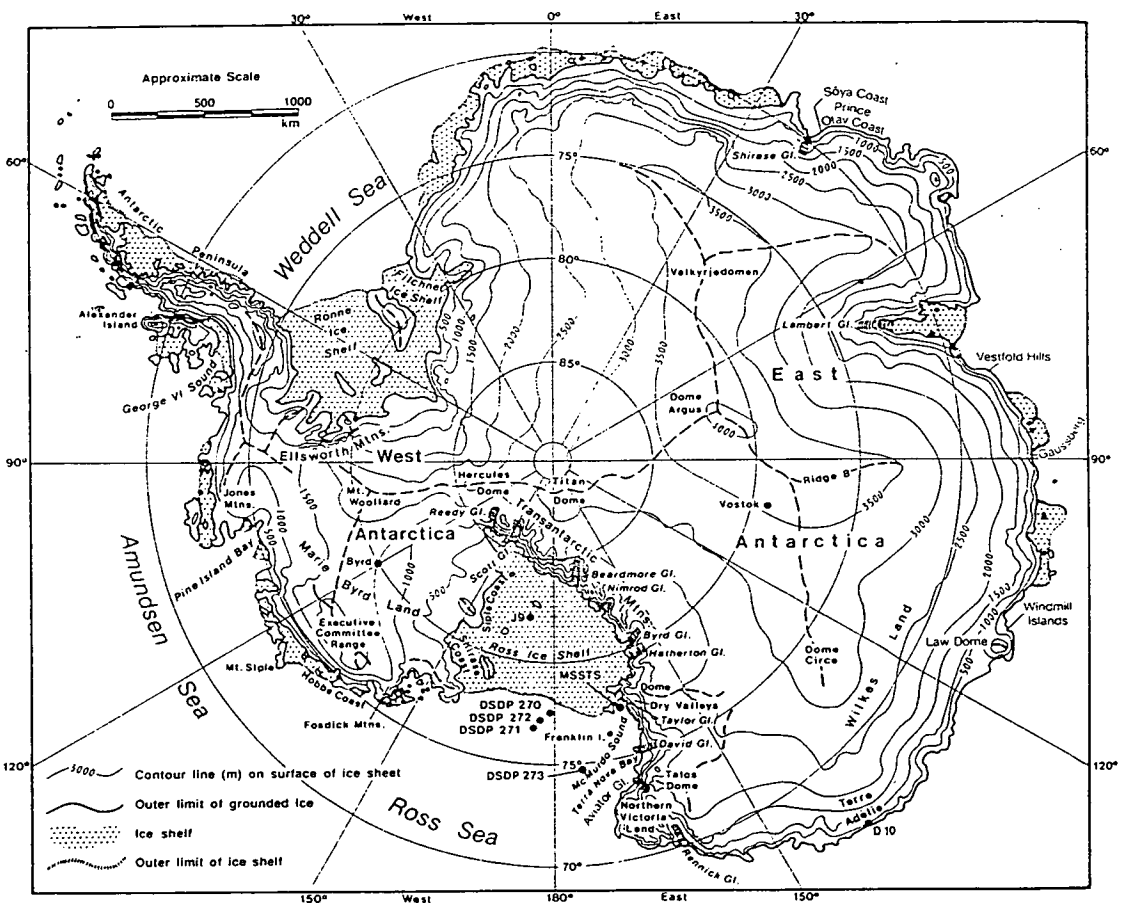

Figure 6.9 Location map showing the Transantarctic Mountains and the major outlet glaciers draining to the Ross Ice Shelf and the Ross Sea (after Denton et al., 1991).

In contrast the alpine glaciers in the northern Transantarctic Mountains, such as those in the Taylor Valley display an asynchronous advance achieving their maximum extent later in the Holocene and remain slightly lower than their Holocene maximum position today (Denton et al., 1989a, 1989b). Stuiver et al. (1978) and Denton et al. (1986) reported that the alpine glaciers in the Dry Valleys and throughout Northern Victoria Land, including the Rennick Glacier and Talos Dome (Figure 6.9) had contracted at ~3,100 years B.P.. This widespread contraction of the alpine glaciers and outlet glaciers in Victoria Land was followed by a period of expansion from ~2,000 years B.P. to the present, during which these glaciers reached their maximum position since before LGM (Denton et al., 1991). Baroni and Orombelli (1994) determined that the Nansen Ice Sheet, which is fed by the Priestley glacier and the Hells Gate Ice Shelf in Terra Nova Bay, Northern Victoria Land, had also retreated during the Mid-Holocene. Raised beaches with ages between 7,500 and 5,000 years B.P. indicate that the coastline of Inexpressible Island was open to the sea during this period. This implies that the Mid-Holocene ice margin of the Nansen Ice Sheet was 5 km further inland than today and similarly the Hells Gate Ice Shelf was 2 km further inland than the present position of the margin. Since 5,000 years B.P. the Nansen Ice Sheet and the Hells Gate Ice Shelf have re-advanced to near their present configuration. Chinn (1986, 1987) and Baroni and Orombelli (1994) reported that small alpine glaciers in the Terra Nova Bay Region of Northern Victoria Land have fluctuated in size during the Neoglacial and are now near their maximum Holocene position. Baroni and Orombelli (1994) interpreted a retreat phase of local alpine glaciers in the Terra Nova Bay regions during the Little Climatic Optimum (~1,000 to 1,200 yr B.P.) and a subsequent re-advance during the Little Ice Age (~400-500 yr B.P.). These fluctuations in the small Terra Nova Bay glaciers are in response to surface mass balance changes in particular, variation in net ablation at the lower elevations.

In general, the Transantarctic alpine glaciers and their drainage basins were severely starved of precipitation during the Late Glacial Maximum and have taken most of the Holocene to accumulate their current mass The advance of the Transantarctic alpine glaciers is synchronous with those alpine glaciers in the Northern Prince Charles Mountains and was probably forced by the increased accumulation in the interior drainage basins since the Early Holocene Climatic Optimum (EHCO) in response to the climate warming and reduced continentality following the retreat of the Late Pleistocene grounded ice sheets in the Ross and Amery Embayments.

6.4 SUMMARY OF GLACIAL GEOLOGICAL EVIDENCE FOR A RE-ADVANCE OF THE EAST ANTARCTIC ICE SHEET AND OUTLET GLACIERS DURING THE MID-LATE-HOLOCENE

Along the East Antarctic coast, the outlet glaciers had retreated to near their present positions by 9,000 to 11,000 years B.P. during the marine transgression (Colhoun and Adamson, 1991, Domack et al., 1991a, and Fitzsimmons, 1991). Ice sheet recession was well underway by ~13,000 years B.P. in the western Ross Embayment with the Ross Sea ice surface within 100 m of the present sea-level between 9,490 and 12,500 yr B.P. (Denton et al., 1989). In contrast, recession of the grounded ice margins lagged the recession of the outlet glaciers. Along the East Antarctic coast, the grounded ice sheet margins retreated to near their present location by 8,000 to 5,000 yr B.P. (Adamson and Pickard, 1986, Colhoun and Adamson, 1991, Fitzsimmons, 1991 and Goodwin, 1993b). There is also regionally widespread evidence that the grounded ice margins retreated further inland than the present position between 5,000 to 4,000 yr B.P. (Adamson and Pickard (1986), and Chapter 5, this study). In the western Ross Embayment, the retreat of the grounded ice margins was completed by ~6,000 yr B.P. (Denton et al., 1989), with the ice margin retreating further inland than the present position in the Terra Nova Bay region between 7,500 to 5,000 yr B.P. (Baroni and Orombelli, 1994).

There is widespread evidence for a Mid-Holocene re-advance of the East Antarctic outlet glaciers between 7,300 to 3,800 yr B.P. along the open Southern Ocean coast, (Domack et al., 1991a) and between 7,400 and 5,300 yr B.P. along the western Ross Embayment coastline (Bockheim et al., 1989) and since 7,500 to 5,000 yr B.P in the Terra Nova Bay region (Baroni and Orombelli, 1994). Along the East Antarctic coast, the grounded ice margins have re-advanced during the Late-Holocene lagging behind the re-advance of the outlet glaciers. The re-advance of the grounded ice margins has occurred since 4,000 yr B.P. on Law Dome (Chapter 5, this study) and since 6,300 yr B.P. in the Bunger Hills (Colhoun and Adamson, 1991). A Late-Holocene re-advance of the Sørsdal Glacier, Vestfold Hills (Fitzsimmons, 1991) and the Edisto Ice Tongue, Bunger Hills (Colhoun and Adamson, 1991) has occurred since 700 yr B.P. and 200 yr B.P. respectively . These glacial advances are synchronous with the second wave of thickening interpreted at the Law Dome ice margin (Chapter 5, this study). Similarly, both the Transantarctic and the Prince Charles Mountains alpine glaciers have re-advanced during the Late Holocene and have slightly retreated from their maximum Holocene position (Chinn, 1987a, Mabin, 1992).

6.5 POSSIBLE FORCINGS AND MECHANISMS FOR THE MID-LATE- HOLOCENE GLACIAL FLUCTUATIONS

The previous sections have identified a large body of consistent evidence for Mid-Late-Holocene glacial fluctuations to have occurred along the margin of the East Antarctic ice sheet, the outlet glaciers and the alpine glaciers. The geological evidence also suggests that the outlet glaciers have led the grounded ice sheet margins and the alpine glaciers both in the Early Holocene contraction and in the Mid-Late Holocene expansion. This pattern of Holocene glacial fluctuations in East Antarctica probably reflects the relative sensitivities of the different glacial morphologies to the dual forcings of relative sea-level and ice sheet accumulation rate changes. Thus the two likely mechanisms controlling the dynamics of the advance are:

- a derived ice sheet thickening due to increased snow accumulation rates forced by Holocene climate warming (Whillans, 1978), and/or;
- a seaward migration of the ice sheet and outlet glaciers' grounding zone forced by relative sea level lowering (Alley and Whillans, 1984).

These mechanisms may have been individually instrumental in determining the nature of the advance, or may have operated together. The characteristics of these mechanisms are discussed in the following sections.

6.5.1 ICE SHEET RESPONSE TO HOLOCENE CLIMATE WARMING

Climate warming affects the mass balance of the Antarctic ice sheet and outlet glaciers by forcing firstly, an increase in accumulation rate and secondly, with some time delay, a warming of the ice along its entire depth. Both of these derivatives of climate warming result in changes to the ice sheet's morphology and consequently, the ice dynamics (Whillans, 1981). In Antarctica, climate warming of the surface air mass and the surrounding oceans forces increased precipitation onto the ice sheet surface (Budd and Simmonds, 1991). The increased air temperatures result in: increased atmospheric moisture flux due to an increase in the saturation water vapour pressure; an increase in open water and hence a closer atmospheric moisture source to the continent, and; changes in the atmospheric circulation. (Huybrechts and Oerlemans, 1990). An increase in atmospheric moisture and cloud cover may also contribute to a decrease in the surface air inversion over the ice sheet resulting in decreased katabatic wind velocities and hence a net decrease in the wind erosion of surface snow. As a result of the above factors snow accumulation rates increase over the ice sheet.

The effect of increasing accumulation rates is immediate, causing an ice sheet thickening corresponding to the excess accumulation. This is initially a static effect since no immediate change in ice dynamics occurs. Whillans (1981) found a numerical solution for the reaction time of the ice sheet or glacier to the thickening process. He found that the ice sheet will continue to thicken in response to the excess accumulation rate until the added thickness changes the surface slope, and hence the basal shear stress, resulting in increased flow by internal shearing. The reaction time is dependent upon the exponent of the ice flow law (**p**), the total ice thickness, **Z** and the steady state accumulation rate, $\mathbf{b_s}$. The reaction time **r** can be calculated from;

- $\mathbf{r = Z/(p+2)\ b_s}$

Whillans (1981) reported typical reaction times for ice sheets (in this case **p=3**) with thicknesses ranging from 2000-3700 m. For example:

- South Greenland ($\mathbf{b_s}$= 0.5 ma^{-1}, **Z**= 2000 m) has a reaction time of 800 years;
- Byrd, Antarctica ($\mathbf{b_s}$= 0.17 ma^{-1}, **Z**= 3000 m) has a reaction time of 3,530 years; and;
- Dome C ($\mathbf{b_s}$=0.035 ma^{-1}, **Z**= 3700 m) has a reaction time of 21,150 years.

The reaction time for ice thicknesses in the range 500-1000 m such as on Law Dome and close to the margin, is much shorter around several hundred years. The final thickness an ice sheet or glacier attains following a sustained accumulation rate increase only, is dependent upon the reaction time and the time duration of the accumulation change. The change in ice thickness $\mathbf{Z_1}$ can be calculated as follows from Whillans (1981):

- $\mathbf{Z_1 = rb_1\ (1 - exp^{-t/r})}$

where $\mathbf{b_1}$ is the change in accumulation rate from the steady state rate, and **t** is the time duration of the accumulation rate change. The ice sheet is 63% adjusted to the accumulation rate change after a time equal to the reaction time **r** and the final change in ice thickness is $\mathbf{rb_1}$ (Whillans, 1981).

Thus on time scales of up to a few 100 years, increased ice thickening due to accumulation, together with increased basal melting beneath ice shelves resulting from surface ocean temperature increases, are the major consequences of short-term climatic warming (Drewry, 1991). These mass balance changes are static responses to climate warming over the first 100 years and directly result in contemporary sea level lowering

by accumulating mass on the ice sheet's surface (Huybrechts and Oerlemans, 1990). It is important to note that increased surface melting is also an important static response to climatic warming for most glaciers and the Greenland Ice Sheet, but is not important in Antarctica where temperature changes of only a few degrees above the present regime occur (Huybrechts and Oerlemans, 1990).

Climatic warming also initiates the penetration of surface temperature increases into deep ice which eventually leads to dynamical changes through more rapid shear deformation and/or basal sliding (Whillans, 1981). These latter changes lead to increased ice flow which causes an advance of the ice sheet or glacier margin and thinning of the ice sheet. The temperature at depth increases by conduction for ice sheets such as East Antarctica where accumulation rates are low. In contrast, in marginal areas where the accumulation rates are high the vertical ice motion carries the temperature increase downwards. The temperature changes are more rapid at depth where the base is cold and temperature fluctuations can penetrate into the subglacial substrate, whereas warm basal conditions where the basal temperature is fixed at the melting point have slower temperature change (Whillans, 1981). These dynamic changes to the ice sheet and/or outlet glaciers as a result of the temperature penetration are delayed with respect to the initial climate warming due to the long time for temperature changes to penetrate to the deeper ice. Typically the ice flow response due to temperature changes begins at the reaction time (**r**) to increased accumulation and thickening and is not completed until a period equivalent to approximately **10r** (Whillans, 1981). A coupled increase in accumulation rates and in temperature will eventually result in net thinning of the glacier at some time equivalent to **5r** . In addition, ice sheets, outlet glaciers and alpine glaciers also have different time responses to climate warming since their catchments range from thousands of square kilometres in the case of the major outlet glaciers and the main ice sheet to just a few square kilometres in the case of small cirque glaciers. Similarly, the ice velocities vary proportionally with total ice flux, from kilometres per year for floating outlet glaciers and wet based glaciers where ice flow is primarily by basal sliding, to less than a metre per year for grounded ice margins and cold based cirque glaciers, where ice flow is by plastic or internal deformation.

The evidence for a Holocene glacial advance has been derived for outlet glaciers, alpine cirque glaciers and grounded ice sheet margins. The majority of the coastal East Antarctic drainage basins generally terminate in grounded ice margins and are dominated by relatively slow divergent flow towards the coast. In contrast, the drainage basins which drain to the three largest ice shelves, the Ross Ice Shelf, the Filcher-Ronne Ice Shelf and the Amery Ice Shelf are characterised by more rapid

convergent ice flow. Hence, an accumulation increase in a basin with convergent ice flow will cause rapid thickening and a significant increase in total ice flux within a relatively short reaction time. The geological evidence shows that the earliest and largest Holocene ice advance, in terms of increased total ice flux from East Antarctic drainage basins comes from the fast flowing Lambert Glacier/Amery Ice Shelf system, the major outlet glaciers in George V Land and Terre Adélie and the major western Ross Embayment outlet glaciers between 7,000-4,000 years B.P. If the advance was forced by climatic warming, then the advance would be the reaction to increased accumulation and glacial thickening during the Late Pleistocene Glacial-Interglacial Transition warming (15,000-11,000 years B.P.) and the Early Holocene Climatic Optimum (EHCO) (11,000-9,000 years B.P.). Surface temperatures increased by ~3.5°C during the Transition, reaching the present mean temperatures by 11,000, before increasing to ~1°C above the present mean temperatures during the EHCO.

The analysis of recent temporal changes in accumulation, temperature and sea ice extent around the coast of East Antarctica in Chapter 3 determined an accumulation-proxy temperature relationship of 20%/°C in the interior of the ice sheet and 25%/°C in the coastal margins . This relationship incorporates the accumulation changes due to changes in surface air temperature and saturation water vapour, the fraction of open water within the sea ice cover and in atmospheric circulation. Assuming that the recent climate and oceanic changes are characteristic of the long-term Holocene changes, the ice sheet palaeo-accumulation rate pattern for the EHCO can be estimated as up to 25% greater than the present long-term accumulation rate pattern in East Antarctica, (defined as the long-term rate for this century) (Chapter 3).

The application of the present accumulation-proxy temperature relationship of 20%/°C in the interior of the ice sheet and 25%/°C in the coastal margins, to the Holocene temperature pattern is supported by the palaeo-accumulation rates determined in the Vostok ice core from ^{10}Be measurements by Raisbeck et al. (1987). Previously, Raisbeck et al. (1981) had reported measurement of cosmogenic ^{10}Be in the Dome C ice core. They found that the ^{10}Be concentration was larger in Last Glacial Maximum (LGM) ice by a factor of 2 to 3 than in the Holocene ice. Raisbeck et al. (1981) suggested that this pattern in the ^{10}Be was due to the ice sheet accumulation rate being 50% less during the LGM than during the Holocene. Hence the mean annual ^{10}Be concentration in ice cores is a function of the dilution of the signal by the accumulation rate. Good correlation between the normalised palaeo-accumulation rates determined from the ^{10}Be and the $\delta^{18}O$ measurements on the Vostok ice core (shown in Figure 6.10) was reported by Jouzel et al. (1989) for the last complete glacial-interglacial cycle. Whilst the normalised palaeo-precipitation rate pattern is similar between the

^{10}Be and $\delta^{18}O$ records, the former describe larger amplitude fluctuations. This is due to the palaeo-accumulation record derived from the $\delta^{18}O$ measurements representing changes in accumulation rate according to changes in the saturation water vapour pressure only. In contrast, the palaeo-accumulation record derived from the ^{10}Be measurements representing direct changes in the dilution of the ^{10}Be signal, which Jouzel et al. (1989) attribute primarily to the precipitation rate. They found that the inverse relationship between ^{10}Be concentration and the precipitation rate at a given latitude was due to the predominance of dry cosmogenic deposition (precipitation independent) over the ice sheet, and the circum-polar atmospheric circulation, rather than a strong meridional atmospheric exchange. Figure 6.10 shows the normalized precipitation rate from ^{10}Be measurements at Vostok for the last full glacial cycle. Unfortunately, a more detailed and specific examination of the Holocene precipitation rate from ^{10}Be measurements is not available.

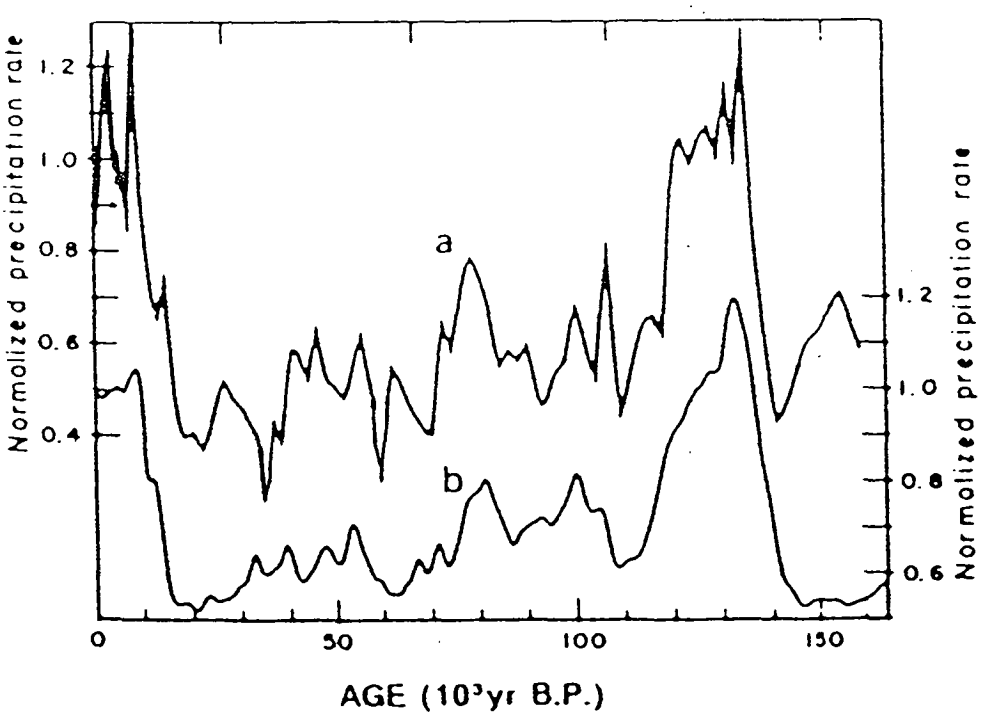

Figure 6.10 Normalised precipitation rate with respect to Holocene mean value (designated as 1.0) for the Vostok ice core. (a) (Upper curve, left scale): from the ^{10}Be concentration record (Raisbeck et al., 1987). (b) (Lower curve, right scale): from the $\delta^{18}O$ isotopic temperature record for comparison (Jouzel et al., 1987).

However, Raisbeck et al. (1987) made a sensitivity analysis of the ^{10}Be peaks to determine the accuracy of the data. They examined the authenticity of the peaks at 35,000, 60,000 and 135,000 yr B.P. by a comparison with independent climate records from Dome C, Byrd and Southern Ocean marine sediments. They determined that the peaks were present in the comparative records and that the dating error at 135,000 yr B.P.was less than 5%. They also showed graphically that the peaks during the Early Holocene and the Mid Holocene were partially dependent upon the inclusion of the detailed peaks at 35,000 and 60,000 yr B.P., and are by inference, real data rather than artefacts of the statistical treatment of the data. Consequently, Figure 6.10 indicates that palaeo-precipitation rates at Vostok were 30% less than the Holocene long-term mean rates at 14,000 to 15,000 yr B.P., and ~50% less than those during the LGM. Figure 6.10 also shows that the precipitation rates increased to 20-25% greater than the Holocene long-term mean rates during the EHCO, and up to 20% greater during the Second Climatic Optimum (SCO) between 3,000 to 4,000 yr B.P.. Therefore, palaeo-accumulation rates determined from the ^{10}Be concentration measurements are equivalent to those estimated using the present accumulation-proxy temperature relationship of 20%/°C in the interior of the ice sheet and 25%/°C in the coastal margins. Further, both these methods describe the total change in palaeo-accumulation rates due to changes in air temperature, the saturation water vapour pressure, sea ice characteristics and moisture sources, and associated changes in the coast parallel cyclone tracks and frequency.

6.5.2 ICE SHEET RESPONSE TO RELATIVE SEA LEVEL LOWERING DURING THE HOLOCENE

Eustatic sea level rise during the Late Pleistocene and Early Holocene beginning at around 15,000 years B.P., initiated the retreat of the Antarctic Ice Sheet where its margins were below sea level, including the major grounded ice shelves and outlet glaciers. (Hollin, 1962). Grounding line retreat begins when the sea-level rise reaches a critical depth and decoupling of the bed occurs. This is determined mainly by the dimensions and the dynamics of the ice sheet or glacier. At the same time the seabed begins to experience uplift in response to the isostatic elastic response of the mantle. However, following this initial elastic response during the Late Pleistocene, isostatic rebound rates were slower and eustatic sea level rise was much faster (Thomas and Bentley, 1978). Consequently, the grounding line of the marine ice sheets retreated significant distances inland until they grounded on subglacial bedrock highs, which enabled a new equilibrium to be reached. By removing the damming effects of ice shelves and grounded margins the total ice flux increased whilst the

grounding line retreated and a thinning of the ice sheet propagated up glacier into the interior (Alley and Whillans, 1984). However, the rate of ice sheet thinning in the interior basins due to coastal retreat was a factor slower than for the coastal margins, with thinning occurring after on the order of 50,000 years in the interior of the ice sheet (W. Budd, pers comm., 1994). Thus any thinning of the interior of the ice sheet due to post-glacial sea-level rise is considered to be insignificant over the Holocene period. The response time of glaciers and ice sheets to sea-level change is approximately the same as that produced by accumulation rate increases. Ice sheets with high accumulation rates and ice streams have the fastest response to sea-level rise.

The geological evidence for a Mid-Late Holocene re-advance of the ice sheet and glaciers indicates that the grounding line of the ice sheet and glaciers retreated further inland than the present position of their termini. It is possible that such a situation could occur through delayed lithospheric rebound (Alley and Whillans, 1984) due to the continental shelf not being in isostatic equilibrium when the rapid eustatic rise was occurring. Thomas and Bentley (1978) concluded that continuing isostatic depression during the Holocene marine transgression may have been just as important in instigating the retreat of the Late Pleistocene ice sheet.

As isostatic rebound progressed during the Holocene, the relative sea level lowered with respect to the ice bed. This would have lead to a progressive increase in the grounded ice sheet area along the coastal margin and eventually to a grounding line advance. Such an advance would result in an increased catchment area and total snow accumulation rate, which would cause further thickening and a positive feedback loop (Thomas and Bentley, 1978). A grounding line advance of a marine ice sheet or outlet glacier would also occur if a seaward ice shelf became progressively grounded by relative isostatic seabed uplift, resulting in the formation of ice rises which retard flow and thus dam the ice flux from inland. This causes a progressive thickening at the grounding line, with the ice sheet eventually advancing onto the ice shelf and absorbing the ice rise. In fact the growth of a marine ice sheet over an undulating seabed, as opposed to an inner shelf bank, is dependent upon the existence of a partially grounded ice shelf. Thomas and Bentley (1978) suggested that self cycling marine ice sheets may advance in response to crustal rebound and retreat in response to crustal depression. Accordingly, the isostatic rebound that occurred to form the present inner shelf topography may have forced an advance of the grounding line to seaward of its present position during the Holocene. They reported that the Ross Ice Shelf is presently thickening in the south east corner along the Siple Coast, and is evidence for this self-cycling mechanism.

6.6 DISCUSSION

The East Antarctic outlet glaciers retreated during the Late Pleistocene-Early Holocene much earlier than the grounded ice margins (before 10,000 yr B.P.) as their beds decoupled in response to a rapid rise in eustatic sea-level. It is also interpreted that these outlet glaciers expanded during the Mid Holocene (7,500-4,000 yr B.P.) at a time when the post-glacial eustatic sea-level rise slowed down. This advance was probably nourished by increased ice drainage due to an increase in accumulation rates due to climate warming during the Late Pleistocene transition (14,000 to 11,000 yr B.P.) and the subsequent EHCO (11,000 to 9,000 yr B.P.), together with a reduction in ice sheet continentality from the LGM maximum extent. By 8,000 years B.P. it is likely that at least half of the total isostatic rebound on the inner continental shelf and present margin had occurred, assuming that deglaciation from the continental shelf had begun by 15,000 years B.P., and a total isostatic response time of 10,000 years (Andrews, 1970). Therefore it is suggested that these outlet glaciers and the margins of the marine based West Antarctic Ice Sheet are very sensitive to eustatic and relative sea-level changes. The sea-level control may also partly explain the interpreted synchronous response of the Southern Ocean and western Ross Embayment outlet glaciers during the Early-Mid Holocene.

The grounded ice margins and alpine glaciers have displayed a different response to the outlet glaciers and retreated much more slowly during the Early Holocene, and probably continued to retreat until between 4,000 to 5,000 years B.P., at the time the outlet glaciers were in advance. The later retreat of the grounded ice margins indicates that they are less sensitive to the eustatic sea-level forcing. The glacial geological evidence suggests that the grounded ice margins and the alpine glaciers advanced during the Mid-Late Holocene, lagging the advance of the outlet glaciers. It is proposed that the fluctuation of the grounded ice margins and the alpine glaciers is primarily in response to increased accumulation due to the climate oscillations during the transition and the Holocene, and partly influenced by post-glacial isostatic uplift of the bedrock.

The relative contributions of the climatic and/or geophysical forcing of the glacial fluctuations during the Holocene are not known. The contributing variables are: (i) LGM maximum ice sheet thickness and the resulting total isostatic rebound amount; (ii) the timing of the isostatic rebound; (iii) the timing and amount of eustatic sea level rise during the Late Pleistocene-Early Holocene; and (iv) the Holocene surface mass balance pattern. The response of the outlet glaciers and ice sheet to these climate and geophysical forcings are examined in a sensitivity analysis in the next chapter.

CHAPTER 7
SENSITIVITY ANALYSIS OF THE RESPONSE OF THE OUTLET GLACIERS AND ICE SHEET MARGINS TO HOLOCENE CLIMATIC FORCINGS AND RELATIVE SEA LEVEL CHANGES

7.1 INTRODUCTION

Widespread geological evidence for Holocene fluctuations in the geographic position of the East Antarctic ice sheet margin and the terminus of major outlet glaciers was presented in the previous chapter. The outlet glaciers led the grounded ice sheet margins and the alpine glaciers both in the Early Holocene contraction and in the Mid-Late Holocene expansion. Here a sensitivity analysis is applied to the Lambert Glacier-Amery Ice Shelf system and the Law Dome ice cap to determine their possible responses to small climate fluctuations and to relative sea level changes produced by eustatic sea level rise and post-glacial isostatic uplift at the margins, during the Holocene.

7.2 LAMBERT GLACIER-AMERY ICE SHELF SYSTEM

7.2.1 ICE DRAINAGE CHARACTERISTICS

The Lambert Glacier is the largest ice stream in Antarctica and has a width of up to 50 km and a total length of 400 km from the grounding line of the Amery Ice Shelf to the southernmost limit of visible flowlines on Landsat Imagery (Allison, 1979). The Lambert Glacier is comprised of a number of confluent streams. The major secondary stream is the Mellor Glacier. The Lambert Glacier feeds into the Amery Ice Shelf forming the central lobe of the ice shelf and discharges ~2% of the total annual outflow from Antarctica. The total Lambert Glacier-Amery Ice Shelf drainage basin is the fourth largest in Antarctica (Giovinetto, 1964); forms a 600 km by 300 km depression in the East Antarctic ice sheet (Trail, 1964); and, can be delineated into three components: the interior basin; the Lambert Glacier; and, the Amery Ice Shelf. These components are shown in Figure 7.1 together with the major sub-basins. The system occupies a major rift valley known as the Lambert Graben extending from the coast to south of latitude 75° S (Wellman and Tingey, 1976). The Amery Ice Shelf is also fed by a number of tributary glaciers from MacRobertson Land and from Princess Elizabeth Land. This drainage pattern results in the three lobes of the ice shelf. The

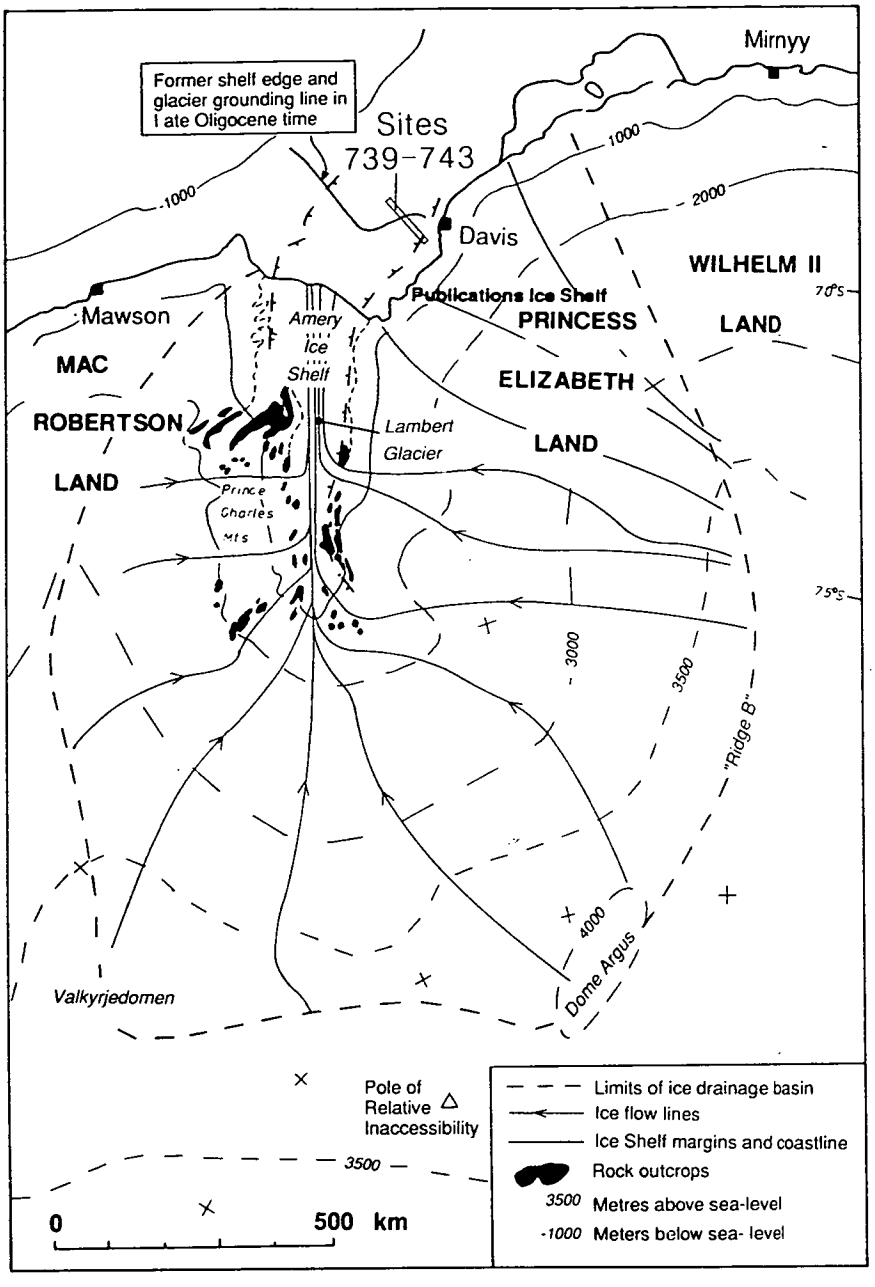

Figure 7.1 The Lambert Glacier-Amery Ice Shelf drainage basin and its ice flowlines (after Drewry, 1983). The sub-drainage basins are defined by these flowlines, together with the individual streams on the Amery Ice Shelf (after Hambrey, 1991). The ODP drilling sites are also shown in Prydz Bay.

western lobe is primarily fed by the Charybdis and Scylla Glaciers which drain the Northern Prince Charles Mountains and enter the ice shelf north of Beaver Lake and Jetty Peninsula, and the grounded ice sheet north of Single Island. The western lobe is relatively stagnant (Allison, 1989) when compared to the central and eastern lobes and discharges approximately 19% of the mass flux at 50-60 km from the ice shelf front (Budd et al., 1982 and Hambrey, 1991). The central lobe which comprises the Lambert, Mellor, and Fisher Glaciers, together with the ice streams from the Eastern Prince Charles Mountains (Hambrey, 1991) discharges approximately 55% of the total mass flux at 50-60 km from the ice shelf front (Budd et al., 1982 and Hambrey, 1991). The eastern lobe is fed by a large ice stream draining the Princess Elizabeth Land from east of the Mawson Escarpment and from the Grove Mountains, together with a second stream draining from Princess Elizabeth Land (in the vicinity of the Reinbolt Hills and Jennings Promontory) and entering the ice shelf to the east of Gillock Island, a major ice rise on the Amery Ice Shelf. The eastern lobe comprises 42% of the total ice shelf (Robertson, 1993) and approximately 26% of the mass flux at 50-60 km from the ice shelf front (Budd et al., 1982 and Hambrey, 1991).

The greater ice flux in the combined central and eastern lobes controls the growth of the ice shelf front towards the north-eastern sector of Prydz Bay and the location of ODP 740 drill hole. The Amery Ice Shelf front is subject to large iceberg calving events, the most recent of which was 11,000 km^2 area and occurred in late 1963 or early 1964 (see section 3.4.4) Budd (1967) and Swithinbank (1969). Robertson (1993) suggested that the periodicity of large calving events for the Amery Ice Shelf front was 60-70 years. Prior to 1963, early maps show that the Publications Ice Shelf which is fed by glaciers draining sections of Princess Elizabeth Land, was joined to the expanded Amery Ice Shelf front. This expanded ice shelf cover was within 100 km of the ODP 740 drill hole. The Amery Ice Shelf front position had re-advanced about 25 km between 1964-1992, as determined from Landsat imagery. The expanded ice shelf cover in Prydz Bay during 7,300 - 3,800 yr B.P. as interpreted by Domack et al. (1991) in ODP 740, would also have been fed by glaciers along the Ingrid Christensen Coast between Davis and the Publications Ice Shelf (Figure 5.1).

7.2.2 MORPHOLOGY OF THE AMERY ICE SHELF GROUNDING ZONE

The grounding zone of the Amery Ice Shelf was determined by ice radar sounding and GPS positioning during ANARE fieldwork in 1989-91 which was reported by Allison and Goodwin (1993). The free floating ice shelf is defined from the northern limit of the grounding zone and is shown in Figure 7.2.

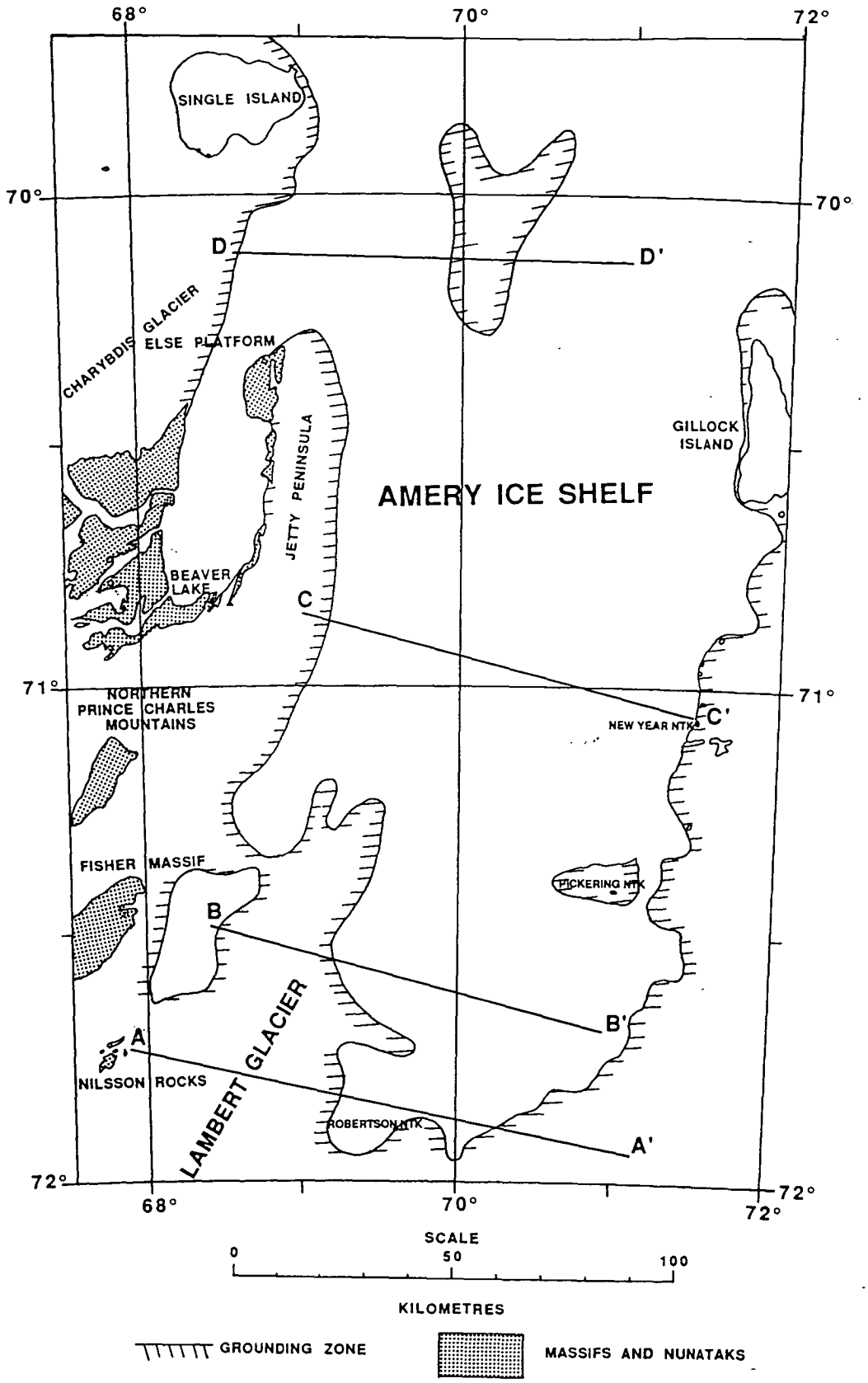

Figure 7.2 Map showing the location of the grounding zone of the Lambert Glacier-Amery Ice Shelf after Allison and Goodwin (1993). The grounding zone was determined by ground and aerial GPS position surveys and aerial ice radar sounding surveys during 1988/89 and 1989/90 austral summers.

Four transverse profiles of ice thickness were constructed across the Amery Ice Shelf from west to east. Profile AA' is located between Nilsson Rocks and Robertson Nunatak and is shown in Figure 7.3a. The ice in profile AA' is mainly grounded or near grounding at 700 m depth with a surface elevation of 100-110 m, giving a typical ice thickness of 800 m. The surface elevation falls from 120 m over the grounded ice to about 90 m over the floating ice shelf. Profile BB' is located between Fisher Massif and a point midway between Pickering Nunatak and Robertson Nunatak and is shown in Figure 7.3b. The ice in profile BB' is also grounded or near to grounding at 700 m depth with a typical ice thickness of 800 m. Profile CC' is located between Beaver Lake, Jetty Peninsula and New Year Nunatak which is along the 1964-70 ANARE stake route through G3 and is shown in Figure 7.4a. The ice is floating across the entire profile with a thickness ranging from 600-750 m. Profile DD' is located between south of Single Island to the northern tip of Gillock Island and is shown in Figure 7.4b. The ice is grounded in the centre of the ice shelf at 400-500 m depth for a distance of 15-20 km which increases in width to the north. This grounded area extends down the ice shelf for 45 km. The ice thickness to the east of the grounded area across to Gillock Island is typically 500 m. To the west of the grounded area the ice thickness increases to 800-900 m where the Charybdis Glacier enters the ice shelf between Jetty Peninsula and Single Island. The ice shelf remains floating from profile DD' to the present terminus. In summary, the major grounding zone of the Lambert Glacier-Amery Ice Shelf extends over a distance of 50 km between Fisher Massif and Robertson Nunatak. Recent work on the buoyancy of the lower Lambert Glacier has indicated that the glacier may be only partially grounded as far inland as Cumpston Massif, which is located a further 50 km inland (I. Allison, pers. comm., 1995). This location is close to the change in bed slope at 350 km in Figure 7.5.

7.2.3 SUBGLACIAL AND SEAFLOOR TOPOGRAPHY

A longitudinal profile of the subglacial and seafloor topography beneath the Lambert Glacier and Amery Ice Shelf, onto the inner continental shelf depression, (known as the Amery Depression) and then further onto the edge of the middle shelf bank, is shown in Figure 7.5. The profile commences beneath the Lambert Glacier at the southern edge of the Mawson Escarpment. Also shown is the ice surface elevation and ice thickness profile. The profile is constructed for a flowline along the Lambert Glacier stream and adjacent to the 'Mawson Escarpment' ice stream (Figure 7.1). This flowline approximates the probable trajectory of ice terminating in the vicinity of ODP 740 in Prydz Bay. The bedrock topography undulates between -700 m to -730 m in the vicinity of profiles AA' and BB' where the ice is grounded. No thinning occurs across the grounding line, but a few tens of kilometres downstream the ice

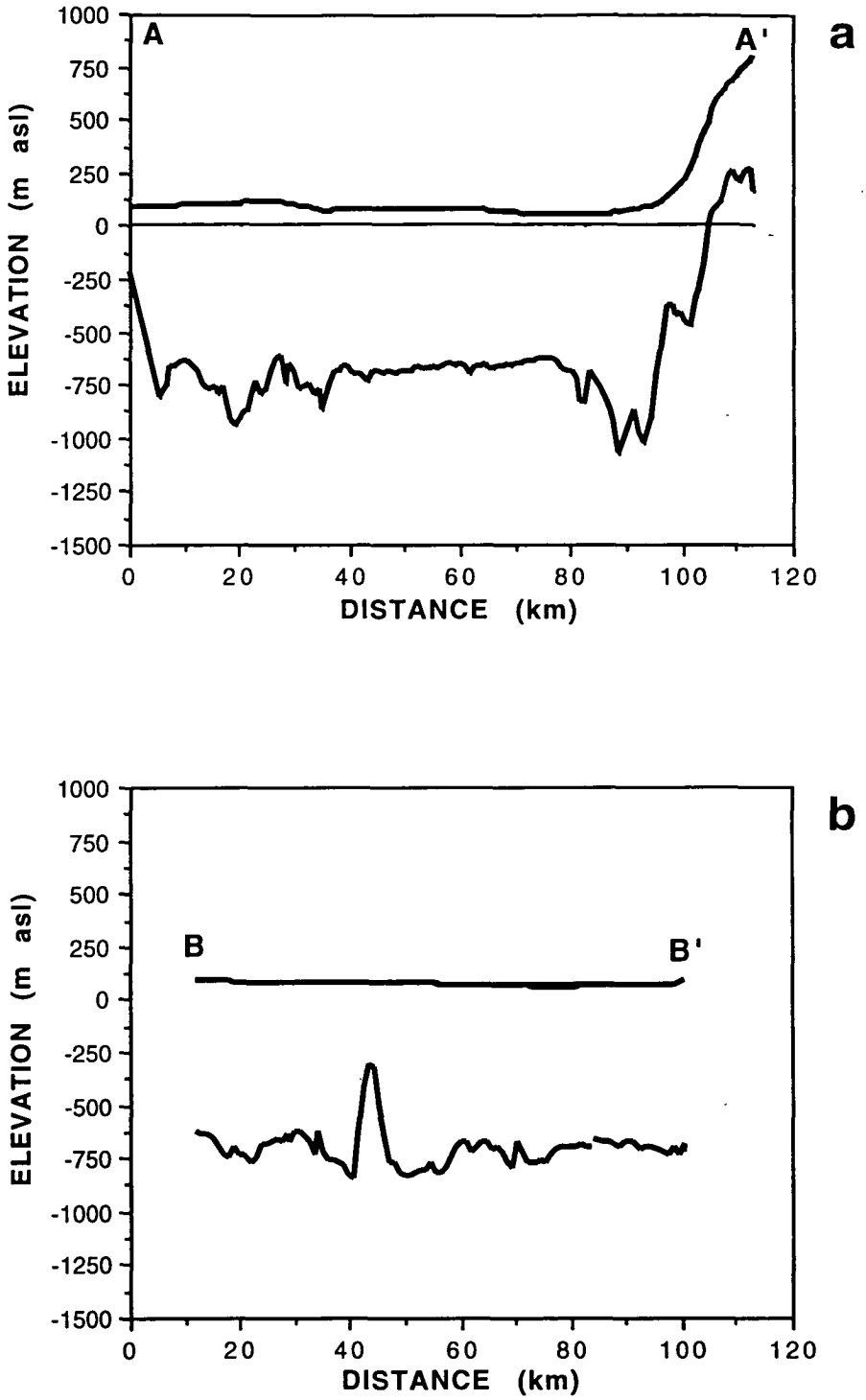

Figure 7.3 Southern Amery Ice Shelf profiles, showing the ice surface and ice base at (a) profile AA'; and (b) profile BB'. Note the ice shelf is floating between the distances 45 and 80 km in profile AA'. The ice shelf is floating between distances 35 to 40 km and between 75 to 100 km in profile BB'.

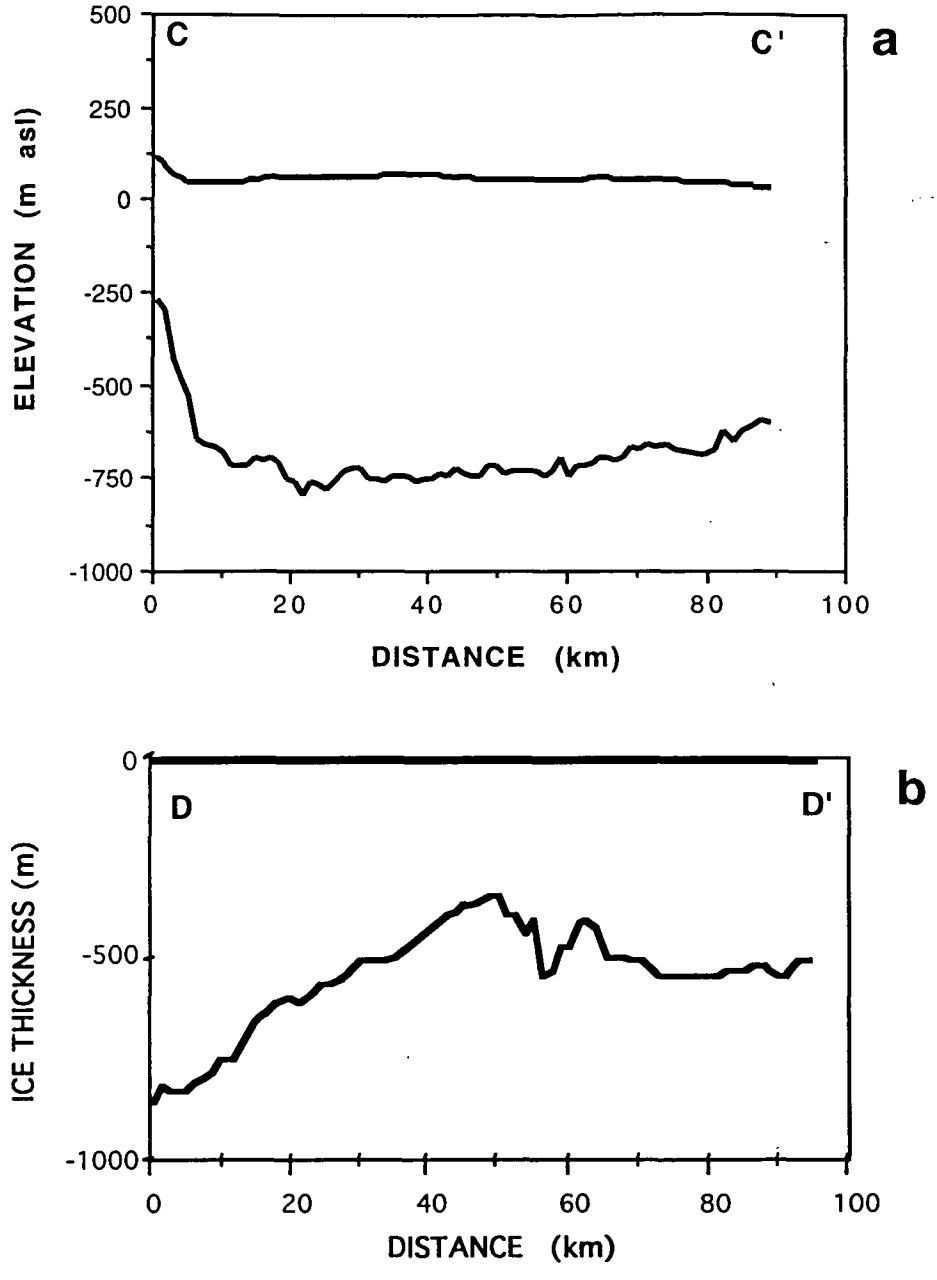

Figure 7.4 (a) Central Amery Ice Shelf profile CC' showing the ice surface and ice base. The ice shelf is floating across the profile except for between the distances 0 km to 10 km. (b) Ice thickness only profile at DD' showing that the ice shelf is grounded between the distances 40 km to 65 km. The surface elevation of the ice shelf across profile DD' is ~80 m (asl).

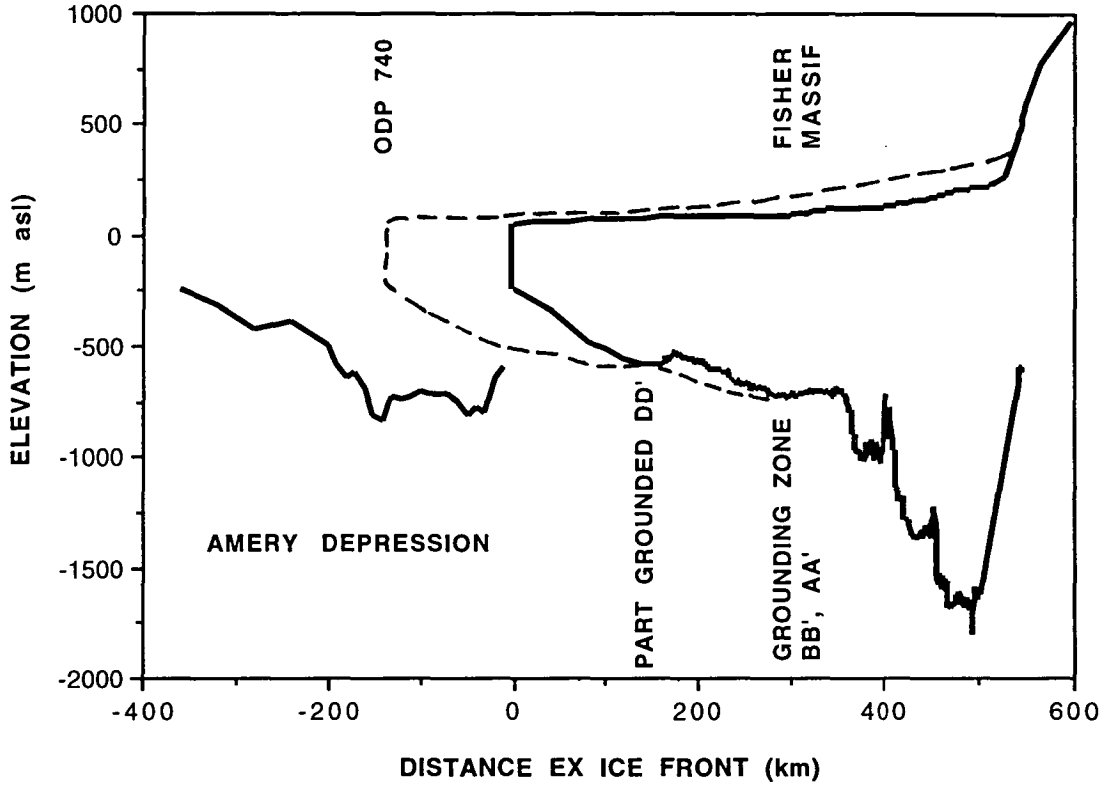

Figure 7.5 The present longitudinal profile (solid line) of the Lambert Glacier, ice surface and bed, together with the ice thickness profile of the Amery Ice Shelf and the sea floor topography in the Amery Depression on the inner continental shelf. The ice surface elevation and thickness data were measured by an ANARE aerial ice sounding program in 1988/89 and 1990/91. The data were reduced and analysed by the author and I. Allison. The reconstructed longitudinal profile (dashed line) of the Lambert Glacier-Amery Ice Shelf system represents the possible morphology during the Mid-Holocene in response to the proposed 150 km expansion of Domack et al. (1991). The reconstructed profile suggests that full grounding of the ice shelf would have occurred up to the location of cross-profile DD', if the system had advanced the full 150 km.

thins by about 50-70 m over a distance of 20-30 km. This thinning is probably due to a zone of basal melting as discussed by Budd et al. (1982) before the zone of basal freeze-on of seawater occurs further down the ice shelf (Hellmer and Jacobs, 1991). The elevation of the seafloor topography has not been determined between profiles BB' and DD'. As stated above, the high point in the bedrock topography at profile DD' is between -300 to -500 m depth. Since the elevation of the seafloor topography ranges from -600 to -700 m at the ice shelf front and there is no evidence for over deepening between profile DD' and the ice shelf front, it is likely that the seafloor topography undulates between -600 to -700 m depth between DD' and the ice shelf front. O'Brien (1994) investigated the sea floor morphology of Prydz Bay from interpretation of 3.5 kHz echo sounding data. He reported that an expansion of the eastern lobe of the Amery Ice Shelf would have flowed north-northeast into the Svenner Channel which is located within the Amery Depression to depths of 800-1000 m. The Svenner Channel in which the ODP 740 drill hole is located, does not cross the continental shelf and terminates within the Amery Depression (Figure 6.2). In contrast the western and much of the central lobes of the Amery Ice Shelf would have discharged ice via the northwest trending Prydz Trough which crosses the outer continental shelf. The Svenner Channel is elongate in a north-north easterly direction indicating that it was eroded by the expanded Lambert Glacier-Amery Ice Shelf system rather than northwesterly flow from the Ingrid Christensen Coast. O'Brien (1994) also concluded that the western side of the Amery Ice Shelf during the Late Pleistocene would have been decoupled from the bed earlier than the eastern side and that the greater grounding depth of the eastern side indicated a higher ice flux in the eastern half of the ice shelf which is consistent with measurements of the present configuration (Budd et al., 1982).

7.2.4 SENSITIVITY OF THE GROUNDING ZONE POSITION TO RELATIVE SEA LEVEL CHANGES DURING THE EARLY-MID HOLOCENE

Whilst the extent and thickness of the expanded and grounded Lambert Glacier-Amery Ice Shelf at LGM is not known, it is probable from the seafloor morphology and marine sediment distribution in Prydz Bay (O'Brien, 1994, and Hambrey 1991) that the system was grounded at least on the inner shelf. It is likely from the glacial geological evidence and weathering state (Mabin, 1992 and the author's observations in 1989) that the Beaver Lake and Jetty Peninsula area near the present grounding zonne was not overridden by the Lambert Glacier during the LGM. Consequently, LGM ice thicknesses would have been of the order of 800-1100 m thick, extending from the present ice shelf grounding zone to profile DD'. It is important to note when

discussing the timing and amount of isostatic uplift following the decoupling of the ice mass from the bed, that isostatic equilibrium may not have been reached and that depression may still have been occurring at the time of decoupling. Such an out of phase isostatic response may have occurred since decoupling was probably initiated by the eustatic sea level rise induced by the melting of the Northern Hemisphere ice sheets (Hollin, 1962). The post-glacial eustatic sea-level modelling of Nakada and Lambeck (1988) indicates that the decoupling of the Antarctic outlet glaciers including the Lambert Glacier, was underway by 13,000 yr B.P.. This is consistent with the 10,700 yr B.P. minimum date for open water conditions in Prydz Bay (Domack et al., 1991) and the 13,000 yr B.P. date for retreat underway in the western Ross Embayment (Denton et al., 1989).

The Amery Embayment between the location of profile DD' and the present grounding zone was partly filled by seawater following the decoupling and retreat of the Late Pleistocene grounding zone. Therefore, the isostatic uplift resulting from the decoupling of an 800-1100 m thick ice mass is calculated from the reduction of the maximum ice load (above sea level) at LGM to that at the point of floating, since the difference in density between seawater and ice is comparatively small. In the vicinity of profile DD' and Jetty Peninsula the height of the Late Pleistocene ice mass above sea level is restricted to <300 m, since it is unlikely that Jetty Peninsula was overridden. Similarly from the glacial geological observations of Mabin (1992) it is unlikely that the surface elevation of the Late Pleistocene Lambert Glacier was higher than 300-400 m above sea level. Thus the maximum isostatic uplift experienced by the Amery Embayment between profile DD' and the present grounding zone is 110 m, between the Early and Mid Holocene. Andrews (1970) showed that in the Arctic total post-glacial isostatic uplift is: 56% completed after 2,000 yr, 80% completed after 4,000 yr, 90% completed after 6,000 yr and 100% completed after 10,000 yr. Consequently, the range of partial isostatic uplift experienced beneath the Amery Ice Shelf in the location of profile DD' would have been: 67 m by: 11,000 yr B.P.; 88 m by 9,000 yr B.P.; 99 m by 7,000 yr B.P. and; 110 m by 4,000 yr B.P..

In the absence of a field derived, Antarctic relative sea level (RSL) curve for the Holocene, the contemporaneous eustatic sea-level changes were calculated from the Barbados eustatic sea-level curve (Fairbanks, 1989) shown in Figure 7.6. Regional differences in post-glacial eustatic sea-level changes occurred across the oceans due to the irregularities in the geoid, the distance from the meltwater sources, and the different meltwater loading isostatic responses of the continental margins and the oceanic islands. Therefore, the Barbados sea-level changes were compared to the equivalent changes in the southern Australasia region, closer to Antarctica. The most

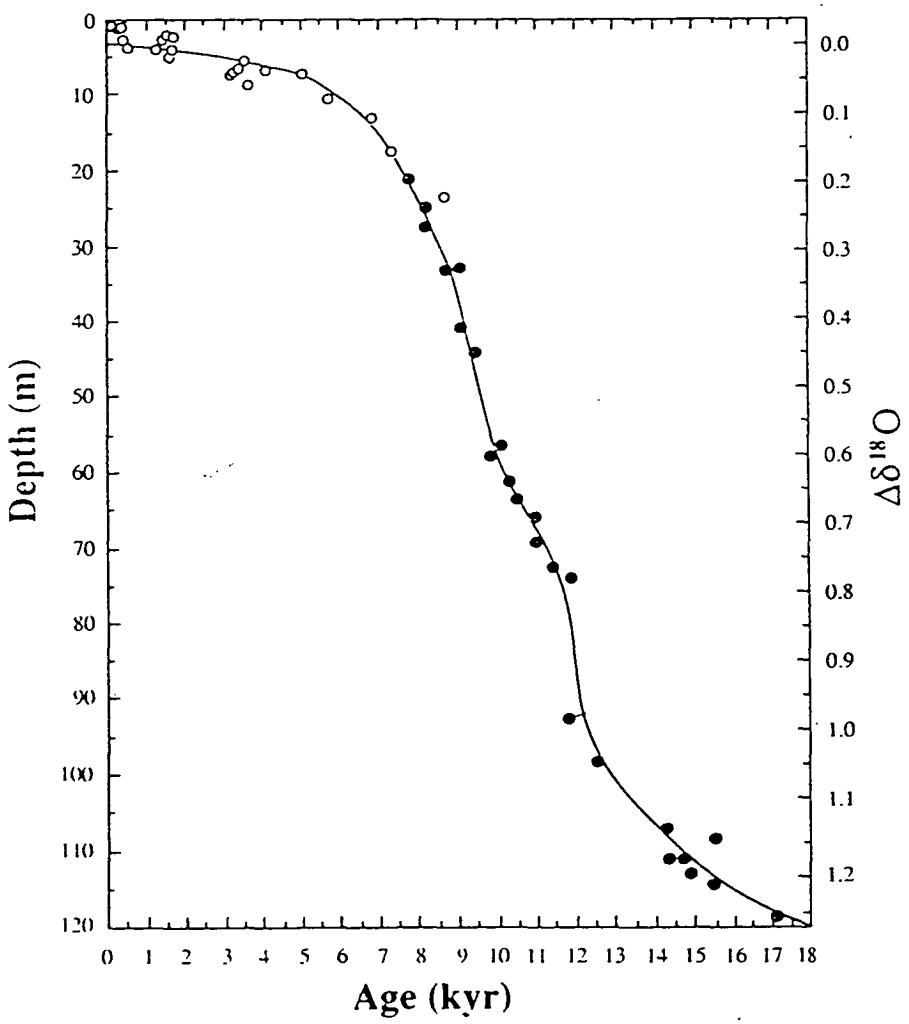

Figure 7.6 Barbados sea-level curve based on radiocarbon-dated (corrected) *Acropora palmata* (reef-crest coral) shown as solid circles, and compared with *A. palmata* age-depth data, shown as open circles for four other Caribbean Island locations (from Fairbanks, 1989).

suitable RSL curve for comparison is from the tectonically stable site at Moruya, NSW, Australia (Nakada and Lambeck, 1988), although this site is subject to the regional hydro-isostatic response of the continental shelf, after 6,000 yr B.P. (after Nakada and Lambeck, 1989). Between 18,000 and 13,000 yr B.P. sea-level generally rose by ~20 m. At Barbados the eustatic sea-level rose rapidly by: 30 m between 13,000 yr B.P. and 11,000 yr B.P.; a further 35 m between 11,000 yr B.P. and 9,000 yr B.P. and ; a further 20 m between 9,000-7,000 yr B.P.. In comparison, the relative sea-level at Moruya rose by 30m , 40 m and 25 m for the 13,000 yr B.P. and 11,000 yr B.P., 11,000 yr B.P. and 9,000 yr B.P., and the 9,000-7,000 yr B.P. respective periods. The regional differences in eustatic sea-level are consistent with the geophysical modelling predictions of Tushingham and Peltier (1991). Eustatic sea-level rose a further 8 m between 7,000 to 4,000 yr B.P., after which it is estimated that eustatic sea-level has been within ± 1m of the present sea-level. Table 7.1 shows the possible relative sea level changes experienced by the bedrock beneath the Amery Ice Shelf between 13,000 and 4,000 yr B.P. as a result of isostatic uplift being in phase with the eustatic sea-level rise.

TABLE 7.1 RELATIVE SEA-LEVEL CHANGES AT THE AMERY ICE SHELF WITH ISOSTATIC UPLIFT AND EUSTATIC RISE IN PHASE

EPOCH	ISOSTATIC UPLIFT	EUSTATIC RISE	RELATIVE SEA LEVEL
13,000-11,000 yr B.P.	67 m	30 m	37 m lowering
11,000-9,000 yr B.P.	21 m	35 m	14 m rise
9,000-7,000 yr B.P.	11 m	20 m	9 m rise
7,000-4,000 yr B.P.	11 m	8 m	3 m lowering
LIMITS (13-7,000 yr B.P.)	+/- 15 m	+/- 5 m	+/- 10 m

Table 7.1 shows that the bedrock beneath the contracted Amery Ice Shelf may have experienced a relative sea level lowering of the order of ~40 m during the Early Holocene. This would have resulted in a shallowing of the Amery Basin from depths of the order of 650-750 m to 610-710 m, close to the depths at the present grounding zone. The relative sea level changes since 9,000 yr B.P. are ~±10 m since both eustatic sea level and isostatic contributions are of a comparable amount. Therefore any decoupling of the bed due to a significant relative sea-level rise would have needed

to occur between 16,000 to 13,000 yr B.P. when sea-level rose by 20 m. However, this sea-level rise seems small in comparison to the ice thickness (~800-1100 m) to cause a catastrophic decoupling and rapid retreat. A more plausible explanation of the likely relative sea-level changes in the Amery Embayment, is that a delayed isostatic rebound of the crust probably followed the decoupling of the ice sheet prior to 11,000 years B. P.. The isostatic rebound may have been delayed due to a disequilibrium in the isostatic depression at LGM, with continued depression occurring during the period 16,000 to 13,000 years B.P.. If isostatic rebound was delayed by 2,000 years, commencing at 11,000 years B.P. instead, then the decoupling and retreat of the outlet glaciers would have occurred in response to a significant relative sea-level rise of 50 m between 18,000 and 11,000 yr B.P.. The relative sea-level contributions due to a delayed isostatic response of 2,000 yr are listed in Table 7.2.

TABLE 7.2 RELATIVE SEA-LEVEL CHANGES AT THE AMERY ICE SHELF WITH A DELAYED ISOSTATIC UPLIFT

EPOCH	ISOSTATIC UPLIFT	EUSTATIC RISE	RELATIVE SEA LEVEL
13,000-11,000 yr B.P.	0 m	30 m	30 m rise
11,000-9,000 yr B.P.	67 m	35 m	32 m lowering
9,000-7,000 yr B.P.	21 m	20 m	1 m lowering
7,000-4,000 yr B.P.	11 m	8 m	3 m lowering
4,000-1,000 yr B.P.	11 m	0 m	11 m lowering
LIMITS (13-7,000 yr B.P.)	+/- 15 m	+/- 5 m	+/- 10 m

A delayed isostatic rebound of the Amery Embayment is consistent with the geological evidence which suggests that the outlet glaciers had contracted to near their present extent by 11,000 yr B.P.. Such a rapid decoupling and contraction was probably completed during a period of rapid eustatic sea-level rise alone, before relative sea-level lowering commenced and slowed the rate of glacial contraction. Table 7.2 shows that between 11,000 to 7,000 yr B.P., a sea-level lowering of ~33 m occurred. This would have resulted in a slight shallowing of the Amery Embayment from depths of the order of 650-750 m to 620-720 m. An additional relative sea-level lowering of ~14 m would have occurred between 7,000 to 1,000 yr B.P..

An advance of the Amery Ice Shelf front by 150 km between 7,300 to 3,800 yr B.P. would also require a grounding zone advance of a similar distance, if the present surface and ice base profiles of the Lambert Glacier-Amery Ice Shelf system are maintained (Figure 7.5). Such an advance of the grounding zone would have resulted in a northerly shift of its location to near that of profile DD'. The dashed line in Figure 7.5 shows the present Lambert Glacier-Amery Ice Shelf profile re-configured for an advance of 150 km (after Domack et al., 1991) with the new grounding line located close to the position of profile DD'. The ice sheet would have been ~100 m thicker at the present grounding zone to maintain the present profiles. Since the present Amery Ice Shelf is only partially grounded or pinned in the centre of the profile at DD', then a thickening due to a mass balance excess is required to achieve a complete grounding at this location by 7,000 yr B.P. subsequent to an expansion of the ice shelf. The system probably contracted around 4,000 yr B.P. with an interpreted 150 km retreat of the grounding zone to near the present location. Therefore, the period of maximum sea-level lowering (33 m) between 11,000 to 7,000 yr B.P. was probably responsible for initiating a re-advance of the grounding zone, whilst a thickening due to a positive surface mass balance in the Lambert Glacier Basin and on the Amery Ice Shelf was required to sustain an expansion between 7,000 to 4,000 yr B.P. and a subsequent contraction. It is probable that the residual isostatic uplift from the LGM deglaciation was slightly offset during the Late Holocene by the subsequent isostatic depression in response to the ice loading between 7,000 to 4,000 yr B.P.. The interpreted glacial fluctuations of the Lambert Glacier-Amery Ice Shelf system during the Mid-Late Holocene suggest that the system is very sensitive to relative sea-level changes and/or ice sheet thickening on the order of 50-100 m close to the grounding zone. In fact the present grounding zone extends over a distance of ~100 km with only small changes in ice thickness of 80-100 m or less than 10% of the ice thickness. Therefore, it is critical in this discussion on the possible forcing mechanisms of a Mid Holocene advance, to determine the possible changes in surface mass balance in the interior basin and on the glacier during the Early to Mid Holocene.

7.2.5 SENSITIVITY OF THE GROUNDING ZONE POSITION TO INCREASED ACCUMULATION DURING THE EARLY HOLOCENE CLIMATIC OPTIMUM

The surface accumulation pattern of the Amery Ice Shelf, described more fully in section 3.5, decreases almost linearly from the ice shelf front (Budd et al., 1982). Thus the pattern shifts seawards as the ice shelf front expands and vice versa. The present accumulation pattern decreases from 500 kg m^{-2} a^{-1} at the shelf front to close

to 0 kg m^{-2} a^{-1} at 300 km inland from the shelf front, near the grounding zone. Net ablation occurs over the Lambert Glacier from the grounding zone to the edge of the interior basin, whilst the peaks and massifs such as Fisher Massif adjacent to the grounding zone experience net accumulation rates of 100-200 kg m^{-2} a^{-1} (Allison, 1979). The mass loss from surface melting on the Lambert Glacier is small since much of the meltwater is redistributed by surface streams to form lakes in the vicinity of the grounding line where they refreeze (Budd et al., 1967). Thus the net surface ablation occurs through evaporative losses (Allison, 1979).

It is likely that the entire Lambert Glacier basin received significantly increased precipitation during the period since 15,000 years B.P. as a result of the climate warming associated with the transition from the Last Glacial to the present Interglacial (Jouzel et al., 1989). However, it is probable that the Lambert Glacier-Amery Ice Shelf system received the highest precipitation rates during this period in the Early Holocene Climatic Optimum (EHCO). The post-glacial contraction of the northern extent of the ice shelf together with reduced sea ice extent (due to the climate warming) would have reduced the continentality of the whole Lambert Glacier Basin. Consequently, the entire basin would have experienced higher precipitation rates as a result of the increased temperature and open water in Prydz Bay during the EHCO. Also as a consequence of the climate warming, increased ablation on the surface of the Lambert Glacier and Amery Ice Shelf would have occurred together with increased basal melting at the grounding line. The following sensitivity analysis will concentrate on the effect of the mass balance changes during the EHCO on the mass budget of the Lambert Glacier-Amery Ice Shelf system.

To hindcast the mass balance of the Lambert Glacier system during the early Holocene it is necessary to define the present state of balance. It is important to note that the timing of the advance at 7,000 yr B.P. lagged the peak warming during the EHCO by at least 2,000 yr B.P. This is largely due to the dynamics of the system and the thickening rate, although the maximum relative sea level lowering by 7,000 yr B.P. is probably the most significant determinant of the triggering of the advance. In contrast the 3,000 year duration of the advance is largely determined by the duration of increased accumulation over the drainage basin. To determine ice sheet thickening forced by increased precipitation during the EHCO it is necessary to define the present mass budget of the system.

7.2.5.1 RECENT MASS BALANCE ESTIMATES

Bentley and Giovinetto (1992) reported the most recent mass balance estimates for the Lambert Glacier-Amery Ice Shelf system, based on the mass budget of Allison (1979) for the Lambert Glacier system and corrected for the best estimate of the drainage basin area as determined from the SPRI atlas (Drewry, 1983) by McIntyre (1985). Both Allison (1979) and McIntyre (1985) calculated a positive mass balance for the system although Allison (1979) had a much larger value of +42 Gt a^{-1} compared to the McIntyre (1985) value of +14 Gt a^{-1}. The difference between the two mass budgets was that McIntyre (1985) argued that a significant area of the interior basin was an area of net ablation characterised by bare ice fields on the basis of his interpretation of Landsat images. Allison et al. (1985) refuted this claim on the basis of identifying similar features on Landsat images in Wilkes Land which were winter wind glazed surfaces in a zone of significant net accumulation. Areas of bare ice have not been encountered by glaciologists on the 1990-94 ANARE oversnow traverses of the Lambert Glacier Basin, and they have found that the region disputed by McIntyre (1985) was instead, an area of net accumulation. Also the recent traverses have confirmed that the accumulation rates in the interior basin were not overestimated by Allison (1979) at an average of 55 kg m^{-2} a^{-1} (Higham, 1994). The components of the revised Allison (1979) mass balance are listed below in Table 7.3.

TABLE 7.3 THE PRESENT ESTIMATE OF MASS BALANCE FOR THE LAMBERT GLACIER SYSTEM after Allison (1979) and McIntyre (1985)*

	Interior drainage basin	Lambert Glacier system	Total drainage basin
Inflow (Gt a^{-1})	-	30	-
Gain in basin (Gt a^{-1})	50	-7 (-10)	43 (40)
Outflow (Gt a^{-1})	30	11	11
Budget (Gt a^{-1})	+20	+12 (+9)	+32 (+29)
Budget limits (Gt a^{-1})	+6, +34	-4.5, +28	+1.5, +62
Area (10^3 km^2)	902*	62	964
Mean annual surface change (ma^{-1} water)	+0.02	+0.19 (+0.15)	+0.03
Surface change limits (ma^{-1} water)	+0.007, +0.04	-0.07, +0.45	+0.002, +0.06

Allison (1979) estimated that mass loss due to evaporation on the Lambert Glacier was small on the order of 0.05-0.10 m water a^{-1} from ablation measurements made for a range of elevations near Mawson by Budd (1967). Allison (1979) estimated that this mass loss would be unlikely to exceed 0.15 m water a^{-1}. Thus the total mass loss was estimated as 5 Gt a^{-1} from the area of blue ice on the Lambert Glacier, whilst the remaining area was considered to be at zero net balance. A re-examination of the mass loss due to evaporation on the Lambert Glacier indicates that for elevations less than 250 m the annual ablation due to evaporation is about 0.26 to 0.3 m water a^{-1}. These ablation rates taken as mean rates would indicate that total mass loss due to evaporation over the blue ice areas of the Lambert Glacier is closer to 8.6 Gt a^{-1} (this revision is shown in brackets in Table 7.3). Mass loss from basal melting was estimated at 2 Gt a^{-1}. In conclusion Table 7.3 shows that a large positive mass balance of +29 to +32 Gt a^{-1} is occurring in the Lambert Glacier system which can be alternatively expressed as approximately +60% out of balance.

Budd et al. (1970) found that the Amery Ice Shelf was 100% out of balance since the calculated balance velocity was twice that of the measured velocities. Bentley and Giovinetto (1992) have also calculated that the whole Amery Ice Shelf system had a positive balance of +83 Gt a^{-1} or +86% out of balance from their assessment of the total outflow through the section between Depot E and Sandefjord Bay. Bentley and Giovinetto (1992) concluded that the system could only be reduced to balance if a bottom melt rate under the ice shelf of 1.5 m a^{-1} was occurring. However, Budd et al. (1982) estimated that to the contrary, bottom freezing at a rate of 0.7 m a^{-1} was presently occurring.

An appropriate explanation for the large positive balance in the system has not been made. Allison (1979) and Budd and McInnes (1978) have suggested that the Lambert Glacier has a high potential for surging and that the positive mass balance may indicate a post surge build-up. However, this view is no longer held (Allison, pers. comm, 1994) and Hambrey (1991) has pointed out from his analysis of glacier structure and foliation on Landsat imagery that there is no surface expression of surge type structures.

Recent studies using satellite radar altimeter data also support a positive mass balance. Lingle et al. (1994) reported that the lower Lambert Glacier in the vicinity of the grounding zone had experienced surface elevation increases of 20-80 mm a^{-1} during the decade from 1978 to 1987-89 from their orbit crossover analysis of Geosat Exact Repeat Mission (ERM) (1987-1989) and Seasat (1978) altimeter data. These surface

elevation increases are less than half of the estimated thickening calculated by Allison (1979). In a companion paper using the same altimeter data, Herzfeld et al. (1994) reported that the surface elevation increases were accompanied by an advance of the Lambert Glacier grounding line of 200-400 m a^{-1} during the same decade.

The large positive imbalance in the Lambert Glacier-Amery Ice Shelf system must be due to either increased accumulation rates over the interior basin or decreased outflow across the grounding line in the last few decades, or may be in response to the continuing post-glacial accumulation rate increase in the interior. It is unlikely that the positive imbalance is due to the latter, since the reaction time before a new equilibrium is reached at the head of the Lambert Glacier is of the order of 8,000 years since LGM (after Whillans, 1981). Such an interval would have been exceeded by the Mid Holocene. The accumulation measurements in the interior basin used by Allison (1979) were made between 1971-74 which agree with those measured during the recent campaign from 1991-94. The accumulation time series obtained from the firn cores at LGB00 and MGA in Kemp Land (shown in Figure 3.5) which are close to the north-western drainage sub-basin of the Amery Ice Shelf, indicate similar accumulation rates for these two epochs. These accumulation records also show that the accumulation rates were close to stable between 1940-1980 after which they decreased markedly, before increasing to the present. Figure 3.7 shows that the Amery Ice Shelf experienced accumulation rates approximately 100 kg m^{-2} a^{-1} higher for the decade 1959-68 than for the period 1969-91, which was probably in part due to a reduction in net ablation estimated as 50 kg m^{-2} a^{-1} in response to a decrease in the summer temperatures (interpreted from the Mawson temperature record, Figure 3.13). Thus the estimate of the accumulation over the interior basin used by Allison (1979) is probably close to the present long-term mean rather than being anomalously high.

This leaves the ice outflow regime as the likely source of the imbalance. If isostatic uplift has continued throughout the Late Holocene in the Lambert graben, then the resulting relative sea-level lowering would have caused a progressive pinning or local grounding of the Amery Ice Shelf. The local grounding depicted in Figure 7.4b for profile DD' may be such an example. As Thomas and Bentley (1978) pointed out for the Ross Ice Shelf, the progressive grounding or pinning of the ice shelf retards the rate of ice outflow across the grounding line which in turn causes thickening of the outlet glacier and an advance of the grounding zone. The thickening and advance of the present grounding zone, interpreted from the recent satellite imagery may support this sequence. The continued isostatic uplift could be due to the out of phase or delayed response to the LGM deglaciation and/or the result of the ice unloading following the Mid-Holocene expansion. However, the large positive imbalance could

also be due to the outflow still responding to the lower LGM accumulation rates in the basin (W. Budd pers. comm., 1994). If this was correct the present accumulation rates are at least twice those for the LGM. On the basis of the relative-sea level history discussed in the previous section it is more likely that the continued relative sea-level lowering due to post-glacial isostatic uplift has retarded ice outflow.

7.2.5.2 ESTIMATING THE MASS BUDGET DURING THE EHCO

The surface air temperature over the ice sheet and the circum-polar oceans was on average 1.0°C warmer during the EHCO (11,000-9,000 years B.P.) than that for the last century prior to 1970 and the recent fluctuations. The temperature record for the last century prior to 1970 is taken as equivalent to the long-term mean for the Holocene (Chapter 1). A mean accumulation increase of 20%/°C greater than the long-term mean is estimated for the 2,000 year period based on the relationships discussed in Chapter 3, and the palaeo-accumulation rates determined from the ^{10}Be measurements on the Vostok and Dome C ice cores (shown in Figure 6.10) by Raisbeck et al. (1987) and Jouzel et al. (1989) . Thus an average accumulation rate of 66 kg m^{-2} a^{-1} is estimated for the interior basin during the EHCO (increased from 55 kg m^{-2} a^{-1}).

The present spatial accumulation pattern in the Lambert Glacier Basin shows that the accumulation rates for a given elevation range are significantly higher below 1800 m in the eastern side of the basin in Princess Elizabeth Land than in the western side in MacRobertson and Kemp Lands. Above 1800 m the spatial patterns are roughly equivalent . This pattern is due to the general atmospheric circulation pattern and katabatic snow redistribution. With open water in Prydz Bay during the EHCO it is possible that the relative accumulation increase would have been even greater for the eastern side of the basin, because of the closer proximity to the moisture source. The eastern drainage basin feeds the eastern lobe of the Amery Ice Shelf. Robertson (1993) examined the pattern and mass budget of the Amery Ice Shelf front with respect to its fluctuations in size between 1936 and 1992 and concluded that the mass budget of the eastern lobe largely drives the mass budget of the total ice shelf front. Thus the ice streams entering from north of the Mawson Escarpment could have made a significant contribution to the excess mass required to thicken and advance the grounding line. It is difficult to test this theory since the present accumulation data from the eastern drainage basins only spans one year in comparison to the three year data for the southern and western drainage basins.

Whilst the advance is initiated by the partial grounding of the Amery Ice Shelf due to the relative sea level changes, the thickening and sustainment of the maximum extent of the advance (from 7,300 to 3,800 yr B.P.) is dependent on increased outflow due to excess accumulation in the interior basin during the Glacial-Interglacial Transition and the EHCO. The mean accumulation rate over the interior basin is equivalent to 0.07 ma^{-1} ice and from the mass budget of Allison (1979) is twice the accumulation rate required to balance the present outflow of 30 Gt a^{-1}. Consequently, the average balance accumulation rate ($\mathbf{b_s}$) for the 902 x 10^3 km^2 area of the basin is estimated as 0.03 ma^{-1}. The dynamic reaction time of an ice sheet to changes in accumulation rate from the steady state rate is also a function of the ice thickness and the flow law parameter as described in section 6.4.2 after Whillans (1981). The reaction time before the ice sheet or glacier achieves a 63% dynamical adjustment to the change in accumulation rate is determined using the following formula:

- $\mathbf{r = Z / (p + 2)\ b_s}$

where $\mathbf{Z}$ = 1200 m (mean ice thickness for the interior basin near the head of the Lambert Glacier is between 1500 m and 2000 m elevation), $\mathbf{p} = 3$, $\mathbf{b_s} = +0.03$ m a^{-1}. Thus the reaction time is calculated as ~11,000 years. In the deep interior of the basin the average ice thickness is ~2,500 m and the corresponding reaction is calculated as 17,000 years.

The estimated mean accumulation rate for the interior basin during the Glacial-Interglacial Transition (14,000 to 11,000 yr B.P.) is estimated to be ~25% less than the present values (Figure 6.8) according to Jouzel et al. (1989) and Ciais et al.(1992). This equates to an average accumulation rate of 0.045 ma^{-1} with an equivalent average surface level change ($\mathbf{b_1}$) of 0.015 ma^{-1} across the interior basin The estimated average accumulation rate for the interior basin during the EHCO is 0.072 ma^{-1} and hence the equivalent average rate of surface level change ($\mathbf{b_1}$) is 0.042 ma^{-1}. The maximum surface elevation rise over the interior basin is estimated from the following formula after Whillans (1981):

- $\mathbf{Z_1 = r b_1 (1 - \exp^{-t/r})}$

where $\mathbf{b_1}$ is the change in accumulation rate from the steady state rate, and $\mathbf{t}$ is the time duration of the accumulation rate change.

The corresponding surface elevation rises for the interior basin are 39 m and 169 m for the accumulation rate changes during the Glacial-Interglacial Transition and the

EHCO, after the respective time periods of 3,000 and 5,000 years. Both these periods were of a significantly shorter duration than the reaction time. Thus the total thickening during the period from 14,000 to 9,000 yr B.P. is estimated at ~156 m; that is ~10% of the present ice thickness between 1500 to 2000 m elevation contours.

Since the duration of the thickening is less than a half of the reaction time the thickening is not significantly affected by dynamical changes, and hence the ice sheet is considered only in static response. The outflow from the interior basin can be estimated for the thickened ice sheet interior as 10% greater than the total mass flux in Allison (1979). Hence, the total mass flux from the interior basin was estimated accordingly as 33 Gt a^{-1} at the end of the EHCO.

Whilst the interior basin was thickening during the peak warming of the EHCO, it is likely that the Amery Ice Shelf grounding zone was still retreating in response to the rapid post-glacial eustatic sea level rise. This has two implications for the mass budget of the whole system. Firstly, the retreat of the Amery Ice Shelf could have resulted in increased outflow from the Lambert Glacier system with faster ice velocities due to the reduction of the damming effect of the grounded ice shelf. Secondly, the retreat of the Amery Ice Shelf would have reduced the continentality of the interior basin leading perhaps to greater increases in precipitation in excess of the estimated 20% increased pattern. The thickening due to the increasing accumulation rates during the Glacial-Interglacial Transition is only significant in the interior basin since shorter reaction times on the glacier, ice shelf and the coastal margins would have resulted in the loss of the positive mass through dynamical adjustments during the Early Holocene. Table 7.4 lists the mass budget components for the response of the total system to the mean estimated accumulation rate increase at the end of the EHCO.

The mean ablation rates on the blue ice area were determined as up to 0.07 m of water a^{-1} (63 kg m^{-2} a^{-1}) higher than the present rates (26 to 0.30 m a^{-1}) in response to the 1°C change in mean annual temperature (after Budd, 1967). A corresponding regional increase of 20% in the Amery Ice Shelf accumulation rates during the EHCO may have reduced the net ablation zone by extending the net accumulation zone 80-100 km further inland than the present if the present decreasing linear pattern with distance from the ice shelf front applied. The present mean accumulation rate over the 80-100 km zone seaward of the grounding zone is close to 75 kg m^{-2} a^{-1} (from Figure 3.7).

TABLE 7.4 THE ESTIMATE OF MASS BALANCE FOR THE LAMBERT GLACIER SYSTEM AT 9,000 YR B.P. IN RESPONSE TO INCREASED ACCUMULATION AND A 1°C WARMING (after the present revised mass budget based on Allison (1979))

	Interior drainage basin	Lambert Glacier system	Total drainage basin
Inflow (Gt a^{-1})	-	33	-
Gain in basin (Gt a^{-1})	60	-12	48
Outflow (Gt a^{-1})	33	11	11
Budget (Gt a^{-1})	+27	+10	+37
Budget limits (Gt a^{-1})	+4, +76	-6, +26	+4, +84
Area (10^3 km^2)	902	62	964
Mean annual surface change (ma^{-1} water)	+0.03	+0.16	+0.04
Surface change limits (ma^{-1} water)	+0.004, +0.084	-0.10, +0.42	+0.004, +0.087

Therefore the increase in accumulation rate at the grounding zone is balanced by the increase in ablation rates, and the ablation area is estimated as the same as the present. Accordingly, the total mass loss due to evaporation was estimated as -11.6 Gt a^{-1} to account for the higher ablation rates over the present area of the Lambert Glacier. The estimate of the present outflow from the lower Lambert Glacier has been applied, since no net change in thickness probably occurred at the grounding zone by 9,000 years B.P., near the end of the EHCO.

Thus the mass budget estimate for the interior basin increases to +27 Gt a^{-1} due to the increased accumulation during the EHCO, and the mass budget estimate for the Lambert Glacier increases marginally to +10 Gt a^{-1} due to the increased inflow from the interior basin. Whilst the mass budget shows an average rate of +0.16 m a^{-1} surface level change for the Lambert Glacier system the thickening takes a further 1,600 years to propagate 400 km down the glacier to the grounding line at the present velocity of 200 m a^{-1}. Thus at 9,000 yr B.P. the actual rate of surface level change on the lower Lambert Glacier near the grounding line would be nearer the lower limit at -0.07 ma^{-1} due to the higher ablation rates. Accumulation measurements made near the grounding line from 1988-90 show that ablation rates are between -0.11 to -0.06

ma^{-1}. Assuming that these rates are close to those required for balance, the reaction time at the grounding line can be calculated as follows;

- $\mathbf{r = Z / (p + 2)\ b_s}$

where $\mathbf{Z}$ = 850 m, mean ice thickness on the lower Lambert Glacier , $\mathbf{p}$ = 3, $\mathbf{b_s}$ = -0.06 m, the steady state accumulation rate. The reaction time is calculated as 2,830 years, an interval after which the glacier is 63% adjusted to the surface level change.

Following the EHCO mean annual temperatures were on average 0.4°C cooler than the long-term Holocene mean during the period between 8,000 to 6,000 B.P. (Mid Holocene Cool Phase) (after Ciais et al, 1992). Hence, ablation rates would have decreased on the lower Lambert Glacier by up to 0.03 ma^{-1} (after Budd, 1967) between 8,000 to 6,000 yr B.P. resulting in a state of net balance at the grounding line. The sustained decrease in ablation rates over the 2,000 year period would result in a thickening at the grounding line equivalent to ~45 m. The present velocity field is characterised by velocities of 50-100 m a^{-1} at the 2000 m contour, which increase to 250 m a^{-1} about 100 km downstream in the upper Lambert Glacier, increasing to 350 m a^{-1} near the grounding line. At a mean velocity of 200 ma^{-1} the ~100 m thickening in the interior basin would propagate down-glacier to the present grounding zone in 2,000 years and to the proposed Mid-Holocene grounding line some 500 km further down-glacier, in a total time of approximately 2,500 years or by 6,500 years B.P.. Alternatively, a thickening on the order of 100 m in the vicinity of Fisher Massif would be transported downstream to the new grounding line near profile DD' in less than 500 years.

With a thickening of ~100 m propagating down the glacier from a mass excess in the interior basin and the synchronous 45 m thickening on the lower Lambert Glacier, the grounding zone would have thickened up to ~150 m by 6,000 yr B.P.. This is equivalent to an 18% increase in total mass outflow from the Lambert Glacier system or an additional 2 Gt a^{-1} greater than the present outflow.. This thickening rate is comparable to that determined for the 1978-1989 decade by satellite altimetry analyses which is coupled to an advance of the grounding line at a rate of 200-400 m a^{-1} (Herzfeld et al., 1994). The timing of this thickening at the grounding zone is synchronous with the interpreted Mid Holocene expansion of the Lambert Glacier-Amery Ice Shelf system by Domack et al. (1991).

The geomorphological constraints on thickening in the vicinity of the present grounding line are the upper elevation limit for the most recent moraine sequence at the base of Fisher Massif at 200 m above the present glacier surface, and that 100 km downstream, the Amery ice did not overrun Else Platform. This constrains the ice thickening to about 150 m above the present surface in this locality. The latter constraint implies that the grounding line advance did not extend much further than the locality of profile DD' in Figure 7.5. A minimum thickening of 100 m at the present grounding line is required to achieve total grounding at profile DD'. This is in accordance with the mass budget estimates. A thickening at the present grounding line would be transported at the present velocity of 300 m a^{-1} to the location of profile DD' in 500 years, assuming a static response. Thus by 7,000 years B.P. total grounding of the Amery Ice Shelf at profile DD' is plausible from the combination of glacier thickening due to climate forcing and to relative sea level lowering.

The reaction time of the Lambert Glacier to the thickening is estimated as less than 3,000 years. The impact of the penetration of temperature change itself in initiating increased outflow is minimal since the basal temperature is already at the melting point and sliding accounts for the majority of the velocity. Consequently, it is likely from the model of Whillans (1981) that dynamical adjustments would be in response to the thickening alone, resulting in slightly increased outflow through the Lambert Glacier after an interval close to the reaction time, or by 5,000 to 4,000 yr B.P.. Further, if glacier movement is predominantly from sliding at the bed, then an increased thickness can cause a retardation of flow, which causes a positive feedback and leads to greater thickening (W. Budd, Antarctic CRC, pers. comm. 1995).

The subsequent retreat of the grounding line, probably commencing as early as 5,000 years B.P. would also have been forced by decreased accumulation rates (~10%) over the interior basin due to the average temperature decrease of 0.4°C between 8,000-6,000 years B.P.. The advance of the ice shelf front between 7,300 to 3,800 years B.P. would also have created a larger ablation area on the lower Lambert Glacier by displacing the ice shelf accumulation profile seawards. This may have resulted in widespread thinning on the lower Lambert Glacier, despite lower ablation rates during this period. The thinning could have led to a decoupling of the grounding zone and subsequent grounding zone retreat towards the location of the present grounding zone. The thinning of the lower Lambert Glacier and the grounding zone retreat would have been maintained by the decreased outflow from the interior basin.

The timing of the retreat of the expanded Amery Ice Shelf is also coincident with the second climatic optimum (SCO) between 4,300 to 3,000 years B.P. (after Ciais et al.,

1992). This warm period was on average 0.4°C above the long-term Holocene mean. The Amery Ice Shelf would have received up to 10% increased precipitation in association with the warmer temperatures during this period (based on the changes observed over the last 30 years in Chapter 3). However, the precipitation increase may have been minimal in the interior basin due to the increased continentality caused by the expanded ice shelf during this period. Hence there is neither the glaciological nor the geological evidence for a later readvance of the Lambert Glacier-Amery Ice Shelf system. However, the alpine glaciers, especially on Fisher Massif, appear to have advanced since 4,000 years B.P. as their termini have eroded the Lambert Glacier lateral moraines (Mabin, 1992) which has been attributed to the Mid Holocene expansion in this study.

7.2.5.3 CONCLUSIONS

It has been demonstrated that the Mid-Holocene advance of the Lambert Glacier-Amery Ice Shelf system was probably grounded in the vicinity of Profile DD' (Figure 7.4b) which is located between Single Island and Gillock Island. Relative sea level lowering by 7,000 years would have enabled partial grounding of the ice shelf similar to the present configuration. However, thickening of the Lambert Glacier on the order of 100 m due to increased accumulation rates over the interior drainage basin during the EHCO (11,000-9,000 yr B.P.) and to a lesser extent the Glacial-Interglacial Transition (14,000-11,000 yr B.P.), together with a reduction in ablation rates on the lower Lambert Glacier during the Mid Holocene Cool Phase (8,000-6,000 yr B.P.), was probably responsible for forcing the complete grounding of the system at this location. The propagation of the thickened ice mass from the interior basin down-glacier over the 4,000 yr period since the end of the EHCO at 9,000 yr B.P., maintained the advance from 7,000 to 4,000 yr B.P.. The total outflow from the system was estimated as 1.5 Gt a^{-1} greater than the present estimates. A thinning of the glacier caused by dynamical adjustments and a reduced accumulation input during the MHCP were the likely causes of the subsequent retreat of the grounding line to the present position. The later and most recent advance of the Fisher Massif cirque glaciers which have eroded the Lambert Glacier moraines is probably the result of increased accumulation during the Holocene but particularly the Late Holocene (during the SCO and the LCO) in response to the reduced continentality of this area due to the retreat of the Amery Ice Shelf front. The present positive imbalance of the Lambert Glacier-Amery Ice Shelf system is possibly due to decreased or obstructed ice outflow across the grounding zone due to progressive local grounding of the Amery Ice Shelf. The latter may be controlled by the isostatic uplift and relative sea-level lowering in response to the ice unloading from the Mid-Holocene expansion.

7.3 LAW DOME ICE CAP

7.3.1 ACCUMULATION RATE DISTRIBUTION AND ICE DRAINAGE CHARACTERISTICS

Law Dome is an independent ice cap (Figure 7.7) separated from the ice flow of the main East Antarctic ice sheet by an arcuate rift valley at the base of its southern flanks . The large Totten and Vanderford outlet glaciers, which occupy the rift valley, discharge significant quantities of ice from the interior Wilkes Land drainage basin (Young et al., 1989a). The accumulation pattern over Law Dome (Figure 7.7) is strongly controlled by topography with an extreme gradient in annual accumulation from east to west (Budd, 1970). For example the accumulation rate at 500 m on the eastern coast is 1600 kg m^{-2} a^{-1} whilst at the same elevation on the western coast the accumulation rate is approximately 100 kg m^{-2} a^{-1}. The east-west gradient across the Law Dome summit area decreases from 800 to 400 kg m^{-2} a^{-1} in 40 km (unpublished ANARE field data, N. Young pers. comm., 1994). The velocities and ice outflow are proportionally higher in the eastern half of Law Dome (Figure 7.7). The present surface ice velocities up to 60 km from the Windmill Islands margin, in the western hemisphere are also shown in more detail in Figure 7.8.

As described in Chapters 4 and 5 the Windmill Islands are located at the north-western margin of the Law Dome where the present ice movement is extremely slow at less than 2 m a^{-1} up to 20 km inland of the margin. Thus the majority of the present ice discharge is divergent to the north and south of the islands. The ice drainage pattern on Law Dome also reflects the east-west rising gradient in bedrock elevation. The characteristic surface and bedrock profiles of the east and west hemispheres of Law Dome are shown in Figure 7.9. The bedrock is at or above sea level along the western margin, rising to the Windmill Islands and Balaena Islets exposure. The bedrock along the eastern margin is 250 m below sea level. There is a marked difference in the surface profiles between Dome Summit to Caper Folger and Dome Summit to Cape Poinsett which reflects the bed slope and flow regime. The former has a close to uniformly sloping profile whilst the latter has a strong convex profile.

Table 7.5 lists the comparative ice sheet physical characteristics for locations in the western and eastern hemispheres of Law Dome at distances up to 60 km from the Løken Moraines and the ice margin, together with DSS (Dome Summit).

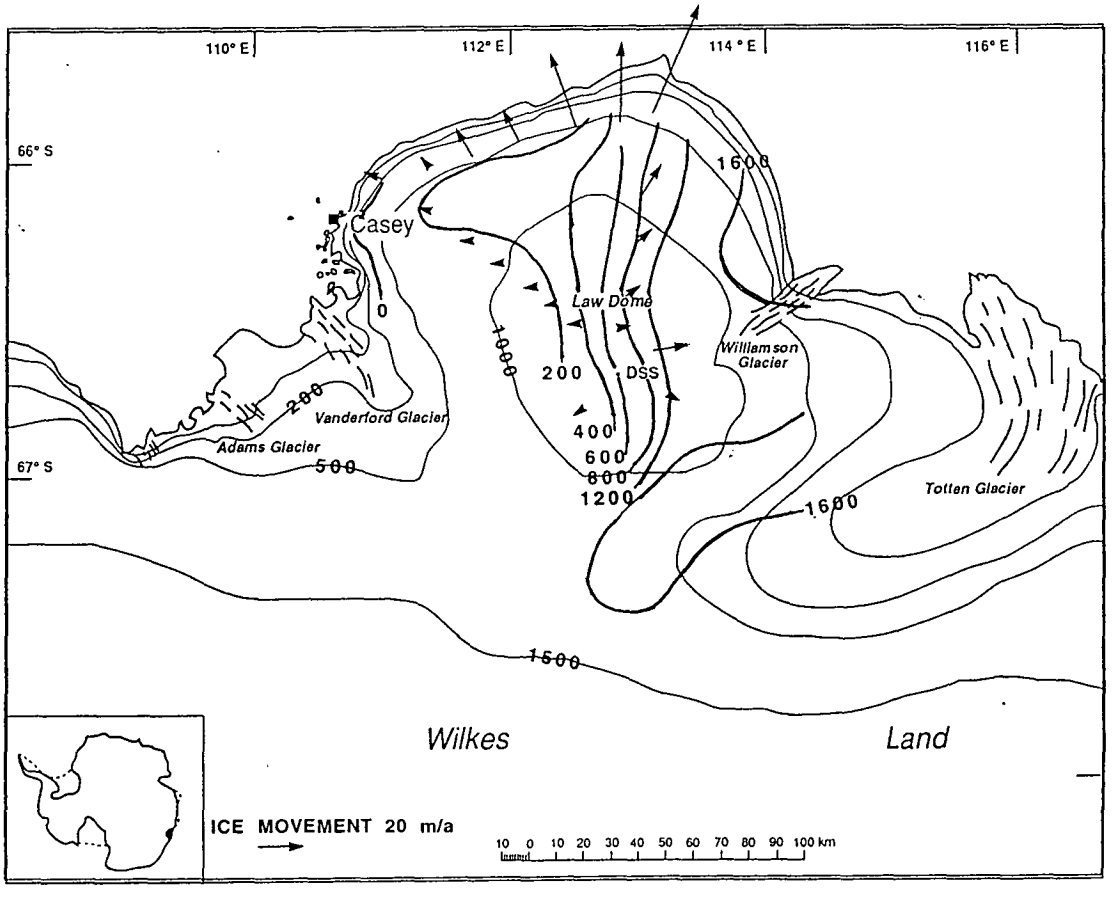

Figure 7.7 Map of Law Dome showing the topography, accumulation rate isopleths (kg m^{-2} a^{-1}) denoted by the bold lines, and the distribution of ice velocity. Note the faster velocities in the eastern hemisphere.

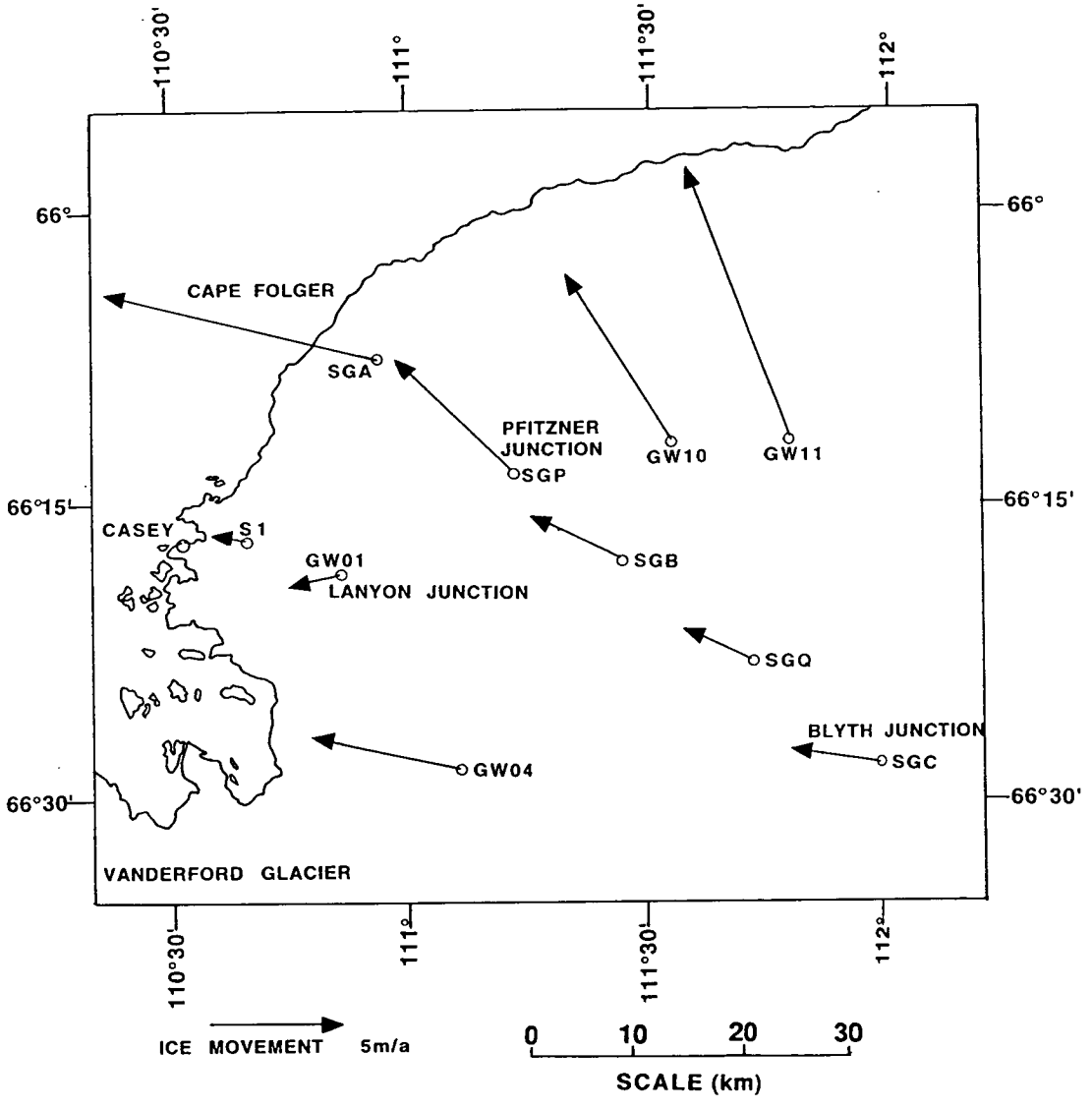

Figure 7.8 Map showing the present (1982-87) surface ice velocities for locations in the western hemisphere of Law Dome at distances up to 60 km from the coast and the Windmill Islands margin (Young et al., 1989). Note the significant reduction in ice velocity from 6.1 ma^{-1} at SGP and 5.3 ma^{-1} at GW04 to 1.7 ma^{-1} at GW01 inland of the Løken Moraines. Note also that the velocities are slower by up to 2 orders of magnitude than that for the outlet glaciers such as the Lambert Glacier-Amery Ice Shelf system.

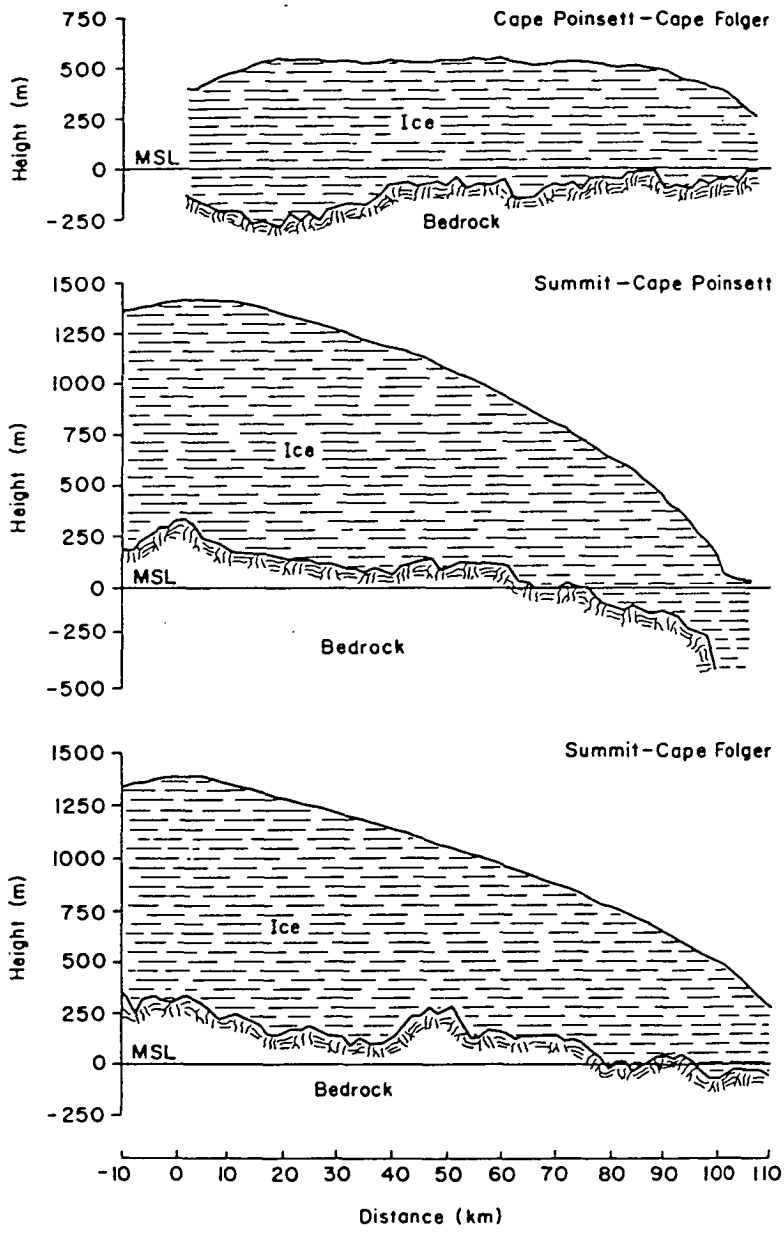

Figure 7.9 Ice surface and bedrock elevation profiles for the eastern and western hemispheres of Law Dome (after Pfitzner, 1980).

TABLE 7.5 LAW DOME PHYSICAL CHARACTERISTICS

Site	Distance ex margin km	Surface elevation m	Ice thickness m	Bedrock elevation m	Acc m a^{-1} snow	Surface velocity m a^{-1}
Western						
S1	4	263	220	43	0.08	1.5
SGA	5	282	322	-40	0.15	10.6
GW01	14	470	370	100	0.18	1.7
SGP	20	610	556	54	0.48	6.1
SGB	33	779	753	26	0.28	3.8
SGQ	49	952	815	137	0.46	2.9
SGC	65	1068	818	258	0.37	3.5
DSS	110	1370	1054	316	1.33	~0
Eastern						
SGJ	20	386	514	-128	1.86	34
SGH	40	788	793	-5	1.90	20
SGG	75	1172	1091	81	1.87	7.5

7.3.2 SENSITIVITY OF THE POSITION OF THE LAW DOME ICE MARGIN TO RELATIVE SEA LEVEL CHANGES DURING THE HOLOCENE

The Holocene glacial history of the Law Dome margin and Windmill Islands was presented in Chapters 4 and 5. In summary, the outer and southern Windmill Islands were deglaciated by 8,000 yr B.P., whilst the coasts of the inner and northern Windmill Islands were deglaciated before 5,500 yr B.P. (Goodwin, 1993). The ice margin retreated to a position further inland than the present position between 5,500-4,000 years. This retreat exposed a larger area of the Clark, Bailey and Mitchell Peninsulas than at present. Since 4,000 yr B.P. an advance of the Law Dome ice margin has occurred. The ice margin has progressively thickened to at least its present configuration between 4,000 to 1,500 yr B.P.. It is likely that a second wave of thickening occurred, producing the outermost ridge of the Løken Moraines in the last 1,500 years.

Therefore, the maximum ice free exposure that the Windmill Islands experienced was between 6,000 and 4,000 yr B.P.. The sensitivity of the Law Dome ice margin to

relative sea-level changes was determined for this period, prior to the readvance. Assuming that significant deglaciation of the grounded ice over the Windmill Islands had begun by 10,000 yr B.P., then at 6,000 yr B.P. and 4,000 yr B.P. approximately 80% and 91% of isostatic uplift would have been completed, assuming that isostatic uplift was not delayed due to disequilibrium (Andrews, 1970). This is consistent with the observed 30 m of isostatic uplift occurring between ~6-8,000 yr B.P. and the present, which is equivalent to 23% of the total estimated uplift. The total maximum ice thickness was estimated as 468 m (Chapter 4) which corresponds to a total isostatic uplift of 128 m after a 10,000 year period. Therefore the isostatic uplift completed by 6,000 years B.P. was 102 m and 116 m by 4,000 years B.P.. By 1,000 years B.P. 97% of the total uplift would have occurred. These estimates include the 3-4 m of postulated emergence since 5,000 years B.P. due to crustal tilting (Clark and Lingle, 1978).

Alternatively, if the isostatic uplift was delayed with respect to the deglaciation of the grounded ice margins similar to that interpreted for the outlet glaciers then the isostatic uplift would have occurred until the present. Consequently the above estimate of the LGM ice sheet thickness over the Windmill Islands would be a minimum value. However, it is likely that the isostatic uplift was in phase with the deglaciation since the rate of retreat of the grounded ice margins was significantly slower than for the outlet glaciers. This is supported by the small difference of 2-3 m in the elevation of the marine limit between the northern Windmill Islands and the southern Windmill Islands, adjacent to the Vanderford Glacier.

The corresponding eustatic sea -level changes were determined from the Barbados sea-level curve (Fairbanks, 1989) which is shown in Figure 7.6. and were compared to the equivalent sea-level changes at the tectonically stable site at Moruya, NSW, Australia (after Nakada and Lambeck, 1988), according to the methods discussed in section 7.2.4. The estimated eustatic sea-level rise between 10,000 and 6,000 years B.P. was estimated as 47 m. Between 6,000 to 4,000 yr B.P. a further 2 m of eustatic sea-level rise occurred. By 4,000 yr B.P. sea-level was within ± 1 m of the present level. In comparison, a rate of relative sea-level change of +5-6 m/1000 years was interpreted from the raised beach study (Chapter 4) between 6,000 years B.P. to present.

Table 7.6 shows the relative sea level changes experienced at the Law Dome ice margin and the Windmill Islands between 10,000 and 1,000 yr B.P.. The limits were estimated from the uncertainties in the ice sheet thickness and the timing of the eustatic sea-level rise.

TABLE 7.6 RELATIVE SEA-LEVEL ESTIMATES FOR THE LAW DOME ICE MARGIN

Epoch	Isostatic uplift	Eustatic rise	Relative sea-level
10,000-6,000 yr B.P.	102 +/- 10 m	47 +/- 4 m	55 m lowering
6,000-4,000 yr B.P.	14 m +/- 5 m	2 +/- 1 m	12 m lowering
4,000-1,000 yr B.P.	8 m +/- 3 m	0 m +/- 1 m	8 m lowering

These estimates of relative sea-level lowering at the Law Dome ice margin are small compared to the changes estimated for the Amery Embayment and the Lambert Glacier Basin. Since 4,000 years B.P. the relative sea-level has lowered ~8-10 m or ~5% of the ice thickness at the margin, contemporaneous with the postulated re-advance. Figure 7.10 shows the surface and bedrock topography along a flowline inland of Bailey Peninsula. Note that the bedrock topography is almost entirely above sea level for 30 km inland of the margin, and that the bedrock slopes upwards to the margin over the last 10-15 km. Flow obstruction due to the latter is likely to be in part responsible for the very slow surface velocities (<2 m a^{-1}) at 10-15 km from the margin. The relative sea-level lowering of approximately 30 m since ~8,000 years B.P. has resulted in a corresponding reduction in surface velocity inland of the margin possibly of the order of 5 m a^{-1} to 2 m a^{-1}.

In addition, the relative lowering of 30 m has resulted in an emergence of parts of the Clark, Bailey and Mitchell Peninsulas. A thin superimposed ice cover has formed over these peninsulas since 4,000 years B.P., creating a more extensive proglacial area. Therefore the emergence of the peninsulas has contributed to the expansion of the Law Dome ice margin. However, the accumulation of the superimposed ice cannot account for the significant thickening and dynamic advance of the Law Dome ice margin. Hence, a thickening of the margin would have been forced by a positive surface mass balance on Law Dome prior to the late Holocene advance. A reduction in ice outflow probably contributed to the thickening as the velocities were progressively decelerated by the relative sea level lowering during the Late Holocene.

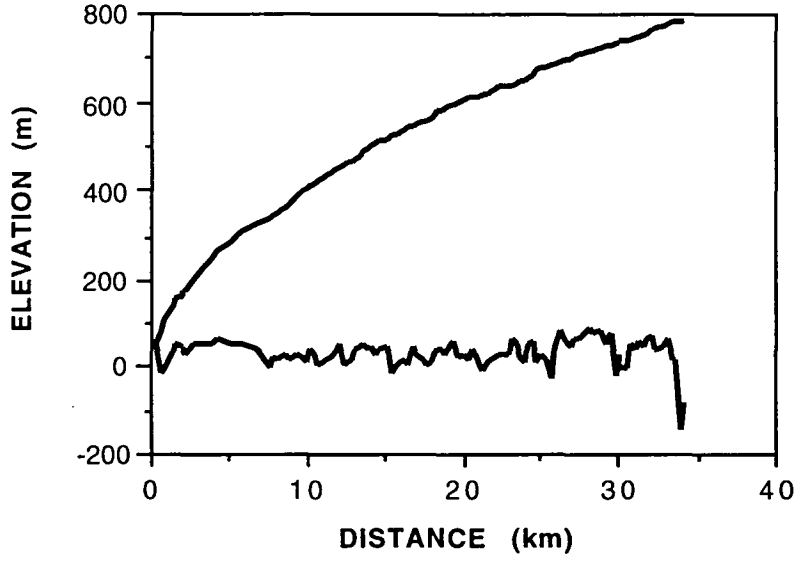

Figure 7.10 Ice surface elevation and bedrock elevation profiles of Law Dome, inland of the Bailey Peninsula. The profiles were measured by optical levelling surveys and ice radar sounding by ANARE during the 1970's. (Unpublished ANARE glaciological data, held by N. W. Young, Antarctic CRC).

7.3.3 SENSITIVITY OF THE POSITION OF THE LAW DOME ICE MARGIN TO SURFACE MASS BALANCE CHANGES DURING THE HOLOCENE

The advance of the Law Dome ice margin and the formation of the Løken Moraines was interpreted to have occurred between 4,000 to 2,000 years B.P. (Chapter 5). Thus the advance was occurring some 4,000-6,000 years after the end of the EHCO (11,000-9,000 years B.P.). The modelled particle paths and isochrones for the Law Dome Summit to Cape Folger profile are shown in Figure 7.11 (after Pfitzner, 1980).

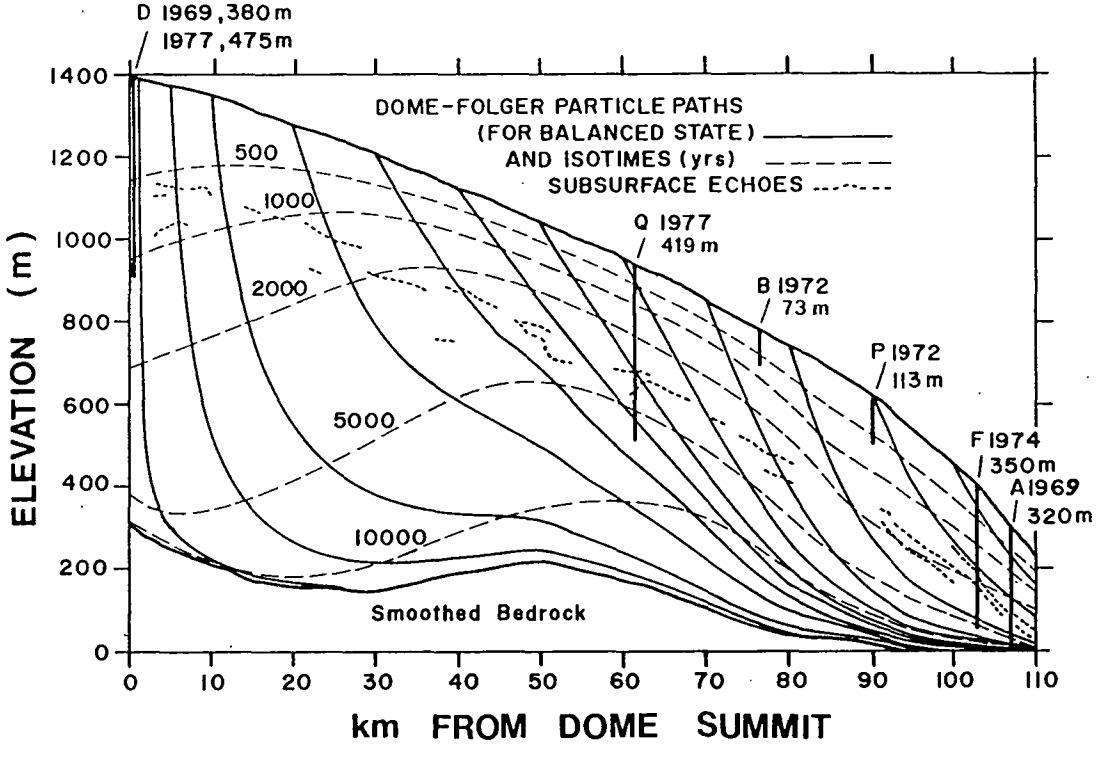

Figure 7.11 Modelled particle paths and isotimes for the Dome Summit to Cape Folger flowline (after Pfitzner, 1980). Sites Q, B, P, F and A correspond to SGQ, SGB, SGP, SGF and SGA.

These particle paths and the present surface velocity field indicate that snow deposited at sites between 5-40 km from the margin (SGB, SGP, SGJ, GW01, SGA and S1) in western Law Dome would require 3,000-8,000 years to travel to the margin. Sites further inland such as SGC and SGG at 65-75 km from the margin would require a travel time to the margin of ~18,500 and ~10,000 years respectively. The travel times for sites located up to 40 km from the margin in eastern Law Dome would be <2,000 years. Thus, at the present ice velocities any thickening of the interior of the Law Dome from increased accumulation rates during the EHCO and the Glacial-Interglacial

Transition would have had little effect on forcing an advance of the margin since 4,000 years B.P.. Alternatively, any changes in ice sheet thickness or flux in the zone up to 40 km from the margin would have been transported to the margin between the end of the EHCO and the time of the Late Holocene readvance. In the eastern Law Dome any changes in ice flux from the EHCO would have reached the margin by the Mid-Holocene, synchronous with the advance of the outlet glaciers. However in western Law Dome any changes in ice flux from the EHCO would have reached the margin much later, probably after 4,000 years B.P.. Thus the interior of the western Law Dome probably thickened during the Early-Mid Holocene whilst the margins continued to slowly retreat.

7.3.3.1 ESTIMATION OF ACCUMULATION RATE AND ICE THICKNESS CHANGES DURING THE EHCO AND THE MID-HOLOCENE COOL PERIOD

To estimate the thickening of the ice sheet during the EHCO, the accumulation rates for this period were determined. The surface air temperature of the EHCO was on average 1°C warmer than the long-term Holocene mean. The accumulation rates on Law Dome were shown in Chapter 3 to vary by ~25%/°C. The long-term Holocene mean accumulation rates were estimated in the DSS core as the mean for this century prior to 1970 (after Morgan et al., 1991). A comparison of mean accumulation rates on Law Dome between SGC and Law Dome Summit (DSS) for the epochs 1964-66 and 1983-87 showed that the latter accumulation rates were 15.2 % higher in accord with the recent decadal changes recorded in the DSS core (Figure 7.12). The 1964-66 accumulation rates are close to the long-term mean rates for this century in the DSS time series. Consequently, the accumulation rates for the 1964-66 period were assumed to be the balance accumulation rates and indicative of the mean for the Holocene. The average accumulation rates over Law Dome during the EHCO were estimated as 25% greater than those for 1964-66. Both the accumulation rates for balance state (1964-66) and the EHCO are shown in Figure 7.13 from the ice margin to Law Dome summit. The balance accumulation rates and those for the EHCO at selected sites within 40 km of the ice margin are shown in Table 7.7 together with the calculated reaction time for ice sheet response to increased accumulation rates, and the total thickening after a time equal to the reaction time.

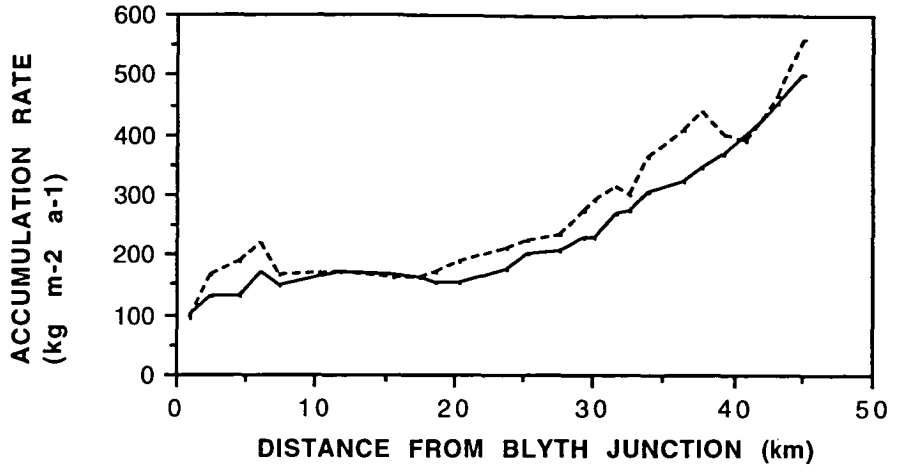

Figure 7.12 Spatial accumulation rate pattern from Blyth Junction (near SGC) to Law Dome summit, for the 1964-66 (solid line) and 1983-87 (dashed line) epochs. The data were obtained from unpublished ANARE annual glaciology field reports.

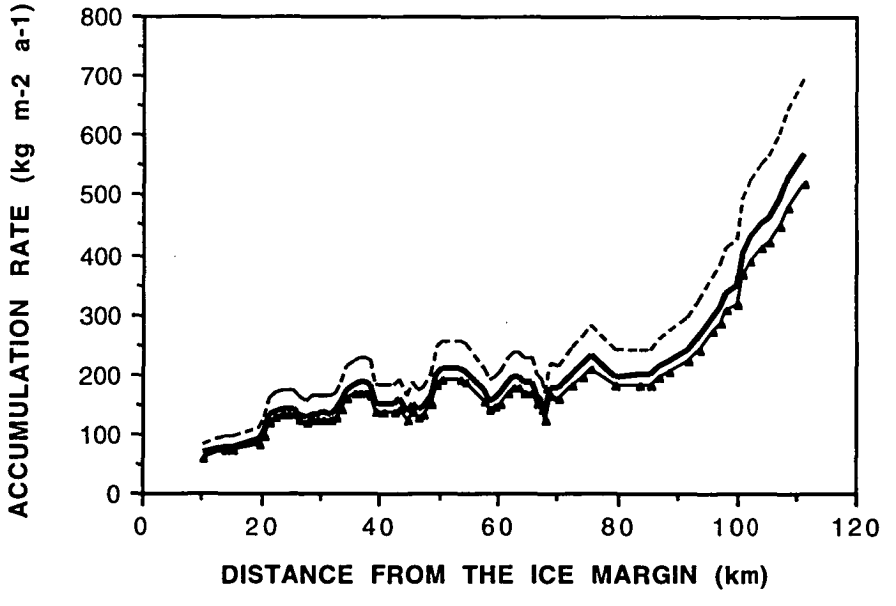

Figure 7.13 Spatial accumulation rate patterns along the Law Dome flowline from the Bailey Peninsula ice margin to Law Dome summit, for the Holocene long-term mean (solid line), taken as the mean for this century from the DSS core, and spatially extrapolated as being equivalent to the 1964-66 epoch. Also shown are the spatial accumulation rate patterns for: the Early Holocene Climatic Optimum (EHCO) (dashed line) which was estimated as 25% greater than the long-term mean; and for the Mid Holocene Cool Period (MHCP) (solid triangles) which was estimated as 10% less than the long-term mean rates.

TABLE 7.7 REACTION TIME AND TOTAL THICKENING IN RESPONSE TO INCREASED ACCUMULATION RATES DURING THE EHCO

Site	Reaction Time r Years	Balance acc. rates b_s m a^{-1}	EHCO acc rates b_1 m a^{-1}	Change in acc. rate b_1 m a^{-1}	Total thickening Z_1 m
GW01	690	0.11	0.13	0.03	19
SGP	560	0.20	0.25	0.05	27
SGB	1270	0.12	0.15	0.03	30
SGH	190	0.85	1.06	0.21	40
DSS	340	0.62	0.78	0.16	54

According to the theory in Whillans (1981) Law Dome would have been 63% dynamically adjusted to this thickening after the reaction times shown in Table 7.7. Since the duration of the EHCO was on average 3-5 times the reaction time, the thickening would have been partially reduced by increased velocities due to the coupled air temperature increase. The ice sheet thickening would also have been partially offset by the decreased accumulation rates expected during the subsequent Mid-Holocene cool period between 8,000-6,000 years B.P.. During this period an average cooling of 0.4°C occurred. The accumulation rates were estimated as ~10% less than those for 1964-66. Table 7.8 lists the accumulation rates and the ice sheet thinning during this period for the same sites as those in Table 7.7.

TABLE 7.8 REACTION TIME AND TOTAL THINNING IN RESPONSE TO DECREASED ACCUMULATION RATES DURING THE MID-HOLOCENE COOL PERIOD

Site	Reaction Time r Years	Balance acc. rates b_s m a^{-1}	Cool period acc rates b_1 m a^{-1}	Change in acc. rate b_1 m a^{-1}	Total thinning Z_1 m
GW01	690	0.11	0.10	0.01	6
SGP	560	0.20	0.18	0.02	11
SGB	1270	0.12	0.11	0.01	10
SGH	190	0.85	0.77	0.09	17
DSS	340	0.62	0.56	0.06	20

Therefore the ice sheet thickening forced by the increased accumulation during the EHCO would have been reduced significantly by the state of negative balance due to the decreased accumulation rates and increased velocities during this period between 8,000 to 6,000 years B.P.. Table 7.9 lists the cumulative ice sheet elevation changes for these sites during the 8,000 to 6,000 years B.P. period.

TABLE 7.9 CUMULATIVE ICE SHEET THICKNESS CHANGES FOR LAW DOME BETWEEN 8,000 TO 6,000 YEARS B.P.

Site	Total change m
GW01	+13
SGP	+16
SGB	+20
SGH	+23
DSS	+34

These cumulative ice sheet thickness changes have not been reduced for additional dynamical adjustments, which have been assumed to be small. Changes in ice flow due to the temperature fluctuations will be small since these do not become important until a period equal to **5r** and the penetration time for the temperature change to reach the bed is equal to **10r** (Whillans, 1981). The effect of temperature on ice flow is more significant in the eastern side of Law Dome since the reaction times are much shorter than the duration of the climate fluctuations. At DSS and similarly at SGG it is expected that a ~1°C temperature change would reach the bed after 3,390 years and 1,300 years respectively. During this period, according to the theory in Whillans (1981), the ice sheet thickening would have been 50% offset by thinning due to warming induced changes in strain rate.

The cumulative ice thickness changes indicate that mass balance fluctuations during the Early-Mid Holocene may have contributed a thickening of 10-20 m at the margin since 4,000 years B.P.. Also between 4,000-3,000 years B.P. the Dome C (Ciais et al., 1992) and DSS ice core oxygen isotope records indicate that the Antarctic was experiencing a second Holocene climatic optimum (SCO). This is also confirmed by the palaeo-accumulation rates determined from ^{10}Be measurements on the Vostok and Dome C cores (Raisbeck et al., 1987) and shown in Figure 6.10. Thus the ice sheet

accumulation rates were higher than the long-term mean during the SCO and would have resulted in an additional thickening of the ice sheet. A sensitivity analysis of this period is discussed below.

7.3.3.2 ESTIMATION OF ACCUMULATION RATE AND ICE THICKNESS CHANGES DURING THE SECOND HOLOCENE CLIMATIC OPTIMUM

The Second Holocene Climatic Optimum period (SCO) (4,000 to 2,500 yr B.P.) experienced a mean increase in surface air temperature of 0.4°C (Dome C) and 0.5°C (DSS) above the long-term mean for the Holocene. This corresponds to an increase in accumulation rates of ~12.5% above the long-term Holocene mean rates on Law Dome. The balance accumulation rates and those for the SCO at selected sites over the eastern and western hemispheres of Law Dome are shown in Table 7.10, together with the calculated reaction time for ice sheet response to increased accumulation rates and the total thickening after a time equal to the reaction time.

TABLE 7.10 REACTION TIME AND TOTAL THICKENING IN RESPONSE TO INCREASED ACCUMULATION RATES DURING THE SECOND HOLOCENE CLIMATIC OPTIMUM

Site	Reaction time r Years	Balance acc. rates b_s m a^{-1}	Warm period acc. rates b_1 m a^{-1}	Change in acc rate b_1 m a^{-1}	Total thickening m
S1	920	0.05	0.05	0.01	8
SGA	720	0.09	0.10	0.01	6
GW01	690	0.11	0.12	0.01	6
SGP	560	0.20	0.23	0.03	16
SGB	1270	0.12	0.13	0.02	18
SGQ	820	0.20	0.23	0.03	21
SGC	1040	0.16	0.18	0.02	16
DSS	340	0.62	0.70	0.08	27
SGJ	190	0.85	0.96	0.11	21
SGH	190	0.85	0.96	0.11	20
SGG	240	0.94	1.06	0.12	29

At sites such as S1, GW01 and SGA near the present ice margin a cumulative thickening of ~20-25 m could have occurred from the surface mass balance fluctuations during the Holocene. These estimates of ice sheet thickening represent an increase of ~10% in the total ice flux. The dynamical adjustments due to the temperature increase are considered to be small. The 1,500 year duration of the SCO is equivalent to less than **1.5r** to **2r** at the lower elevations near the margin and the strain rate changes are insignificant after this short time interval. At the lower elevation sites the ice sheet base is likely to be at the melting point (N. Young pers. comm) especially nearer the margin at GW01, SGA and S1 from both temperature profiles and the observed jökulhlaup event at the margin (Goodwin, 1988). Thus at these sites the effect of a temperature increase of <1°C on the vertical velocity field is negligible, since the bed was probably already sliding.

Estimates of the scale of advance required to thicken the ice sheet by the above cumulative amounts were scaled from the ice sheet profiles for DSS to Cape Folger and the DSS to Cape Poinsett in Figure 7.8 assuming that the equilibrium ice sheet profile is maintained. These are listed in Table 7.11.

TABLE 7.11 ESTIMATES OF ICE SHEET ADVANCE FOR LAW DOME

Location	Net thickening (m)	Advance of profile (km)
Western		
S1	21	2
SGA	22	3
GW01	19	2-3
SGP	32	3
Eastern		
SGJ	55	3

The reaction times at S1, SGA and GW01 are comparable to the duration of the maximum warming between 4,000 to 3,000 years B.P.. Thus the total thickening at each of these sites would have been achieved. The preliminary DSS oxygen isotope record in Figure 1.5 implies that the SCO continued until 2,500 years B.P. on Law Dome and that the Little Climatic Optimum of equivalent warming occurred between 1,500-1,000 years B.P. (Morgan, 1985) with the intervening period at or slightly above the long-term mean (Chapter 1). Therefore, higher than the Holocene mean accumulation rates were probably maintained for much of the period between 4,000-

1,000 years B.P. on Law Dome. It is probable that a further 5-10 m of ice thickening at the margin occurred in response to the increased accumulation during the Little Climatic Optimum.

7.3.3.3 DISCUSSION ON THE IMPLICATIONS FOR TIMING AND DURATION OF THE ADVANCE

The estimates of ice sheet advance listed in Table 7.11, indicate that the margin would have advanced between 2-3 km in response to the estimated thickening of the ice sheet during the Late Holocene. This implies that during the Mid-Holocene the ice margin was located near S1, 2-3 km inland of the present ice margin. The rate of retreat is not known but was determined primarily by the eustatic sea-level rise and the slope of the bedrock. Thus it is likely that the East Antarctic coastline may have experienced similar rates of retreat to the 2-3 km/1000 years reported in the Vestfold Hills by Adamson and Pickard (1986) during the Mid-Holocene. At 5,500 yr B.P. the majority of the Clark, Bailey and Mitchell Peninsulas were at or below sea-level with their coastlines recently deglaciated. A further 1000 years duration for the retreat across the peninsulas would indicate that the Law Dome probably reached its maximum Holocene retreat position by 4,500 yr B.P.. This is supported by evidence from the location of Holocene raised beaches abutting the present ice margin at the inland edge of the emerged Clark Peninsula which are of an equivalent height to those dated at ~4,500 years B.P. on Browning Peninsula.

An estimate of the timing of the advance can be determined from the present surface ice velocities inland of the margin. The base of the ice ramp in the Clark Peninsula no. 3 ice margin profile (Figure 5.5c) is located ~2.5 km along the flowline from S1 which has a present surface velocity of ~1.5 m a^{-1}. At this velocity the advance of the ice margin forming the Løken Moraines, would have required 1,700 years. The thickening and advance of the ice margin was probably synchronous with the emergence of the peninsulas. It is likely that the ice velocity inland of the margin has decreased over the last few thousand years due to the ~20 m relative sea-level lowering, and the damming of the outflow by the bedrock high of the Windmill Islands. Present velocities along the margin to the north and south of the Windmill Islands are ~4-5 m a^{-1} (Figure 7.8) and may be indicative of the velocities at the commencement of the advance. Therefore, with similar velocities the advance of the margin over the 2-3 km could have been completed in 500-600 years. The margin would have continued to thicken for at least a time interval equivalent to the 1,500 year period of increased accumulation rates.

These time intervals agree well with the formation of the inland ridge of the Løken Moraines inland of Clark Peninsula. The earliest date from lichenometry for the formation of the Løken Moraine inland ridge at Clark Peninsula no. 3 profile is 3,250 years B.P. (Chapter 5), although the absolute date of formation may be younger depending upon the actual growth rate of the lichens. The ice margin between Bailey and Clark Peninsulas was advancing during this time period and the Bailey terminal moraine was dated by lichenometry at 2,550 years B.P. (Chapter 5). As the ice margin continued to thicken, the successive moraine ridges developed down-glacier. This down-glacier migration of the active basal shear plane and corresponding moraine ridges occurred since 2,000 years B.P. as a result of the increased thickening at the margin. This thickening of the ice margin was probably forced by higher accumulation rates forced by the Little Climatic Optimum between 1,500-1,000 yr B.P..

In the eastern hemisphere of Law Dome the advance may have been more rapid. The difference between the eastern and western hemispheres is that the reaction times are much faster in the east. For example the reaction time at SGJ, 20 km from the ice margin at Cape Poinsett is only 200 years and the surface velocity significantly faster at 34 m a^{-1}. Thus the eastern Law Dome ice margin would have advanced in under 400 years after the maximum thickening was attained. It is probable that the eastern hemisphere ice margin which is below sea-level has subsequently retreated, since a negative imbalance would have occurred over the last 1,000 years, with accumulation rates lower than the long-term Holocene mean.

7.4 IMPLICATIONS FOR THE MID TO LATE HOLOCENE GLACIAL HISTORY OF THE EAST ANTARCTIC MARGIN FROM PRINCESS ELIZABETH LAND TO GEORGE V LAND

The above sensitivity analyses show that the geological evidence for a mid to late Holocene advance of the East Antarctic ice margin and outlet glaciers after the early-Holocene marine transgression can be substantiated by glaciological theory. These analyses are based on a number of assumptions which include:

- That the oxygen isotope records from the Dome C, Vostok, Komsomolskaya and Law Dome Summit ice cores, together with those from the oceanic sediment cores, describe the broad temperature fluctuations across Antarctica during the Holocene;

- That major changes to the atmospheric circulation pattern have not occurred during the Holocene;
- That long-term accumulation rates have fluctuated similar to their present variation with temperature, sea ice extent and concentration; and,
- That the western Pacific, Indian and Atlantic Ocean sectors of the East Antarctic ice sheet would have experienced similar climatic trends over timescales of 1000 years, based on the comparable sea surface temperature records from oceanic sediment cores (Labracherie et al., 1989, Charles and Fairbanks, 1992), in contrast to the often opposing interdecadal climatic fluctuations observed and interpreted between regions over the last few decades (Chapter 3).

Whilst it is assumed that the ice sheet experienced similar climate fluctuations during the Holocene, large spatial variation in the accumulation rate occurs across Antarctica. The following examines whether the different coastal regions developed different scales of surface mass balance response to the climate fluctuations.

The recent spatial accumulation pattern of East Antarctica is highly variable both inter and intra drainage basins (Chapter 2). This is particularly obvious in the accumulation rate compilations for the whole of Antarctica presented by Giovinetto and Bull (1987) and shown in Figure 7.14. One of the most striking features in the accumulation pattern is a marked decrease in accumulation between the coastal slopes of Wilkes Land and Dronning Maud Land. The Wilkes Land coastline is located approximately at 67°S and is not surrounded by fringing ice shelves. In contrast the Dronning Maud Land coastline is located further south at 70-73°S and is surrounded by fringing ice shelves with an average width of 60-80 km. Thus the Dronning Maud Land coastal margins have a greater continentality. They also have a more extensive sea-ice cover. Both of these factors are probably responsible for the reduced ice sheet precipitation in Dronning Maud Land.

What was the likely effect of these regional differences in the recent spatial accumulation patterns on the response of the ice sheet to an Antarctic wide warming during the EHCO ? Did the warming produce greater increases in accumulation rate in Wilkes Land than Dronning Maud Land and hence a greater glacial expansion ? The following sensitivity analysis is applied to sites at the same elevation (2100 m) in Wilkes Land, MacRobertson/Kemp Land, Enderby Land and Dronning Maud Land to determine whether different responses were likely. The 2100 m elevation was selected because the comparative data was available and have been analysed in chapter 2, and

because the accumulation rates at 2100 m are less affected by topography than at lower elevations close to the coast.

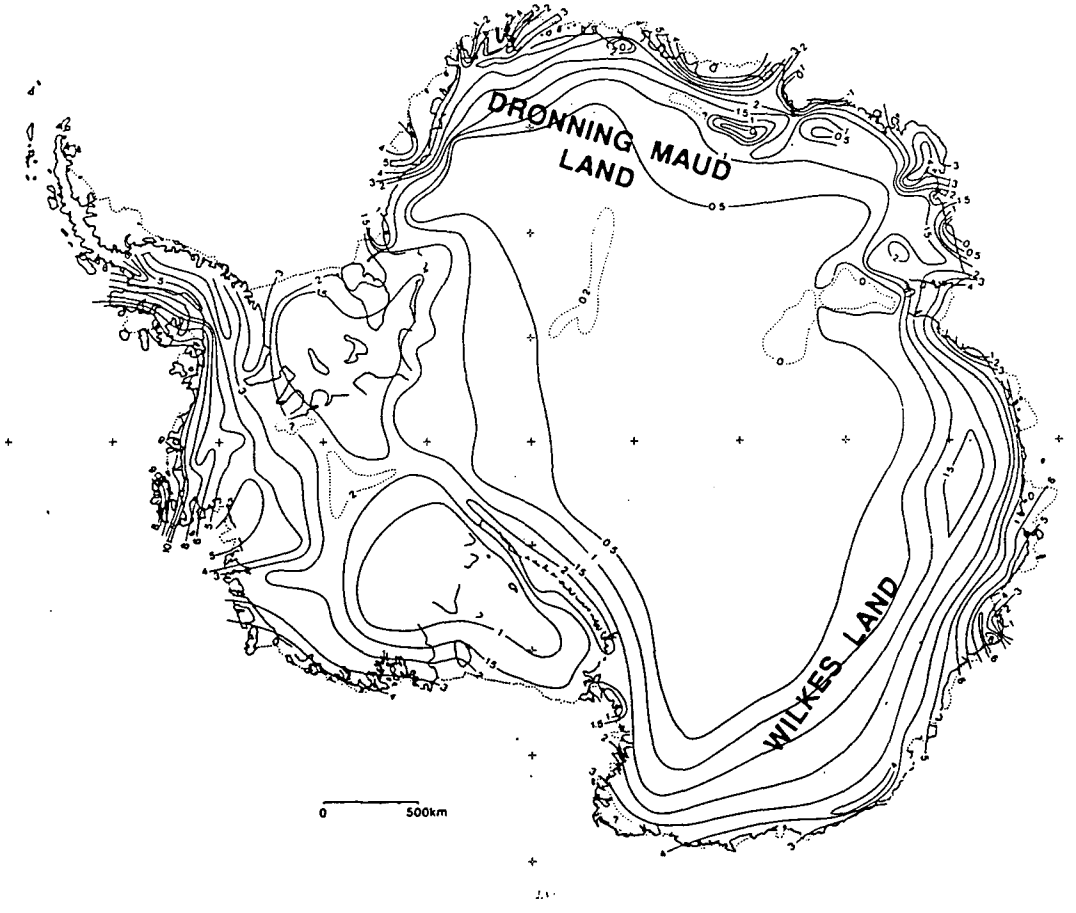

Figure 7.14 Accumulation rate (surface balance) isopleths (10 gm^{-2} a^{-1}), after Giovinetto and Bull (1987). Note the significantly greater accumulation rates in Wilkes Land than in Dronning Maud Land.

Table 7.12 lists the sites with their recent accumulation rates, together with the estimated steady state accumulation rates, accumulation rate increase during the EHCO, the reaction time to thickening and the maximum thickening. The recent accumulation rates were assumed to be equivalent to the long-term Holocene mean rates. The steady state rates were approximated by these long-term rates, and the EHCO rates were taken as 20% greater than the present rates according to the ^{10}Be measurements of Raisbeck et al. (1987). The Mizuho accumulation rate is from Watanabe et al. (1988) and the Dronning Maud Land (DML) rate from Isaksson and Karlen (1994).

TABLE 7.12 SENSITIVITY ANALYSIS OF ACCUMULATION RATE INCREASES IN COASTAL EAST ANTARCTICA AT 2100 M ELEVATION

Region	Recent acc rates kg m^{-2}	Ice thickness m	Acc rate b_s	Acc rate increase b	Reaction time a	Total thickness change m
EWL NE	375	2580	0.35	0.09	1480	99
WWL NE	323	2670	0.30	0.08	1780	96
SWL NE	288	2100	0.26	0.07	1620	80
EWL NW	218	2440	0.20	0.05	2440	68
WWL NW	241	1630	0.22	0.06	1480	66
LGB NE	83	1500	0.15	0.04	2000	51
MIZUHO	60	2200	0.13	0.03	3390	45
DML	74	~1500	0.15	0.04	2000	51

Whilst the reaction times are comparable except for Mizuho, which is twice as long as in Wilkes Land, the variation in thickening of 45 to 100 m corresponds to potential differences in ice sheet expansion of ~7-25 km between the Dronning Maud Land basin and the Wilkes Land basin, according to the idealised ice sheet profile of Hollin (1962). He proposed the formula:

- $\mathbf{H = 149\ D^{0.5}}$, where **H** is the ice sheet thickness in metres and **D** is the distance in kilometres from the margin.

Similarly, the expansion of the outlet glaciers during the Mid Holocene would have been synchronous since the initiation of the re-advance was probably controlled by

relative sea-level lowering, when the post-glacial sea-level rise was nearly complete. However, the extent of the outlet glacier expansion between regions would have been controlled by the relative differences in accumulation rates and ice velocities. It is consistent with the accumulation rate differences between Dronning Maud Land and Wilkes Land in Table 7.12, to conclude that the outlet glacier expansion was probably greater in Wilkes Land than in Dronning Maud Land. However, the response of the outlet glaciers and the ice sheet margins to relative sea-level lowering and climate fluctuations would also have been a function of the bathymetric slope on the inner continental shelf, which may have masked some of the regional differences in the ice sheet response.

The investigations outlined above in section 7.3 for the Lambert Glacier-Amery Ice Shelf system indicate that this system advanced on the order of 150 km in response to an equivalent 18% increase in total ice outflow and to relative sea-level lowering. It is consistent from these analyses to conclude that the major outlet glaciers draining the East Antarctic coast behaved in a similar fashion, although with the greatest responses in the sector between MacRobertson Land to George V Land.

It can be concluded that the outlet glaciers advanced initially in response to relative sea-level lowering due to delayed isostatic rebound, with subsequent thickening of the glaciers due to increased accumulation during the EHCO. From the evidence in the Windmill Islands, the Vestfold Hills and along the western Ross Sea coast, the outlet glaciers probably also expanded on a lesser scale in response to the SCO and the LCO. The grounded ice sheet margins were probably in retreat until 4,500-5,000 years B.P. (Chapters 5 and 6). These margins advanced during the Late Holocene in response to relative sea-level lowering and to a net thickening of the ice sheet in response to the climatic fluctuations during the Holocene. The slower moving grounded ice sheet margins and alpine glaciers are presently close to their maximum Holocene extent. The outlet glaciers led the grounded ice sheet margins in their expansion and subsequent contraction.

These sensitivity analyses support the glacial marine geological evidence (Domack et al, 1991) for the 15-20 km advance of the Astrolabe and Zelee Glacier ice shelf front in Terre Adélie, and the 40-50 km advance of the Mertz Glacier ice shelf front in George V Land. Therefore it can be concluded that the major glaciers such as the Denman Glacier, the Scott Glaciers, the Totten Glacier and the Mertz and Ninnis Glaciers may have advanced during the mid Holocene by up to 40-50 km, whilst the minor glaciers typified by the Astrolabe and Zelee Glaciers in Terre Adélie, and including the Wilkes Land glaciers such as the Vanderford Glacier on the Budd Coast

and the Princess Elizabeth Land glaciers such as the Polar Record and Sørsdal Glaciers, are likely to have advanced on the order of 10-15 km during the mid-Holocene .

If the coastal Wilkes Land sector of East Antarctica maintained a relatively higher spatial accumulation pattern and a relatively narrow sea ice extent throughout the Holocene, it is expected that the most widespread and significant ice sheet and outlet glacier advance occurred along the Wilkes Land coast. The implications of the glacial fluctuations on the late-Holocene eustatic sea-level history are discussed in the following Chapter.

CHAPTER 8
CONCLUSIONS ON THE ANTARCTIC CONTRIBUTION TO RECENT AND HOLOCENE GLOBAL SEA-LEVEL CHANGES

8.1 INTRODUCTION

This thesis has examined the variation in mass balance in East Antarctica over the last few decades, together with the effect of mass balance fluctuations on the extent and volume of East Antarctica throughout the Holocene. In this concluding chapter, the contribution of these mass balance fluctuations to both present and Holocene global sea-levels is determined. The accumulation-temperature relationships determined for East Antarctica (in chapters 2 and 3) are applied to the proxy Holocene temperature record derived from the deep ice core oxygen isotope records (Figure 1.5, after Ciais et al., 1992), to estimate the palaeo-accumulation distribution throughout the Holocene. An equivalent Holocene eustatic sea-level contribution for Antarctica is derived from the fluctuating palaeo-accumulation distribution, and the Late Pleistocene-Holocene glacial fluctuations of Antarctica (investigated in chapters 4, 5, 6, and 7). The validity of this Antarctic equivalent sea-level contribution is tested against the relative sea-level records on mid-oceanic islands, and compared to a geophysical model of continuing exponential melting and retreat of the Antarctic Ice Sheet throughout the Holocene (Nakada and Lambeck, 1988, 1989). The implications of the Antarctic equivalent sea-level contribution are discussed with respect to Holocene sea-level modelling, especially of the mid-oceanic islands.

8.2 THE CONTRIBUTION OF RECENT ANTARCTIC MASS BALANCE VARIATION TO SEA-LEVEL

Most recent mass balance studies have concluded that Antarctica is either close to balance or in slight positive balance and is causing a negative or lowering contribution to sea-level. The estimates of the sea-level lowering contribution are 0.1-1.1 mm a^{-1} (Bentley and Giovinetto, 1991), 0-1.2 mm a^{-1} (Budd and Smith, 1985), 1.0-1.2 mm a^{-1} (Morgan et al., 1991) and 0.2-1.1 m a^{-1} (Warrick and Oerlemans, 1990). These estimates are based on similar data sets and it is not surprising that they present a similar estimate, despite their different approaches to the problem. Inherent in these estimates is a ±20% uncertainty in the estimation of mass input and mass output

(Bentley and Giovinetto, 1991). An independent study by Patterson (1993) determined the source and contribution of the observed rate of sea-level rise this century around the globe. The residual component of this global water mass balance study was equivalent to a sea-level rise of 0.65 ± 0.61 mm a^{-1}, and was assigned to the Antarctic Ice Sheet. In a comparable analysis the author calculated 0.46 ± 0.80 mm a^{-1} using the most recent global water mass balance estimates (Chapter 1).

In contrast to the other studies, Jacobs et al. (1992) and Jacobs (1992) conducted mass balance studies which included estimates for ice shelf melting (±50% errors), and meltwater outflow from the grounded ice sheets in their analyses. They reported the likelihood of a negative mass balance equivalent to a +1.3 mm a^{-1} rise in sea-level, if all of the mass imbalance was derived from the grounded ice alone. The previously mentioned mass balance studies did not include these parameters in their estimates except for Bentley and Giovinetto (1991) who included ice shelf melting component, since the latter does not directly contribute to sea-level changes.

Ice shelf melting does not impact on sea-level directly since the ice is buoyant. However, the argument to include ice shelf melting in the mass balance equation is based on the role of ice shelves in controlling a significant volume of outlet glacier flow. Jacobs et al. (1992) argue strongly that increased ice shelf melting rates in response to increased ocean temperatures and a changed thermohaline circulation could lead to substantial ice shelf thinning. This in turn would reduce the back pressure on the grounding zone and allow an increased ice volume to be discharged from the outlet glaciers. However, field evidence is sparse and often contradictory to suggest that this is presently occurring (Jacobs et al., 1992). As an example, the best evidence for the present mass balance of the Lambert Glacier-Amery Ice Shelf system examined in Chapter 7, would indicate that the grounding zone was probably thickening slightly rather than thinning. Shabtie and Bentley (1987) reported evidence for the retreat of the Ross Ice Shelf grounded ice. Previously, Thomas and Bentley (1978) suggested that continuing isostatic rebound in the Ross Embayment may be causing local grounding and partially offsetting a thinning of the ice shelf. Large iceberg calving events from the ice shelves and glacier tongues over the last 30 years appear to be regular components of ice shelf dynamics rather than indicative of a catastrophic collapse, except for the Antarctic Peninsula ice shelves, such as the Wordie Ice Shelf and the Larsen Ice Shelf which are very sensitive to ocean temperature changes, which may be responsible for their latest calving events.

One of the problems with the estimation of the current mass balance of Antarctica, is the definition of the best estimates of the long-term accumulation rates across the ice

sheet. The measurement of accumulation rates across the ice sheet has been both geographically sparse and sporadic. The accumulation rate estimates included in all the mass balance studies have been measured or extrapolated from measurements made over the last few decades (since the IGY in 1957-58). These accumulation rates are derived from measurements over periods of 1 year to 3 decades and have a large variation due to spatial and temporal effects. Most recent studies of the temporal variation of accumulation rates report a large fluctuation on the timescales of decades (Goodwin, 1992, Morgan et al, 1991, Peel 1992 and Isaksson et al. submitted). The best method to determine whether the measured and compiled spatial accumulation patterns (such as Giovinetto and Bentley, 1987) are typical of the Holocene long-term rates is by reference to temporal records derived from firn and ice cores, such as those presented in Chapter 3. Whilst the interdecadal changes in accumulation rate provide an immediate change in the sea-level contribution through simple mass transfer from the ocean to the ice sheet and vice-versa, the long-term trends over timescales of 100 years or more provide the best method of determining trends in sea-level. The latter are more suitable for correlation with Holocene relative sea-level records from far-field sites, since it is difficult to resolve fluctuations in sea-level of less than a few hundred years in the geological record.

The following discussion is based on the firn core records presented in Chapter 3 and others from the Antarctic Peninsula, and will attempt to clarify the best estimate of the long-term mass input to Antarctica. The impact of accumulation changes on the sea-level contribution is most marked in the regions of highest accumulation per surface area. These areas include the Antarctic Peninsula, where 23% of the total annual accumulation falls over 7% of the continents area (Drewry and Morris, 1992). Also the ice shelves receive 29% of the total annual accumulation with only 12% of the area (Jacobs et al., 1992). The remaining high accumulation areas are located along the coastal margins in Wilkes Land, Oates Land and Queen Mary Land, and in West Antarctica.

In Wilkes Land and Queen Mary Land the majority of the spatial accumulation measurements were made during the 1980's. The accumulation rates for this period, when compared to the temporal ice core records determined for the DSS and DE08 sites at Law Dome, are 15-23% higher than the long-term means for 1930-1987 and 1806-1987 (Morgan et al, 1991). These long-term periods were considered to be representative of the Holocene long-term mean from the comparison of the oxygen isotope profiles for DSS, DE08 and the 30,000 year record for Dome C. Thus the accumulation rates are interpreted to have recently increased by 20% above the long-term mean in the last 1-2 decades. This pattern is considered to be representative of

the coastal margins and interior of Wilkes Land to Oates Land, including the South Pole, from the interpretation of the temporal comparisons of Pourchet et al. (1983). Bentley and Giovinetto (1991) estimated that the combined drainage system of Wilkes Land presently has a small positive balance of 4 Gt a^{-1}. However, using the long-term accumulation rates (20% < present) the mass balance is calculated as a negative balance of 11.8 Gt a-1, or 19% of the input. Whilst this is not a statistically significant imbalance since it is equivalent to the 20% error estimates, it does indicate that prior to 1970 the Wilkes Land system was likely to be close to balance or slightly negative.

A similar pattern of increasing accumulation and temperature in recent decades, superimposed on a more gradual long-term increase, has been reported for the Antarctic Peninsula (Peel, 1992). A 17-25% increase in accumulation rate was observed since 1955 in the Antarctic Peninsula when compared to the long-term mean since 1805. Thus the total long-term accumulation input for the Antarctic Peninsula is possibly 100 Gt a^{-1} less than the 500 Gt a^{-1} estimated by Drewry and Morris (1992).

In contrast to these areas, Isaksson et al. (submitted) reported that accumulation in the coastal margin of Dronning Maud Land has decreased by 18-25% between 1932-1991, with the last decade showing the greatest decrease. No trend in accumulation rates was observed in the firn core record from the interior of Dronning Maud Land. A similar pattern was reported for the Filchner-Ronne Ice Shelf in Jacobs (1992). Mosley-Thompson et al. (1991) reported that accumulation rates were stable at Siple Station, West Antarctica between 1966-85.

The accumulation rate records determined from firn cores in the coastal margin region of the Lambert Glacier Basin show that accumulation has decreased by ~20% in the period 1955-1991 (Chapter 3). Similarly the accumulation rate had decreased by 20% on the Amery Ice Shelf between 1968 and 1990. On the basis of these accumulation trends and the temperature record at Mawson it was estimated that the accumulation rates measured between 1970-74 (Allison, 1979) were likely to have been close to the long-term mean in the Lambert Glacier Basin. The accumulation rates between 1990-94 are equivalent to the 1970-74 rates.

The above summary highlights the widespread temporal variation of accumulation rates across Antarctica, on the timescale of decades. There are a number of major problems with extrapolating these accumulation rate changes and regional total estimates to the whole of the Antarctic Ice Sheet since these sites are not evenly spaced, may not be entirely representative of the regions, and are more concentrated in

the coastal margins (Jacobs, 1992). Nevertheless, the large accumulation increases in Wilkes Land and the Antarctic Peninsula since 1970 need to be taken into account when assessing typical long-term mass balance and sea-level contributions of Antarctica, for this century. This is particularly important if the Antarctic sea-level contribution is to be compared to the global sea-level record determined from tide gauges over the last century.

Table 8.1 lists the estimated mass balance components determined from various studies. The best current estimates of the grounded and total ice sheet accumulation rates are 1,528 and 2,144 Gt a^{-1} (Jacobs et al., 1992). The combined accumulation rate for George V Land, Terre Adélie, Wilkes Land and Queen Mary Land is estimated as approximately 200 Gt a^{-1} (after Bentley and Giovinetto, 1991). The accumulation rate estimates were adjusted by taking into account the temporal accumulation variation over the last 20-30 years, to determine the average mass balance estimate for this century. This gave long-term (1900-1970) estimates of the grounded and total ice sheet accumulation rates for the whole of Antarctica of 1,388 and 2,004 Gt a^{-1} respectively (comprising -40 Gt a^{-1} from the combined George V Land, Terre Adélie, Wilkes Land and Queen Mary Land regions, and -100 Gt a^{-1} from the Antarctic Peninsula). All other regions were assumed to have experienced no significant change in accumulation rates during this century. The total ice sheet accumulation estimate of 2,004 Gt a^{-1} is close to that determined by Giovinetto and Bentley (1985) of 1,963 Gt a^{-1}.

Table 8.1 lists three forms of mass attrition which are calving icebergs (-2016 Gt a^{-1}), ice shelf melting (-544 Gt a^{-1}) and runoff (-53 Gt a^{-1}) (Jacobs et al., 1992). However on-going retreat of the grounded ice margins following the late Holocene advance may be contributing an additional significant component of mass attrition. The field evidence from the Law Dome margin at the Windmill Islands indicates that surface lowering of approximately 40 m in the last 400 years has occurred up to the present, which is equivalent to -0.1 m a^{-1}. Evidence from the temporal comparison of aerial photographs of the Law Dome margin north of the Windmill Islands also indicates a recession of the ice margin by up to 100 m between 1962-1985 through calving and melting events. If an equivalent thinning and retreat of the ice margin was occurring around the total coastal ablation area of Antarctica (estimated as 2% of the grounded ice area after Robin, 1987) then an additional mass loss of 22 Gt a^{-1} would be discharging to the ocean. When combined with the estimate of surface runoff for balance state of -36 Gt a^{-1} (Robin, 1987) and the estimate of basal meltwater discharge of -17 Gt a^{-1} (Jacobs et al., 1992) then the total melting contribution from the grounded ice sheet could be as high as 75 Gt a^{-1}.

TABLE 8.1 ANTARCTIC MASS BALANCE ESTIMATES (Gt a^{-1})

ACCUMULATION			ATTRITION				BALANCE	REFERENCE
Grounded Ice	Ice Shelf	Total	Calving Icebergs	Ice Shelf Melting	Runoff	Ice Margin Thinning		
		2000	-1879 *				+121	Budd and Smith (1985)
1468	495	1963						Giovinetto and Bentley (1985)
1660							+180	Bentley and Giovinetto (1991)
1528	616	2144	-2016	-544	-53		-469	Jacobs et al. (1992)
								With Ice Shelf Melting
1388	616	2004	-2016	-544	-53	-22	-631	Long-term 1900-1970 this study
1528	616	2144	-2016	-544	-53	-22	-491	Since 1970 this study
								Without Ice Shelf Melting
1388	616	2004	-2016		-53	-22	-87	Long-term 1900-1970 this study
1528	616	2144	-2016		-53	-22	+53	Since 1970 this study

* Note that the attrition estimate of Budd and Smith (1985) is calculated as the mass flux across the grounding line.

This estimate was used in the following mass balance calculations. The Antarctic mass balance was calculated with and without the ice shelf melting component of Jacobs et al. (1992) for the period 1900-1970 and since 1970, using the respective total accumulation estimates of 2004 and 2144 Gt a^{-1}. The results are listed in Table 8.1 and discussed below.

The mass balance during the period 1900-1970 was estimated as an imbalance of -631 Gt a^{-1} with the ice shelf melting component and -87 Gt a^{-1} without the component. This imbalance is equivalent to a sea-level contribution of +0.24 to +1.8 mm a^{-1}. Similarly, the mass balance during the period since 1970 was calculated as an imbalance of -491 with the ice shelf melting component and +53 Gt a^{-1} without the component. This imbalance is equivalent to a sea-level contribution of +1.4 to -0.15 mm a^{-1}. These results suggest that the ice sheet is close to balance if the ice shelf melting component is not included.

The estimated sea-level rise contributions which include the ice shelf melting component for both the periods, are significantly greater than those estimated as the residual contribution from the global water mass balance study for this century. The latter are equivalent to a sea-level rise of $+0.65 \pm 0.61$ mm a^{-1}, (Patterson, 1993) and $+0.46 \pm 0.80$ mm a^{-1} (Chapter 1 this study). Consequently, it is considered that ice shelf melting is not contributing to significant changes in ice shelf thickness, nor in the ice discharge from the adjacent outlet glaciers and to an overall ice sheet imbalance as postulated by Jacobs et al. (1992). Therefore, the best estimates of the Antarctic contribution to sea-level are considered to be $+0.24 \pm 0.05$ mm a^{-1}, between 1900-1970, and -0.15 ± 0.05 mm a^{-1} since 1970. During the latter period, the slightly positive balance of +53 Gt a^{-1} (due to the increased accumulation in George V Land, Wilkes Land and Queen Mary Land sector of East Antarctica and in the Antarctic Peninsula) has probably balanced the mass loss from the thinning of the ice margins. For Antarctica to be in positive balance and contributing a sea-level lowering of the order of 1.0 mm a^{-1} (as suggested by some previous studies outlined above) then the observed rate of accumulation increase in Wilkes Land and the Antarctic Peninsula would need to be occurring over the entire grounded ice area. The temporal accumulation records from ice cores suggest that this is probably not the case.

8.3 THE SEA-LEVEL CONTRIBUTION FROM HOLOCENE GLACIAL FLUCTUATIONS ACROSS ANTARCTICA

8.3.1 ANTARCTIC PENINSULA

The Antarctic Peninsula experiences the warmest climate in Antarctica and its mass balance is very sensitive to the equilibrium line elevation which is largely determined by the mean annual surface temperature (Drewry and Morris, 1992). Doake (1985) reported that the Antarctic Peninsula is characterised by two distinct climate regimes with a divide close to the eastern escarpment of the Peninsula. Surface temperatures are up to 7°C lower on the Weddell Sea side and ice shelves much more extensive than on the Pacific Ocean side. This is due to the persistent summer sea ice cover in the Weddell Sea. The accumulation rate increases rapidly with altitude near the coast, and consequently, a small shift in the equilibrium line elevation can result in an exaggerated effect on the mass balance of the coastal margins (Doake, 1985). The majority of the Antarctic Peninsula experiences mean annual surface temperatures lower than -11°C, with 2% of the area experiencing warmer temperatures (Drewry and Morris, 1992). As outlined in section 8.2 the recent changes in coastal air temperature and ice sheet accumulation rates are comparable between the Antarctic Peninsula and those in Wilkes Land.

Clapperton (1990) made an assessment of the Late Pleistocene and Holocene glacial fluctuations on the Sub-Antarctic Southern Ocean islands and the Antarctic Peninsula. He acknowledged that stratigraphical and chronological evidence for glacial fluctuations in this region was scarce due to the sea level control on ice extent, differential tectonics and the lack of material for radiometric dating. Nevertheless, he established a possible pattern of glacial fluctuations during the Holocene. Hansom and Flint (1989) and Ingolfsson et al. (1992) also reported field evidence for Holocene glacial fluctuations on Brabant Island and James Ross Island, Antarctic Peninsula, respectively. These patterns indicate that it is likely that a glacial advance occurred during the Early-Holocene climatic optimum at around 10,000 years B.P. on South Georgia, the South Shetland Islands and the Antarctic Peninsula. Similarly a second glacial advance was interpreted to have occurred at ~ 2,200 years B.P. on South Georgia and since 6,500 years B.P. on the South Shetland Islands and the Antarctic Peninsula. Similarly, on James Ross Island a glacial advance was interpreted between 7,000-5,000 years B.P. and a later one at 3,000 years B.P. The George VI ice shelf which is particularly sensitive to sea temperature changes, was interpreted to have disappeared at ~6,500 years B.P. (Clapperton and Sugden, 1982). Clapperton (1990) reported field evidence which indicates that the George VI ice shelf reformed since

5,000 years B.P. in response to Neoglacial cooling which is thought to have occurred in South Georgia (Clapperton et al., 1989) and Patagonia (Mercer, 1978) during this period. Sea-level is a primary control of glacier extent in the Antarctic Peninsula region and together with the variable bathymetry on the inner shelf may explain the variation in extent during the Early-Mid Holocene when sea-level was rapidly rising. The glacial advances reported between 5,000-2,000 years B.P. may have been forced by the climate warming associated with the Late Holocene climatic optimum which occurred in East Antarctica. It is unclear from the above glacial geological evidence whether the Antarctic Peninsula experienced Holocene climatic fluctuations in phase with those interpreted in East Antarctica or with those in South America (Mercer, 1978).

However, it is possible to make some comment on the possible sea-level contributions that the Antarctic Peninsula would be likely to make in response to the small climatic fluctuations which have occurred throughout the Holocene. In the majority of the Peninsula where mean annual surface air temperatures are below -11°C the glacier reaction time to changes in accumulation rate is ~200-400 years, based on an average accumulation rate of 0.5 m a^{-1} and an equilibrium ice divide thickness of 500-1000 m (Drewry and Morris, 1992). With such a short reaction time compared to that of the order of 10,000 years in East and West Antarctica the Antarctic Peninsula would have reached a new equilibrium within the duration of the Holocene climatic fluctuations. Hence, increased accumulation rates in response to warmer temperature would be partly offset by the effect of temperature on ice viscosity and faster ice flow (Drewry and Morris, 1992). Thus, the total volume of grounded ice would not significantly change after ~500 years when a new equilibrium is reached. In the coastal margins where the mean annual surface air temperature is less than -5°C, the changes in accumulation rate vary non-linearly with changes in temperature. An increase in temperature results in a decrease in accumulation tending towards a negative or ablation rate which reduces the equilibrium ice thickness and leads to a positive sea-level contribution. Similarly, increased sea temperatures would also result in increased basal melt rates of glacier tongues and ice shelves. The increase in the combined basal and surface melt rates of the ice shelves lead to their disintegration which results in the increased ice flow of the adjacent glaciers.

On the basis of the above it is clear that the Antarctic Peninsula would make short-term contributions to global sea-level change for periods of a few hundred years before new equilibriums were reached. Drewry and Morris (1992) calculated that the transient response of the Antarctic Peninsula to climate fluctuations of 1-2°C over short time periods of decades would contribute to sea-level at rates of 0.01-0.03 mm a^{-1}. Despite

the large total accumulation the Peninsula receives (23% of the whole of Antarctica), the entire ice mass is equivalent to only 0.54 m of equivalent sea-level. Therefore, it is likely that net mass balance changes in the Antarctic Peninsula contributed less than 0.1 m to sea-level in response to Holocene climate fluctuations over periods of a few thousand years. It is probable that such a contribution is more likely for short-term fluctuations such as the Little Climatic Optimum and the Little Ice Age during the Neoglacial. Further, there is no field evidence to support large changes in the ice volume of the Antarctic Peninsula during the Holocene, in addition to the contraction since LGM.

8.3.2 EAST AND WEST ANTARCTICA

Evidence from glacial geological studies for a widespread advance of East Antarctic outlet glaciers during the Mid-Holocene has been described and examined in Chapter 6. In summary, outlet glacier thickening and grounding line advances between 7,000 to 4,000 years B.P. have been reported for the Lambert Glacier-Amery Ice Shelf system, the Mertz-Ninnis Glaciers in George V Land, and the smaller Terre Adélie glaciers by Domack et al. (1991). Denton et al. (1989a) have reported thickening of the Transantarctic outlet glaciers draining the East Antarctic interior to the western Ross Embayment, during the Early to Mid-Holocene. The geographic spread of these similar morphological changes together with their synchroneity suggested that these outlet glaciers were driven by the same forcing mechanisms, of relative sea-level lowering and increased accumulation due to Early Holocene climate warming. A sensitivity analysis of the response of the Lambert Glacier-Amery Ice Shelf system to both increased accumulation and relative sea-level changes near the grounding line (Chapter 7) indicated that the Mid-Holocene expansion could have been initially forced by relative sea-level lowering causing local grounding of the Amery Ice Shelf. This occurred at 9,000 to 7,000 yr B.P. when the rate of post-glacial eustatic sea-level rise was decreasing and the isostatic uplift of the Amery Basin, which probably lagged the eustatic rise by ~2,000 years, was occurring at a greater rate. The subsequent 150 km advance of the grounding zone was probably forced by a 20% increase in accumulation above the Holocene long-term rates during the Early Holocene Climatic Optimum (EHCO) (11,000 to 9,000 years B.P.) in conjunction with a 7% decrease in ablation rates during the Mid Holocene Cool Period (MHCP) (8,000 to 6,000 yr B.P). A 20% increase in EHCO accumulation and a 7% decrease in MHCP ablation rates were estimated using recent accumulation and temperature relationships, and the ablation-temperature relationships of Budd (1967), together with the proxy Holocene temperature records obtained from the deep ice cores (Ciais et al., 1992). The combined effect of increased accumulation and decreased ablation on the Lambert

Glacier was to cause a thickening of ~100-150 m equivalent to an increase in total ice outflow by 18%, assuming a negligible change in the ice flow rate.

An additional sensitivity analysis of the spatial accumulation pattern of the East Antarctic katabatic slope indicated that the greatest outlet glacier expansion would have occurred in the regions with the highest present accumulation rates, such as the western Ross Embayment, George V Land and Wilkes Land sectors. The least expansion would have occurred in Dronning Maud Land and Enderby Land where the present coastal margin accumulation rates are the lowest. The probable synchroneity of the expansion of the East Antarctic outlet glaciers was principally controlled by the decrease in the post-glacial eustatic sea-level rise during the Mid Holocene.

Widespread geographical evidence for a re-advance of the East Antarctic ice sheet margins during the Mid-Late Holocene was interpreted from a number of glacial geological studies, including a detailed study of the evolution of the Law Dome ice margin in Chapter 5. The glacial geological evidence extends from George V Land to Kemp Land and implies a similar forcing. Synchronous with this advance of the East Antarctic ice sheet margins has been an advance of Transantarctic alpine glaciers (Denton et al. 1989a) and the alpine glaciers in the Northern Prince Charles Mountains (Mabin, 1992). A sensitivity analysis of the response of the Law Dome ice sheet to increased accumulation during the EHCO and during the later warm period between 4,000 to 2,500 years B.P. indicated that the latter warming was responsible for forcing a 3 km wide advance of the ice margin between 4,000 to 1,000 years B.P.. It is postulated that relative sea-level lowering caused by isostatic and eustatic changes contributed a minor role to the advance. Thus it was concluded that the Mid-Late Holocene advance of the East Antarctic ice sheet margin and the alpine glaciers lagged the Mid Holocene expansion of the outlet glaciers, and was probably forced by the combination of accumulation increases during the EHCO and more importantly, the later SCO. It is consistent to infer that the West Antarctic ice sheet probably experienced similar glacial fluctuations on the basis of the spatial accumulation patterns outlined in Chapter 2 and the similar Holocene sea-surface temperature records determined for both the Indian Ocean and Atlantic Ocean sectors of the Southern Ocean (Labracherie et al., 1989, Charles and Fairbanks, 1992).

In summary, the glaciological sensitivity analyses suggest that the evidence in the glacial geological studies is consistent with the variation of ice sheet accumulation rates throughout the Holocene, and that synchronous or teleconnected episodes of glacial advance and retreat of the ice sheet and the outlet glaciers occurred. This strongly suggests that the Antarctic mass balance contribution to sea-level has fluctuated

throughout the Holocene, in addition to the continuation of the retreat of the LGM ice sheet margins. This is particularly the case in the period during the Mid-Late Holocene. In contrast many glacial geologists and geophysicists have previously assumed that Antarctica has been stable since the LGM deglaciation was completed at 5,000 years B.P., with a subsequently negligible effect on sea-level.

One way to estimate the Antarctic mass balance contribution to sea-level is to determine the magnitude of the major fluctuations in ice sheet accumulation rates throughout the Holocene, in combination with the estimated Early-Mid Holocene melting rates. The method involves the determination of the relative differences in the total Antarctic accumulation rate (excluding the Antarctic Peninsula) throughout the Holocene, with respect to the long-term mean rate. The palaeo-accumulation rate change with respect to the long-term Holocene mean rates during each of the major Holocene warm and cool climatic periods (as defined in Figure 1.5 after Ciais et al., 1992), was determined according to the proxy accumulation-temperature relationships of 20%/°C in the ice sheet interior and 25%/°C in the coastal margins (Chapter 3). These relationships were based on the observed rate of accumulation and temperature change over the last few decades at Dome C (Pourchet et al., 1983), in Wilkes Land and the Lambert Glacier Basin (this study), and in Dronning Maud Land (Isaksson et al, submitted). Accumulation rate estimates for the Holocene climate fluctuations using the above method are calculated as 20% and 25% higher during the EHCO, 8% and 10% lower during the MHCP, and 8% and 10% higher during the SCO, for the interior and coastal regions respectively. These are in good agreement with the palaeo-accumulation rates shown in Figure 6.10 (relative to the Holocene long-term mean), as determined from ^{10}Be measurements on the Vostok and Dome C ice cores (Jouzel et al., 1989). These measurements suggest palaeo-accumulation rates during the EHCO were ~20-25% higher than the Holocene long-term mean, 10% lower during the MHCP, and similarly ~15-20 % higher during the SCO.

The best estimate of the long-term Holocene mean accumulation rate for Antarctica is considered to be the mean for the last century (Lorius et al., 1979). The total accumulation rate for Antarctica was calculated accordingly as 2004 Gt a^{-1} in the previous section. This was proportioned into the total rate for the interior (>1500 m elevation) and coastal margin zones (<1500 m elevation) of the ice sheet according to Drewry and Morris (1992). They reported that the interior zone receives 40% of the total annual accumulation whilst the coastal margins excluding the Antarctic Peninsula receives 8% of the total annual accumulation. The total annual accumulation rates for the interior and coastal margin zones of the East and West Antarctic ice sheet are; 802 Gt a^{-1} and 160 Gt a^{-1}, respectively. According to Jacobs et al. (1992) an accuracy of

±20% applies to these most up-to-date accumulation estimates. The remaining 52% of the total annual accumulation occurs on the ice shelves and on the Antarctic Peninsula.

Table 8.2 lists the accumulation rate changes for an equivalent 20%/°C relationship for the ice sheet interior together with those for a 25%/°C relationship for the coastal margins. The cumulative accumulation rate changes were multiplied by the duration of the climate interval to deduce the total change in relative surface mass balance across Antarctica. These relative surface mass balance changes are expressed as equivalent sea-level contributions in Table 8.2. The total change in sea-level contribution is also shown for the duration of the temperature fluctuations between 11,000 years B.P. to the present.

TABLE 8.2 HOLOCENE RELATIVE SURFACE MASS BALANCE CHANGES AND SEA-LEVEL CONTRIBUTIONS FOR PERIODS WHERE CLIMATE DEVIATED FROM THE HOLOCENE LONG-TERM MEAN

Holocene period (ka B.P.)	Long-term accumulation rate (Gt a^{-1})	Change in total accumulation (Gt)	Sea-level Contribution (m)
Interior		for 20%/°C	
11-9 (EHCO)	802	+320,800	-0.88
8-6 (MHCP)	802	-192,480	+0.53
4.0-2.5 (SCO)	802	+96,240	-0.26
Coastal Margin		for 25%/°C	
11-9 (EHCO)	160	+80,000	-0.22
8-6 (MHCP)	160	-32,000	+0.09
4.0-2.5 (SCO)	160	+24,000	-0.07
Combined			
11-9 (EHCO)	962	+400,800	-1.10
8-6 (MHCP)	962	-224,480	+0.62
4.0-2.5 (SCO)	962	+120,240	-0.33

The calculations in Table 8.2 show that excess surface mass balance over steady state (Holocene long-term mean) would have accumulated over both regions during the Early-Mid Holocene. The sea-level contributions are used to construct comparative equivalent sea-level curves for Antarctica during the Holocene in the following Section 8.4.

During the EHCO an excess ice mass equivalent to ~1.1 m of sea-level probably accumulated on the ice sheet (Figure 8.1) and would have partially offset the sea-level rise contribution of the concurrent deglaciation of the margins of the LGM ice sheet. From the glacial geological evidence it is postulated that such an ice sheet thickening led to an expansion and grounding line advance of the major East Antarctic outlet glaciers, culminating at 5,000 years B.P. with retreat under way by 4,000 years B.P.. During this period of glacial expansion, the thickening forced by the accumulation increases during the EHCO was partially offset by decreased accumulation rates during the intervening MHCP. Thus the possible ice sheet thickening between 11,000 to 5,500 years B.P. is reduced to an ice mass equivalent to a sea-level change of -0.35 m for the interior region and to -0.13 m for the coastal margin region (Figure 8.1). Since velocities are slow, typically less than 20 m a^{-1} in the ice sheet interior and the typical ice sheet reaction time to accumulation rate changes is between 15,000-20,000 years, the excess accumulation would remain stored in the ice sheet above 2500 m elevation throughout the Holocene. A net thickening of 10-15 m for the ice sheet interior zone above 2500 m, was calculated for the period 11,000-5,500 years B.P., based on a mean Holocene accumulation rate of 0.03 ma^{-1} ice for the interior zone. This thickening or excess mass is equivalent to ~0.2 m of sea-level and has remained in the ice sheet interior during the Holocene because of the very long reaction times. The remaining 0.15 m of equivalent sea-level stored on the interior region between the 1500-2500 m elevation contours may have been discharged via the outlet glaciers by ~4,000 years B.P.. At this time, the outlet glaciers and the ice sheet margins would also have discharged the 0.13 m sea-level contribution accumulated in the coastal margin region back to the ocean using the present ice velocity estimates. Thus Antarctica probably contributed a sea-level rise of +0.28 m via the outlet glaciers between 5,500 to 4,000 years B. P., in addition to the mass loss from the retreating margins. The retreat of the outlet glaciers by 4,000 yr B.P. was probably due to a negative mass balance in the interior of the drainage basin from decreased accumulation and increased glacier velocities.

Between 4,000 to 2,500 years B.P. during the SCO, increased ice sheet accumulation rates would have been responsible for an equivalent sea-level change of -0.33 m,

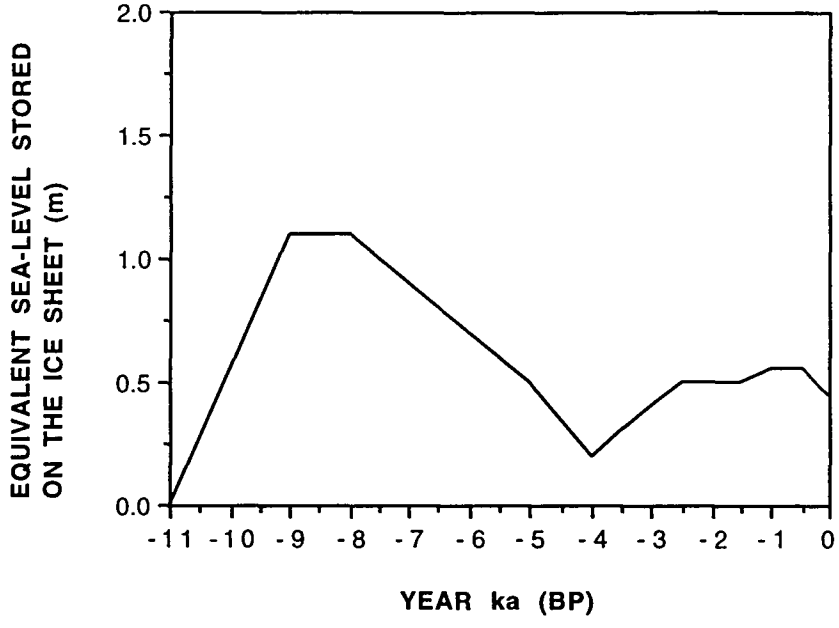

Figure 8.1 The Holocene equivalent sea-level contribution of excess surface mass balance (above that required for balance) stored on the Antarctic ice sheet. The cumulative curve was constructed from the sea-level contributions caused by fluctuations in palaeo-accumulation rates as calculated in Table 8.2, together with the geological evidence for glacial fluctuations (Chapters 4, 5, 6 and 7), and the morphology and present ice dynamics of the ice sheet (Chapters 2, 3 and 7).

although the continued retreat of the outlet glaciers during this period, possibly offset this sea-level change by up to +0.1 m. The Late Holocene glacial history at Law Dome (Chapter 5), Vestfold Hills (Fitzsimons, 1991) and in Northern Victoria Land (Baroni and Orombelli, 1994) indicates that the coastal margins and outlet glaciers were probably in an expansion phase since 3,500 to 4,000 years B.P.. In the subsequent period to 1,000 years B.P., accumulation rates were interpreted from the $\delta^{18}O$ records at DSS and Dome C to be close to the long-term mean, except for during the LCO (1,000 to 1,400 years B.P.). The higher (+10%) accumulation rates during the LCO possibly contributed a further sea-level lowering of 0.06 m. The decrease in accumulation rates during the Little Ice Age possibly contributed a slight sea level change of +0.035 m. Since 500 years B.P. there is some evidence for a 0.5-1 km retreat or contraction of the Law Dome ice margin north of the Løken Moraines (Chapter 5) and a similar contraction of the Sørsdal Glacier, an East Antarctic outlet glacier in the Vestfold Hills (Fitzsimons, 1991). If such an ice margin retreat of 0.5-1.0 km was widespread around the total Antarctic Ice Sheet margin, a sea-level rise of +0.05-0.1 m of sea-level may have occurred (after Walcott, 1975). Thus, Antarctica possibly contributed a sea-level rise of up to +0.1 m since 500 years. This contribution is equivalent to the Antarctic contribution of +0.24 mm a^{-1} calculated in section 8.2 for the period 1900-1970.

Without detailed glacial geological evidence of Holocene ice sheet and glacier fluctuations across Antarctica, the spatial variation in accumulation patterns has not been able to be taken fully into account in the determination of sea-level contributions. Hence, these estimates of the sea-level contribution of the Mid-Late Holocene glacial fluctuations across Antarctica are biased towards the glacial history of Wilkes Land and the Lambert Glacier-Amery Ice Shelf drainage basins in particular.

8.4 THE DETERMINATION OF A HOLOCENE EQUIVALENT SEA-LEVEL CURVE FOR ANTARCTICA

There have been numerous estimates of the total eustatic sea-level contribution from the Late Pleistocene deglaciation of Antarctica. These have been discussed in Chapter 4 and can be summarised as follows; 25 m from the CLIMAP reconstruction (Stuiver et al., 1981) comprising of 8.4 m from East Antarctica and 16.3 m from West Antarctica; 8 m from the glacial geological evidence in Drewry (1979); 2.5 m from Colhoun et al. (1992); and 12 m from the modelling study of Huybrechts (1992) based on the most recent glacial marine geological evidence for the Weddell Sea (Grobe et al., 1993) and for the Ross Sea (Denton et al. 1989).

Relative sea-level modelling by Clark and Lingle (1979) used a eustatic contribution of 25 m for Antarctica in conjunction with a total post-glacial eustatic sea-level rise of 100 m. More recently, Nakada and Lambeck (1988) used a eustatic contribution of 37 m for Antarctica and a total post-glacial eustatic sea-level rise of 130 m. The other major work by Tushingham and Peltier (1991) calculated a eustatic contribution of 27 m for Antarctica and used a total post-glacial eustatic sea-level rise of 120 m. The latter is in agreement with the best field evidence of 121 ± 5 m from Fairbanks (1989).

The discrepancies between the glacial geological evidence and the modelling is exacerbated by the estimates of the timing and duration of the Antarctic deglaciation. Peltier (1988) concludes from his ICE-2 model that the Antarctic ice sheet did not commence deglaciation prior to 11,000 years B. P. and was complete by 6,000 years B.P. whilst Tushingham and Peltier (1991, 1992) developed their relative sea-level model (ICE-3G) on the basis that the Antarctic ice sheet commenced deglaciation by 9,000 years B.P. with melting completed by 4,000 years B.P.. Nakada and Lambeck (1988, 1989) have based their ANT-3a and 3b models on the commencement of deglaciation at 17,000 years B.P. or synchronous with the deglaciation of the Northern Hemisphere ice sheets. The ANT-3a + b models in contrast to the other models have melting continuing after 4,000 years B.P., following a rapid eustatic sea-level rise of 25 m between 12,000 years B.P. and 6,000 years B.P..

In contrast, the current body of glacial geological evidence allows a substantially different interpretation of the Late Pleistocene-Holocene glacial and melting history of Antarctica. This is summarised as follows. The glacial geological evidence indicates that deglaciation was well under-way along the Southern Ocean segment of the East Antarctic coast before 11,000 years B.P. with the Lambert Glacier-Amery Ice Shelf close to its present configuration by 10,700 years B.P. (Domack et al., 1991) together with outlet glaciers adjacent to the Bunger Hills by 11,600 years B.P. (Bolshiyanov et al., 1991). Denton et al. (1989a) reported that the deglaciation of the Ross Ice Sheet was initiated by 16,000 years B.P. and was well underway by as early as 13,040 years B.P. along the western Ross Embayment. Lorius et al. (1985) reported that climate warming and increased accumulation rates had commenced at Dome C by 15,000 years B.P. from the interpretation of oxygen isotope records. Denton et al. (1989a) reported that deglaciation in the western Ross Embayment was complete by 6600-6020 years B.P. whilst Goodwin (1993b) reported that deglaciation of the grounded Law Dome ice margin on the East Antarctic coast was completed on the southern and outer Windmill Islands by 8,000 years B.P. with a continued retreat and emergence of the inner coastline to between ~4,500 years B.P. (Chapter 5). The grounded ice margin at this time was located further inland than the present margin.

The pattern of deglaciation of the grounded East Antarctic ice margin reported by Goodwin (1993) and in Chapter 5 is supported by field evidence in Colhoun and Adamson (1991, 1992) for the Bunger Hills, in Fitzsimons (1990) and Adamson and Pickard (1986) for the Vestfold Hills, and in Gillieson et al. (1990) for the Larsemann Hills.

Whilst the Antarctic deglaciation had commenced by 16,000 years B.P., the bulk of the deglaciation lagged the Northern Hemisphere deglaciation since the main mechanism for deglaciation was the marine ice bed decoupling in response to rapidly rising eustatic sea-level (Hollin, 1962, Thomas and Bentley, 1978). Thomas and Bentley (1978) suggested that retreat rates of 25-70 km/yr would have been possible during the decoupling of the Ross Ice Sheet. Since the outlet glaciers along the East Antarctic coast had retreated to near their present termini by 10,000 years B.P. it is probable the bulk of the deglaciation of the marine based ice sheets and ice shelves had occurred between 14,000-10,000 years B.P. during which the eustatic sea-level had rapidly risen approximately 50-60 m (Fairbanks, 1989) and the climate warming of the Early Holocene climatic optimum had commenced. It is also likely that the grounded ice sheet margins were progressively deglaciated over this period and perhaps accelerated between 10,000 to 8,000 years B.P., following the removal of the buttressing by fringing ice shelves and the rapid climate warming of the Early Holocene climatic optimum. The retreat of the remaining grounded ice margins to inland of their present configurations occurred between 8,000-4,500 years B.P., probably at a much slower rate (from evidence in the Windmill Islands and the Vestfold Hills). The slowing was due to the eustatic sea-level rise tailing off, and in part due to the ice sheet thickening in the interior in response to increased accumulation rates during the Early Holocene and the Glacial Transition period. This thickening led to the Mid-Late Holocene glacial expansion of the Antarctic coast between 7,000 to 4,000 years B.P.. This study has proposed that the subsequent retreat possibly contributed a sea-level rise of 0.3 m between 5,500 to 4,000 years B.P..

On the basis of this glacial history, equivalent sea-level curves were constructed from the net contributions of excess mass stored on the ice sheet from surface mass balance fluctuations, and from the contraction of the LGM ice sheet margins and outlet glaciers during the Holocene. The net sea-level curves (shown in Figure 8.2) were calculated by subtracting the cumulative curve of excess mass (above that required for balance) stored on the ice sheet (Figure 8.1) from the Late Glacial melting curves estimated for the minimum LGM contribution of 2.5 m (Colhoun et al., 1992) and the estimate of 12 m (Huybrechts, 1992), which was taken as a plausible maximum estimate, for comparison. In the absence of a relative sea-level curve for Antarctica it was assumed

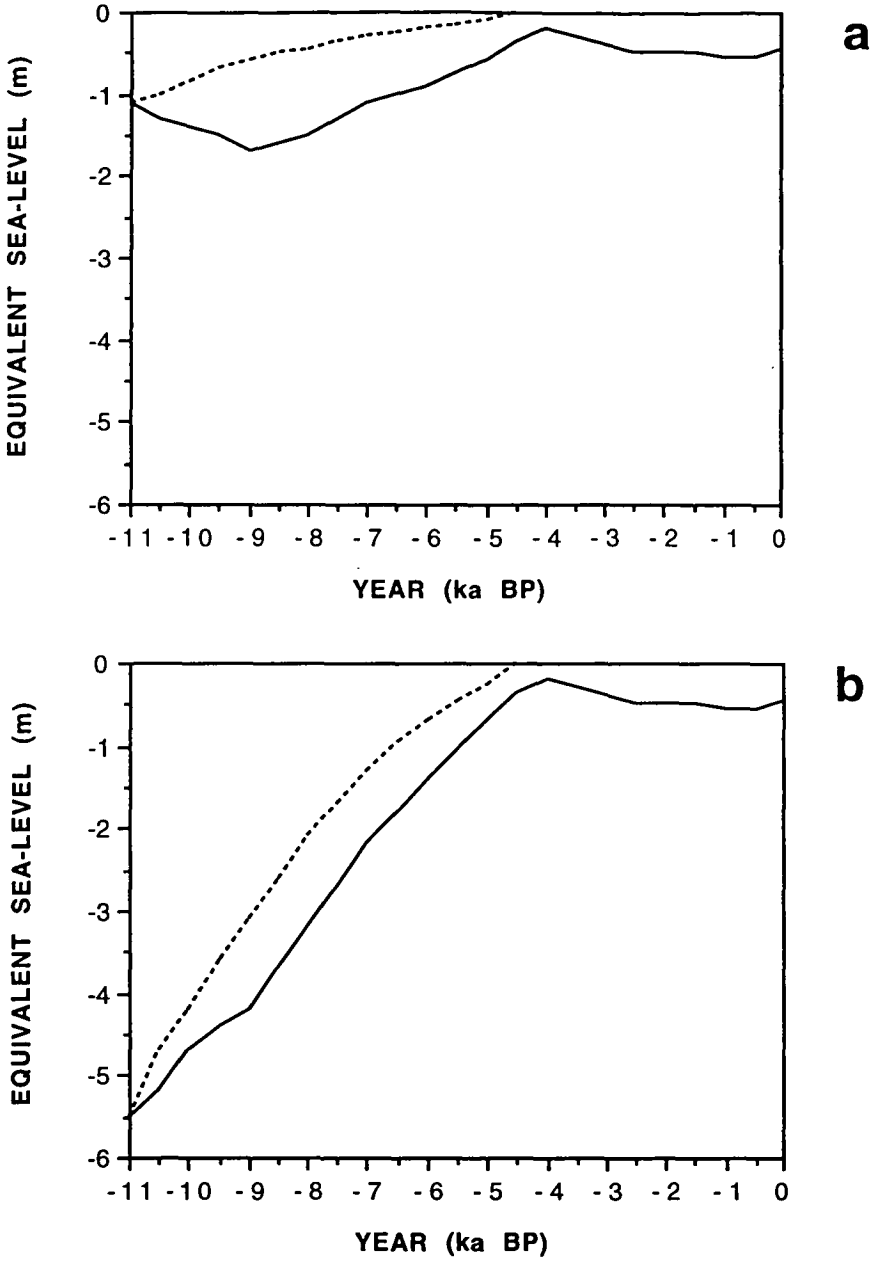

Figure 8.2 Equivalent net sea-level curves for Antarctica (solid lines), constructed from the addition of the post-glacial meltwater contribution from the retreat of the LGM ice margins (dashed lines), and the Holocene excess surface mass contribution (above that required for balance) which has accumulated on the ice sheet as a result of climatic fluctuations (calculated from Table 8.2 and shown in Figure 8.1). Figure (a) is constructed using the minimum post-glacial meltwater contribution of 2.5 m (Colhoun et al., 1992) (dashed curve). Figure (b) is constructed from the plausible maximum postglacial meltwater contribution of 12 m (Huybrechts, 1992) (dashed curve).

from the glacial geological evidence that two-thirds of the meltwater volume was probably added to the oceans between 16,000 to 10,000 years B.P.. The minimum and maximum Holocene curves for the melt contribution from the retreat of the LGM ice sheet margins together with the net sea-level curves are shown in Figures 8.2a and 8.2b, respectively.

The ice sheet thickening during the EHCO resulted in a simultaneous slowing of the sea-level rise contribution, due to the continuing deglaciation of the LGM margins (Figure 8.2b). Alternatively, Figure 8.2a shows that ice sheet thickening during the Early Holocene could have offset the small post-glacial meltwater contribution proposed by Colhoun et al. (1992), resulting in a net sea-level contribution of -0.6 m between 11,000-9,000 yr B.P.. Between 8,000-4,000 years B.P. Antarctica probably contributed a sea-level change of between +1.3 m (Figure 8.2a) to +3.0 m (Figure 8.2b) from the recession of the ice margins culminating at 4,500 years B.P. and the retreat of the outlet glaciers following the Mid-Holocene expansion. A sea-level change of -0.35 m was probably contributed between 4,000-2,500 years B.P. as a result of increased ice sheet accumulation. The magnitude of the net sea-level change between 4,000-2,500 years B.P. is dependent upon the volume of meltwater added to the oceans from the retreat of the outlet glaciers and was estimated as ~-0.3 m. It is likely that the majority of the outlet glaciers had retreated by 4,000 yr B.P.. Between 2,500-1,000 years B.P. Antarctica probably contributed a slight sea-level change of -0.05 m as a result of sustained higher accumulation rates than the long-term mean rates. Since 500 years B.P. Antarctica has probably contributed a sea-level change of +0.1 m up to the present, due to increased outflow, decreased average accumulation rates and recession of the ice margins. The equivalent sea-level curves in Figure 8.2a and 8.2b, indicate that the present ice volume of the Antarctic ice sheet is slightly greater (equivalent to -0.2 m of sea-level change) than at 4,000 years B.P. due to a net thickening of the ice sheet.

8.5 VALIDATION OF THE HOLOCENE ANTARCTIC SEA-LEVEL CURVE

The following discussion compares the calculated Antarctic equivalent sea-level curve (Figure 8.2a and b) with that previously applied in geophysical modelling, and the relative sea-level histories of oceanic islands for the Mid-Late Holocene. The dependence of the global sea-level models on the Antarctic glacial history during the Mid-Late Holocene , is also discussed together with their implications for future modelling. These comparisons enable a validation of the proposed Antarctic sea-level

curve, and its implications for the geomorphological interpretation of Mid-Late Holocene sea-level fluctuations.

8.5.1 SUMMARY OF HOLOCENE RELATIVE AND EUSTATIC SEA-LEVEL HISTORY AS DETERMINED BY MODELLING

Clark et al. (1978) reported the results of a global isostatic model of the sea-level response to changing earth and meltwater loads which predicted six sea-level zones with a distinct relative sea-level curve for the Mid-Late Holocene. These sea-level zones were defined on the basis of distance from the LGM ice sheets and areas of glacio-isostatic rebound in the Northern Hemisphere and are highly dependant upon the lithospheric thickness, and the upper and lower mantle viscosity of the continental margins and the ocean floor. Their model did not include the partial deglaciation of Antarctica which was rectified in a subsequent paper Clark and Lingle (1979). The inclusion of Antarctica into the global isostatic model has significant effects on the delineation of these zones in the Southern Hemisphere. Figure 8.3 shows the distribution of these six sea-level zones and typical sea-level curves as defined by the model of Clark and Lingle (1979) under the assumption that meltwater was added to the oceans as a linear function since 18,000 years B.P. and no eustatic change has occurred since 5,000 years B.P.. The importance of this modelling is that it shows that the type of relative sea-level response is varied across the globe rather than the fluctuations being synchronous or monotonic. Clark and Lingle (1979) determined that each zone characterised either submergence or emergence during the Mid-Late Holocene. The relative sea-level history of Zones 3 and 5 are particularly sensitive to further meltwater additions during this period. The latter have been assigned to Antarctic sources by Clark and Lingle (1979) and later by Tushingham and Peltier (1991) and Nakada and Lambeck (1988, 1989) to explain the relative sea-level histories. Clark and Lingle (1979) calculated that the Zone 5 region would be reduced to a small band in the Southern Ocean (including New Zealand) if as little as 0.7 m of eustatic sea-level rise from continued exponential melting of Antarctica had occurred between 5,000 years B.P. and the present. The Zone 3 entirely disappears with a meltwater addition. Alternatively, Nakada and Lambeck (1988, 1989) have shown through similar lithospheric modelling that Mid-Late Holocene emergence can be expected for the entire Zone 5 region in Figure 8.3, even if continued melting of Antarctica occurred throughout the Late Holocene.

The relative sea-level history at the far field sites in Zone 5 is not sensitive to the ice-load in Antarctica (Nakada and Lambeck, 1989) and would not be significantly different if the meltwater originated in the Northern Hemisphere. Therefore, the

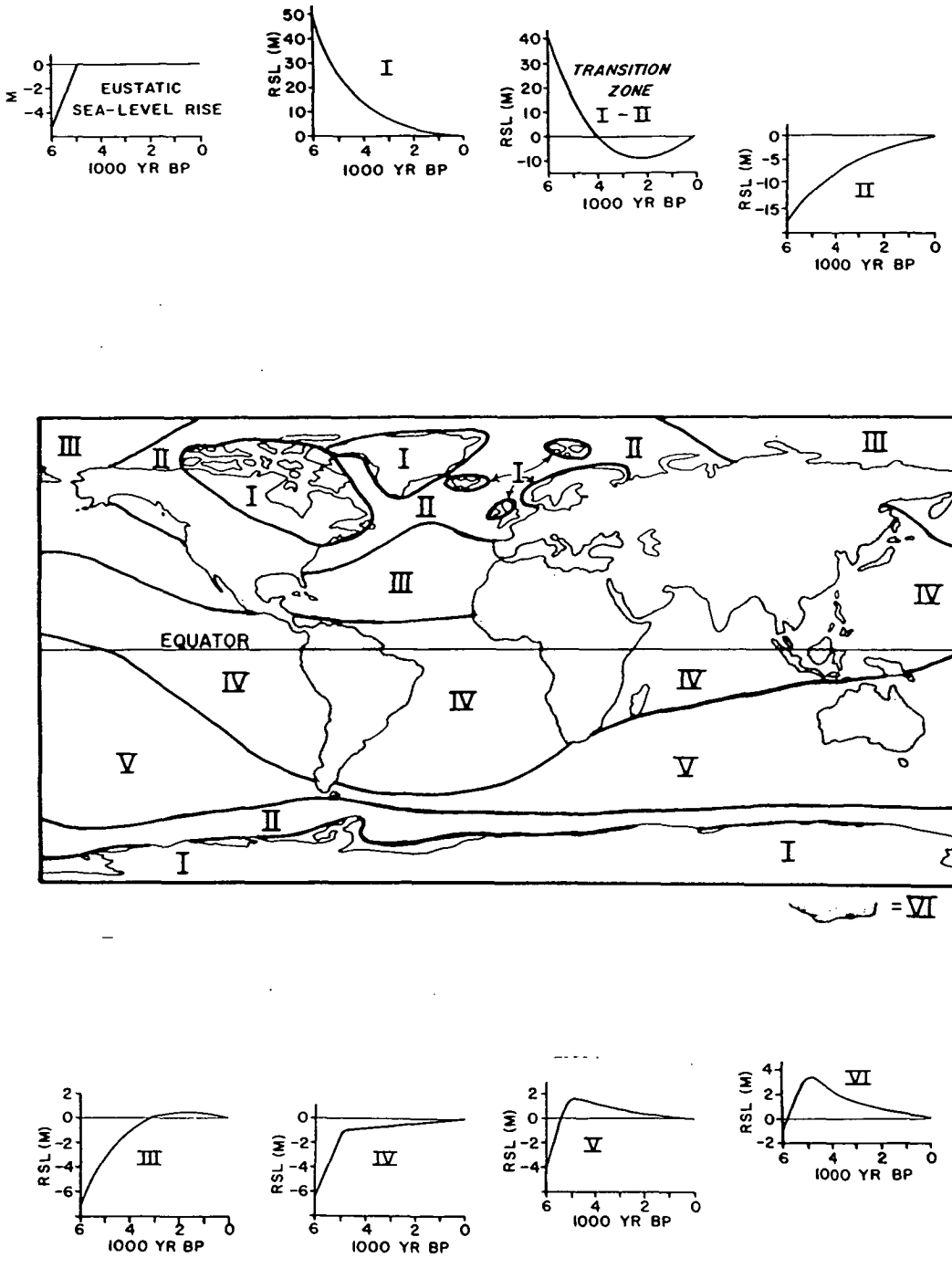

Figure 8.3 The global distribution of Holocene sea-level change zones predicted by Clark and Lingle (1979) for the Antarctic linear ice retreat history, together with the typical relative sea-level curves predicted for each zone by Clark et al. (1978) under the assumption that no eustatic change has occurred since 5,000 yr B.P.. Zone 6 (not shown) includes all continental margins except those that lie in zone 2 (from Clark and Lingle, 1979). The Antarctic continental shelf lies in the transition zone 1-2 and zone 2.

modelling of the Mid-Late Holocene sea-level history in Zone 5 by Clark and Lingle (1979), Tushingham and Peltier (1991) and Nakada and Lambeck (1988, 1989) is largely independent of the disputed Late-glacial to Holocene total meltwater contribution from the contraction of the LGM Antarctic ice sheet. In addition, the disputed volume of meltwater equivalent to 12-25 m of sea-level from Antarctica must have been contributed to the oceans prior to 5,000-6,000 years B.P. on the basis of the geological evidence and irrespective of its origin. The most likely alternate source of this meltwater must be from the deglaciation of the Northern Hemisphere ice sheets.

The Zone 5 represents the far-field, a region remote from the effect of glacio-isostatic rebound where the relative sea-level history reflects the changes in ocean volume, isostatic crustal deformation due to ocean basin loading with increased water volume and tectonic deformations (Lambeck, 1990 and Nakada, 1986). Geomorphological studies (reviewed in Pirazzoli, 1991) have determined that the relative sea-level change at the continental margins in Zone 5 is typified by a rapid rise in sea-level up to 6,000 years B.P., culminating in a high-stand of 1-2 m above the present level, and followed by a subsequent uniform decrease to the present. The amplitude and timing of the high-stand varies significantly, depending upon coastline geometry, the rate of sea-level rise and the isostatic response of the mantle to the water load (Lambeck, 1990). Alternatively, similar studies determined that the relative sea-level change at the oceanic islands in Zone 5 is typified by a similar rapid rise in sea-level culminating in a much smaller amplitude high-stand of <1 m occurring between 4,000 to 2,000 years B.P. (Pirazzoli and Montaggioni, 1988, Lambeck, 1990).

Bloom (1967) recognised that the regional variations in the high stands were indicative of the different response of the Earth to the time-dependent meltwater and ice loads as the ice mass was transferred to the oceans. He also demonstrated that the relative sea-level history was much simpler to understand on oceanic islands than around the continental margins. Figure 8.4 shows the relative sea-level model of Bloom (1967). This shows that the relative sea-level histories on the continental margins reflect the displacement and deformation of both the continental shelves and the ocean basins to the hydro-isostatic effects of meltwater loading. In contrast, Bloom's model shows that the relative sea-level histories on oceanic islands predominantly reflect only eustatic sea-level changes. He concluded that 'oceanic islands were dipsticks which recorded the true magnitude of glacially-controlled sea-level changes'. In a subsequent work Nakada (1986) reported that the relative sea-level history of these oceanic islands has a significant dependency on the upper mantle rheology for islands with a radius greater than 10 km, and is independent of the upper mantle rheology for islands with a radius less than 10 km. Therefore, the relative sea-level history of these smaller

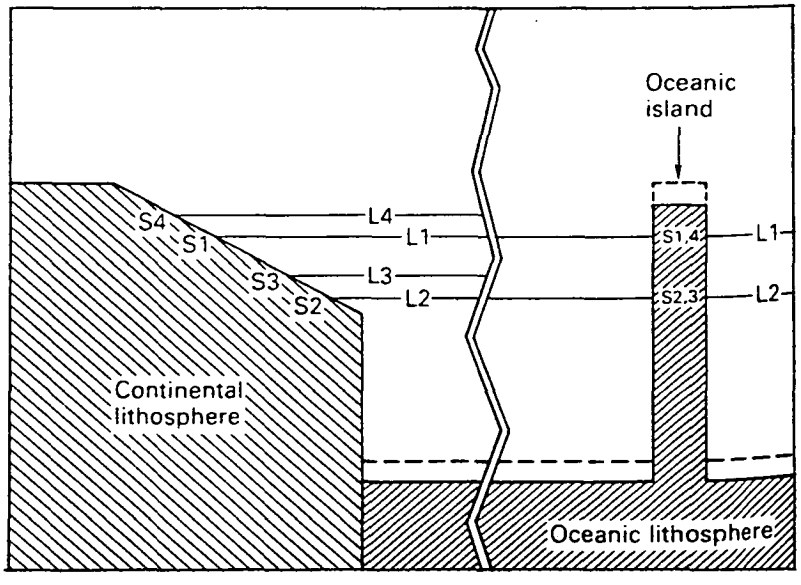

Figure 8.4 Analogue model of the development of Pleistocene shorelines on continental and oceanic island coasts (after Bloom, 1967). The diagram shows that the record of shoreline displacement on most oceanic islands does not include a significant hydro-isostatic component, which is experienced by the continental margins. Initial interglacial sea-level L1 produces shoreline S1. Glacial sea-level L2 produces shoreline S2. Isostatic rebound of the ocean floor carries the island up with it so, although the sea-level rises to L3, the shoreline position remains the same. Subsequent post-glacial sea-level rise is followed by a slow isostatic sinking of the ocean floor which lowers sea-level to initial position L1, but lowers the island the same amount, so that shorelines S4 and S1 remain superimposed.

islands, particularly small atolls, reflects the eustatic sea-level rise and global (ocean basin) isostatic adjustment (lower mantle viscosity) due to meltwater loading only, without the additional local hydro-isostatic adjustment due to differential loading of meltwater between the inside and the outside of larger islands. This makes the small islands and atolls ideal 'dipsticks' to determine the eustatic sea-level changes particularly if the lower mantle viscosity and the tectonic history of the islands can be determined.

8.5.2 COMPARISON OF THE ANTARCTIC SEA-LEVEL CURVE WITH THE SEA-LEVEL HISTORY DETERMINED FROM FIELD EVIDENCE ON MID-OCEANIC ISLANDS

Geomorphological and geological evidence of Holocene sea-level history on oceanic islands in the Atlantic, Indian and Pacific Oceans is summarised in Hopley (1987), Pirazzoli (1991) and Nunn (1994). The bulk of the relative sea-level history on the oceanic islands has been interpreted from coral reef stratigraphy since coral reefs generally respond to sea-level changes by maintaining their surface at or near sea-level. Other sea-level indicators which have provided chronological control include peat deposits, intertidal molluscs, and beachrock, together with erosional features such as tidal notches which have been undercut at the base of limestone formations (van de Plassche, 1986, Nunn, 1994). The following discussion of the geomorphological evidence concentrates on the sea-level histories derived from coral reef stratigraphy, including coral microatolls, reef framework, coralline algal crusts, and coral conglomerates.

There is a large variation in the Mid-Late Holocene sea-level history derived from coral reef stratigraphy between oceanic islands. This geographic variation in relative sea-level is primarily due to the variability of the vertical accretion rates of the coral reefs, and the regional tectonic history. Some of the variation may also be due to regional irregularities in the geoid and ocean basin lithospheric structure (Nunn, 1994). The variation in the sea-level data due to coral reef accretion rates can be minimised through the use of data which has been derived from coral reefs which have kept up with sea-level changes.

Neumann and MacIntyre (1985) classified coral reefs on the basis of their species composition into reefs which keep-up, catch-up or give-up in response to sea-level changes. Keep-up reefs are fringing and/or barrier in form and are found on windward, open narrow shelf environments, at depths less than 3 m. Catch-up reefs are found in protected shelf and back reef environments and give-up reefs are found

on broad, open and deep shelf environments. The keep-up reefs maintain shallow, frame-building communities throughout sea-level rise, and generally maintain a core facies of *Acropora palmata* . The keep-up reef builds by lateral accretion once the sea-level stabilises, and often become capped by reef flat rubble and fore reef pavement (Neumann and MacIntyre, 1985).

The variation in sea-level response during the Mid-Late Holocene between islands, atolls and regions can often be explained by tectonics, with some islands and atolls having experienced recent uplift, subsidence or stability. These atolls and islands have a volcanic origin. The smaller islands and atolls have formed on submerged seamounts which have generally experienced either stability or slight subsidence during the Mid-Late Holocene. The larger islands, such as Tahiti and Moorea in the Society Islands, have experienced downwarping and subsidence of the oceanic crust associated with active volcano-isostasy. This downwarping forms a concentric raised rim at distances up to a few hundred kilometres away (Pirazzoli and Montaggioni, 1985). Some islands have experienced both gradual and abrupt vertical movements during the Mid-Late Holocene which are associated with their youthful stage of volcanic development. Whilst this tectonism affects the potential for reconstructing eustatic sea-level changes, it does not preclude the interpretation of the Holocene high-stand, since this can be determined from relative elevation changes. Further, some studies such as those for the Fijian Islands in Nunn (1994), have shown that the tectonic movements can be interpreted and subtracted from the sea-level record to determine the eustatic component.

Table 8.3 lists the field evidence for the timing and magnitude of the Mid-Late Holocene high-stand on selected mid-oceanic islands in Zone 5 of the Indian and Pacific Oceans. The selected islands have been identified as being tectonically stable or subject to slight tectonism during the Mid-Late Holocene, by the respective researchers. They were also selected because the emergence dates were measured on samples from keep-up reefs in fringing or barrier reef complexes. Therefore, the widespread field evidence from the Pacific and Indian Oceans in Table 8.3 probably best describes the eustatic sea-level on the mid-oceanic islands. The mean emergence date and magnitude from Table 8.3 are 3,830 ± 520 yr B.P. and 1.0 ± 0.4 m, respectively.

TABLE 8.3 MID-LATE HOLOCENE HIGH STANDS ON SELECTED MID-OCEANIC ISLANDS

ISLAND	EMERGENCE DATE (yr B.P.)	EMERGENCE MAGNITUDE (m)	REFERENCE
Cocos-Keeling Atoll (Indian Ocean)	3000	1.0	Woodroffe et al., 1990
Rota and Guam, Mariana Islands (Zone iv)	4200	1.8	Kayanne et al., 1993
Vanua Levu, Fiji	4000	2.0	Miyarta et al., 1988
New Caledonia	3500	>1.0	Coudray and Delibrias, 1972
Enewetak Atoll, Marshall Islands	3500	>1.0	Buddemeier et al., 1975
Mangaia Island, Cook Islands	3700	1.1	Yonekura et al., 1988
Starbuck Atoll	3950	1.0	Tracey, 1972
Suwarrow Atoll, Cook Is	4220	0.5	Scoffin et al., 1985
Mopelia, Society Islands	3450	0.8	Pirazzoli and Montaggioni, 1988
Tupai, Society Islands	3580	0.7	Pirazzoli and Montaggioni, 1988
Takapoto, Tuamotu Islands	3540	>0.55	Pirazzoli and Montaggioni, 1988
Rangiroa Island, Tuamotu Island	3150	>0.85	Pirazzoli and Montaggioni, 1986
Mataiva Island, Tuamotu Islands	5210	0.75	Pirazzoli and Montaggioni, 1986
Vahitahi Atoll, Tuamotu Islands	4300	>0.65	Pirazzoli and Montaggioni, 1988
Reao Atoll, Tuamotu Islands	4250	>0.85	Pirazzoli and Montaggioni, 1988
Hereheretue Atoll, Tuamotu Islands	3825	>0.9	Pirazzoli and Montaggioni, 1988
Temoe Atoll, Gambier Islands	3740	0.7	Pirazzoli, 1987

The Mid-Late Holocene high-stand has been universally accepted as the time of the cessation of the Antarctic meltwater contribution since the Antarctic melting lagged behind the melting of the Northern hemisphere ice sheets (Clark and Lingle, 1979, Peltier, 1988 and Tushingham and Peltier, 1991). The field evidence reviewed in Table 8.3 would suggest that the timing of the high-stand is clustered around 3,800 years B.P. and supports the hypothesis presented in this study for a maximum Antarctic meltwater contribution terminating at 4,000 yr B.P. (Figure 8.2a and b). This contradicts the assumptions used in the lithospheric and sea-level modelling of Nakada and Lambeck (1988, 1989) for a continuation of the post-glacial meltwater contribution from Antarctica from 4,000 yr B.P. to the present.

Since the present sea-level was not reached on the majority of islands until ~5,000-6,000 yr B.P. (Pirazzoli, 1991) it is difficult to validate the Antarctic contribution during and prior to this time. However, the magnitude of the sea-level rise between 6,000-4,000 yr B.P. is important to determine since there is general agreement that the increase in sea-level from 6,000 yr B.P. to the high-stand at ~4,000 yr B.P. on oceanic islands is thought to be the result of the continued contribution of Antarctic meltwater. A few studies have reported field evidence of the magnitude of the sea-level rise between 6,000-4,000 yr B.P.. Kayanne et al. (1993) reconstructed sea-levels during this period on Rota and Guam Islands in the Mariana Island group. They dated emergent reef crests (54 samples) and tidal notches in the base of low limestone cliffs, and concluded that 1.8 m of sea-level rise had occurred at both islands during the period from 6,000 to 4,000 yr B.P.. In the Fiji Islands, along the southern coast of Vanua Levu, Miyarta et al. (1988) reported a sea-level rise of 1 m between 6,000 to 4,000 yr B.P. from a series of dated coral reefs and geomorphological observations. In the Tuamotu Islands of French Polynesia, Pirazzoli and Montaggioni (1988) reconstructed a sea-level rise of ~1.2 m for the period 6,000 to 4,000 yr B.P., from dated in situ coral microatolls and reef framework, and coral conglomerates. It is not possible to determine from this sparse body of field evidence, which of the two estimated Antarctic sea-level contributions (Figure 8.2a and b) better represent the eustatic changes during this period. Alternatively, the geophysical modelling of Nakada and Lambeck (1989) provides some indication of the likely Antarctic contribution to sea-level during the 6,000 to 4,000 yr B.P. period. Their Antarctic meltwater model known as ANT-3B (shown in Figure 8.5) in combination with regional estimates of the upper and lower mantle viscosity and lithospheric thickness, produces a good fit to the field evidence for

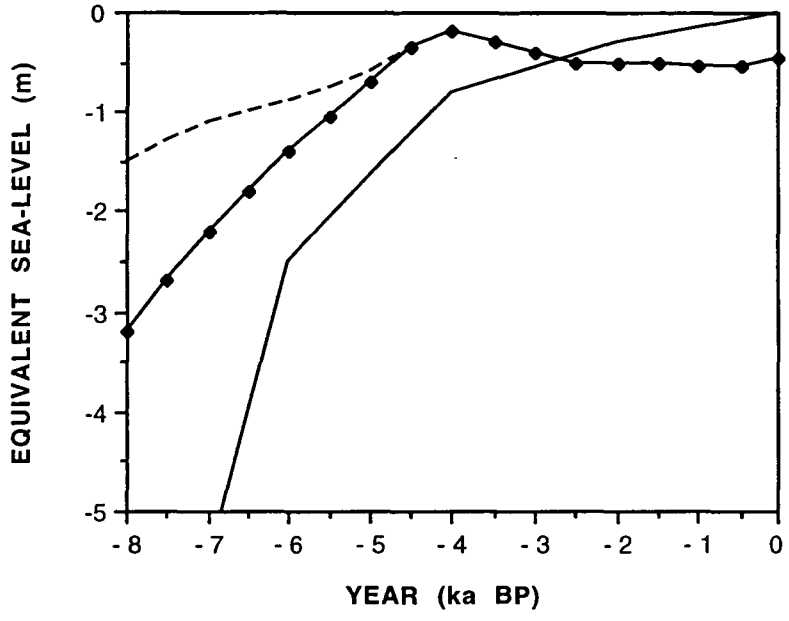

Figure 8.5 A comparison of the estimated Antarctica sea-level contributions in this study, with that known as the ANT-3B model used by Nakada and Lambeck (1989), in their global sea-level and lithospheric modelling. The ANT-3B model is shown by the solid line. The estimated maximum contribution from this study (derived from Huybrechts, 1992, Figure 8.2b) is shown by the solid line with the diamonds, and the estimated minimum contribution from this study (derived from Colhoun et al., 1992, Figure 8.2a) is shown by the dashed line with the diamonds.

Holocene high-stands at 6,000 yr B.P. around the Australian continental margin, and at 4,000 yr B.P. on the mid-oceanic islands. Their model simulates an Antarctic sea-level contribution of 1.7 m between 6,000 and 4,000 yr B.P.. The two estimated Antarctic sea-level contributions from Figure 8.2a and b are also shown in Figure 8.5 for comparison. The Antarctic sea-level contribution of 1.2 m (from Figure 8.2b) derived from the combination of Holocene accumulation changes and the post-glacial contribution (12 m) of Huybrechts (1992) is closer to both the limited field evidence and the ANT-3B contribution than the 0.7 m (from Figure 8.2a) calculated from the minimum post-glacial contribution (2.5 m) of Colhoun et al. (1992) and the Holocene accumulation changes. Further, the minimum estimate of 0.7 m (Figure 8.2a) would be reduced to ~0.2 m for the post-glacial meltwater contribution without the addition of the Holocene accumulation changes. Similarly, the maximum estimate of 1.2 m (Figure 8.2b) would be reduced to ~0.6 m. This suggests that Antarctica could not have contributed a sea-level contribution >1 m between 6,000 to 4,000 yr B.P. unless increased accumulation during the Holocene had partly forced a Mid-Holocene expansion and subsequent contraction of the outlet glaciers, and contributed a further 0.5 m to sea-level. Further, this analysis suggests that the minimum estimate (2.5 m) of post-glacial melting in Antarctica (Colhoun et al., 1992) may be considered an underestimate, since a greater post-glacial sea-level contribution is necessary to account for an Antarctic sea-level contribution > 1 m between 6,000 to 4,000 yr B.P..

The relative sea-level history on the mid-oceanic islands was examined further to compare the Antarctic sea-level contribution with the interpreted mid-ocean eustatic sea-level changes during the Late Holocene, since 4,000 yr B.P.. Whilst a large body of sea-level data on oceanic islands has been reconstructed from geomorphological observations and coral stratigraphy, few sea-level curves have been determined which are both relatively free of tectonic influences, and span the entire Mid-Late Holocene. The largest body of sea-level data which spans this period, has been interpreted from geomorphological surveys on 38 islands in French Polynesia (Pirazzoli and Montaggioni, 1988). French Polynesia spans approximately 2,500 km of the South Pacific Ocean and comprises the Society Islands, Marquesas Islands, the Tuamotu Islands, the Austral Islands and the Gambier Islands (Figure 8.6). The palaeo mean sea-level data summarised by Pirazzoli and Montaggioni (1988) were interpreted from a detailed study of radiocarbon-dated exposed corals, abandoned algal ridges and reef frameworks in the growth position, emerged tidal notches, and skeletal reef conglomerates. The palaeo mean sea-level data from a total of 38 islands are plotted against time in Figure 8.7 (after Pirazzoli and Montaggioni, 1988).

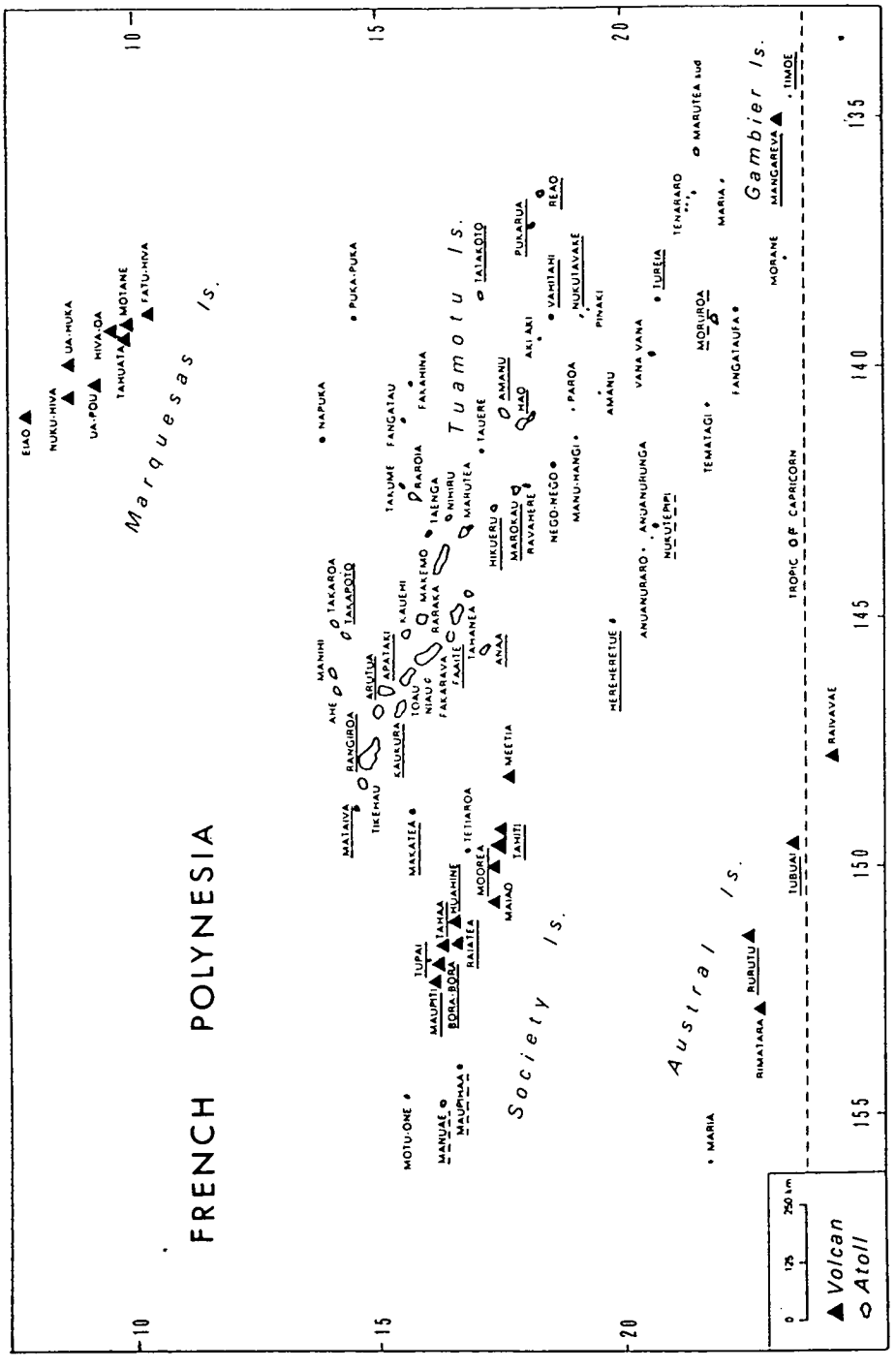

Figure 8.6 Location map of French Polynesia. Sea-level data were determined from coral stratigraphy and geomorphological observations on the islands underlined (after Pirazzoli and Montaggioni, 1988).

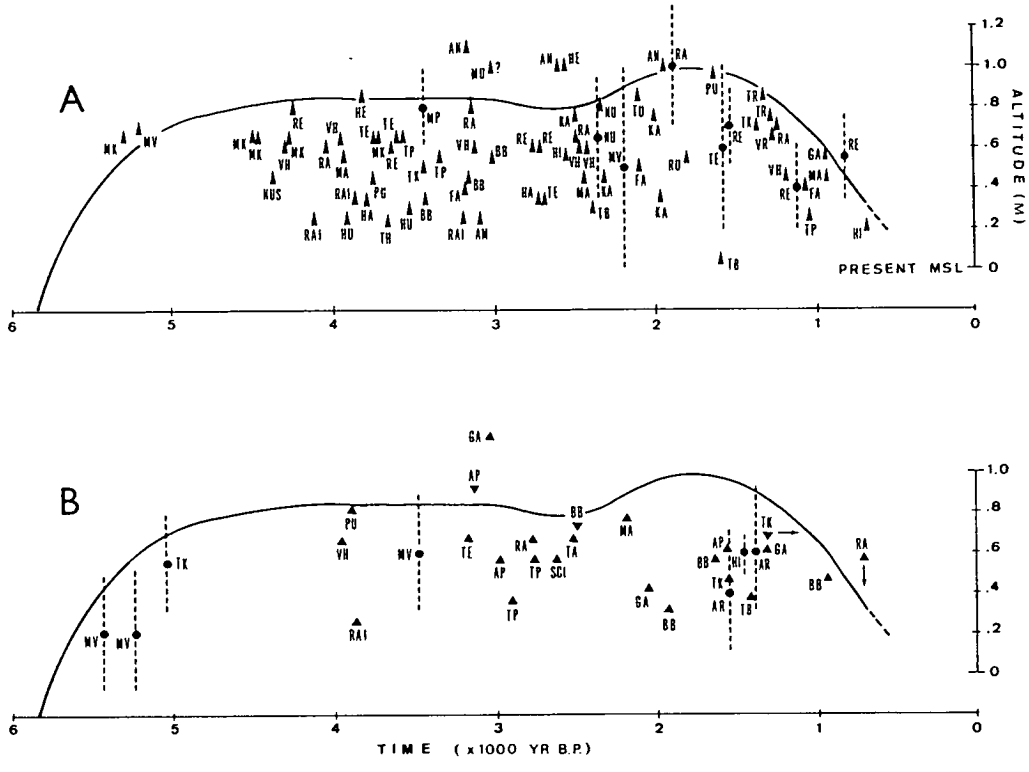

Figure 8.7 Temporal plot of radiocarbon-dated, palaeo mean sea-level data from French Polynesia (Pirazzoli and Montaggioni, 1988). Figure A. Samples collected in growth position with reliable radiocarbon ages for the corresponding MSL; arrows are minimum positions of reconstructed MSL; circles and vertical dashed lines represent estimated positions of reconstructed MSL and uncertainty limits. Figure B. Data deduced from reworked coral conglomerate and beachrock material. The corresponding radiocarbon ages are considered to be maximum ages for the corresponding MSL; triangles are minimum (upward vertex) and maximum (downward vertex) positions of reconstructed MSL; circles and dashed lines as for Figure A. The solid lines represent the best fitting MSL curves, as defined by the upper limit of the sea-level data.

The volcanic islands which form the Society Islands have experienced volcano-isostatic movement during the Holocene, due to lithospheric flexure centred on the volcanic edifices of the Leeward Islands and the Moorea-Tahiti group (Pirazzoli and Montaggioni, 1985). Thus the palaeo sea-level data from these islands do not represent the regional eustatic signal alone. In contrast, the 1,700 km long Tuamotu Island archipelago comprises entirely of atolls, formed on submerged truncated cones. These atolls are presently considered to be in volcano-isostatic equilibrium and relative vertical stability, since the vulcanism and hotspots on the ocean floor which probably formed their parent seamounts are located some 1,000 km to the south-east of the Tuamotu Island archipelago, near the East Pacific Rise (Pirazzoli and Montaggioni, 1985). Thus palaeo sea-level data from this archipelago most likely represents the regional eustatic sea-level history. Consequently, palaeo mean sea-level data from the atolls in the Tuamotu Island archipelago and the Gambier Islands were compiled from Pirazzoli and Montaggioni (1988), for comparison with the estimated Late Holocene Antarctic sea-level contribution. Only, palaeo mean sea-level data from atolls and islands less than 10 km in radius were selected, since they were not affected by local hydro-isostatic adjustments. The potential eustatic sea-level data were further culled to include only reliable data (estimated errors $<\pm 0.2$ m) from in situ coral, reef framework and coralline algal crusts which formed windward fringing or barrier, keep-up reefs. Palaeo mean sea-level data from beachrocks and coral conglomerates were excluded from the analysis because they generally had reliability estimates $>\pm 0.2$ m. The palaeo mean sea-level data were collected between 1980-85, during which the central south Pacific Ocean experienced fluctuations in sea-level of ± 0.1 m associated with El Niño-Southern Oscillation (ENSO) events (Wyrtki, 1985). Woodroffe and McLean (1990) examined microatolls of *Porites* corals in Kiribati, in the Pacific Ocean and Cocos (Keeling) Islands in the Indian Ocean, and determined excellent proxy sea-level records from the annual growth rings of the *Porites* microatolls, which were consistent with the sea-level variations recorded by tide gauges during the same period (1974-1988). Consequently, the French Polynesian palaeo sea-level data of Pirazzoli and Montaggioni (1988) are relative to mean sea-level (MSL) with an annual range of ± 0.1 m, since they were measured over a five year period, during which the major El-Niño event occurred in 1982-83 (Wyrtki, 1985).

The selected palaeo mean sea-level data are shown in Figure 8.8 and indicate that eustatic sea-level in French Polynesia reached a high-stand at 3,800 yr B.P. Subsequently, sea-level fell slightly by ~0.3 m until ~3,000 yr B.P.. A stable sea-level stand occurred between 3,000 and 1,300 yr B.P., which was followed by a gradual decrease in sea-level of 0.7 m to the present. A comparison between the sea-level curve from French Polynesia with the equivalent sea-level curve representing the

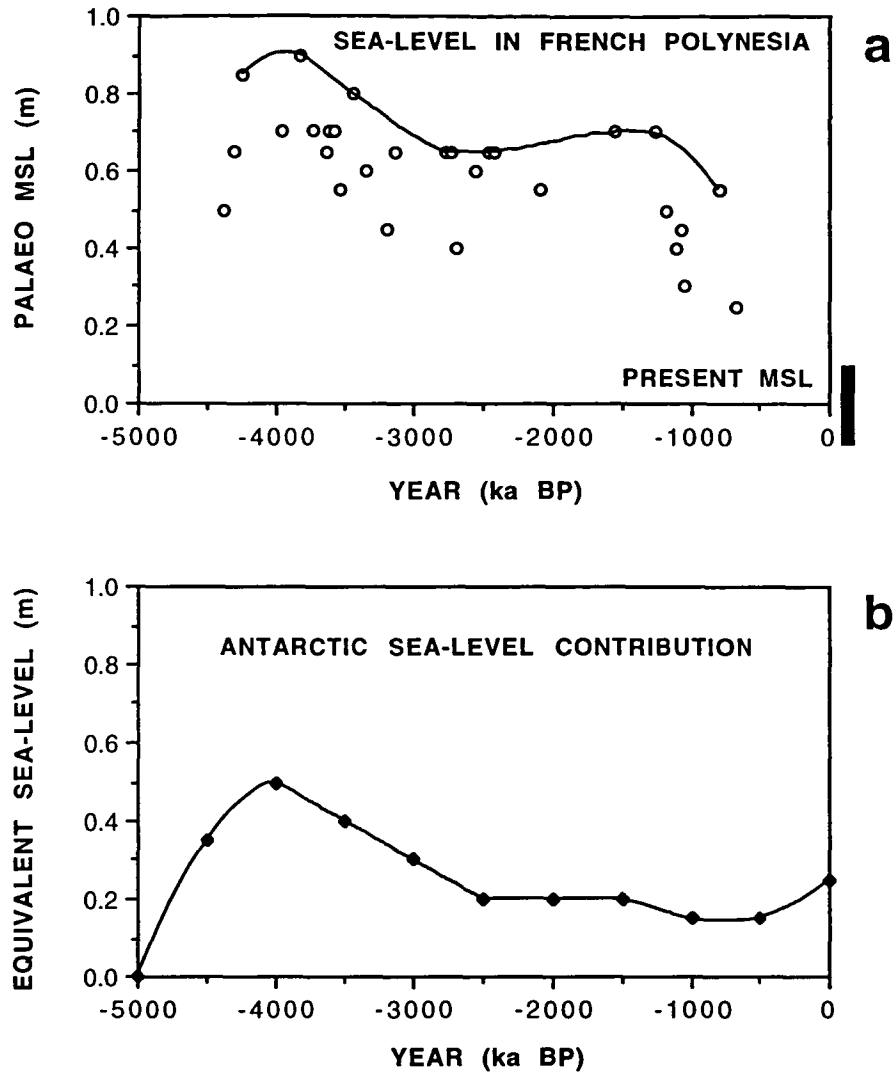

Figure 8.8 (a) Plot showing the selected (from Pirazzoli and Montaggioni, 1988) palaeo-sea-level data (open circles) for the Mid-Late Holocene, from: Tupai Atoll in the Society Islands; Temoe Atoll in the Gambier Islands, and the following atolls in the Tuamotu Islands; Mataiva Atoll, Faaite Atoll, Taiaro Atoll, Hikueru Atoll, Amanu Atoll, Vahitahi Atoll, Reao Atoll, Vairaatea Atoll, Nukutipipi Atoll, and Hereheretue Atoll. The regional palaeo mean sea-level curve (shown by the solid line) was reconstructed through the maximum elevation data, since all the palaeo mean sea-level data are considered to be minimum estimates. All palaeo MSL data are relative to the present MSL range (solid bar) which is associated with fluctuations in the ENSO (Wyrtki, 1985) (b) For comparison the Antarctic equivalent sea-level curve (from Figure 8.2b) is shown. Note that the data which suggest an apparent high stand at 1800-2000 yr B.P. in Figure 8.7 are not included in Figure 8.8a above. It is interpreted that the high elevation of these sea-level data are due to tectonic uplift as determined for one of the sites, Anaa Atoll by Pirazzoli et al. (1988).

Antarctic contribution in Figure 8.8 , indicates a remarkably strong similarity between the Antarctic contribution and the eustatic curve between 4,000 to 1,500 yr B.P.. This suggests that the variation in the total Antarctic accumulation is most likely the primary determinant of the eustatic sea-level during this period. Further, the good agreement between the two curves, supports the hypothesis presented in this study, for the temporal variation in Antarctic palaeo-accumulation, synchronous with climate fluctuations throughout the Holocene.

However, there is a major departure between the two curves from 1,000 yr B.P. to the present. The French Polynesian sea-level curve describes a continuous sea-level fall of 0.4-0.6 m during this period whilst Antarctica probably contributed a slight (0.1 m) rise to sea-level. This sea-level fall has also been interpreted at Suwarrow Atoll in the Northern Cook Islands (Scoffin et al., 1985), at Enewetak Atoll, Marshall Islands (Buddemeier, 1975) and at New Caledonia (Coudray and Delibrias, 1972). This difference between the curves may be due to: a delayed global isostatic adjustment of the oceanic lithosphere, a long-term shift in the ENSO pattern, and/or thermal contraction of the ocean.

According to the geophysical models of Nakada and Lambeck (1989), Tushingham and Peltier (1991) and Clark and Lingle (1979), the combination of local and global hydro-isostatic adjustments to the increase in post-glacial ocean volume, would have caused a typical relative sea-level curve for the South Pacific Ocean. This curve describes an increase in sea-level to an inflection point at 4,000-5,000 yr B.P., followed by a gradual decrease in sea-level to the present (shown in Figure 8.3). This is not represented by the actual sea-level curve for French Polynesia in Figure 8.8. It is possible that in the mid-ocean basins a delayed global isostatic adjustment of the oceanic lithosphere may have occurred, some 2,500 years after the cessation of major meltwater contributions. Such a delay may have occurred due to the great distance between the continental margins and the central South Pacific Ocean, combined with regional differences in the lithospheric thickness and lower mantle viscosity. Tushingham and Peltier (1991) proposed the hypothesis that such a delayed sea-level fall in the equatorial ocean may occur because postglacial rebound of the polar margins increases the gravitational attraction of the equatorial water to the polar regions. Both the models of Tushingham and Peltier (1991) and Nakada and Lambeck (1989) indicate that the Late Holocene sea-level fall in the mid-oceans, should have occurred <1,000 years after the attainment of the high-stand.

Alternatively, it is possible that thermal contraction of the ocean may have contributed to this sea-level fall in the mid-oceans. The period of sea-level fall spans the same

period in which climate variations produced the Little Climatic Optimum (LCO) and the Little Ice Age (LIA). The LCO generally occurred between 1,200 to 650 yr B.P. with average temperatures 0.5-1.0°C higher than the present (Grove, 1988). Morgan (1985) reported evidence for the widespread occurrence of the LCO, including Antarctica. The LIA occurred from 650 to 150 yr B.P. with average temperatures ~1.5°C lower than during the LCO, or equivalent to 0.5-1°C lower than at present (Grove, 1988). There is some evidence from a few data points in Figure 8.8 that sea-level in French Polynesia reached a second Holocene peak during the LCO, which has also been suggested for other islands in the South Pacific Ocean such as in the Northern Cook Islands (Scoffin et al., 1985). A temperature change of 1°C in the middle to deep South Pacific Ocean over 1,000 years could account for up to 0.4 m of the sea-level change since 1,000 yr B.P., given an ocean with an average depth of 3,000 m and a thermal expansion coefficient of 1.4×10^{-4} (after Bindoff and Church, 1992). This sea-level change would have been equivalent to the present rate of sea-level rise due to the thermal expansion of the ocean which is estimated as 0.45 ± 0.2 mm a^{-1}, in response to an average 1°C temperature warming (Wigley and Raper, 1993). Further, it is possible that long-term variations in the ENSO pattern may also have contributed to the sea-level fall. Regional variations in sea-level associated with ENSO events have been as large as $\pm$ 0.3 m across the Pacific Ocean (Wyrtki, 1985). Therefore, it is possible that climate variations may be responsible for at least part of the sea-level fall in the South Pacific Ocean since 1,000 yr B.P..

Therefore, the combination of a delayed global hydro-isostatic adjustment and climate-induced oceanic contraction may account for the divergence between the mid-ocean sea-level record and the Antarctic sea-level contribution. Clearly, it is difficult to separate out the contributions since the palaeo sea-level data are sparse with only moderate temporal resolution during the last 1,000 years. Both the sea-level curve for French Polynesia and the equivalent sea-level curve for Antarctica strongly suggest that Antarctica did not add significant quantities of meltwater from continuing deglaciation of the margins, between 4,000 yr B. P. to the present, as assumed in the geophysical modelling of Nakada and Lambeck (1989). They proposed a continuation of Antarctic meltwater (equivalent to 0.8 m of sea-level) added to the oceans at a rate of 0.2 mm a^{-1} from 4,000 years B.P. to the present. This implies that global hydro-isostatic adjustments in the mid-oceanic islands were less than those determined by the visco-elastic numerical models of Nakada and Lambeck (1989). The results in this study also suggest that geophysical modelling of both the earth response to meltwater loading and of relative sea-level history, need to incorporate a total post-glacial meltwater contribution of Antarctica to a value closer to 10-12 m rather than 25-37 m. In addition, the cumulative sea-level contribution due to variations in the total Antarctic

accumulation mass during the Glacial-Holocene Transition and the Holocene periods, should also be added to the revised post-glacial melting contribution. The timing of the Antarctic melting models should also be adjusted to allow for the earlier completion of the major post-glacial Antarctic melting contribution by 11,000-10,000 yr B.P..

However, more detailed data on the timing and geographical extent of Holocene glacial fluctuations of the Antarctic ice margin are required to refine the Antarctic sea-level contribution and the eustatic sea-level history during the Mid-Late Holocene. The refinement of the Holocene Antarctic sea-level contribution is critical to the determination of the hydro-isostatic and tectonic history of oceanic islands, and hence the prediction of relative sea-level changes in response to future climate forcings, such as global warming and the regional effects of ENSO phenomena. This study suggests that the net sea-level curve (Figure 8.2b) based on a post glacial melt contribution of 12 m (after Huybrechts, 1992) between 16,000 to 4,500 yr B.P. and partially offset by excess accumulation during the Holocene, better fits the relative sea-level history of mid oceanic islands than the continuous exponential melting of the Antarctic ice sheet margins throughout the Late Holocene.

REFERENCES

Adamson, D. A. and Colhoun, E. A. (1992). Late Quaternary glaciation and deglaciation of the Bunger Hills, Antarctica.. *Antarctic Science* **4** (4), 435-446.

Adamson, D. A. and Pickard, J. (1986). Cainozoic history of the Vestfold Hills. In *"Antarctic Oasis: Terrestrial Environments and History of the Vestfold Hills"* (J. Pickard, Ed.), pp.63-97. Academic Press.

Allan, R. J. and Haylock, M. R. (1993). Circulation features associated with the winter rainfall decrease in southwestern Australia. *Journal of Climate*, **6**(7), 1356-1367.

Alley, R. B. (1988). Concerning the deposition and diagenesis of strata in polar firn. *Journal of Glaciology*, **34**(118), 283 - 290.

Alley, R. B. and Whillans, I. M. (1984). Response of the East Antarctica ice sheet to sea level rise. *Journal of Geophysical Research*, **89** C4, 6487-6493.

Allison, I. (1979). The mass budget of the Lambert Glacier drainage basin, Antarctica. *Journal of Glaciology*, **22** (87), 223-235.

Allison, I. (1985). Diurnal variability of the surface wind and air temperature at an inland site: 2 years of AWS data. *ANARE Research Notes* **28**, 81-92.

Allison, I, Higham, M and Kiernan, R. (1992). Preliminary results from the Lambert-Amery Regional Glaciological Experiment (LARGE). Unpublished Antarctic CRC and Australian Antarctic Division report.

Allison, I , Wendler, G. and Radok, U. (1993). Climatology of the East Antarctic Ice Sheet (100°E to 140°E) derived from automatic weather stations. *Journal of Geophysical Research* **98**, D5, 8815-8823.

Allison, I. and Goodwin, I. D. (1993). The grounding zone of the Amery Ice Shelf. *Fifth International Symposium on Antarctic Glaciology.* Cambridge, United Kingdom. September 1993 (Abstract)

Anderson, J. B., Domack, E. W. and Kurtz, D. D. (1980). Observations of sediment-laden icebergs in Antarctica waters: implications to glacial erosion and transport. *Journal of Glaciology* **25** (93), 387-396.

Andrews, J. T. (1970). "A geomorphological study of post-glacial uplift with particular reference to Arctic Canada". *Institute of British Geographers Special Publication No. 2.* 156pp.

Bagnold, R. A. (1941). The Physics of Blown Sand and Desert Dunes. Methuen, London, 265pp.

Ball, F. K. (1960). Winds on the ice slopes of Antarctica. *Proceedings of the symposium on Antarctic meteorology,* Melbourne, 1959. Pergamon Press, 9-16.

Barnes, P. W. and Lien, R. (1988). Icebergs rework shelf sediments to 500 m off Antarctica. *Geology*, **16**, 1130-1133.

Baroni, C. and Orombelli, G. (1991). Holocene raised beaches at Terra Nova Bay, Victoria Land, Antarctica. *Quaternary Research* **36**, 157-177.

Baroni, C. and Orombelli, G. (1994a). Abandoned penguin rookeries as Holocene paleoclimatic indicators in Antarctica. *Geology*, **22**, 23-26.

Baroni, C. and Orombelli, G. (1994b). Holocene glacier variations in the Terra Nova Bay area (Victoria Land, Antarctica). *Antarctic Science* **6** (4): 497-505.

Bentley, C. R. and Giovinetto, M. B. (1991). Mass balance of Antarctica and sea-level change. In Weller et al. (Eds) *Proc. Int. Conf. of Polar Regions in Global Change*, June 11-15, 1990, Univ. of Alaska, 481-488.

Bindoff, N. L. and Church, J. A. (1992). Warming of the water column in the southwest Pacific Ocean. *Nature* **357**, 59-62.

Bird, M. I., Chivas, A. R., Radnell, C. J. and Burton, H. R. (1991). Sedimentological and stable-isotope evolution of lakes in the Vestfold Hills, Antarctica. *Palaeogeography, Palaeoclimatology, Palaeoecology*, **84**, 109-130.

Bishop, B. C. (1957). Shear moraines in the Thule Area, Northwest Greenland. *U.S Snow, Ice and Permafrost Research Establishment Technical Report* **17**, 52pp.

Black, H. P. and Budd, W. (1964). Accumulation in the region of Wilkes, Wilkes Land, Antarctica. *Journal of Glaciology*, **5** (37), 3-15.

Blight, D. F. and Oliver, R. L. (1977). The metamorphic geology of the Windmill Islands, Antarctica: a preliminary account. *Geological Society of Australia Journal* **24**, 239-262.

Bloom, A. L. (1967). Pleistocene shorelines: a new test of isostasy. *Geological Society of America Bulletin*, **78**, 1477-1494.

Bockheim, J. G., Wilson, S. C., Denton, G. H., Andersen, B. G. and Stuiver, M. (1989). Late Quaternary ice-surface fluctuations of Hatherton Glacier, Transantarctic Mountains. *Quaternary Research* **31**, 229-254.

Bolshiyanov, D., Verkulich, S., Pushina, Z. and Kirienko, E. (1991). Some features of the Late Pleistocene and Holocene history of the Bunger Hills (East Antarctica). Abstracts, *Sixth International Symposium on Antarctic Earth Sciences*, Saitama, Japan, 9-13 September, 1991, Tokyo, National Institute of Polar Research, 66-71.

Bromwich, D. H. (1988). Snowfall in high southern latitudes. *Reviews of Geophysics*, **26**(1), 149 - 168.

Bromwich, D. H. (1990). Estimates of Antarctic precipitation. *Nature* **343**, 627-629.

Bromwich, D. H. and Weaver, C. J. (1983). Latitudinal displacement from main moisture source controls $\delta^{18}O$ of snow in coastal Antarctica. *Nature* **301**, (5896), 145-147.

Bronge, C. (1992). Holocene climatic record from lacustrine sediments in a freshwater lake in the Vestfold Hills, Antarctica. *Geografiska Annaler* **74A**, 1, 47-58.

Budd, W. F. (1966). The dynamics of the Amery Ice Shelf. *Journal of Glaciology*, **6**, 335-358.

Budd, W. F. (1967). Ablation from an Antarctic ice surface. In Oura, H., *Physics of Snow and Ice, Proceedings of the International Conference on Low Temperature Science*, 1966, Sapporo Japan, volume 1, part 1 431-446..

Budd, W. F. and Morgan, V. I. (1977). Isotopes, climate and ice sheet dynamics from core studies on Law Dome, Antarctica. In: *Isotopes and impurities in snow and ice (Proc. Grenoble Symp., 1975)*, IAHS Publ. No. **118**, 312-321,.

Budd, W. F. and McInnes, B. (1978). Modelling surging glaciers and periodic surging of the Antarctic ice sheet. In Pittock, A. B., Frakes, L. A., Jenssen, D., Peterson, J. A. and Zillman, J. W. (Eds.)., *Climate change and variability: a southern perspective*, Cambridge University Press, 228-233.

Budd, W. F. and Smith, I. N. (1985). The state of balance of the Antarctic Ice Sheet - an updated assessment 1984. In DOE (United States Department of Energy) (1985). *Glaciers, Ice Sheets and Sea Level: Effect of a CO_2-induced climatic change.* Report of a workshop held in Seattle, Washington, September 13-15, 1984, 172-177.

Budd, W. F. and Simmonds, I. (1991). The impact of global warming on the Antarctic mass balance and global sea level. In Weller, G., McCauley, L. L. and Wilson C. (eds) *Proceedings of International Conference on the Role of Polar Regions in Global Change*, June 11-15, 1990. University of Alaska, Fairbanks, 489-494.

Budd, W. F., Corry, M. J. and Jacka, T. J. (1982). Results from the Amery Ice Shelf Project. *Annals of Glaciology* **3**, 36-41.

Budd, W. F., Jenssen, D. and Radok, U. (1970). The extent of basal melting in Antarctica. *Polarforschung*, Bd. **6**, Jarhrg. 39, No. 1, 1969, 293-306.

Budd, W. F., Landon-Smith, I. and Wishart, E. (1967). The Amery Ice Shelf. In Oura, H., *Physics of Snow and Ice, Proceedings of the International Conference on Low Temperature Science, 1966*, Sapporo Japan, volume 1, part 1 447-467. Hokkaido University, Institute of Low Temperature Science.

Budd, W. F., Reid, P. A. and Minty, L. J. (1994). Antarctic moisture flux and net accumulation from global atmospheric analyses. *Annals of Glaciology*, **21**, in press.

Budd, W. F., Young, N. W. and Austin, C. R. (1976). Measured and computed temperature distributions in the Law Dome ice cap, Antarctica. *Journal of Glaciology*, **16** (74), 99-110.

Budd, W. F., Jenssen, D. and Radok, U. (1984). Derived physical characteristics of the Antarctic Ice Sheet (Mark 1). University of Melbourne Meteorology Department, Publication No. 18, 178pp, 2nd printing.

Buddemeier, R. W., Smith, S. V. and Kinzie, R. A. (1975). Holocene windward reef-flat history, Enewetak Atoll. *Geol. Soc. Am. Bull.*, **86**, 1581-1584.

Burgess, J. S., Spate, A. P. and Shevlin, J. (1994) The onset of deglaciation in the Larsemann Hills, Eastern Antarctica. *Antarctic Science* **6** (4), 491-495.

Burckle, L. H. and Cirilli, J. (1987). Origin of diatom ooze belt in the Southern Ocean: implications for late Quaternary palaeoceanography. *Micropaleontology*, **29**, 6-10.

Cameron, R. L. (1964). Glaciological studies at Wilkes Station, Budd Coast, Antarctica. In, "*Antarctic Snow and Ice Studies*" (M. Mellor, Ed.). American Geophysical Union 1-36, Antarctic Research Series 2, pp 1-36, Washington D.C.

Cameron, R. L., Løken, O., and Molholm, J. (1959). Wilkes Station glaciological data 1957-58. *Ohio State University Research Foundation Report* **825-1**, part 3, 173pp.

Chappell, J. and Shackleton, J. J. (1986). Pleistocene sea-levels and the oxygen isotope record: A reconciliation. *Nature* **324**, 137-140.

Charles, C. D. and Fairbanks, R. G. (1992). Evidence from Southern Ocean sediments for the effect of North Atlantic deep-water flux on climate. *Nature* **355**, 416-419.

Chinn, T. J. H. (1986). Structure and equilibrium of the Dry Valley Glaciers. *New Zealand Antarctic Record, Special Issue: The proceedings of the Dry Valleys and McMurdo region Conference*, University of Waikato, Hamilton, New Zealand, 14th-16th, May, 1985, 73-88.

Chinn, T. J. H. (1987). Single folds at the margins of dry-based glaciers as indicators of a glacial advance. Unpublished paper, Soil Conservation Group, Ministry of Works and Development, Christchurch New Zealand.

Chinn, T. J., Whitehouse, I. E. and Höfle, H-C. (1987). The glaciers of the Terra Nova Bay are, Antarctica. Report No Ws 1213, Soil Conservation Group, Ministry of Works and Development, Christchurch New Zealand.

Church, J. A., Godfrey, J. S., Jackett, D. R. and McDougall, T. J. (1991). A model of sea level rise caused by ocean thermal expansion. *Journal of Climate*, **4**(4), 438-456.

Ciais, P., Petit, J. R., Jouzel, J., Lorius, C., Barkov, N. I., Lipenkov, V. and Nicolaiiev, V. (1992). Evidence for an early Holocene climatic optimum in the Antarctic deep ice-core record. *Climate Dynamics* **6**, 169-177.

Clapperton, C. M. (1990). Quaternary glaciations in the Southern Ocean and Antarctic Peninsula area. *Quaternary Science Reviews* **9**, 229-252.

Clapperton, C. M. and Sugden, D. E. (1982). Late Quaternary glacial history of George VI Sound Area, West Antarctica. *Quaternary Research* **18**, 243-267.

Clapperton, C. M., Sugden, D. E., Birnie, J. and Wilson, M. J. (1989). Late-glacial and Holocene glacier fluctuations and environmental change on South Georgia, Southern Ocean. *Quaternary Research* **31**, 210-228.

Clark, J. A. and Lingle, C. S. (1979) Predicted relative sea-level changes (18,000 years B.P. to present) caused by late-glacial retreat of the Antarctic Ice Sheet. *Quaternary Research* **11**, 279-298.

Clark, J. A., Farrell, W. E. and Peltier, W. R. (1978). Global changes in postglacial sea-level: a numerical calculation. *Quaternary Research* **9**, 265-278.

Colhoun, E. A. (1991). Geological evidence for changes in the East Antarctica ice sheet (60°-120° E) during the last glaciation. *Polar Record* **27** (163), 345-355.

Colhoun, E. A., Mabin, M. C. G., Adamson, D. A. and Kirk, R. M. (1992). Antarctic ice volume and contribution to sea-level fall at 20,000 yr B.P. from raised beaches. *Nature* **358**, 316-319.

Colhoun, E. A. and Adamson, D. A. (1991). Raised beaches of the Bunger Hills. In *"Quaternary Research in Australian Antarctica: Future Directions"*, D. Gillieson and S. Fitzsimons, Eds.) 79-84. Special Publication No. 3, Department of Geography and Oceanography, University College, Australian Defence Force Academy, Canberra.

Colhoun, E. A. and Adamson, D. A. (1992). Raised beaches of the Bunger Hills, Antarctica. *ANARE Reports* **136**, Antarctic Division, DASET.

Coudray, J. and Delibrias, G. (1972). Variations du niveau marin au-dessus de l'actuel en Nouvelle Calédonie depuis 6000 ans. *C. R. Acad. Sc. Paris, D*, **275**, 2623-2626.

Craig, H. (1961). Variations in meteoric waters. *Science* **133**, 1702-1703.

Currie, P. J. (1984). The structure and origin of the Strand Moraines, Antarctica. Unpublished BSc thesis, Victoria University of Wellington. (99 pp).

Dansgaard, W. (1964). Stable isotopes in precipitation. *Tellus* **16**, 436-68.

Davies, P. J. and Hopley, D., (1983). Growth fabrics and growth rates of Holocene reefs in the Great Barrier Reef, *Bur. Min. Res. J. Aust. Geol. Geophys.*, **8**, 237-251.

De Decker, P., Kiss, E. and Chivas, A. R. (1991). The suitability of lakes on the Windmill Islands in Antarctica for palaeolimnological studies. In *"Quaternary Research in Australian Antarctica: Future Directions"*, D. Gillieson and S. Fitzsimons, Eds.) 69-77. Special Publication No. 3, Department of Geography and Oceanography, University College, Australian Defence Force Academy, Canberra.

Denton, G. H., Armstrong, R. L. and Stuiver, M. (1971). The late Cenozoic glacial history of Antarctica. In "*The late Cenozoic glacial ages* " (ed. K. K. Turekian), pp 267-306. Yale University Press, New Haven, Connecticut.

Denton, G. H. and Hughes, T. J. (1981). *The Last Great Ice Sheets. Wiley*, New York, 484pp.

Denton, G. H., Prentice, M. L. and Burkle, L. H. (1991). Cainozoic history of the Antarctic Ice Sheet. In Tingey, R. J. (ed), *The Geology of Antarctica.* Clarendon Press, Oxford, 365-433.

Denton, G. H., Bockheim, J. G., Wilson, S. C., and Schluchter, C. (1986). Late Cenozoic history of Rennick Glacier and Talos Dome, northern Victoria Land. In *Geological investigations in northern Victoria Land*, Antarctic Research Series, Vol. **46** (ed E. Stump), 339-375. American Geophysical Union, Washington D.C..

Denton, G. H., Bockheim, J. G., Wilson, S. C. and Stuiver, M. (1989a). Late Wisconsin and Early Holocene glacial history, inner Ross Embayment, Antarctica. *Quaternary Research* **31**, 151-182.

Denton, G. H., Bockheim, J. G., Wilson, S. C., Leide, J. E. and Andersen, B. G. (1989b). Late Quaternary ice-surface fluctuations of Beardmore Glacier, Transantarctic Mountains. *Quaternary Research* **31**, 183-209.

Devoy, R. J. N. (ed) (1987). *Sea surface studies: A global view.* Croom Helm, Sydney, pp 649

Doake, C. S. M. (1985). Antarctic mass balance: glaciological evidence from Antarctic Peninsula and Weddell Sea sector. In *Glaciers, ice sheets and sea-level: effect of a CO_2 induced climatic change*, pp 197-209. Report of a workshop held in Seattle, Washington, September 13-15, 1984. United States Department of Energy, DOE/EV/60235-1.

DOE (United States Department of Energy) (1985). *Glaciers, Ice Sheets and Sea Level: Effect of a CO_2-induced climatic change.* Report of a workshop held in Seattle, Washington, September 13-15, 1984, 330pp.

Domack, E. W. (1982). Sedimentology of glacial and glacial marine deposits on the George V - Adélie continental shelf, East Antarctica. *Boreas* **11**, 79-97.

Domack, E. W., Jull, A. J. T., and Nakao, S. (1991a). Advance of East Antarctic outlet glaciers during the Hypsithermal: Implications for the volume state of the Antarctic ice sheet under global warming. *Geology*, **19**, 1059-1062.

Domack, E. W., Jull, A. J. T., Anderson, J. B. and Linick, T. W. (1991b). Mid-Holocene ice sheet recession from the Wilkes Land continental shelf, East Antarctica. In *"Geological Evolution of Antarctica"*, (M. R. A. Thomson, J. A. Crame and J. W. Thomson, Eds.) 693-698. Proc. of the Fifth Int. Symp. on Antarctic Earth Sciences. Cambridge University Press, Cambridge.

Domack, E. W., Jull, A. J. T., and Donahue, D. J. (1991c). Holocene chronology for the unconsolidated sediments at hole 740A: Prydz Bay, East Antarctica. In Barron, J., Larsen, B. et al., *Proceedings of the Ocean Drilling Program, Scientific Results*, Vol **119**, 747-750.

Doumani, G. A. (1967). Surface structure in snow. *In.;* Oura, H., *ed Physics of Snow and Ice.* Sapporo, 1119-1136.

Drewry, D. J. (1979). Late Wisconsin reconstruction from the Ross sea region, Antarctica. *Journal of Glaciology*, **24**, 231-243.

Drewry, D. J. (Ed.) (1983). *Antarctica: Glaciological and geophysical folio.* Scott Polar Research Institute, Cambridge.

Drewry, D. J., Jordan, S. R. and Janowski, E. (1982). Measured properties of the Antarctic Ice Sheet: surface configuration, ice thickness, volume and bedrock characteristics. *Annals of Glaciology* **3**, 83-91.

Drewry, D. J. (1991). The response of the Antarctic ice sheet to climate change. In *Antarctica and global climatic change* (ed). C. M. Harris and B. Stonehouse, pp 90-106. London: Bellhaven Press.

Drewry, D. J. and Morris, E. M. (1992). The response of ice sheets to climatic change. *Phil. Trans. R. Soc. Lond. B.* **338**, 235-242.

Duplessy, J. C., Shackleton, N. J., Fairbanks, R. G., Labeyrie, L., Oppo, D. and Kalles, N. (1988). Deepwater source variations during the last climatic cycle and their impact on the global deepwater circulation. *Paleoceanography*, **3**, 343-360.

Fairbanks, R. G. (1989). A 17,000-year glacio-eustatic sea level record; influence of glacial melting rates on the Younger Dryas event and deep-ocean circulation. *Nature* **342**, 637-642.

Filson R. B. (1974). Studies in Antarctic lichens II: Lichens from the Windmill Islands, Wilkes Land. *Muelleria* **3** (1), 9-36.

Fitzsimons, S. J. (1990). Geomorphic development of the Vestfold Hills: Questions regarding Holocene deglaciation. In *"Quaternary Research in Australian Antarctica: Future Directions"*, D. Gillieson and S. Fitzsimons, Eds.) 25-36. Special Publication No. 3, Department of Geography and Oceanography, University College, Australian Defence Force Academy, Canberra.

Flint, R. F. (1955). *Glacial Geology and the Pleistocene Epoch.* John Wiley and Sons, New York, 590 pp.

Fortuin, J. P. F. and Oerlemans, J. (1990). Parameterization of the annual surface temperature and mass balance of Antarctica. *Annals of Glaciology*, **14**, 78-84.

Fujiwara, K. and Endo, Y. (1971). Preliminary report of glaciological studies. *In :* Murayama, M., *ed. Report of the Japanese traverse, Syowa-South Pole 1968-1969.* Polar Research Centre, National Science Museum, Tokyo, 71-104.

Gillieson, D. (1991a). Diatom stratigraphy in Antarctic freshwater lakes. In *"Quaternary Research in Australian Antarctica: Future Directions"*, D. Gillieson and S. Fitzsimons, Eds.) 55-68. Special Publication No. 3, Department of Geography and Oceanography, University College, Australian Defence Force Academy, Canberra.

Gillieson, D. (1991b). An environmental history of two freshwater lakes in the Larsemann Hills, Antarctica. *Hydrobiologia* **214**, 327-331.

Gillieson, D., Burgess, J., Spate, A. and Cochrane, A. (1990). An atlas of the lakes of the Larsemann Hills, Princess Elizabeth Land, Antarctica. *ANARE Research Notes* **74**, 171 p. Australian Antarctic Division.

Giovinetto, M. B. (1964). The drainage systems of Antarctica: accumulation. In Mellor, M. ed. *Antarctic snow and ice studies*. Antarctic Research Series, Vol. 2, Washington, D. C..

Giovinetto, M. B. and Bentley, C. R. (1985). Surface balance in ice drainage systems of Antarctica. *Antarctic Journal of the U.S.* **20**, 6-13.

Giovinetto, M. B. and Bull, C. (1987). Summary and analysis of surface mass balance compilations for Antarctica, 1960-1985. *Byrd Polar Research Center, Report* No. **1**, Ohio State University, Columbus, Ohio.

Giovinetto, M. B., Waters, N. M. and Bentley, C. R. (1990). Dependence of Antarctic surface mass balance on temperature, elevation and distance to open ocean. *Journal of Geophysical Research*, **95** (D4), p 3517-3531, March 20, 1990.

Gloersen, P., Campbell, W. J., Cavalleri, D. J., Comiso, J. C., Parkinson, C. L. and Zwally, H. J. (1992). Arctic and Antarctic sea ice, 1978-1987: satellite passive-microwave observations and analysis. *NASA SP-511*, 201-204.

Goodwin, I. D. (1988a). Ice sheet topography and surface characteristics in eastern Wilkes Land, East Antarctica. *ANARE Research Notes,* 64, 100 pp. Australian Antarctic Division, Hobart.

Goodwin, I. D. (1988b). Firn core data from shallow drilling investigations in eastern Wilkes Land, East Antarctica. ANARE Research Notes **65**, 74 pp. Australian Antarctic Division, Hobart.

Goodwin, I. D. (1988c). The nature and origin of a jokulhlaup near Casey Station, Antarctica. *Journal of Glaciology,* **34** (116), 95-101.

Goodwin, I. D. (1990). Snow accumulation and surface topography in the katabatic zone of eastern Wilkes Land, Antarctica. *Antarctic Science* **2** (3), 235-242.

Goodwin, I. D. (1991). Snow-accumulation variability from seasonal surface observations and firn-core stratigraphy, eastern Wilkes Land, Antarctica. *Journal of Glaciology*, **37**, 127, p 383-387.

Goodwin, I. D. (1993a). Basal ice accretion and debris entrainment within the coastal ice margin, Law Dome, Antarctica. *Journal of Glaciology* **39,** no. 131, 157-166.

Goodwin, I. D. (1993b). Holocene deglaciation, sea-level change and the emergence of the Windmill Islands, Budd Coast, Antarctica. *Quaternary Research*, **40**, 70-80.

Goodwin, I. D. and Fraser, D. (1987). Antarctic snow dune fields and surface wind fields from Landsat MSS data. Abstract in *Proc. 4th Australasian Remote Sensing Conference,* Adelaide, Volume **2**, p 831.

Goodwin, I. D., Higham, M., Allison, I. and Jiawen, R. (1994). Accumulation variability in eastern Kemp Land, Antarctica. *Annals of Glaciology*, **20**, 202-206.

Gornitz, V. (1993). Mean sea level changes in the recent past. In Warrick, R. A., Barrow, E. M. and Wigley, T. M. L. (eds) (1993), *Climate and sea level change: observations, projections and implications.* Cambridge University Press, 25-44.

Gornitz, V., Rosenzweig, C. and Hillel, D. (1994). Is sea level rising or falling?. *Nature*, **371**, 481.

Goudie, A. (1983). *Environmental Change*. Oxford University Press, Oxford, 258 pp.

Gow, A. J. and Epstein, S. (1972). On the use of stable isotopes to trace the origins of ice in a floating ice tongue. *Journal of Geophysical Research* **77** (33), 6552-6557.

Gow, A. J., Epstein, S. and Sheehy, W. (1979). On the origin of stratified debris in ice cores from the bottom of the Antarctic ice sheet. *Journal of Glaciology*, **23** (89), 185-192.

Grobe, H. and Mackensen, A. (1992). Late Quaternary climatic cycles as recorded in sediments from the Antarctic continental margin. In, Kennett, J. P., and Warnke, D. (eds), *'The Antarctic Paleoenvironment: A perspective on global change'*. Antarctic Research Series, **56**, Part 1, 349-376, American Geophysical Union.

Grobe, H., Huybrechts, P. and Futterer, D. K. (1993). Late Quaternary record of sea-level changes in the Antarctic. *Geologische Rundschau* **82**, 263-275.

Grootes, P. M. and Stuiver, M. (1987). Ice sheet elevation changes from isotope profiles. In *The Physical Basis of Ice Sheet Modelling* (Proceedings of the Vancouver Symposium, August 1987), IAHS Publ. no. **170**, 269-281.

Grove, J. M. (1988). *The Little Ice Age*. London, Methuen.

Hambrey, M. J. (1991). Structure and dynamics of the Lambert Glacier-Amery Ice Shelf system: implications for the origin of Prydz Bay sediments. In Barron, J., Larsen, B. et al., *Proceedings of the Ocean Drilling Program, Scientific Results,* Vol **119**, 61-75.

Hambrey, M. J., Ehrmann, W. U. and Larsen, B. (1991). Cenozoic glacial record of the Prydz Bay continental shelf, East Antarctica. In Barron, J., Larsen, B. et al., *Proceedings of the Ocean Drilling Program, Scientific Results*, Vol **119**, 77-128.

Hammer, C. U. (1980). Acidity of polar ice cores in relation to absolute dating, past volcanism and radio-echoes. *Journal of Glaciology* **25**, 359-372.

Hansom, J. M. and Flint, C. P. (1989). Holocene ice fluctuations on Brabant Island, Antarctic Peninsula. *Antarctic Science* **1**, 165-176.

Harkness, D. D. (1979). Radiocarbon dates from Antarctica. *British Antarctic Survey Bulletin*, **47**, 43-59.

Hayashi, M. and Yoshida, Y. (1994). Holocene raised beaches in the Lutzow-Holm Bay region, East Antarctica. In Berkman, P. A. and Yoshida, Y. (eds), *Holocene environmental changes in the Antarctic coastal areas.* Memoirs of National Institute of Polar Research Special Issue No. **50**, 49-84. National Institute of Polar Research, Tokyo.

Hays, J. D., Imbrie, J. and Shackelton, N. J. (1976). Variations in the earth's orbit: pacemaker of the ice ages. *Science*, **194**, 1121-32.

Hazelton, B. (1987). 1986 Casey Glaciological Program, Volume 1, Data report. Unpublished internal Australian Antarctic Division Report, 166 pages.

Hellmer, H. H. and Jacobs, S. S. (1991). Sensitivity study of the thermohaline circulation beneath Amery Ice Shelf, Antarctica. *Journal of Geophysical Research*, **97** (C12), 20305-20317.

Herzfeld, U. C., Lingle, C. S. and Lee L.-H (1994). Recent changes in the position of the grounding line of Lambert Glacier, Antarctica, from kriging of satellite radar altimetry. *Annals of Glaciology*, **20**, ?.

Heusser, C. J. and Streeter, S. S. (1980). A temperature and precipitation record of the past 16,000 years in southern Chile, *Science* **210**, 1345-1347.

Higham, M. (1994). Surface mass balance and snow surface properties from the Lambert Glacier basin traverses, 1990-94. Submitted as Antarctic CRC Research Note, Australian Antarctic Division.

Hollin, J. T. (1962). On the glacial history of Antarctica. *Journal of Glaciology* **4**, 173-195.

Hollin, J. T. and Cameron, R. L. (1961). I.G.Y. Glaciological work at Wilkes Station, Antarctica *Journal of Glaciology.* **3** (29), 833-842.

Hooke, R. Le b. (1970). Morphology of the ice sheet margin near Thule, Greenland. *Journal of Glaciology*, **9**, 57, 303-323.

Hopley, D. (1987). Holocene sea-level changes in Australasia and the southern Pacific. In Devoy, R. J. N., *Sea Surface Studies: A Global Perspective.* 375-408, Croom Helm, New York.

Hubbard, B and Sharp, M. (1989). Basal ice formation and deformation: a review. *Progress in Physical Geography*, **13**, 529-558.

Hudleston, P. J. (1976). Recumbent folding in the base of the Barnes Ice Cap, Baffin Island, Northwest Territories, Canada. *Geological Society of America Bulletin*, **87**, 1684-1692.

Hughes, T., Denton, G., Anderson, B. G., Schilling, D. H., Fastook, J. L. and Lingle, C. S. (1981). The last great ice sheets: A global view. In *"The Last Great Ice Sheets"* (G. H. Denton and T. J. Hughes Eds). John Wiley and Sons, New York.

Huybrechts, P. (1992). The Antarctic ice sheet and environmental change: a three-dimensional modelling study. *Rep. Polar Res.* **99**: 241 pp.

Huybrechts, P. and Oerlemans, J. (1990). Response of the Antarctic ice sheet to future greenhouse warming. *Climate Dynamics* **5**, 93-102.

Ingolfsson, O., Hjort, C., Bjorck, S. and Lewis Smith, R. I. (1992). Late Pleistocene and Holocene glacial history of James Ross Island, Antarctic Peninsula. *Boreas* **21**, 209-222.

Isaksson, E and Karlen, W. (1994a). Spatial and temporal patterns in snow accumulation, western Dronning Maud Land, Antarctica. *Journal of Glaciology*, **40**, 135, 399-409.

Isaksson, E. and Karlen, W. (1994b). High resolution climatic information obtained from short firn cores, western Dronning Maud Land, Antarctica. *Climatic Change* **26**, 421-434.

Isaksson, E., Karlen, W., Gundestrup, N., Mayewski, P., Whitlow, S. and Twickler, M. (Submitted). A century of accumulation and temperature changes in Dronning Maud Land, Antarctica. Submitted to *Journal of Geophysical Research.*

Jacka, T. H. (1983). A computer data base for Antarctic sea ice extent. *ANARE Research Notes* **13**, 54 pages.

Jacka, T. H., Christou, L., Cook, B. J. (1984). A data bank of mean monthly and annual surface temperatures for Antarctica, the Southern Ocean and the South Pacific Ocean. *ANARE Research Notes* **22**. 97 pages. Antarctic Division, Department of Science and Technology.

Jacka, T. H. (1987). Unpublished update of *ANARE Research Notes* **13**.

Jacka, T. H. (1992). Unpublished update of *ANARE Research Notes* **22**.

Jacka, T. H. and Budd, W. F. (1991). Detection of temperature and sea ice extent changes in the Antarctic and Southern Ocean. In Weller et al. (Eds) *Proc. Int. Conf. of Polar Regions in Global Change*, June 11-15, 1990, Univ. of Alaska, 63-70.

Jacobs, S. S., (1992). Is the Antarctic ice sheet growing. *Nature* **360**, 29-33.

Jacobs, S. S., Hellmer, H. H., Doake, C. S. M., Jenkins, A. and Frolich, R. M. (1992). Melting of ice shelves and the mass balance of Antarctica. *Journal of Glaciology* **38** (130), 375-387.

Jenne, R. L., Crutcher, H. L., van Loon, H. and Taljaard, J. J. (1974). *A selected climatology of the Southern Hemisphere: Computer methods and data availability.* NCAR-TN/STR-92, National Centre for Atmospheric Research, Boulder, Colorado, 91pp.

Johnsen, S. J., Dansgaard, W., Clausen, H. B. and Langway, C. C. (1972). Oxygen isotope profiles through the Antarctic and Greenland ice sheets. *Nature* **235**, 429-434.

Jones, D. J. (1983). Snow stratigraphy observations in the katabatic wind region of eastern Wilkes Land, Antarctica. *ANARE Research Notes*, **17**, 18pp. Australian Antarctic Division, Hobart.

Jones, P. D. and Wigley, T. M. L. (1988). Antarctic gridded sea level pressure data: an analysis and reconstruction back to 1957. *Journal of Climate*, 1, 1199-1220.

Jouzel, J. and Merlivat, L. (1984). Deuterium and oxygen 18 in precipitation: modelling of the isotopic effects during snow formation. *Journal of Geophysical Research* **88** (C4), 2693-703.

Jouzel, J. and Souchez, R. A. (1982). Melting-refreezing at the glacier sole and the isotopic composition of the ice. *Journal of Glaciology*, **28** (98), 35-42.

Jouzel, J., Lorius, C., Petit, J. R., Genthon, C., Barkov, N. I., Kotlyakov, V. M. and Petrov, V. M. (1987). Vostok ice core: a continuous isotope temperature record over the last climatic cycle (160,000 years). *Nature* **329**, 403-408.

Jouzel, J., Raisbeck, G., Benoist, J. P., Yiou, F., Lorius, C., Raynaud, D., Petit, J. R., Barkov, N. I., Korotkevich, Y. S. and Kotlyakov, V. M. (1989). A comparison of deep Antarctic ice cores and their implications for climate between 65,000 and 15,000 years ago. *Quaternary Research* **31**, 135-150.

Kayanne, H., Ishii, T., Matsumoto, E. and Yonekura, N. (1993). Late Holocene sea-level change on Rota and Guam, Mariana islands, and its constraint on geophysical predictions. *Quaternary Research* **40** (2), 189-200.

Knight, P. G. (1987). Observations at the edge of the Greenland ice sheet: boundary condition implications for modellers. *In The physical basis of ice sheet modelling* (Proceedings of the Vancouver Symposium, August 1987). *IAHS Publ.* **170**, 359-366.

Knight, P. G. (1989). Stacking of basal debris layers without bulk freezing-on: isotopic evidence from West Greenland. *Journal of Glaciology* **35** (120), 214-216.

Korotkevich, E. S. and Timofeev, B. V. (1964). The age of the rocks of East Antarctica from spore analysis. Information *Bulletin Soviet Antarctic Expedition* , II (English translation), 63-71.

Kotlyakov, A. M. (1961). *The snow cover of the Antarctic and it's role in the present day glaciation of the continent.* Available from the U.S. Department of Commerce, translated from Russian by the Israel Program for Scientific Translations, 182-186.

Labeyrie, L. D., Pichon, J. J., Labracherie, M., Ippolito, P., Duprat, J. and Duplessy, J. C. (1986). Melting history of Antarctica during the past 60,000 years. *Nature* **322**, 701-706.

Labeyrie, L. D., Duplessy, J. C. and Blanc, P. L. (1987). Variations of mode of formation and temperature of oceanic deep waters over the past 125,000 years. *Nature* **327**, 477-482.

Labracherie, M., Labeyrie, L. D., Duprat, J., Bard, E., Arnold, M., Pichon, J. J. and Duplessy, J. C. (1989). The last deglaciation in the Southern Ocean. *Palaeoceanography* **4**, 629-638.

Lambeck, K. (1990). Late Pleistocene, Holocene and present sea-levels: constraints on future change. *Palaeogeography, Palaeoclimatology, Palaeoecology (Global and Planetary Change Section)* **89**, 205-217.

Landon-Smith, I. (1965). Glaciological Studies at Mawson and on the Amery Ice Shelf 1962. Unpublished MSc. Thesis, Department of Meteorology, University of Melbourne, 108 p.

Lawson, D. E. (1979). Sedimentological analysis of the western terminus of the Matanuska Glacier, Alaska. *CRREL Rep.* **79**-9, 96pp.

Lingle, C. S., Lee, L.-H., Zwally, H. J. and Seiss, T. C. (1994). Recent elevation changes on Lambert Glacier, Antarctica, from orbit crossover analysis of satellite radar altimetry. *Annals of Glaciology*, **20**, in the press.

Lock, W. W., Andrews, J. T. and Webber, P. J. (1979). A manual for lichenometry. *British Geomorphological Research Group, Technical Bulletin* No. **26**, pp47.

Loewe, F. (1974). Considerations concerning the winds of Adelie Land. *Z. Gletscherkunde Glazialgeologie* **10**, 189-197.

Loewe, F. J. (1962). On the mass economy of the interior of the Antarctic Ice cap. *Journal of Geophysical Research*, **67**, 5171-5177.

Lorius, C. (1968). A physical and chemical study of the coastal ice sampled from a core drilling in Antarctica. *IASH Publ.* **79**, 141-148.

Lorius, C. and Merlivat, L. (1977). Distribution of mean surface stable isotope values in East Antarctica: observed changes with depth in the coastal area. *International Association of Hydrological Sciences Publication*, No **118**, 127-137.

Lorius, C., Jouzel, J., Ritz, C., Merlivat, L.,, Barkov, N. I., Korotkevich, Y. S. and Kotlyakov, V. M. (1985). A 150,000 year isotope climate record from Antarctic ice. *Nature* **316**, 591-596.

Lorius, C., Merlivat, L., Duval, P., Jouzel, J. and Pourchet, M. (1979). Evidence of climatic change in Antarctica over the last 30, 000 years from the Dome C ice core. In Allison, I. (ed) Sea Level, Ice and Climatic Change (Proceedings of the Canberra symposium, December 1979) *IAHS Publ.* no. **131**, 217-225.

Lorius, C., Merlivat, L., Jouzel, J. and Fouchet, M. (1979). A 30 000 year isotope climatic record from Antarctic ice. *Nature* **280**, 644-648.

Løken, O.(1959). Evidence of higher sea levels in the Windmill Islands. In " Wilkes Station glaciological data 1957-58". (R. L. Cameron, O. H. Løken and J. R. L. Molholm Eds.) *Ohio State University Research Foundation Rep*ort **825-1**, part 3, 28-32.

Mabin, M. C. G. (1992). Late Quaternary ice-surface fluctuations of the Lambert Glacier. *Recent Progress in Antarctic Earth Science.* Edited by Y. Yoshida et al., p683-687. TERRAPUB, Tokyo.

Mabin, M .C. G. (1986). ^{14}C ages for "Heroic Era" penguin and seal remains from Cape Evans, McMurdo Sound. *New Zealand Antarctic Record* 7(2), 19-20.

Markgraf, V. (1983). Late and postglacial vegetational and paleoclimatic changes in Subantarctic temperate and arid environments in Argentina. *Palynology* **7**, 43-70.

Martinerie, P., Lipenkov, V. Y., Raynaud, D., Chappellaz, J., Barkov, N. I. and Lorius, C. (1994). Air content palaeo record in the Vostok ice core (Antarctica): A mixed record of climatic and glaciological parameters. *Journal of Geophysical Research* **99**, D5, 10,565-10,576.

Martinson, D. G., Pisias, N. G., Hays, J. D., Imbrie, J., Moore, T. C. and Shackleton, N. J. (1987). Age dating and the orbital theory of the ice ages: Development of a high-resolution 0-300,000 yr chronostratigraphy. *Quaternary Research* **27**, 1-29.

Mayewski, P. A. (1975). Glacial geology and Late Cenozoic history of the Transantarctic Mountains, Antarctica. *Institute of Polar Studies (Ohio) Report*, **56** 1-168, Ohio State University, Columbus.

McIntyre, N. F. (1985). A re-assessment of the mass balance of the Lambert Glacier drainage basin, Antarctica. *Journal of Glaciology*, **31** (107), 34-38.

Medhurst, T. G. (1984). Unpublished Glaciology Data Report, 1983 Casey Glaciological Program. Australian Antarctic Division Internal Report.

Meier, M. F. (1993). Ice, climate and sea level; do we know what is happening. In Peltier, W. R. (ed) *Ice in the Climate System*, NATO ASI Series I12, Springer-Verlag, Berlin, 141-160.

Mellor, M. (1964). Remarks concerning the Antarctic mass balance. *Polarforschung* **5**, 33, 179-180.

Mercer, J. H. (1976). Glacial history of southernmost South America. *Quaternary Research* **6**, 125-166.

Mitchell, J. F. B., Manabe, V., Tokioka, T., Meleshko, V. (1990). Equilibrium climate change. In Houghton, J. T. et al. (Eds) *Climate Change: The IPCC Scientific Assessment.* Cambridge University Press, 131-172.

Miyarta, T., Maeda, Y., Matsumoto, E., Matsushima, Y., Rodda, P. and Sugimura, A. (1988). Emerged notches and microatolls on Vanua Levu, Fiji. In: *Sea-level changes and tectonics in the Middle Pacific.* Rep. HIPAC Proj. in 1986 and 1987. Univ. Tokyo, 67-76.

Montaggioni, L. F. (1988). Holocene reef growth history in mid-plate high volcanic islands. *Proc. 6th International Coral Reef Symposium, Australia*, Vol. 3, 455-460.

Morgan, V. I. (1982). Antarctic ice sheet surface oxygen isotope values. *Journal of Glaciology* **18**, (99), 315-323.

Morgan, V. I. (1985). An oxygen isostope - climate record from Law Dome, Antarctica. *Climate Change* **7**, 415-426.

Morgan, V. I. and Jacka, T. H. (1979). Mass balance studies in East Antarctica. In Allison, I. (Ed) *Sea Level, Ice and Climatic Change.* Proceedings of the Canberra Symposium, December, 1979. IAHS Publ **131**, 253-260.

Morgan, V. M., Goodwin, I. D., Etheridge, D. M., and Wookey, C. W. (1991). Evidence from Antarctic ice cores for recent increases in snow accumulation. *Nature*, **354**, 58-60.

Mosley-Thompson, E., Thompson, L. G., Grootes, P. M. and Gundestrup, N. (1990). Little Ice Age (Neoglacial) palaeoenvironmental conditions at Siple Station, Antarctica. *Annals of Glaciology* **14**, 199-204.

Muszynski, I. and Birchfield, G. E. (1985). The dependence of Antarctic accumulation rates on surface temperature and elevation. *Tellus* 37A, 204-208.

Nakada, M. (1986). Holocene sea-levels in oceanic islands: implications for the rheological structure of the Earth's mantle. *Tectonophysics* **121**, 263-276.

Nakada, M. and Lambeck, K. (1988). The melting history of the Late Pleistocene Antarctic ice sheet. *Nature* **333** , 36-40.

Nakada, M. and Lambeck, K. (1989). Late Pleistocene and Holocene sea-level change in the Australian region and mantle rheology. *Geophysical Journal* **96**, 497-517.

Neumann, A. C. and MacIntyre, I. (1985). Reef response to sea level rise: keep-up, catch-up or give-up. *Proceedings of the Fifth International Coral Reef Congress, Tahiti*, 1985, Volume 3, 105-110.

Nichols, R. L. (1961). Characteristics of beaches formed in polar climates. *American Journal of Science*, **259**, 694-708.

Nougier, J. and Lorius, C. (1969). Etude geologique et physico-chimique de carottes profondes de glace (Terre Adelie). *Rev. Geog. Phys. Geol. Dyn.* **11** (2), 165-170.

Nunn, P. D. (1986). Implications of migrating geoid anomalies for the interpretation of high-level fossil coral reefs. *Geological Society of America Bulletin*, **97**, 946-952.

Nunn, P. D. (1994). *Oceanic Islands*. Blackwell Publishers, Oxford, 413 pp.

O'Brien, P. E. (1994). Morphology and late glacial history of Prydz Bay, Antarctica, based on radio-echo sounding. Internal Australian Geological Survey Organisation Report. (Unpublished).

Oerlemans, J. (1993). Possible changes in the mass balance of the Greenland and Antarctic ice sheets and their effects on sea level. In Warrick, R. A., Barrow, E. M. and Wigley, T. M. L. (eds) (1993), *Climate and sea level change: observations, projections and implications*. Cambridge University Press, 144-161.

Omoto, K. (1977). Geomorphic development of the Soya Coast, East Antarctica - Chronological interpretation of raised beaches based on levellings and radiocarbon datings. *Science Reports of the Tohoku University, 7th Series (Geography)* Vol. 27 No. 2, pp148.

Omoto, K. (1983). The problem and significance of radiocarbon geochronology in Antarctica. In *"Antarctic Earth Science"* (R. L. Oliver, P. R. James and J. B. Jago Eds), Australian Academy Science, Canberra, 450-452.

Paren, J. G., Doake, C. S. M. and Peel, D. A. (1993). The Antarctic Peninsula contribution to future sea level rise. In Warrick, R. A., Barrow, E. M. and Wigley, T. M. L. (eds) (1993), *Climate and sea level change: observations, projections and implications*. Cambridge University Press, 162-168.

Parish, T. R. (1988). Surface winds over the Antarctic continent: a review. *Reviews of Geophysics*, **26** (1), 169-180.

Parish, T. R. and Bromwich, D. M. (1987). The surface windfield over the Antarctic ice sheets. *Nature*, **328** (6125), 51-54.

Paterson, W. S. B. (1981). *The Physics of Glaciers*. 2nd Edition. Pergamon Press, 380pp.

Paterson, W. S. B. (1993). World sea level and the present mass balance of the Antarctic Ice Sheet. In Peltier, W. R. (ed) *Ice in the Climate System*, NATO ASI Series I12, Springer-Verlag, Berlin, 131-140.

Payne, A. J., Sugden, D. E. and Clapperton, C. M. (1989). Modelling the growth and decay of the Antarctic Peninsula Ice Sheet. *Quaternary Research* **31**, 119-134.

Peel, D. A. (1992). Ice - core evidence from the Antarctic Peninsula region. *In* Bradley, R. S. and Jones, P. D. , eds. *Climate since 1500 A.D.* Harper Collins Academic, London.

Peltier, W. R. (1988). Lithospheric thickness, Antarctic deglaciation history, and ocean basin discretization effects in a global model of postglacial sea level change: A summary of some sources on non-uniqueness. *Quaternary Research* **29**, 93-112.

Petit, J. R., Jouzel, J., Pourchet, M. and Merlivat, L. (1982). A detailed study of snow accumulation and stable isotope content in Dome C (Antarctica). *Journal of Geophysical Research*, **87** (C6), 4301-4308.

Pettre, P., Pinglot, J. F., Pourchet, M. and Reynaud, L. (1986). Accumulation in Terre Adelie, Antarctica: effect of meteorological parameters. *Journal of Glaciology*, **32** (112), 486-500.

Pfitzner, M. L. (1980). The Wilkes Ice Cap project 1966. *ANARE Scientific Reports, series A (4) Glaciology*, Publication No. **127**. Australian Government Publishing Service, Canberra.

Pielou, E. C. (1991). *After the ice age*. University of Chicago Press, Chicago, 366 pp.

Pirazzoli, P. A. (1987). A reconnaissance and survey of Temoe Atoll (South Pacific Ocean). *Journal of Coastal Research*, **3**(3), 307-322.

Pirazzoli, P. A. (1991) *World Atlas of Holocene Sea-Level Changes*. Elsevier Oceanography Series 58, Elsevier, Amsterdam, 300 pp.

Pirazzoli, P. A. (1993). Present and near-future sea-level changes: an assessment. In Paepe R. et al.(eds), *Greenhouse Effect, Sea-level and Drought*. Kluwer Academic Publishers, 153-163.

Pirazzoli, P. A. and Montaggioni, L. F. (1985). Lithospheric deformation in French Polynesia (Pacific Ocean) as deduced from Quaternary shorelines. *Proceedings of the 5th International Coral Reef Congress, Tahiti*, Vol. **3**, 195-200.

Pirazzoli, P. A. and Montaggioni, L. F. (1986). Late Holocene sea-level changes in the Northwest Tuamotu Islands, French Polynesia. *Quaternary Research*, **25**, 350-368.

Pirazzoli, P. A., and Montaggioni, L. F. (1988). Holocene sea-level changes in French Polynesia. *Palaeogeography, Palaeoclimatology, Palaeoecology*, **68**, 153-175.

Pirazzoli, P. A., Koba, M., Montaggioni, L.F. and Person, A. (1988). Anaa (Tuamotu Islands, central Pacific): an incipient rising atoll? *Marine Geology*, **82**, 261-269.

Pirazzoli, P. A., Montaggioni, L. F., Vergnaud-Grazzini, C. and Saliege, J. F. (1987). Late Holocene sea-levels and coral reef development in Vahitahi Atoll, eastern Tuamotu Islands, Pacific Ocean. *Marine Geology*, **76**, 105-116.

Plassche, O. van de (Ed) (1986). *Sea-level research.* Geo Books, Norwich, 618 pp.

Pourchet, M., Pinglot, F. and Lorius, C. (1983). Some meteorological applications of radioactive fallout measurements in Antarctic snows. *Journal of Geophysical Research*, **88**(C10), 6013 - 6020.

Quilty, P. G. (1985). Distribution of foraminiferids in sediments of Prydz Bay, Antarctica. *Spec. Publ. S. Aust. Dep. Mines Energy*, **5**:329-340.

Quilty, P. G. (1993). Coastal East Antarctic neogene sections and their contribution to the ice sheet evolution debate. In *The Antarctic Paleoenvironment: A Perspective on Global Change*. Antarctic Research Series, Volume **60**, p251-264. American Geophysical Union.

Raisbeck, G. M., Yiou, F., Fruneau, M., Loiseaux, J. M., Lieuvin, M., Ravel, J. C. and Lorius, C. (1981). Cosmogenic ^{10}Be concentrations in Antarctic ice during the past 30,000 years. *Nature* (London) **292**, 825-826.

Raisbeck, G. M., Yiou, F., Bourles, D., Lorius, C., Jouzel, J., and Barkov, N. I. (1987). Evidence for two intervals of enhanced ^{10}Be concentrations in Antarctic ice during the last glacial period. *Nature* (London) **326**, 273-277.

Raynaud, D. and Lebel, B. (1979). Total gas content and surface elevation of polar ice sheets, *Nature*, **281**, 289-291.

Raynaud, D., Lorius, C., Budd, W. F. and Young, N. W. (1979). Ice flow along an IAGP flow line and interpretation of data from an ice core in Terre Adélie, Antarctica. *Journal of Glaciology*, **24** (90), 103-115.

Robertson, F. B. (1993). Amery Ice Shelf front mass budget. Unpublished BSc (Hons) thesis, IASOS, University of Tasmania.

Robertson, R. (1959). Preliminary report on the bedrock geology of the Windmill Islands. *Ohio State University Research Foundation Report* **825-2**, part 6, 25pp.

Robin, G. de Q. (1977). Ice cores and climatic change. *Phil Trans. R. Soc*, **B280**, 143-168.

Robin, G. de Q. (1976). Is the basal ice of a temperate glacier at the melting point ? *Journal of Glaciology,* **16**, 183-196.

Robin, G. de Q. (1983). Ice sheets: isotopes and temperatures. In Robin, G. de Q (ed) *The Climatic Record in Polar Ice Sheets*, Cambridge University Press, p180-184.

Robin, G. de Q. (1983). The δ value-temperature relationship. In Robin, G. de Q (ed) *The Climatic Record in Polar Ice Sheets*, Cambridge University Press, p180-184.

Robin, G. de Q.. (1986). Changing the sea level: projecting the rise in sea level caused by warming of the atmosphere. In Bolin, B., Doos, B., Jager, J. and Warrick, R. (eds), *The Greenhouse Effect, Climatic Change and Ecosystems*. Scope 29, ICSU, WMO, Wiley, New York, 323-359.

Sahagian, D. L., Schwartz, F. W. and Jacobs, D. K. (1994). Direct anthropogenic contributions to sea level rise in the twentieth century. *Nature*, **367**, 54-57.

Schwerdtfeger, W. (1984). *Weather and Climate of the Antarctica,* Development in Atmospheric Science , 15, Elsevier, Amsterdam.

Scoffin, T. P., Stoddart, D. R., Tudhope, A. W. and Woodroffe, C. D. (1985). Exposed limestones of Surarrow Atoll. *Proc. Fifth International. Coral Reef Congress., Tahiti,* **3,** 137-140.

Shackleton, N. J. (1978). Some results of the CLIMAP project. In: *Climatic Change and Variability, a Southern Perspective* (ed. A. B. Pittock, L. A. Frakes, D. Jenssen, J. A. Peterson and J. W. Zillman), 69-76, Cambridge University Press.

Sigg, A. and Neftel, A. (1988). Seasonal variations in hydrogen peroxide in polar ice cores. *Annals of Glaciology*, **10**, 157-162.

Simmonds, I. and Budd, W. F. (1991). Sensitivity of the southern hemisphere circulation to leads in the Antarctic pack ice. *Q. J. R. Meteorological Society*, **117**, 1003-1024.

Simmonds, I. and Wu, X., (1993). Cyclone behaviour response to changes in winter southern hemisphere sea-ice concentration. *Q. J. R. Meteorological Society*, **119**, p 1121-1148.

Souchez, R. A. (1967). The formation of shear moraines; An example from South Victoria Land, Antarctica. *Journal of Glaciology*, **6**, 837-843.

Souchez, R. A and De Groote, J. M. (1985). δD - $\delta^{18}O$ relationships in ice formed by subglacial freezing: palaeoclimatic implications. *Journal of Glaciology*, **31** (109), 229-232.

Souchez, R. A. and Lorrain, R. D. (1978). Origin of the basal ice layer from Alpine glaciers as indicated by its chemistry. *Journal of Glaciology*, **20** (83), 319-328.

Souchez, R. A. and Lorrain, R. D. (1992). *Ice Composition and Glacier Dynamics.* Springer-Verlag, Berlin, 200 pp.

Souchez, R. A. and Tison J.-L. (1981). Basal freezing of squeezed water: its influence on glacier erosion. *Annals of Glaciology,* **2**, 63-66.

Souchez, R. A., Lorrain, R. Tison, J.-L. and Jouzel, J. (1988). Co-isotopic signature of two mechanisms of basal ice formation in arctic outlet glaciers. *Annals of Glaciology,* **10**, 163-166.

Souchez, R., Meneghel, M., Tison, J.-L., Lorrain, R., Ronveaux, D., Baroni, C., Lozej, A., Tabacco, I. and Jouzel, J. (1991). Ice composition evidence of marine ice transfer along the bottom of a small Antarctic ice shelf. *Geophys. Res. Lett*, **18** (5), 849-852.

Stillwell, F. L. (1918). The metamorphic rocks of Adélie Land. *Australasian Antarctic Expedition 1911-1914, Scientific Reports, Series A*, Volume **3**, Part 1, 15-24.

Stuiver, M. and Braziunas, T. F. (1985). Compilation of isotopic dates from Antarctica. *Radiocarbon* **27**(2a), 117-304.

Stuiver, M., Denton, G. H., Kellogg, T. B. and Kellogg, D. E. (1978). Glacial geologic studies in the McMurdo Sound region. *Antarctic Journal of the United States*, **XIII**, 44-45.

Stuiver, M., Denton, G. H., Hughes, T. J. and Fastook, J. L. (1981). History of the marine ice sheet in West Antarctica during the last glaciation. In *"The Last Great Ice Sheets"* (G. H. Denton and T. J. Hughes Eds) 319-436. John Wiley and Sons, New York.

Sugden, D. E., Knight, P. G., Livesey, N., Lorrain, R. D., Souchez, R. A., Tison, J. -L. and Jouzel, J. (1987). Evidence for two zones of debris entrainment beneath the Greenland ice sheet. *Nature* , **328**, 238-241.

Swithinbank, C. W. M. (1969). Giant icebergs in the Weddell Sea, 1976-68. *Polar Record*, **14**: 477-478.

Thomas, R. H. and Bentley, C. R. (1978). A model for Holocene retreat of the West Antarctic Ice Sheet. *Quaternary Research*, **2**: 150-170.

Thwaites, R. J. (1984). 1984 Casey Glaciological program Data Report. Unpublished Report, Glaciology Program, Australian Antarctic Division, Hobart.

Thwaites, R. J. (Unpublished). Accumulation and ten metre firn temperature variations and their relationships, in Wilkes Land, Antarctica. Unpublished Report, Glaciology Program, Australian Antarctic Division, Hobart.

Tison, J.-L., Souchez, R. and Lorrain, R. (1989).On the incorporation of unconsolidated sediments in basal ice: present-day examples. *Zeitschrift für Geomorphologie,* **72**, 173-183.

Tison, J. -L., Petit, J. -R., Barnola, J. -M. and Mahaney, W. C. (1993). Debris entrainment at the ice-bedrock interface in sub-freezing temperature conditions (Terre Adélie, Antarctica). *Journal of Glaciology*, **39**, 132, 303-315.

Tracey, J. L. (1972). Holocene emergent reefs in the central Pacific. In *2nd Conference of the American Quaternary Association*, Abstracts, 51-2.(from Nunn, 1994).

Trail, D. S. (1970). Geological traverses on the MacRobertson Land and Kemp Land Coast. *ANARE Interim Reports, Series A (lll) Geology*, Publication No. **116**, Antarctic Division, Melbourne, pp37.

Trupin, A. S., Meier, M. F. and Wahr, J. M. (1992). Effect of melting glaciers on the Earth's rotation and gravitational field: 1965-1984. *Geophysical Journal International* , **108**: 1-15.

Tushingham, A. M. and Peltier, W. R. (1991). Ice 3G: A new global model of Late Pleistocene deglaciation based upon geophysical predictions of post glacial relative sea level change. *Journal of Geophysical Research*, **96**, B3, 4497-4523.

Tushingham, A. M. and Peltier, W. R. (1992). Validation of the ICE-3G model of Wurm-Wisconsin deglaciation using a global data base of relative sea-level histories. *Journal of Geophysical Research*, **97**, B3, 3285-3304.

Walcott, R. I. (1975). Recent and Late quaternary changes in water level. *EOS. Trans. Am. Geophys. Un., 56*, 62-72.

Warren, S. G., Roesler, C. S., Morgan, V. I., Brandt, R. E., Goodwin, I. D. and Allison, I. (1993). Green icebergs formed by freezing of organic-rich seawater to the base of Antarctic ice shelves. *Journal of Geophysical Research*, **98**, C4, 6921-6928.

Warrick, R. and Oerlemans, J. (1990). Sea Level Rise. In Houghton, et al. (Eds) *Climate Change The IPCC Scientific Assessment.* Cambridge University Press.

Watanabe, O. (1978). Distribution of surface features of snow cover in Mizuho Plateau. *In Memoirs of National Institute of Polar Research, Special Issue* No. 7, Tokyo, 44-62.

Watanabe, O., Fujii, Y. and Satow, K. (1988). Depositional regime of the katabatic slope from Mizuho Plateau to the coast, East Antarctica. *Annals of Glaciology*, **10**, 188-192.

Weertman, J. (1961). Mechanism for the formation of inner moraines found near the edge of cold ice caps and ice sheets. *Journal of Glaciology*, **6** (44), 191-207.

Wellman, P. and Tingey, R. J. (1976). Gravity evidence for a major crustal fracture in eastern Antarctica. *BMR Journal of Australian Geology and Geophysics*, **1** (2), 105-108.

Whillans, I. M. (1981). Reaction of the accumulation zone portions of Glaciers to climatic change. *Journal of Geophysical Research*, **86**, C5, 4274-4282.

Whitehouse, I. E., Chinn, T. J., and Höfle, H. C. (1988). Radiocarbon contaminated penguin bones from Terra Nova Bay, Antarctica. *New Zealand Antarctic Record* **8**(3), 11-23.

Whitehouse, I. E., Chinn, T. J., and Höfle, H. C. (1989). Radiocarbon dates from raised beaches, Terra Nova Bay, Antarctica. *Geologisches Jahrbuch* **E38**, 321-334.

Wigley, T. M. L. and Raper, S. C. B. (1993). Future changes in global mean temperature and sea level. In Warrick, R. A., Barrow, E. M. and Wigley, T. M. L. (eds) (1993), *Climate and sea level change: observations, projections and implications.* Cambridge University Press, 111-133.

Woodroffe, C. and McLean, R. (1990). Microatolls and recent sea-level change on coral atolls. *Nature*, **344**, 531-534.

Woodroffe, C., Maclean, R., Polach, H. and Wallensky, E. (1990). Sea-level and coral atolls: Late Holocene emergence in the Indian Ocean. *Geology*, **18**, 62-66.

Worby, A. P. and Allison, I. (1991). Ocean-atmosphere energy exchange over thin, variable concentration Antarctic pack ice. *Annals of Glaciology*, **15**, 184-190.

Wyrtki, K. (1985). Water displacements in the Pacific and the genesis of El Niño cycles. *Journal of Geophysical Research*, **90**, 7129-32.

Xie, Z. (1983). Snow stratigraphy and ice formation on Law Dome. Unpublished Glaciology Section, Australian Antarctic Division Report.

Yevteyev, S. A. (1959). Opredeleniye kolichestva morennogo materiala, perenosimogo lednikami vostochnogo poberezh'ya Antarktidy. *Informatsionnyy Byulleten' Sovetskoy Antarkticheskoy Ekspeditsii* **11**, 14-16.

Yonekura, N., Matsushima, Y., Maeda, Y. and Kayanne, H. (1984). Holocene sea-level changes in the southern Cook Islands. In: Sea-Level Changes in the Middle Pacific. Rep. HIPAC Proj. in 1981, 1982 and 1983. Kobe University, 113-136.

Yoshida, Y. and Moriwaki, K. (1979). Some consideration on elevated coastal features and their dates around Syowa Station, Antarctica. In *"Proc. of the Seminar III on Dry Valley Drilling Project, 1978.* National Institute of Polar Research, 220-226.

Young, N. W, Raynaud, D., de Angelis, M., Petit, J-R., and Lorius, C. (1984). Past changes of the Antarctic Ice Sheet in Terre Adélie as deduced from ice core data and ice modelling. (Abstract), *Annals of Glaciology* , **5**, 239.

Young, N. W., Goodwin, I. D., Hazelton, N. W. J. and Thwaites, R. J. (1989a). Measured velocities and ice flow in Wilkes Land, Antarctica. *Annals of Glaciology*, **12**, 192-197.

Young, N., Malcolm, P., Mantell, P. and McGibbon, E. (1989b). Velocity and surface-lowering measurements on Law Dome, Antarctica (abstract). *Annals of Glaciology*, **12**, 220.

Young, S. B. and Schofield, E. K. (1973). Pollen evidence for late Quaternary climate changes on Kerguelen Islands. *Nature* , **245**, 311-312.

Zhang, Q. and Peterson, J. A. (1985). A geomorphology and Late Quaternary geology of the Vestfold Hills, Antarctica. *Australian National Antarctic Research Expeditions Scientific Report* , **133**, 1-84.

Zwally, H. J., Comiso, J. C., Parkinson, C. L., Campbell, W. J., Carsey, F. D. and Gloersen, P. (1983). *Antarctic sea ice, 1973-1976: Satellite passive-microwave observations..* NASA Sci. Tech. Inf. Branch, NASA Spec. publ. **459**.